

INTERIM REPORT

Examination of Airborne FDEM System Attributes for UXO Mapping and Detection

SERDP Project MM-1633

November 2009

Dr. William Doll
Battelle

This document has been approved for public release.



Strategic Environmental Research and
Development Program

This report was prepared under contract to the Department of Defense Strategic Environmental Research and Development Program (SERDP). The publication of this report does not indicate endorsement by the Department of Defense, nor should the contents be construed as reflecting the official policy or position of the Department of Defense. Reference herein to any specific commercial product, process, or service by trade name, trademark, manufacturer, or otherwise, does not necessarily constitute or imply its endorsement, recommendation, or favoring by the Department of Defense.

Table of Contents

Executive Summary.....	i
1. Objective.....	1
2. Materials and Methods	1
3. Results and discussion.....	2
3.1 Computer modeling.....	2
3.1.1 Background.....	2
3.1.2 Signal Response Model.....	3
3.1.3 Modeling Considerations	4
3.1.4 Sensor Configurations.....	6
3.1.5 Soil Properties.....	10
3.1.6 Modeling Results	10
3.1.7 “Perturbation” Noise.....	18
3.1.8 Ground Response.....	21
3.1.9 Passive Noise Level Determination	27
3.1.10 Comparison to Time Domain.....	33
3.1.11 Ground-based transmit loop.....	42
3.2 Helicopter Noise Measurements	46
3.2.1 Noise Measurements During Takeoff and Landing.....	46
3.2.2 Noise Spectra, Transmitter off, at 500 ft AGL	48
3.3 Design constraints for nulling and mock-up testing.....	49
3.4 Primary Field Removal Assessment	52
3.4.1 Dynamic Range Issues: FDEM vs TEM.....	52
3.4.2 Transmitter-Receiver Configurations	52
3.4.3 Dynamic Range Compression Methods Testing.....	53
3.5 Mock-up Tests.....	54
3.5.1 Mock-up Apparatus	54
3.5.2 Results from Preliminary Mock-up Tests.....	58
3.6 Discussion	61
3.6.1 Preferred model configurations.....	61
3.6.2 Comparison of Observed and Modeled FDEM and TEM Performance.....	61
3.6.3 Semi-Airborne Configuration (ground-based transmitter)	65
4. Conclusions to Date and Recommendations for Remainder of this Project	68
5. Literature Cited.....	72
Appendix 1A. Signal strength modeling results for five sensor configurations.....	A1A-1
Appendix 1B. Modeling results of the change in coupling due to coil perturbations	A1B-1
Appendix 2A. Signal strength for a ground based transmitter	A2A-1
Appendix 2B. Perturbation levels for receive coils and a 1 km square transmit coil.	A2B-1

Executive Summary

In this project, we have conducted computer modeling and mock-up tests to assess the benefits of several airborne frequency-domain electromagnetic system configurations for mapping and detection of UXO, and have projected their likely performance in comparison to an existing time-domain airborne system. The goal of the first year of the project was to identify preferred configurations that would be analyzed in greater detail during the second year of the project.

Most of the designs that were evaluated had both transmitter and receivers mounted on booms that are attached directly to the helicopter. Two of these designs were shown to have low sensitivity to vibration and flexure and modest response amplitudes. Both had horizontal coplanar transmitters and receivers. Comparisons of the FDEM models with TEM models have used the Battelle-TEM-8 system for reference, as this is the only known airborne TEM system for UXO mapping and detection. This suggested that the S/N performance of the quadrature output of the two FDEM designs would be similar to the observed S/N of TEM systems, though differences in the numerical modeling procedures for the two methods adds some uncertainty to the comparison. Mock-up testing of FDEM systems and ground-based offset measurements of ordnance, conducted as part of the TEM-8 development and assessment, indicated that FDEM measurements may yield up to 4 times more signal than TEM measurements, with noise levels being comparable between the two methods. A S/N improvement of 4X for FDEM relative to TEM designs would enable detection of standard ordnance items at approximately 1 m higher altitude than with current TEM systems. The diameter of the transmitter loop was shown to be a key factor in determining the S/N performance of these systems, with larger diameters than have been flown to date yielding better S/N due to lower rates of primary field strength attenuation at the target level.

Another potential route to improvement in S/N was found for configurations that use a ground-based transmitter in combination with airborne receivers. Systems which use this approach for mineral prospecting are referred to as “semi-airborne”. This approach would have many practical advantages over configurations with helicopter-mounted transmitters. First, these configurations would involve much less weight and associated moment of inertia on the helicopter, making them easier and safer to fly. The ground-based transmitter would allow for receivers to be placed across the entire array (sidebooms and foreboom) so that they would be more operationally efficient than the current TEM-8 system. The emplacement of a large (up to 15 km²) ground-based transmitter loop for the semi-airborne Turair and FLAIRTEM mineral prospecting systems was reported to be very efficient, sometimes requiring as little as an hour to deploy.

Given the Year 1 results, we recommend that the remaining year of the project be focused on evaluating the semi-airborne configuration. Many important questions remain unanswered and would need to be addressed in order for this to prove a viable design, but the initial indications are very favorable and encouraging. Among the tasks to be addressed are the following:

1. Detailed assessment of anticipated signal and noise arising from various sources for two receiver configuration styles (vertical and horizontal gradient receive coil pairs) with ground-based transmitter:
 - a. Model variable ground response as a function of height for these configurations. Modeling work to date is unable to assess the ground effects for the semi-airborne configuration. We propose to extend the current SAIC codes to address this need, and to perform additional modeling using codes that are available within the EM research community
 - b. Model frequency-dependent susceptibility response as a function of height for a realistic source layer thickness (this should be compared with the halfspace response)
 - c. Measure ambient noise amplitudes as a function of receiver height for these receiver configurations
 - d. Measure helicopter noise emissions for these receiver configurations. We plan to measure noise using a ground-based transmitter with the existing receivers on the TEM-8 system. Additional airborne measurements will be made with Cases 2 and 4 receiver configurations to assess degree of noise cancellation obtained with these arrays.
 - e. Model and measure vibration effects in ground-based transmitter field for these receiver configurations
 - f. Model and measure the above effects as a function of horizontal position relative to ground-based transmitter. Determine effective useful area.
2. Although modeling indicates a significant signal performance improvement for a FDEM semi-airborne system over a fully airborne TEM configuration, it does not address comparison with a semi-airborne TEM configuration. As part of the above measurements, we will compare the benefits of TEM and FDEM systems which both use a ground-based transmitter.
3. Consider operational constraints on system viability:
 - a. Analyze Case 2 and Case 4 receiver coil array requirements for ambient noise rejection performance under airborne conditions, effective area, rigidity, weight, thermal noise and electrical characteristics, and build mock-up for bench and ground-based testing
 - b. Assess required transmitter capabilities (current, voltage, timebase stability)
 - c. Assess transmitter cable diameter and weight for the likely range of transmitter size and currents
 - d. Consider practical cable deployment and retrieval procedures
 - e. Assess available transmitter safety mechanisms and related operating procedures
 - f. Analyze modifications to TEM-8 console required to accommodate a high-stability, GPS-disciplined timebase.
4. Conduct simple ground-based signal and noise measurements using frequencies that would be operationally suitable for airborne deployment, using the Battelle airborne UXO test grid near Columbus, Ohio

1. Objective

The objective of this project was to provide new capabilities for wide-area mapping and detection of UXO, by developing airborne frequency-domain electromagnetic (FDEM) systems as an alternative to magnetometer and time-domain electromagnetic systems. At the first level, these could be used to assess ordnance density in areas where site conditions are unfavorable for magnetometers. In the longer term, we anticipated that an airborne FDEM system could consistently perform better than magnetometer systems (analogous to the performance of ground-based EM systems vs. magnetic systems), even at those sites where geologic conditions are less problematic for magnetic surveys. The proposed system assessment would focus on mapping and detection, rather than discrimination, of unexploded ordnance.

This report provides a summary of progress to date on the project during the first of two years effort. The predominant task in the first year consisted of computer modeling of selected system designs to assess optimal configurations and to weigh likely performance of the FDEM architecture in comparison with existing TEM architectures. The culmination of the first year is a go/ no-go decision based on the projected improvement in sensitivity of FDEM systems over existing TEM systems.

2. Materials and Methods

A diagram of the task sequence for the project is shown in Figure 1.

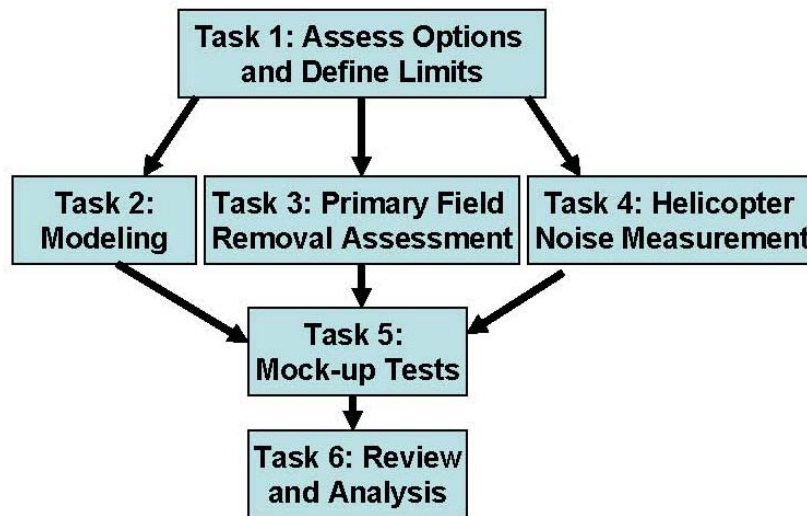


Figure 1. Block diagram of tasks for this project.

The first task was for the project team to meet and discuss system architecture strengths and weaknesses, and to specify constraints on subsequent computer modeling. The discussion was broad-based and led to the selection of models that are described below. In addition to extensive computer modeling (Task 2), helicopter noise data have been

acquired and processed (Task 4), as was the primary field removal method assessment (Task 3). The final task to validate the modeling results, namely the initial phase of mock-up testing (Task 5) that was scheduled for Year 1, was also completed. The remainder of the project as proposed includes additional modeling and considerable effort in detailed mock-up testing using inert UXO and for a variety of operational noise sources to include vibration testing, flexure tests, and altitude simulations.

It was determined that the focus of modeling and assessment should be on relatively low-frequency, quadrature measurements for three reasons.

First, the inphase response of small, magnetically susceptible targets such as UXO can range from positive to negative values, depending on frequency, orientation and sensor-target geometry, so that the inphase component of such target responses can approach zero amplitude. This contrasts with low-frequency quadrature responses from such targets, which are always positive for the principal FDEM arrays considered.

Second, the quadrature output of an FDEM system in free space is decoupled from small changes in transmitter-receiver geometry, so that distortions of the FDEM array due to vibration and externally applied forces do not generate significant responses that can act as noise when measuring the quadrature component of measured target responses.

Third, at low frequencies, the quadrature response of weakly or moderately conductive, magnetically susceptible soils for the FDEM arrays under consideration is very weak. Inphase responses from such soils can be stronger, due to magnetic polarization. The quadrature response of frequency-dependent susceptible soils to these in airborne configurations was not well understood at the outset of this project.

3. Results and discussion

3.1 Computer modeling

3.1.1 Background

Measurements made by ground based EMI sensors over buried UXO have been closely matched with a basic dipole response model. The dipole response strength for a given conducting, magnetically permeable object is given by its magnetic polarization terms along its major body axes. These polarizations can be determined analytically for simple shapes such as spheres and have been measured for a wide range of ordnance items. Given these response terms, the signal strength from any EMI sensor can be predicted. It is just a matter of calculating the fields from the given coil configurations. To go from ground based to a helicopter platform, this involves scaling up the coil sizes. In a similar fashion, various EMI noise sources, such as response from ground, can be predicted as well.

3.1.2 Signal Response Model

For a frequency domain EMI sensor operating in a continuous transmit wave mode at a single frequency f , the voltage induced in an arbitrary receive coil by the presence of a metallic object can be expressed as

$$\mathbf{V} = -i\mu_0\omega n_R n_T I_T \mathbf{C}_R \cdot \mathbf{C}_T \mathbf{B} \quad (1)$$

In equation (1), μ_0 is the magnetic permeability of free space ($4\pi \times 10^{-7}$ Volt-sec/Amp-m); $\omega = 2\pi f$ is the angular frequency; n_T and n_R are the number of turns in the transmit and receive coils, respectively; I_T is the peak current amplitude at frequency f ; \mathbf{C}_T and \mathbf{C}_R are coil sensitivity functions for the transmit and receive coils, respectively, with units of m^{-1} ; and \mathbf{B} is the magnetic polarizability matrix of the object at frequency f , in m^3 . \mathbf{C}_T and \mathbf{C}_R depend on the respective coil geometries and are functions of the location of the coils relative to the object. They are defined in terms of integrals around the coil involving the vector from the coil to the object:

$$\mathbf{C}_{T,R}(\mathbf{r}_0) = \frac{1}{4\pi} \oint_{T,R} \frac{d\mathbf{l} \times (\mathbf{r}_0 - \mathbf{r})}{|\mathbf{r}_0 - \mathbf{r}|^3} \quad (2)$$

where \mathbf{r}_0 is the location of the object and \mathbf{r} is the location of a point on the coil. Note that the vector $n_T I_T \mathbf{C}_T \mathbf{B}$ in (1) describes the strength of the induced dipole response of the object at frequency f in $\text{Amp}\cdot\text{m}^2$.

The voltage induced in the receive coil directly by the transmit field can be expressed as

$$\mathbf{V}_{\text{Norm}} = -i\mu_0\omega n_R n_T I_T \int_{A_R} \mathbf{C}_T(\mathbf{r}_{dA_R}) \cdot d\mathbf{A}_R \quad (3)$$

where $\mathbf{C}_T(\mathbf{r}_{dA_R})$ is defined by (2) with \mathbf{r}_0 replaced by \mathbf{r}_{dA_R} , and \mathbf{r}_{dA_R} is the location of an infinitesimal area with normal vector $d\mathbf{A}_R$ within the receive coil area A_R . The integral represents a summation of all the infinitesimal areas that make up A_R .

A unit used to compare the voltage induced by the object to the voltage induced by the transmit field is the parts-per-million (ppm) unit, defined as

$$\text{ppm} = \frac{\mathbf{V}}{\mathbf{V}_{\text{Norm}}} \cdot 10^6 = \frac{\mathbf{C}_R \cdot \mathbf{C}_T \mathbf{B}}{\int_{A_R} \mathbf{C}_T(\mathbf{r}_{dA_R}) \cdot d\mathbf{A}_R} \cdot 10^6 \quad (4)$$

In examining the expressions for the voltage induced and the ppm unit given by (1) and (4), respectively, it is clear that the voltage induced depends linearly on f , n_R , n_T and I_T , whereas the ppm does not depend on these quantities. Furthermore, as specified by (2), for a fixed sensor configuration at a fixed distance from the object, \mathbf{C}_T , \mathbf{C}_R and the ppm

denominator increases as the respective coil size increases; and for a fixed sensor configuration with fixed coil sizes, \mathbf{C}_T and \mathbf{C}_R decreases as the distance from the object increases, while the ppm denominator remains constant. More explicitly, in the far-field regime (i.e. $|\mathbf{r}_0| \gg |\mathbf{r}|$ in (2)),

$$|\mathbf{C}_{T,R}| \sim \frac{A_{T,R}}{2\pi|\mathbf{r}_0|^3}$$

and so, at this fixed far-field distance from the object, \mathbf{C}_T and \mathbf{C}_R depend linearly on the respective coil areas; while for fixed coil sizes, \mathbf{C}_T and \mathbf{C}_R depend inversely on the object distance cubed.

For the special case where both transmit and receive coils are circular, coaxial and concentric, the integral in (3) can be expressed analytically. Specifically,

$$\int_{A_R} \mathbf{C}_T(\mathbf{r}_{dA_R}) \cdot d\mathbf{A}_R \equiv \pi a_T a_R \int_0^\infty J_1(\lambda a_T) J_1(\lambda a_R) d\lambda$$

where a_T and a_R are the transmit and receive coil radii, J_1 denotes a Bessel function of the first kind and of order one, and λ is the variable of integration. Assuming this same specialized coil configuration at a height h above a soil half-space, the voltage induced by the presence of the soil can similarly be expressed as [Das, 2004 & 2006]

$$V_{\text{Soil}} = -i\mu_0 \omega n_R n_T I_T \pi a_T a_R \int_0^\infty \Gamma(\lambda, u, \mu) \exp(-2\lambda h) J_1(\lambda a_T) J_1(\lambda a_R) d\lambda \quad (5)$$

with

$$\Gamma(\lambda, u, \mu) = \frac{\lambda\mu - u\mu_0}{\lambda\mu + u\mu_0}, \quad u = \sqrt{\lambda^2 + i\sigma\mu\omega} \quad (6)$$

In (5), the influence of the soil enters through the function $\Gamma(\lambda, u, \mu) \exp(-2\lambda h)$, which depends on the magnetic permeability μ and electrical conductivity σ of the soil, the frequency, the variable of integration and the height above ground.

3.1.3 Modeling Considerations

In this section, we present details on the select assortment of modeled coil configurations (i.e. coil shapes and relative placement) and state all the accompanying assumptions made in computing the quantities of (1) and (4) for each. In addition, for those specialized coil configurations where (5) is applicable and consequently computable, assumptions regarding soil properties are also detailed. Since both quantities of (1) and

(4) depend directly on the object-dependent matrix \mathbf{B} , we first justify the matrix element values used.

Test Object

The magnetic polarizability matrix \mathbf{B} of the object can be expressed as

$$\mathbf{B} = \mathbf{U}\mathbf{B}_0\mathbf{U}^T \quad (7)$$

with

$$\mathbf{B}_0 = \begin{bmatrix} \beta_1 & 0 & 0 \\ 0 & \beta_2 & 0 \\ 0 & 0 & \beta_3 \end{bmatrix}, \quad (8)$$

where $\beta_1, \beta_2, \beta_3$ correspond to the complex responses induced along each of the object's principal axes by a continuous transmit wave of frequency f , and \mathbf{U} is the rotation matrix that transform these responses to the X, Y and Z coordinate directions.

Since we are particularly interested in modeling signal levels due to larger-sized UXO items, appropriate estimates for the β 's of such items are necessary. To this end, we draw upon β 's derived from multi-frequency FD EMI data (collected with the NRL GEM-3 Array [Nelson, et al., 2002]) of a 105mm and a 155mm projectile placed in a pit under different orientations. For axially symmetric shapes such as cylinders, prolate or oblate spheroids, and many UXO items, there is a basic longitudinal response along its length and two equal responses transverse to this (i.e. $\beta_1, \beta_2=\beta_3$). Figure 2 shows the two different possibilities for β_1 (i.e. the 'Nose Down' and 'Nose Up' orientations), as well as β_2 and β_3 (i.e. the 'Horizontal' orientation), for both the 105mm and 155mm projectiles. The solid curves represent the in-phase component of the complex β 's as a function of frequency, while the dashed curves represent the quadrature component. For these larger ordnance items, the in-phase response β crosses from negative to positive values in this frequency range; at the wrong frequency, it would be "invisible". The quadrature response is positive, but decreasing, with frequency. The peak longitudinal quadrature response of large ordnance is below 10 Hz. The transverse quadrature response peaks in the 100 Hz to several kHz range. In calculating signal strengths, we will consider two nominal response factors of $\beta = 0.0075 \text{ m}^3$ at 150 Hz and $\beta = 0.005 \text{ m}^3$ at 1 kHz. These values are plotted in green and red in Figure 2. They closely match the "Nose Up" and "Nose Down" quadrature response of the 105mm and the "Nose Down" and "Horizontal" response of the 155mm. The 105mm "Horizontal" has a weaker response and the 155mm "Nose Up" a stronger one. Overall, the signal strength in PPM scales linearly with β and any calculated strength can be scaled to another by multiplication. The 150 Hz response of 0.0075 is just 1.5 times the 1 kHz response of 0.005.

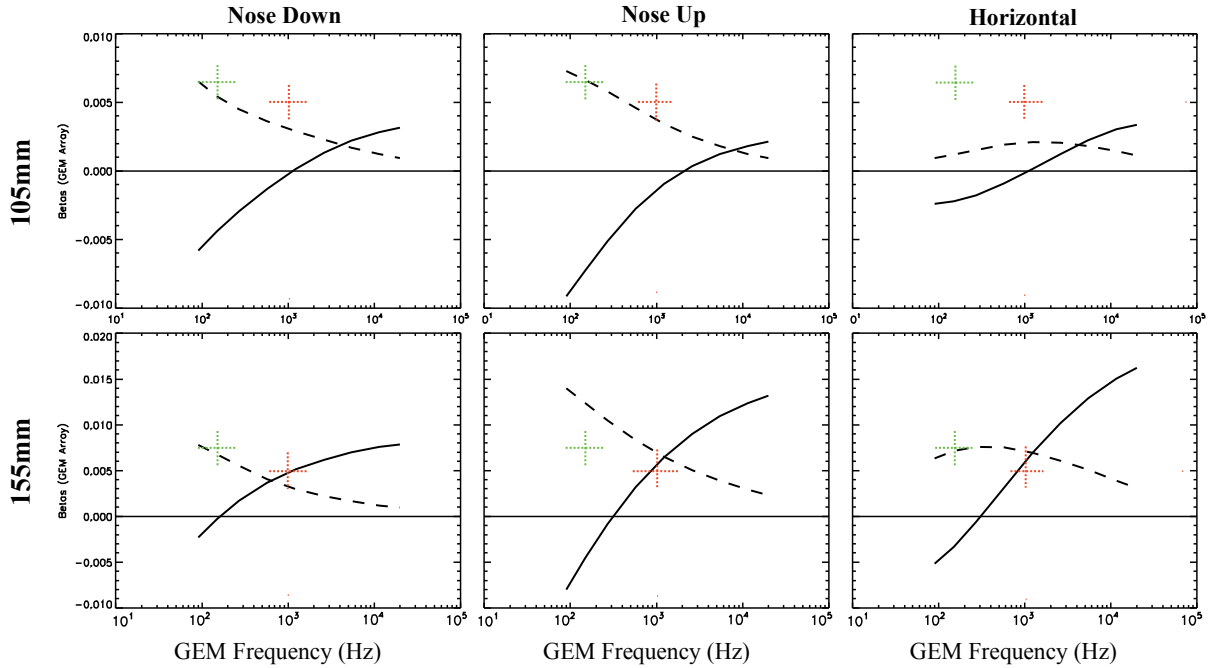


Figure 2. β 's (In-phase = solid curves; Quadrature = dashed curves) derived from GEM-3 array data for a 105mm and a 155mm projectile. Green and red crossings indicate β values selected at 150 Hz and 1000 Hz for general comparison.

3.1.4 Sensor Configurations

The coil configurations we consider include both helicopter-borne and ground-based transmit coils.

Helicopter-borne Transmit Coil Systems

For these systems, two types of primary field nulling (PFN) are examined: active PFN using transmit coils to cancel the primary field in the receive coil; and passive PFN (or bucking) using receive coils to cancel the primary field. In order to simulate the active PFN method used by the GEM-3 sensor, while also retaining the ability for direct cross-comparison of these results with passive PFN configurations, circular transmit and receive coils are utilized throughout. All the different cases considered are bulleted below and portrayed in Figure 3:

- CASE 1 – Vertical Transmit Coil with a Concentric and Coaxial Receive Coil
- CASE 2 – Vertical Transmit Coil with a Concentric and Coaxial Vertical Gradient Receive Coil Pair
- CASE 3 – Vertical Transmit Coil with a Concentric Horizontal Receive Coil
- CASE 4 – Vertical Transmit Coil with a Concentric Horizontal Gradient Receive Coil Pair

- CASE 5 – GEM-3 Style Vertical Transmit Coil with a Concentric and Coaxial Receive Coil

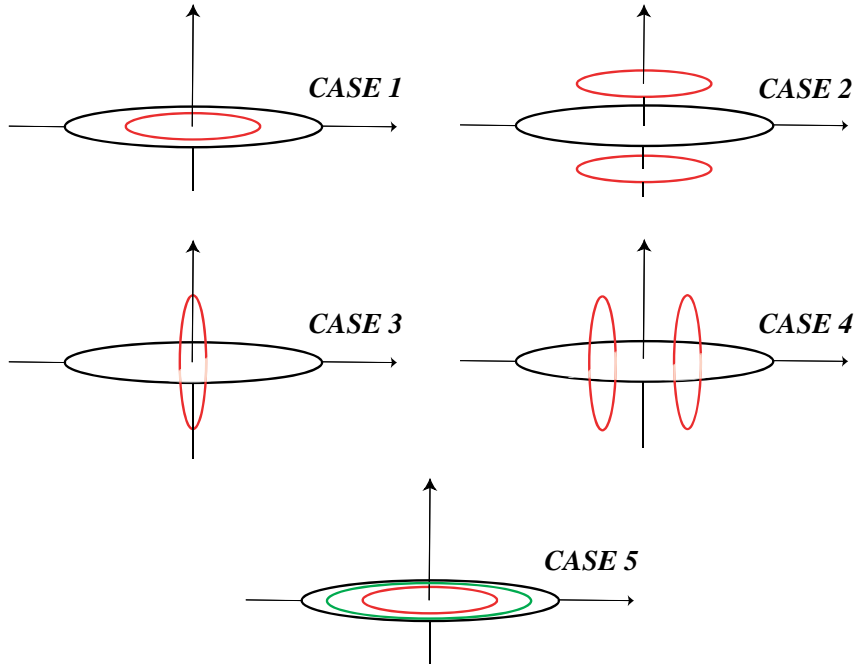


Figure 3. All the helicopter-borne transmit coil configurations considered in our modeling efforts. Red represents receive coils, black represents transmit coils, and green represents the GEM-3 style bucking coil.

For each of these cases, a single-turn vertical transmit coil configuration carrying a current of 1 Amp (i.e. $n_T=1$ and $I_T=1$ Amp) is considered, along with a single-turn receive coil configuration (i.e. $n_R=1$). In order to provide modeling results that can be readily compared, we choose a transmit coil diameter of 3m (comparable to width of TEM-8) and compute the signal strength in nano-Volts using (1), and the ppm unit using (4), as a function of both the transmit coil height above ground and the horizontal profile above the object, with receive coil diameters of 0.1m, 0.2m, 0.5m and 1 m, respectively. The object is always assigned a depth of 1 m; and recall that we previously chose $\beta_1 = \beta_2 = \beta_3 = 0.005 \text{ m}^3$ as an approximate quadrature response strength for a large ordnance item at a frequency of 1 kHz. The nominal quadrature response strength at 150 Hz is 1.5 times this with $\beta = 0.0075 \text{ m}^3$.

The gradient receive coil configurations will have an additional dependency on the signal strength through the coil separation Δl . For the purpose of direct comparison between results of all configurations, we choose a coil separation distance of 0.5 m and generate the same curves as outlined above. In addition, we fix the receive coil diameter at 1 m and generate the same curves for coil separation distances of 0.1 m, 0.25 m, 0.5 m and 1 m, respectively. As before, an explicit dependence in the far-field (with the added condition that $|\mathbf{r}_1| \gg \Delta l$), can be established via (2) as:

$$|\mathbf{C}_R| \equiv |\mathbf{C}_{R_1} - \mathbf{C}_{R_2}| \sim \frac{A_R}{2\pi} \left(\frac{1}{|\mathbf{r}_1|^3} - \frac{1}{(|\mathbf{r}_1| + \Delta l)^3} \right) \sim \frac{3A_R \Delta l}{2\pi |\mathbf{r}_1|^4} \quad (9)$$

where $|\mathbf{r}_1|$ is the distance from the closest receive coil to the object. Clearly, in the far-field, the signal strength (i.e. (1) and (4)) does not only depend linearly on Δl , but now also depends inversely on the object distance to the power of 7.

In computing the denominator of (4) for horizontal receive configurations, the results tend toward zero yielding undefined ppm units. For such cases, we follow the general convention of computing the denominator by replacing horizontal coils with vertical ones. For the gradient receive coil pair configurations, either of the coil locations may be used since the magnitude of the transmit field in each coil will be identical due to symmetry.

The GEM-3 style coil configuration consists of a planar concentric pair of transmit coils (i.e. an outer coil and a smaller inner coil) balanced such that the oppositely flowing current in the inner coil produces a field that exactly cancels the field formed by the outer coil within the receive coil. Using (3) with $n_T=1$, the condition is simply:

$$\mathbf{V}_{\text{Norm}}^{\text{Outer}} - g \mathbf{V}_{\text{Norm}}^{\text{Inner}} = 0 \quad (10a)$$

where g is a gain factor that can ultimately be realized practically with an appropriate number of turns, i.e.,

$$g = \frac{n_T^{\text{Inner}}}{n_T^{\text{Outer}}} \cdot \quad (10b)$$

for a given set of outer and inner transmit coil diameters and receive coil diameter.

Since, for our current purposes, our intention is to be able to directly compare results across configurations, we use exactly the same outer transmit and receive diameter choices as before, fixing the inner coil diameter to be 1.25 m. However, to examine the dependency of the inner coil diameter choice on the signal strength, we also fix the receive diameter to be 1 m and compute (1) and (4) using an inner transmit coil diameter of 1.25, 1.75, 2.25 and 2.75 m. To get an explicit dependence of the inner transmit coil on the signal strength in the far-field, we examine the ratio of the GEM-3 style transmit signal to the transmit signal due to just the outer coil, i.e.:

$$\frac{n_T^{\text{Outer}} |\mathbf{C}_T^{\text{Outer}}| - n_T^{\text{Inner}} |\mathbf{C}_T^{\text{Inner}}|}{n_T^{\text{Outer}} |\mathbf{C}_T^{\text{Outer}}|} \sim 1 - \frac{n_T^{\text{Inner}}}{n_T^{\text{Outer}}} \frac{A_T^{\text{Inner}}}{A_T^{\text{Outer}}} = 1 - \frac{n_T^{\text{Inner}}}{n_T^{\text{Outer}}} \left(\frac{D_T^{\text{Inner}}}{D_T^{\text{Outer}}} \right)^2 \quad (11)$$

The second term in the above result represents the far-field signal strength loss due to the addition of a concentric and coplanar oppositely polarized inner transmit coil of

diameter D_T^{Inner} . As D_T^{Inner} gets larger, the loss gets larger and thus the signal strength gets smaller.

Finally, in an effort to determine the relative stability of the configurations given in Figure 3 to the effects of vibration and flexure, we compute and compare the change in primary field coupling to small perturbations in the positioning and orientation of the receive coil relative to a fixed transmit coil. The perturbations considered are illustrated in Figure 4. For the gradient receive configurations, the coils are perturbed both individually and as a pair. For the GEM-3 style configurations, in addition to the receive coil being perturbed relative to the transmit configuration, we also perturb the inner transmit coil relative to the fixed set of remaining coils (i.e. the outer transmit and inner receive coils).

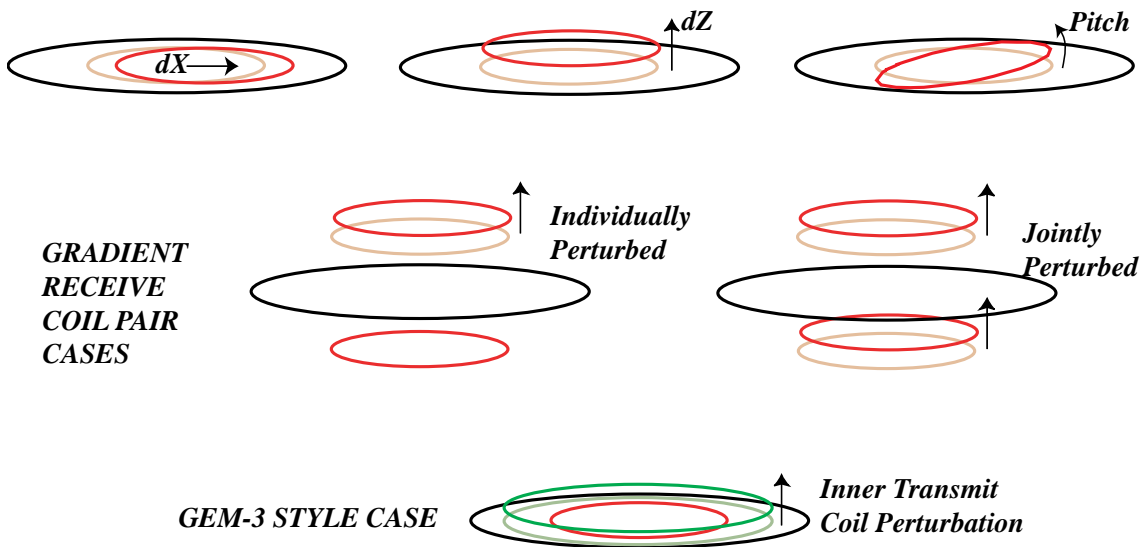


Figure 4. Types of perturbations considered.

For the special cases where there is complete insensitivity to certain perturbations due to geometrical symmetry, we examine the perturbation in question by breaking the symmetry via a minute change in coil position. An example would be that of Case 2 under pitch perturbations: when placed concentrically, any pitch perturbation occurring on the vertical gradient receive coil pair (as a rigid structure) will have absolutely no effect due to symmetry; however, if placed 1mm off-center in x or z, the same pitch perturbations will have a pronounced effect.

Ground-based Transmit Coil System

For these systems, a ground-based 1 km² square coil is considered with either a vertical receive coil or a vertical gradient receive coil pair placed parallel to and above the ground. We shall refer to these as CASE 1 and CASE 2, respectively. As before, we determine the signal strength in nano-Volts using (1), and the ppm unit using (4), this

time not only as a function of both the receive coil height above ground and the horizontal profile above the object, but also as a function of the horizontal profile above the extent of the transmit coil, with receive coil diameters of 0.1 m, 0.2 m, 0.5 m, 1 m and 2 m, respectively. Again, $f=1$ kHz, $n_R=1$, $n_T=1$ and $I_T=1$ Amp are used in our computations, along with the same assumptions for the object (i.e. depth=1m and $\beta_1=\beta_2=\beta_3=0.005\text{m}^3$). The response at 150 Hz is 1.5 times the 1 kHz response ($\beta=0.0075\text{m}^3$).

3.1.5 Soil Properties

Based on GEM-3 soil measurements taken at Blossom Point, Maryland [ESTCP MM-0508, 2006] and other work [West, 2009] we assume a frequency-independent σ and use the same frequency-dependent model for μ used by [Das 2004,2006], i.e.

$$\mu = \mu_0(1 + \chi(\omega)) \quad , \quad \chi(\omega) = \chi_0 \left(1 - \frac{1}{\ln(\tau_2 / \tau_1)} \cdot \ln \frac{i\omega\tau_2 + 1}{i\omega\tau_1 + 1} \right) \quad . \quad (12)$$

In (12), $\chi(\omega)$ is the frequency-dependent susceptibility of the soil and is a complex-valued function; χ_0 is the d.c. value of susceptibility; and τ_1 and τ_2 are, respectively, the lower and upper bound magnetic relaxation time constants considered in the soil model. For our purposes, the complex-valued signal strength due to the soil as a function of height is determined via (5). A moderate soil conductivity of $\sigma=0.005$ S/m is used. A set of three magnetic susceptibility values ($\chi_0=2 \cdot 10^{-4}$, $20 \cdot 10^{-4}$, and $200 \cdot 10^{-4}$) are applied ranging from benign to severe magnetic conditions. The time constants in (12) are set to very high and low values resulting in a linear inphase response across the frequency range of 10 Hz to 10 kHz ($\tau_1=1/(2\pi \cdot 10^{11})\text{s}$ and $\tau_2=1/(2\pi \cdot 10^0)\text{s}$). Recall, however, that (5) is only applicable for the CASE 1 and CASE 5 sensor configurations of Figure 2. For the CASE 5 sensor configuration, however, $J_1(\lambda a_T)$ has to be replaced with $J_1(\lambda a_T^{\text{Outer}}) - g a_T^{\text{Inner}} J_1(\lambda a_T^{\text{Inner}}) / a_T^{\text{Outer}}$, where g is the gain factor that satisfies condition (10).

3.1.6 Modeling Results

In this section, we present results of computing (1), (4) and (5) for the assortment of cases outlined in the previous section.

3.1.6.1 Transmit Field

To begin, however, we examine the on-axis (and maximum) field strength from two standard transmit coil geometries – square and circular – and make a few observations. Figure 5 shows such results for single-turn coils with a 1 Amp current and lengths/diameters of 1, 3, and 4 m. It is clear that the square and circular coil results are

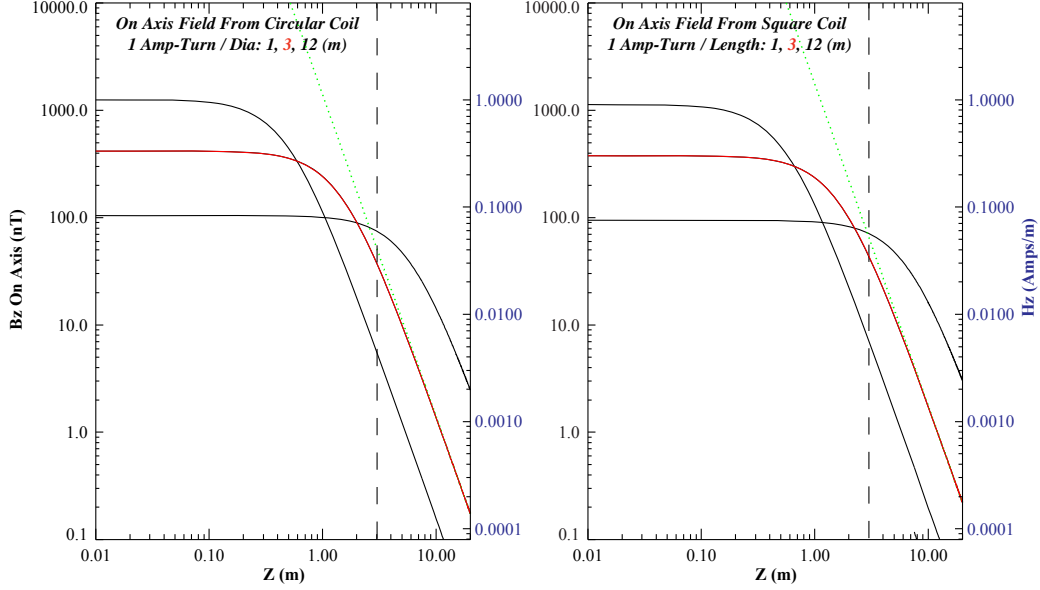


Figure 5. On axis field strength from circular (left) and square (right) transmit coils. Coil diameter/lengths are 1, 3, and 12 meters. Green dotted line indicates far field $1/r^3$ fall off.

comparable. Indeed, the far-field asymptote of (2) as discussed in that section (and shown as the green dotted lines in Figure 5 for the 3 m length and diameter cases) explicitly states that, at a fixed (far off) distance, the square coil field strength is greater than the circular coil field strength by a factor of only $4/\pi$. It is equally clear that a large coil is necessary if we want to be in the slowly varying transmit regime at a distance of several meters below the coil.

Figure 6 shows profiles of the B field Z-component in the plane of the coil ($Z=0$) and at $Z=2$ m below due to large rectangular transmit coils similar to those tested on the ORAGS-TEM helicopter system. These include 12m x 3m, 4m x 3m, and pairs of 4m x 3m symmetric and anti-symmetric rectangular coils. Note that directly under the coils ($X=\pm 4$ m) the transmit fields are comparable. In addition, the long rectangular coils scale with the narrower 3m dimension.

3.1.6.2 Signal Strengths

Plots of the signal strength modeling results for the sensor configurations of Figure 3 are shown in Appendix 1A. As described in the previous section, the signal strengths (in nano-Volts and ppm units) in the presence of an object are computed as a function of both the transmit coil height above ground and the horizontal profile above the object, for receive coil diameters of 0.1 m, 0.2 m, 0.5 m and 1 m. Again, for all cases, we have chosen $f=1$ kHz, $n_R=1$, $n_T=1$, $I_T=1$ Amp, a transmit coil diameter of 3 m, an object at 1 m depth with $\beta_1=\beta_2=\beta_3=0.005$ m³, a coil separation distance of 0.5 m for the two gradient receive coil configurations (i.e. CASE 2 and CASE 4), and an inner transmit coil diameter of 1.25 m for the GEM-3 style configuration (i.e. CASE 5). For the signal strength at 150 Hz, multiply these curves by a factor of 1.5.

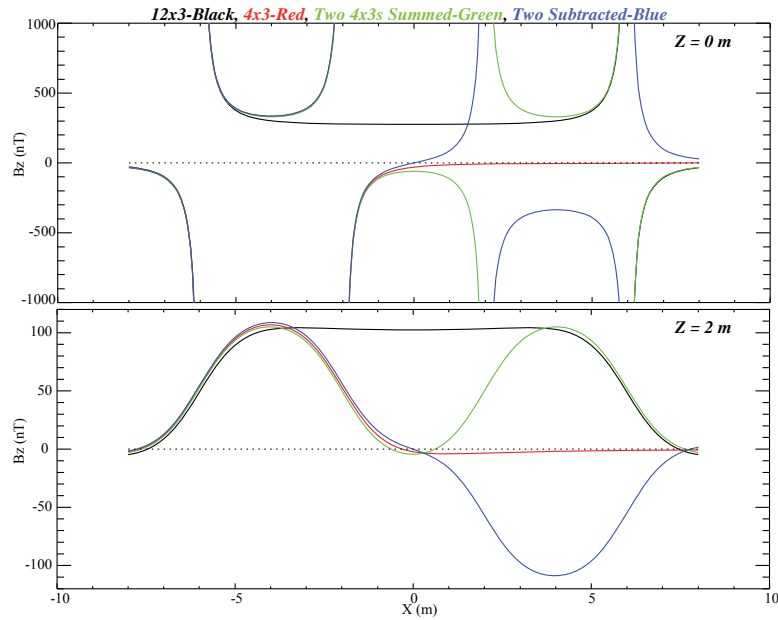


Figure 6. Transverse profiles of vertical component of B field from various rectangular transmit coil configurations similar to those tested on ORAGS-TEM. Top plot is field in plane of transmit coil(s) and bottom plot is field 2 meters below transmit coil(s).

In addition, for a receive coil diameter of 1 m, the same signal strength curves are generated for coil separation distances of 0.1 m, 0.25 m, 0.5 m and 1 m (for CASE 2 and CASE 4), and inner transmit coil diameters of 1.25, 1.75, 2.25 and 2.75 m (for CASE 5). Finally, the signal strengths are also determined as a function of coil separation distance (for CASE 2 and CASE 4), where the same receive coil diameters of 0.1m, 0.2m, 0.5m and 1m, are considered.

Focusing on results for the 1 m diameter receive coil (with a coil separation of 0.5 m for CASE 2 and CASE 4 and an inner transmit coil diameter of 1.25 m for CASE 5) and a transmit coil height above ground of 2 m, we note that over all configurations the maximum signal amplitudes range from 1 – 5 nano-Volts and 0.5 – 2.5 ppm units. The actual values for the various cases are listed in Table 1 below. As is evident from equations (1) and (4), the nano-Volt results can be increased by increasing the parameters n_R , n_T and/or I_T , whereas the ppm unit results do not depend on these latter parameters. These results are for the response at 1 kHz and signals will be 1.5 times stronger at 150 Hz.

Sensor Configuration	nano-Volt	ppm
CASE 1	5.23	2.42
CASE 2	2.60	1.26
CASE 3	1.24	0.58
CASE 4	-1.41	-0.64
CASE 5	4.87	2.25

Table 1 – The maximum modeled signals (in nV and ppm) for a receive coil diameter of 1m when the transmit coil is 2m above ground.

It should be noted that the maximum signal for CASE 3 in Table 1 occurs when the horizontal position of the sensor relative to the object is 1.15m; for all other sensor configurations, the maximum signal occurs when the sensor is directly over the object. Recall that the signal strengths listed in Table 1 are for a sensor height above ground of 2m. The signal strengths as a function of sensor height above ground, with otherwise identical parameters, are presented in Figure 7 for all sensor configurations. CASE 1 generally represents the upper bound on signal strength, while CASE 3 generally represents the lower bound. CASE 2 and CASE 5 are examples of CASE 1 with passive PFN and active PFN, respectively, and are both generally less than CASE 1 in signal strength, as expected. As seen from Figure 8, however, for a coil separation choice of 1m instead of the 0.5m previously considered, signal strength performance for CASE 2 exceeds that of CASE 1 especially towards the lower end of the plot sensor height range.

The three paneled plot of Figure 9 shows the horizontal profiles of the transmit field Z-component for CASE 5 – in the plane of the sensor; 2m from the plane of the sensor; and 10m from the plane of the sensor. These demonstrate both the PFN at the receive coil and the asymptotic tendency of the far field reduction in signal strength due to the presence of the inner TX coil. Recall from (11) that,

$$loss = \frac{n_T^{Inner}}{n_T^{Outer}} \left(\frac{D_T^{Inner}}{D_T^{Outer}} \right)^2 = 0.305 \left(\frac{1.25}{3} \right)^2 = 0.053 \quad .$$

At 2m from the plane of the sensor the loss is at 9%, while at 10m from the plane of the sensor the loss is at 5.4%, which approaches the 5.3% value calculated above. By comparison, the loss for the case of the 2.75m diameter inner TX coil is 76.4% in the far field. This explains why the CASE 5 signal strengths for the 2.75m diameter inner TX coil case are much reduced, as seen in Figure 8.

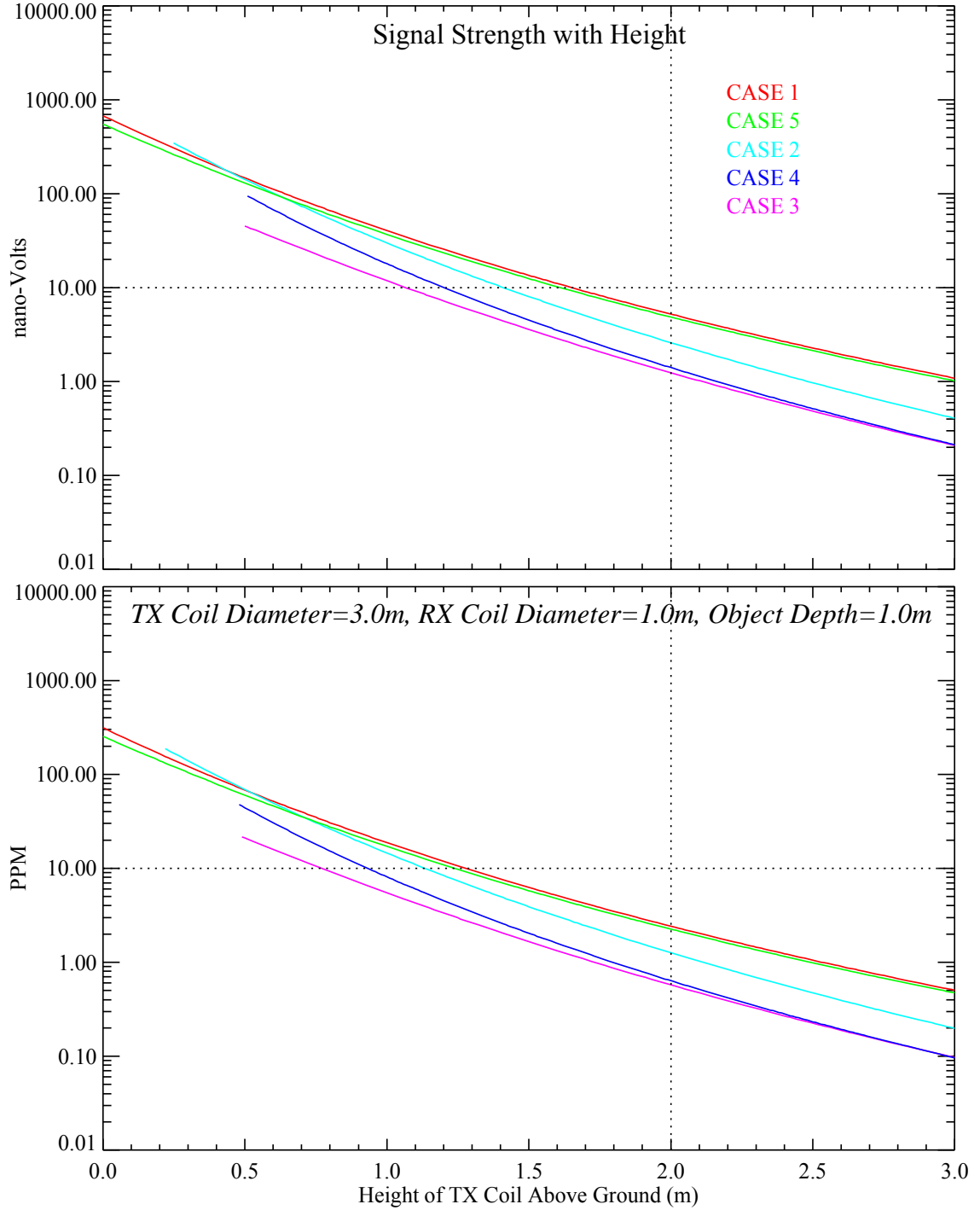


Figure 7. The signal strength for all the sensor configurations of Figure 2 as a function of sensor height above ground. For all cases, we have chosen $f=1\text{kHz}$, $n_R=1$, $n_T=1$, $I_T=1\text{Amp}$, a transmit coil diameter of 3m, an object at 1m depth with $\beta_1=\beta_2=\beta_3=0.005\text{m}^3$, a coil separation distance of 0.5m for the two gradient receive coil configurations (i.e. CASE 2 and CASE 4), and an inner transmit coil diameter of 1.25m for the GEM-3 style configuration (i.e. CASE 5).

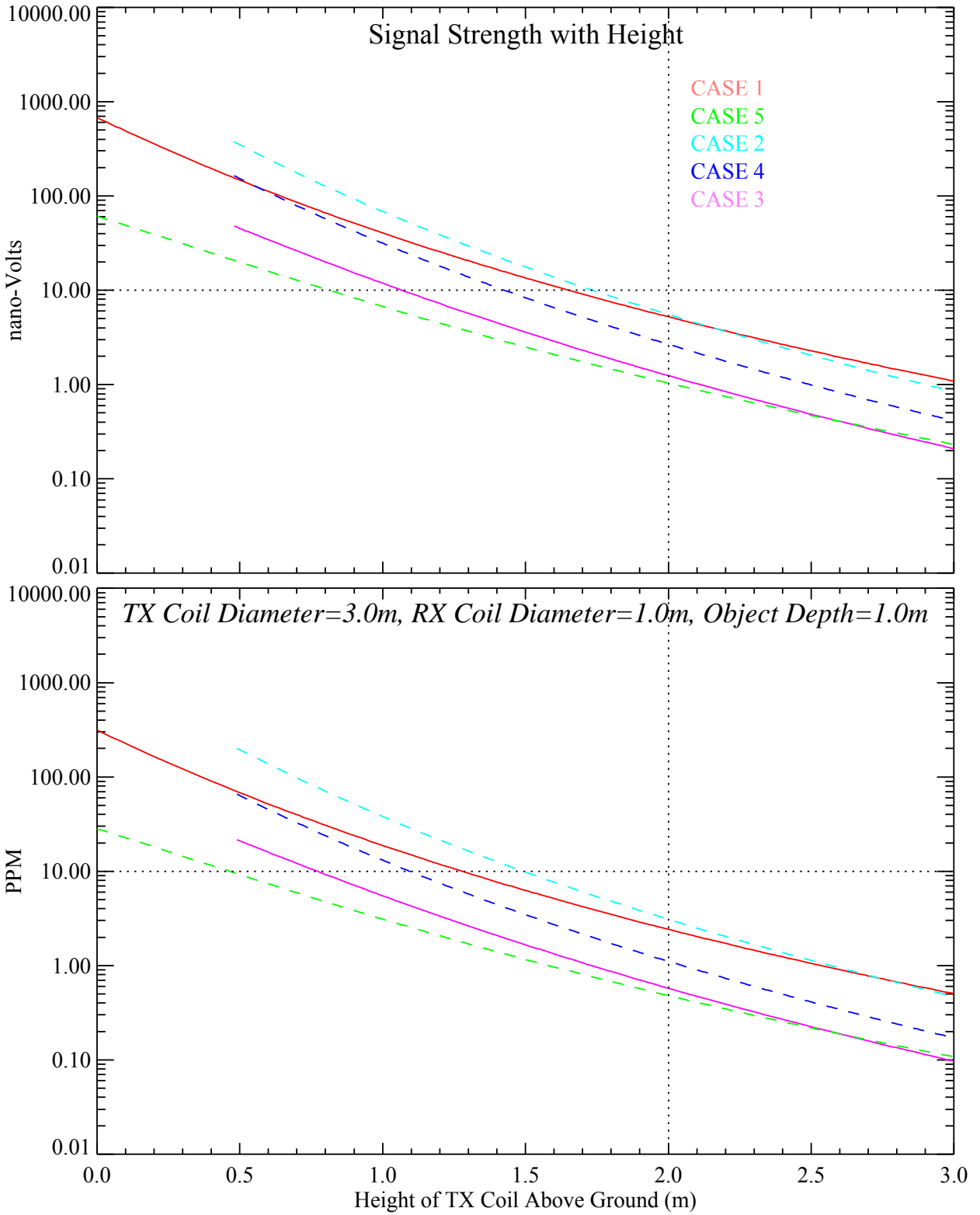


Figure 8. The “gradient” signal strength curves of CASE 2 and CASE 4 with an increased coil separation of 1.0m instead of 0.5m, and CASE 5 with an increased inner transmit coil diameter of 2.75m instead of 1.25m. CASE 1 and CASE 3 (non-gradient) are the same.

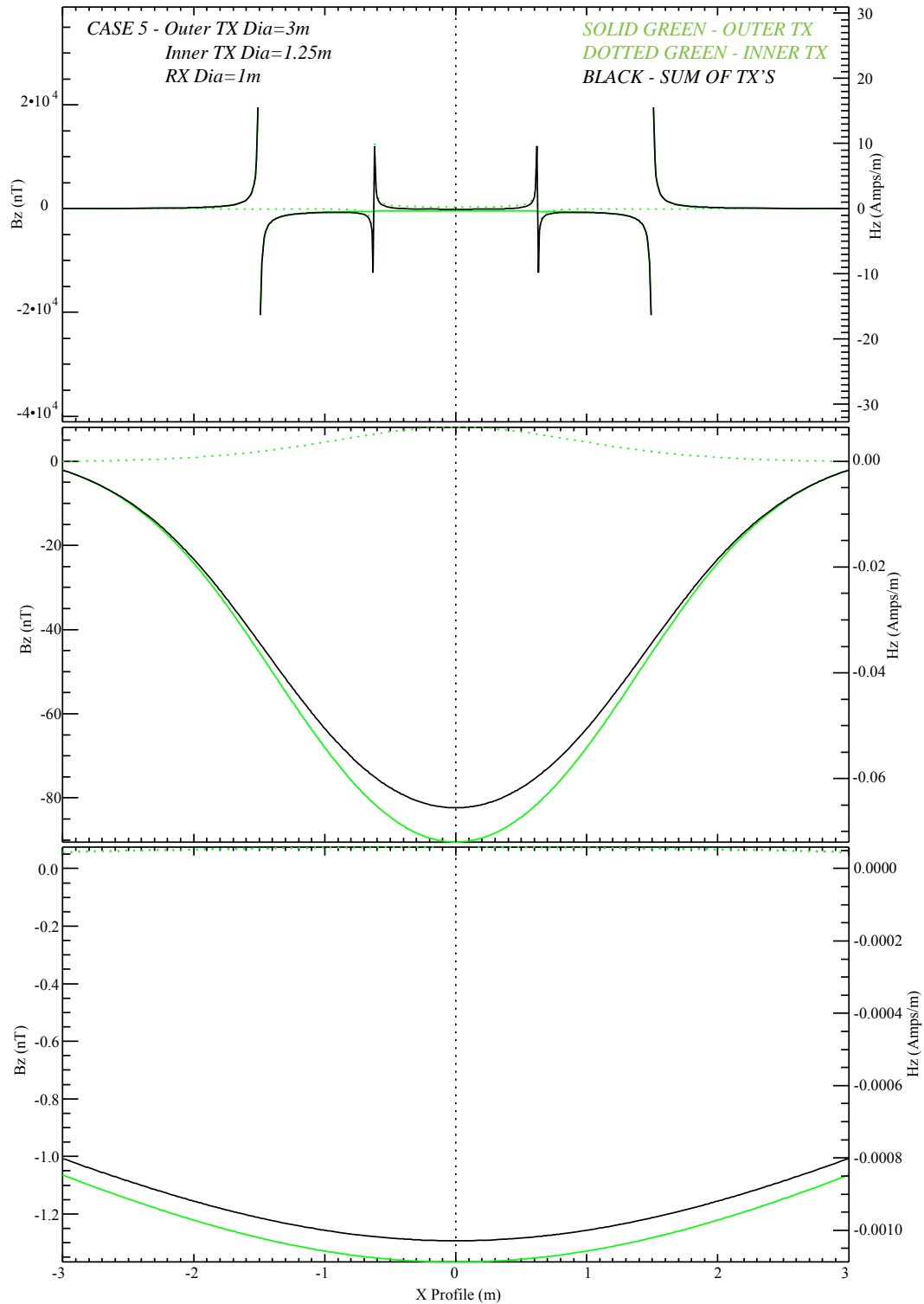


Figure 9. Horizontal profiles for the transmit field z-component for CASE 5 in the plane of the sensor (top panel); 2m from the plane of the sensor (center panel); and 10m from the plane of the sensor (bottom panel).

The measured voltage in the receive coil can be increased by changing a number of parameters: receive coil size, number of turns, transmit current, and transmit frequency. All of these changes result in a larger primary signal in the receive coil and no change in the relative signal strength in terms of PPM. Relative signal strength can be increased by changing the transmit coil size which both reduces the primary coupling to the receiver and increases the transmit field at the buried item. To significantly increase the field requires a very large change in coil diameter as can be seen from Figure 5. Table 2 and Figure 10 give the results for a 12 m diameter transmit coil combined with a 1 m receive coil. The results are, again, for an assumed object response of $\beta = 0.005 \text{ m}^3$ at 1 kHz and a 1.5 times larger response is expected at 150 Hz.

Sensor Configuration	3m dia. TX Coil (ppm)	12m dia. TX Coil (ppm)
CASE 1	2.42	20.19
CASE 2	1.26	10.06
CASE 3	0.58	8.24
CASE 4	-0.64	-5.43
CASE 5	2.25	20.02

Table 2 – The maximum modeled signals in ppm for a receive coil diameter of 1 m and a transmit coil of 12 m when the transmit coil is 2 m above ground.

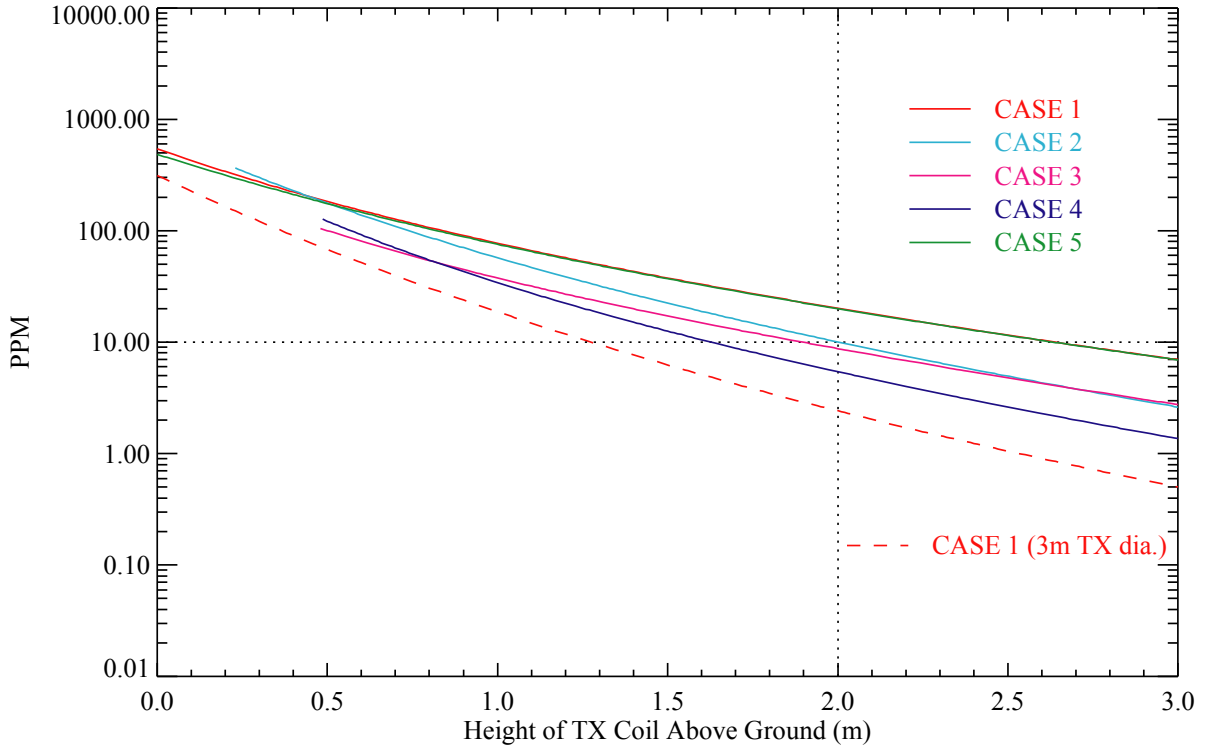


Figure 10. Signal strength as a function of height for a 12 m diameter transmit coil. All other parameters the same as Figure 7.

3.1.7 “Perturbation” Noise

Plots showing modeling results of the change in primary (i.e. transmit) field coupling due to perturbations are given in Appendix 1B. The specific perturbations that are considered were described in the previous section and illustrated in Figure 4, and are applied to the sensor configurations of Figure 3. In all cases, we have chosen a 3m diameter transmit coil, with a 0.5m coil separation for CASE 2 and CASE 4, and a 1.25m inner diameter transmit coil for CASE 5. Although explicitly absent from the plots, it should be noted that all curves tend to a zero change in primary field coupling when zero perturbations are applied.

Focusing on the results of the 1m diameter receive coil, the changes in primary field coupling (in nano-Volts and ppm units) due to very small perturbations (i.e. $dZ=1\text{mm}$, $dX=1\text{mm}$ and $\text{Pitch}=\frac{1}{2}^\circ$) are listed in Table 3.

Sensor Configuration		nano-Volt			ppm		
		dZ	dX	Pitch	dZ	dX	Pitch
CASE 1		-1.72	0.86	-82.24	-0.80	0.40	-38.077
CASE 2	Individually perturbed	784.06	0.65	-78.33	381.14	0.31	-38.08
	Jointly perturbed	1570.71	→0 (Z=1mm: 0.00303)	→0 (X=1mm: -26.20)	763.54	→0 (Z=1mm: 0.00147)	→0 (X=1mm: -12.74)
CASE 3		→0 (X=1mm: -1.72)	→0 (Z=1mm: -1.72)	18848.13	→0 (X=1mm: -0.80)	→0 (Z=1mm: -0.80)	8726.54
CASE 4	Individually perturbed	-461.75	→0 (Z=1mm: -2.12)	19334.10	-208.41	→0 (Z=1mm: -0.96)	8726.54
	Jointly perturbed	-923.51	→0 (Z=1mm: -0.0035)	→0 (X=1mm: 25.35)	-416.83	→0 (Z=1mm: -0.0016)	→0 (X=1mm: 11.44)
CASE 5	Receive coil perturbed	-39.16	19.59	-0.17	-18.13	9.07	-0.077
	Inner Transmit Coil perturbed	-40.88	20.45	-82.41	-18.93	9.47	-38.154

Table 3 – Results of the change in primary field coupling due to very small perturbations of dZ=1mm, dX=1mm and Pitch= $\frac{1}{2}^\circ$ for a 1m diameter receive coil and a 3m diameter transmit coil, with a 0.5m coil separation for CASE 2 and CASE 4, and a 1.25m inner diameter transmit coil for CASE 5.

Overall, the simple vertical, coaxial coils of CASE 1 and CASE 5 are the least sensitive to perturbations. The gradient and horizontal cases are all sensitive to at least one of the perturbations. Some of these perturbations could be reduced if the receive coil(s) were in a more uniform transmit field. Just as it increases signal strength, a very large diameter transmit coil reduces some of the perturbations. Table 4 compares perturbation noise in PPM between a 3 m and 12 m diameter transmit coil.

Sensor Configuration		3m dia. TX Coil (ppm)			12m dia. TX Coil (ppm)		
		dZ	dX	Pitch	dZ	dX	Pitch
CASE 1		-0.80	0.40	-38.077	-0.042	0.021	-38.077
CASE 2	Individually perturbed	381.14	0.31	-38.08	20.97	0.021	-38.077
	Jointly perturbed	763.54	→0	→0	42.03	→0	→0
CASE 3		→0	→0	8726.54	→0	→0	8726.54
CASE 4	Individually perturbed	-208.41	→0	8726.54	-10.55	→0	8726.54
	Jointly perturbed	-416.83	→0	→0	-21.09	→0	→0
CASE 5	Receive coil perturbed	-18.13	9.07	-0.077	-18.89	9.45	-0.077
	Inner Transmit Coil perturbed	-18.93	9.47	-38.154	-18.93	9.47	-38.154

Table 4 Comparison of perturbation sensitivity between 3 m and 12 m diameter transmit coils.

3.1.8 Ground Response

The soil model discussed in Section 3.1.5 is used to calculate ground signal strengths as a function of sensor frequency and sensor height above ground. The Case 1 coil configuration is applied with a receive coil diameter of 1.0 meter and transmit diameters of both 3 and 12 meters. The soil conductivity is set at a moderate level of 0.005 S/m. Three different ranges of the magnetic susceptibility are applied to the frequency dependent model with the time constants set to very low and high values to produce the linear dependency observed by others for the inphase soil response. These levels are $\chi_0 = 2.0, 20.0,$ and 200.0×10^{-4} in dimensionless SI units. The first value is reasonable for the benign, non-magnetic soils often found at eastern test sites. The second value is typical of numbers reported for western magnetic soils and the third is representative of some extreme values reported at some spots like Kaho’lawe in Hawaii [West, 2009, Simms et al., 2004, Pasion, 2002].

As a function of frequency, Figure 11 plots the response from the ground at a 2.0 meter height for the 3 (left plots) and 12 (right plots) meter TX diameters. The three curves are for the three levels of susceptibility (black-low, green-moderate, and red-high). The top plots are the inphase response and the bottom plots quadrature. The inphase response shows the log-linear trend with frequency out to 10 kHz (due to susceptibility) and then curves up in response to conductivity at high frequencies. The quadrature response has a small offset due to the complex susceptibility at low frequencies and then curves rapidly up in response to soil conductivity. The lowest amplitude soil response is at low quadrature frequencies. The two vertical dashed lines indicate the frequencies of interest at 150 Hz and 1000 Hz for a helicopter based system.

Figure 12 plots the ground response as a function of height for the two frequencies of interest (150 Hz – solid, 1000 Hz – dashed). Figure 13 plots the gradient of the ground response in ppm/cm for the two frequencies. The three colors again indicate the three levels of magnetic susceptibility. The top plots are inphase and the bottom quadrature. The left plots are for a 3 meter TX diameter and the right ones are 12 meter diameter. Table 5 presents a synopsis of these results for the coil height of interest, 2 meters above the ground.

As the helicopter flies over the ground, the coil to ground height will vary and produce changing sensor output from the ground. This ground “noise” has the potential to hide signals from UXO of equal or lesser amplitude. The ground signal gradients in Figure 13 can be used to calculate the level of noise for a given level of height variation over the scale length of a UXO signal. As a reasonable estimate, we will assume 25 cm height variations. Figure 14 plots the signal strengths as a function of height in the top two plots for the two transmit coil diameters. The large UXO, quadrature response parameters of $\beta = 0.0075$ and 0.005 m^3 at the frequencies of 150 Hz (solid) and 1 kHz (dashed) have been used. At 2 meters above ground, the two coil sizes produce signals on the order of several ppm and several tens of ppm. The lower plots divide this signal strength by the estimated ground noise to graph the signal-to-noise ratio (SNR) for a large UXO item relative to

possible ground noise. The solid and dashed curves indicate low and high frequencies and the three colors indicate increasing levels of soil magnetic susceptibility (black – 2×10^{-4} , green – 20×10^{-4} , and red – 200×10^{-4}). The SNR levels at 1 kHz are significantly lower due to ground response from soil conductivity. At 150 Hz, the 3 m transmit coil has SNR levels greater than 4 at the weak and moderate magnetic soil levels and less than 1 in the strongly magnetic soil. The height dependency of the SNR is relatively flat for the 3 m coil because both the signal and the ground gradient are falling off at similar rates. The 12 m coil case has a relatively flat gradient response to soil and the SNR falls off with height. The signal levels, however, are sufficiently stronger for this case that the SNR levels stay above 3 for the weak and moderate magnetic soils. The strongly magnetic case exceeds an SNR of 1 for heights below 1.75 m.

It is worth noting that the quadrature component of the ground response, which at low frequencies arises primarily from frequency-dependent susceptibility (FDS) effects, is probably overstated by some of the assumptions made in this analysis. First, while FDS is a well-known effect, it is not simply correlated with DC soil susceptibility. FDS appears to be strongly correlated with local precipitation during weathering of iron-bearing rocks, and is typically weak or not present in relatively unweathered rocks and in many arid areas. Second, the fine-grained magnetite responsible for FDS is often concentrated near the top of the soil profile. Thus, modeling a soil layer with FDS as a halfspace should strongly overestimate the effect of FDS on airborne EM measurements made over the soil layer.

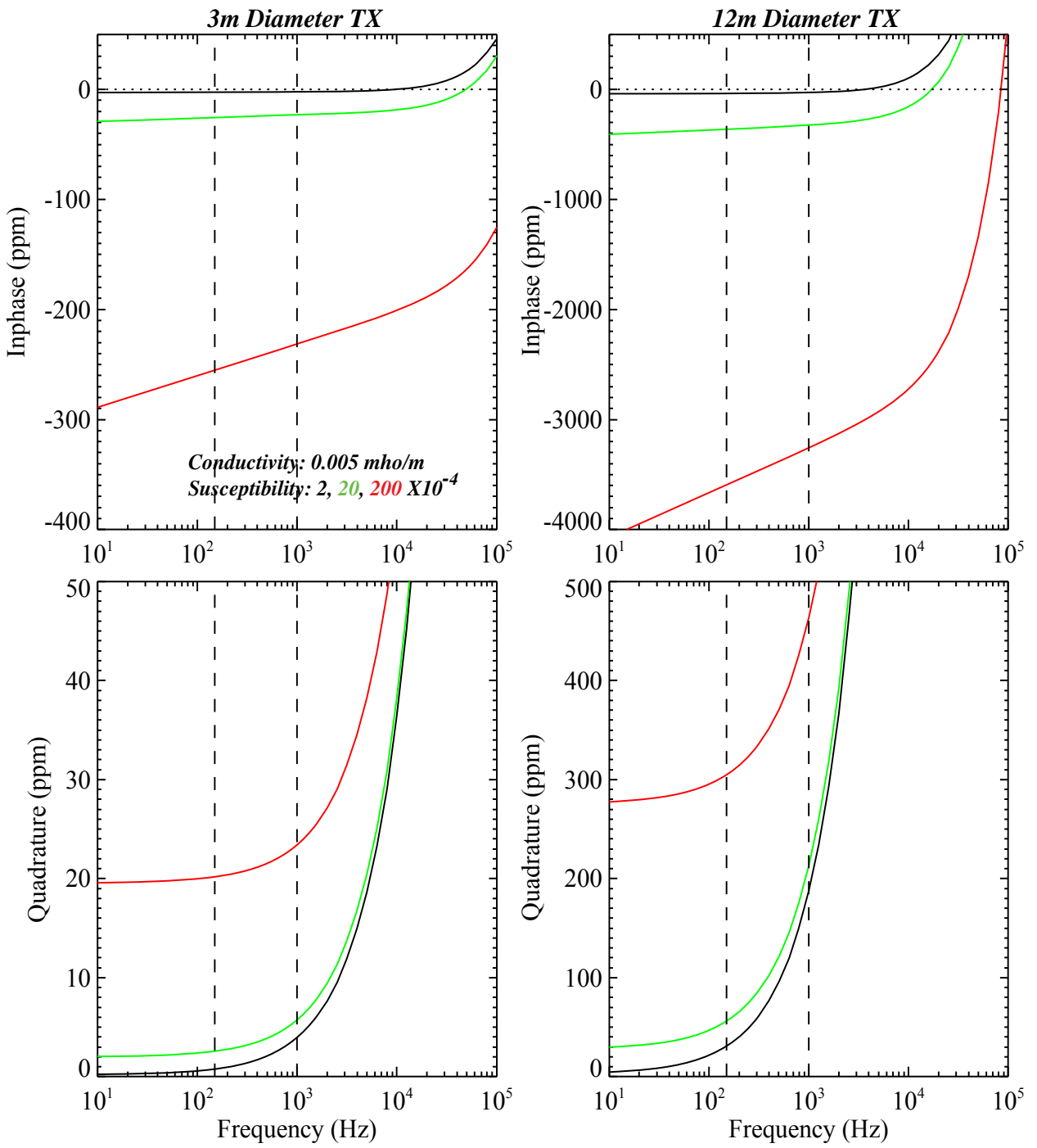


Figure 11. Ground response as a function of frequency for three levels of magnetic susceptibility.

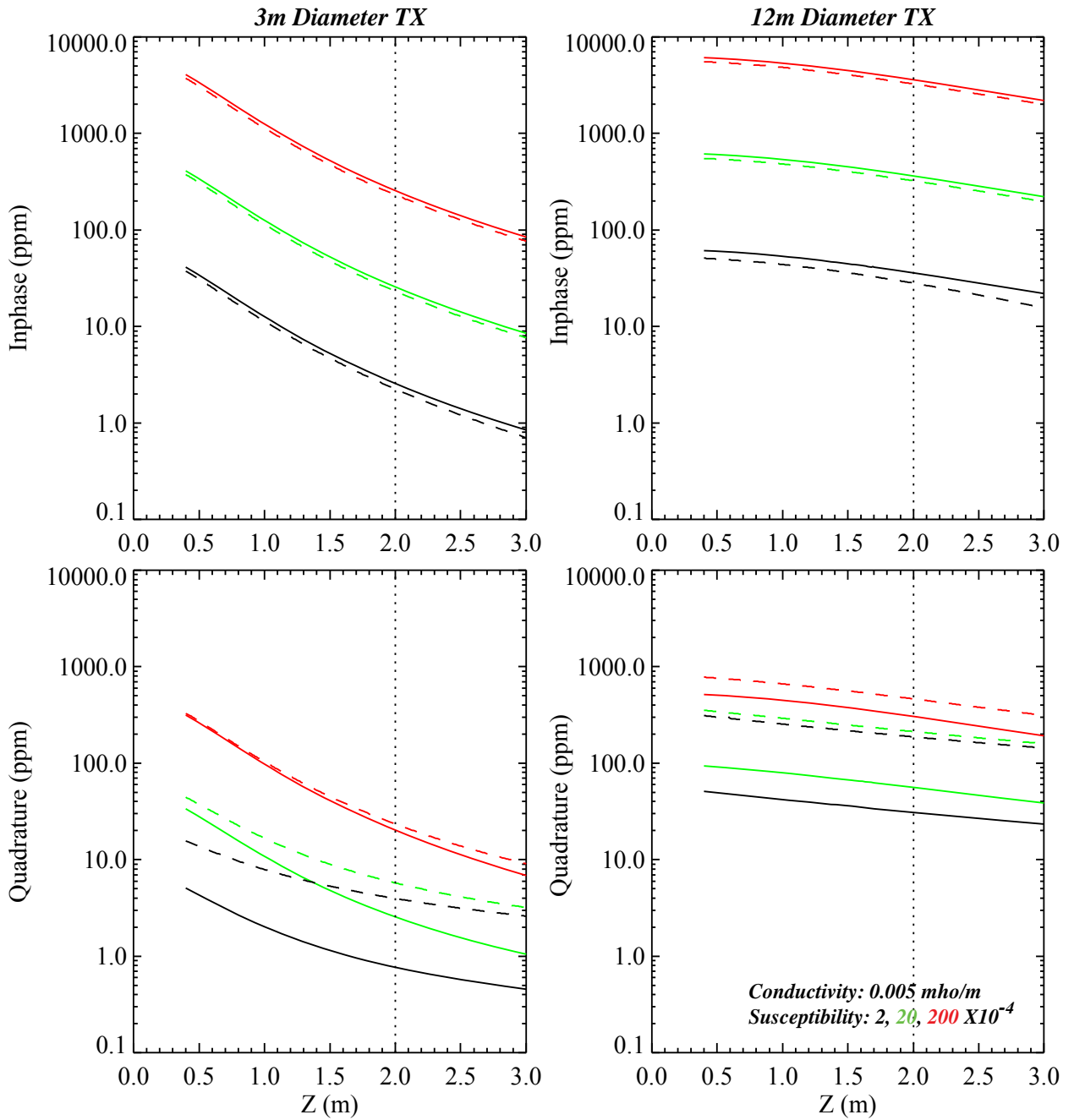


Figure 12. Ground response as a function of height at two frequencies (150 Hz – solid, 1 kHz – dashed) for three levels of magnetic susceptibility.

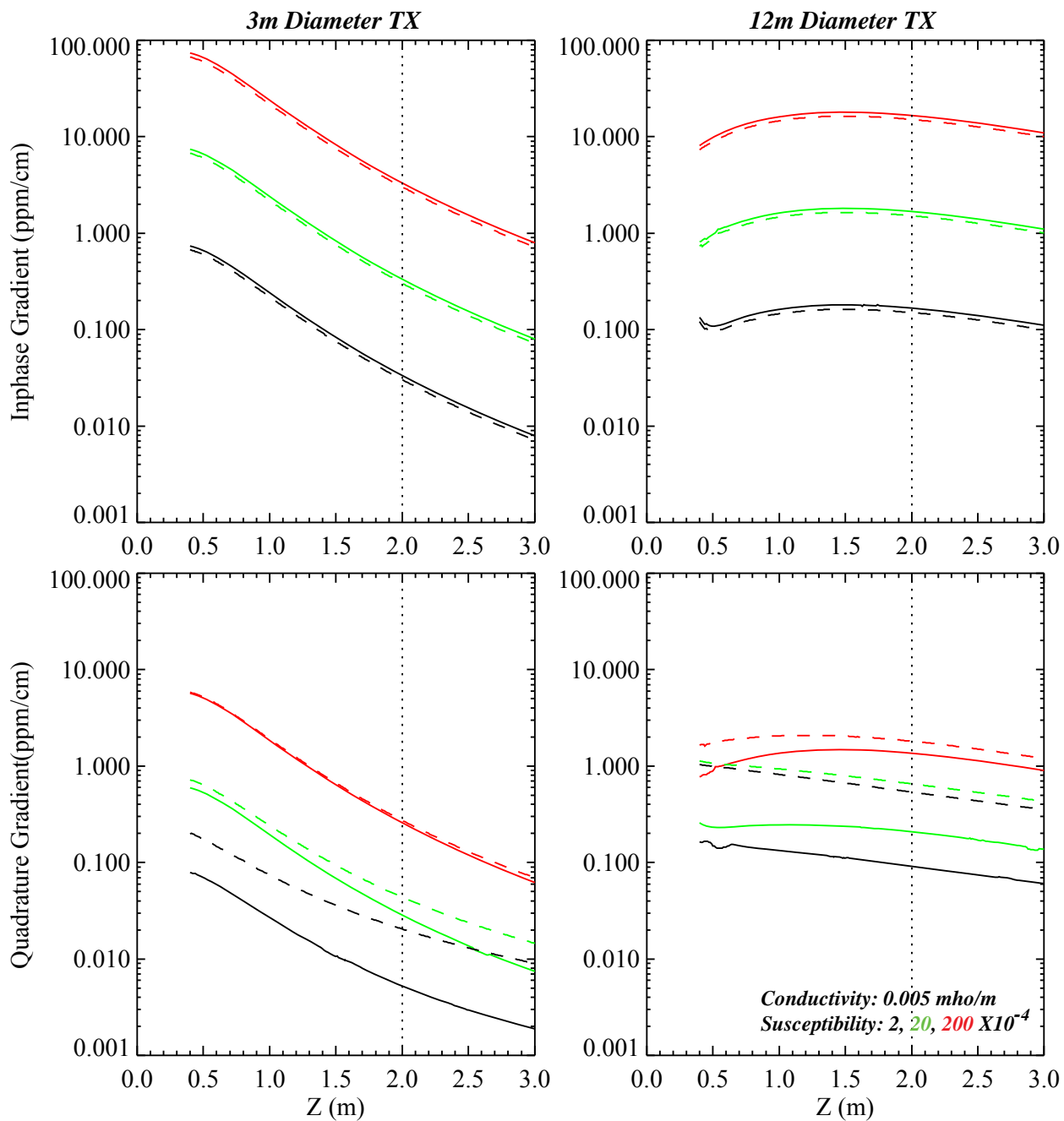


Figure 13. Gradient of the ground response as a function of height at two frequencies (150 Hz – solid, 1 kHz – dashed) for three levels of magnetic susceptibility.

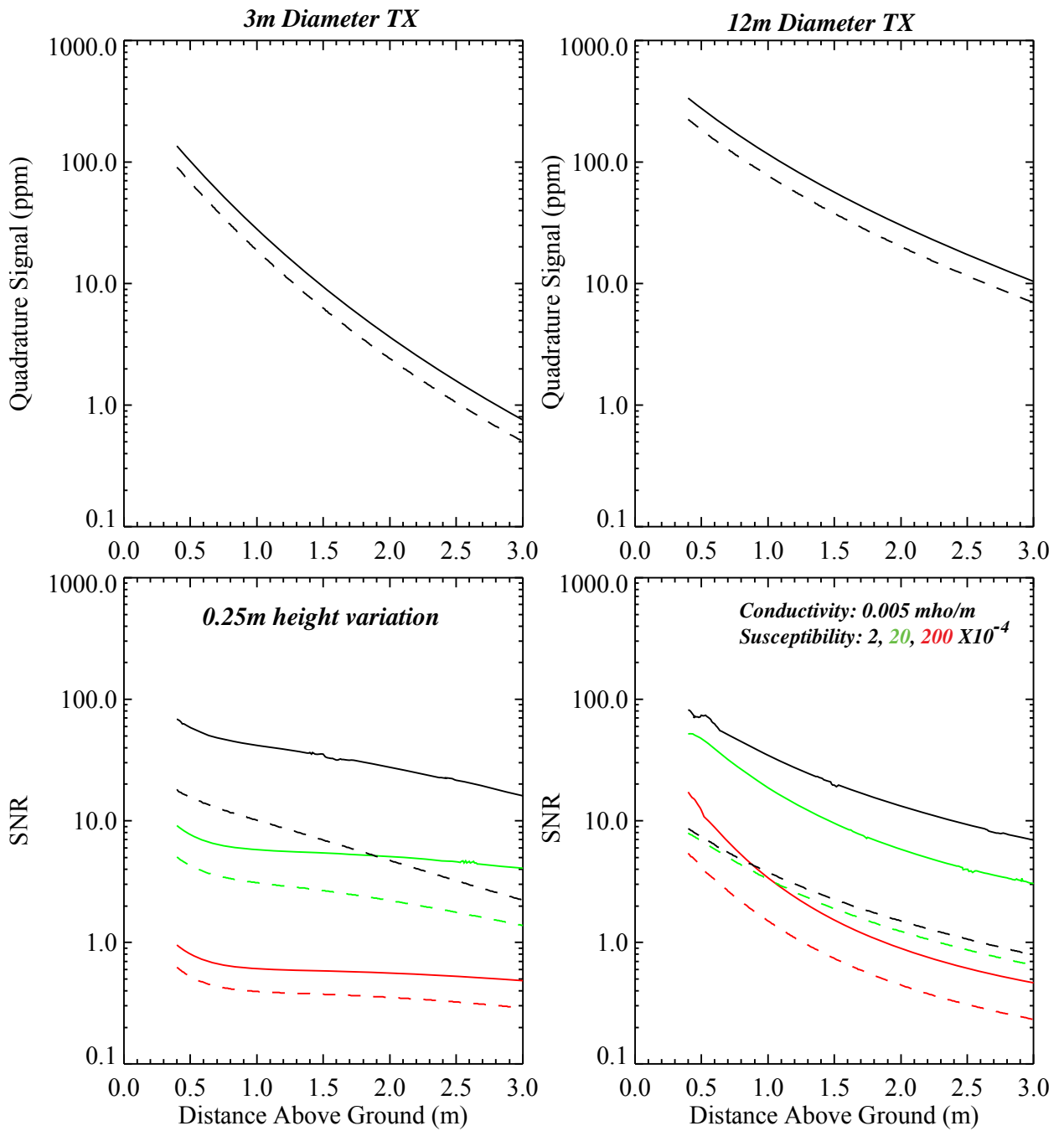


Figure 14. Signal strength from standard object as a function of height (top plots) and resulting signal-to-noise ratio for 25 cm height variations over ground with three levels of magnetic susceptibility.

$\chi = 2 \times 10^{-4}$	3m (ppm)	12m (ppm)	3m (ppm/cm)	12m (ppm/cm)
Inphase (150 Hz)	-2.5625695	-35.888121	0.03349055	0.1674826
Inphase (1000 Hz)	-2.2570161	-28.148385	0.030325175	0.15034473
Quadrature (150 Hz)	0.76928662	30.944977	-0.005272324	-0.091751686
Quadrature (1000 Hz)	3.9656354	187.32538	-0.020473988	-0.53795426
$\chi = 20 \times 10^{-4}$	3m (ppm)	12m (ppm)	3m (ppm/cm)	12m (ppm/cm)
Inphase (150 Hz)	-25.646514	-361.26678	0.33472237	1.6742343
Inphase (1000 Hz)	-23.195557	-323.13941	0.30346686	1.5166468
Quadrature (150 Hz)	2.5544995	56.11298	-0.028546598	-0.20823275
Quadrature (1000 Hz)	5.7530436	212.65456	-0.043766664	-0.6547364
$\chi = 200 \times 10^{-4}$	3m (ppm)	12m (ppm)	3m (ppm/cm)	12m (ppm/cm)
Inphase (150 Hz)	-255.0627	-3594.9416	3.3284711	16.650356
Inphase (1000 Hz)	-231.32493	-3256.6005	3.0194416	15.101518
Quadrature (150 Hz)	20.173468	304.6718	-0.25841082	-1.3587487
Quadrature (1000 Hz)	23.42687	463.09728	-0.27408098	-1.8113887

Table 5 - Ground response signal strength (ppm) and signal gradient (ppm/cm) at a TX coil height of 2 meters over the ground.

3.1.9 Passive Noise Level Determination

In order to get a representative measure of the expected passive noise level which the modeling results can be compared against, we draw on segments of induced voltage data collected passively (i.e. with transmitters turned off) at a sampling rate of 10.8kHz in two of the TEM-8 receive coils during a straight section of flight. The top panel of Figure 15 shows the data segments for the innermost (black) and outermost (red) receive coils, relative to the helicopter, scaled to units of nano-Volts over single-turn 1m diameter receive coils. The bottom panel of Figure 15 shows a close up of the first tenth of a second of the data, and clearly reveals the influence of the terrestrial 60Hz power lines on the signals.

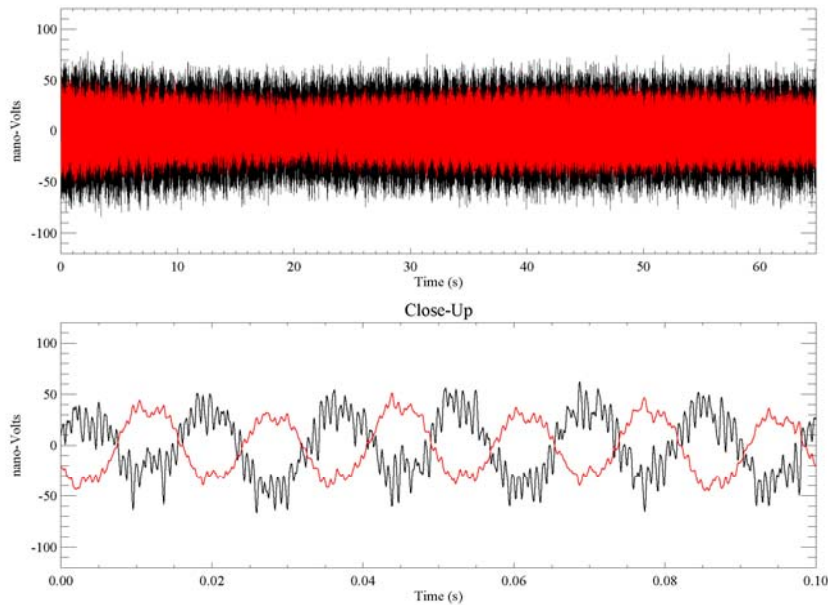


Figure 15. Voltages induced during a straight section of flight in the innermost (black) and outermost (red) of the TEM-8 receive coils, when the transmitter is turned off and the sensor is in the passive mode. The top panel shows the entire data segments collected at a sampling rate of 10.8kHz, while the bottom panel shows a close up.

The top panels of Figure 16 and Figure 17 show the power spectra of the passive signals of Figure 15 with, respectively, logarithmic and linear frequency scales. Clearly an abundance of narrow lines and broad peaks exist in the spectra. These occur from a multitude of sources – from terrestrial power lines, to helicopter sources (blades, rotor, generator, electronics, etc), to mechanical vibrations of the receive coil, as well as other unknown sources. The harmonics of the 60Hz power sources are all slightly smaller in amplitude in the outermost receive coil than in the innermost receive coil. Note, however, that the dominant odd harmonics are percentage-wise very nearly the same in both receive coils, suggesting the possibility of removing the influence of terrestrial power lines by differencing the channels.

Since we are ultimately interested in obtaining FDEM in-phase and quadrature noise level estimates from the data of Figure 15, it will be necessary to convolve these data with sines and cosines of the operating transmit frequency over an appropriate base period. The shortest choice in base period that will minimize the 60Hz power source noise is 1/30th of a second. With this choice in base period, the allowable transmit frequency (i.e. the frequency such that the transmit waveform starts and ends at zero) is any multiple of 30Hz. However, to avoid 60Hz and any harmonic, the obvious choice in transmit frequency has to be any *odd* multiple of 30Hz. The dotted vertical lines on the spectra represent all the possible odd multiples of 30 Hz ranging from 210Hz to 2250Hz.

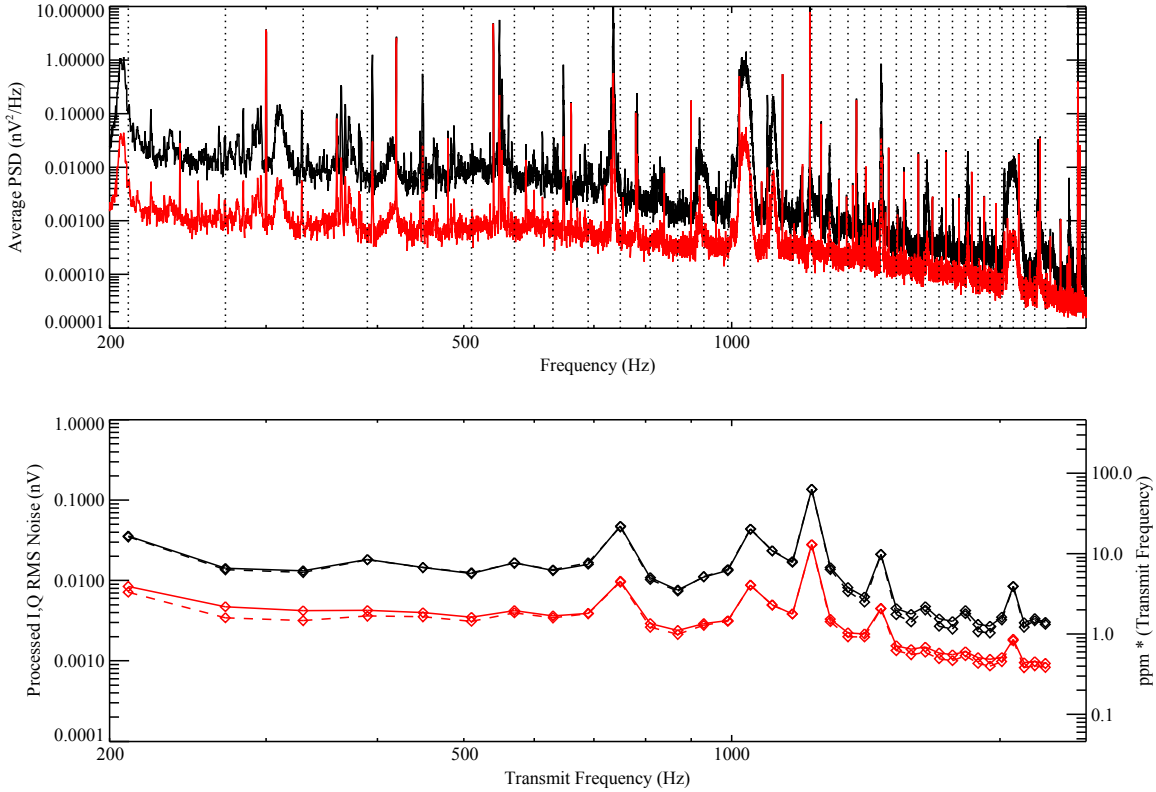


Figure 16. The top panel shows the power spectra of the innermost (black) and outermost (red) receive coil data of Figure 15. The vertical dotted lines represent all frequencies of odd multiples of 30Hz ranging from 210Hz on the left end to 2250Hz on the right end. The bottom panel shows a plot of the RMS values of the processed in-phase (solid) and quadrature (dashed) signals for transmit frequencies of odd multiples of 30Hz ranging from 210Hz to 2250Hz.

The bottom panels of Figure 16 and Figure 17 plot the RMS noise of the processed in-phase and quadrature signals for transmit frequencies of odd multiples of 30 Hz ranging from 210Hz to 2250Hz. Again, Figure 16 has a logarithmic transmit frequency scale while Figure 17 has a linear one. Despite the multitude of lines in the spectra, there are some operating transmit frequencies where quieter signals can be found. Indeed, two of the quieter operating frequencies close to 1kHz are 870Hz and 1590Hz. Reading from the plot, at 870Hz the quadrature RMS noise is 0.0074nV and 0.0039ppm for the innermost coil and 0.0021nV and 0.0011ppm for the outermost coil, while at 1590Hz the quadrature RMS noise is 0.0030nV and 0.0009ppm for the innermost coil and 0.0012nV and 0.0003ppm for the outermost coil.

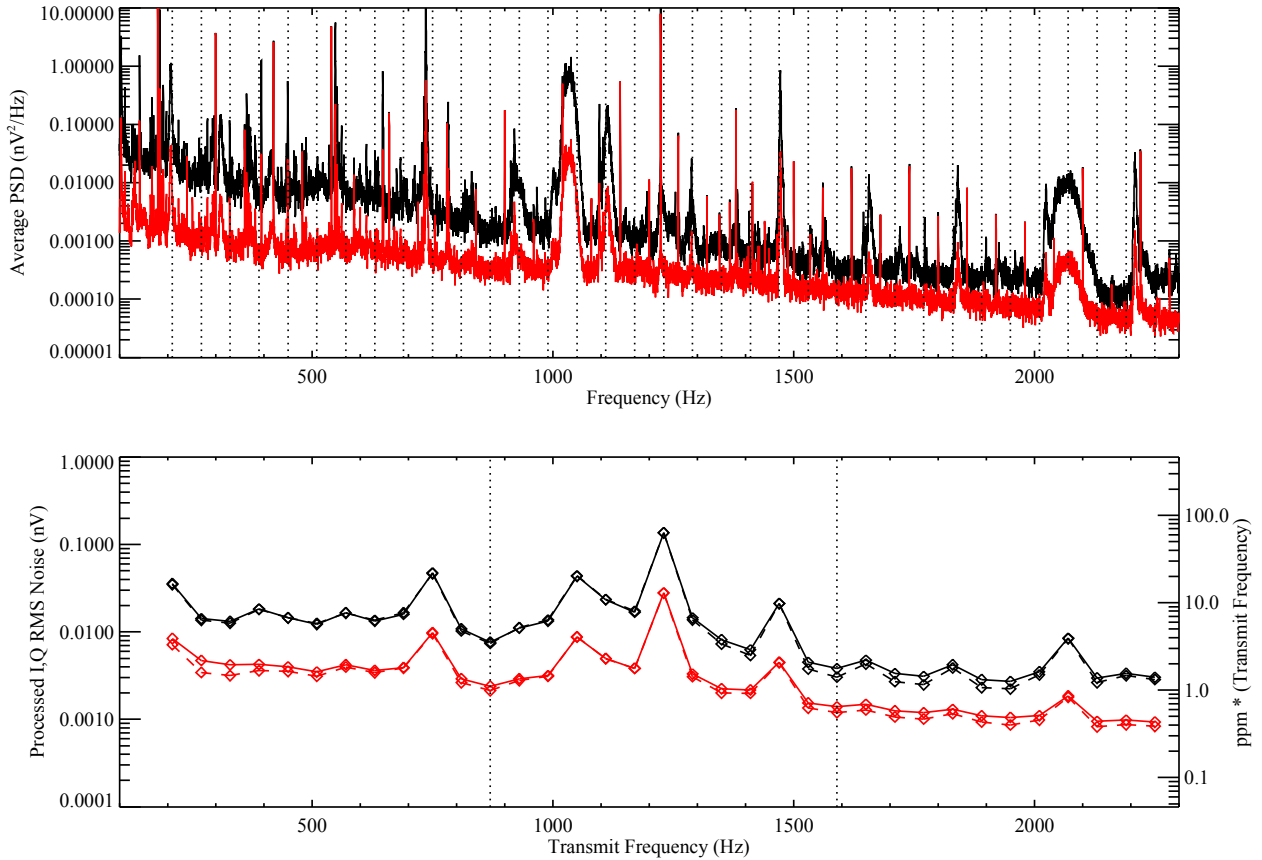


Figure 17. Identical plots to Figure 16, but with linear rather than logarithmic abscissa scales.

Reading off the PSD for 225 Hz in Fig. 17, top panel gives $0.001 \text{ nV}^2/\text{Hz}$. Integrating for $\pm 15 \text{ Hz}$ around this frequency to match the nominal 30 Hz output bandwidth gives 0.03 nV^2 . A slightly higher noise level would be observed at 150 Hz . Taking the square root, picking off the $\text{ppm} \cdot \text{frequency}$ value of 430 ppm-Hz per nV from the lower panel of this figure and dividing by 225 Hz gives $0.17 \text{ nV} \cdot 430 / 225 = 0.33 \text{ ppm}$ RMS noise.

Figures 18 and 19 are the same sets of spectra on logarithmic and linear scales. The top plots are the spectra for the measured passive voltage with the outer receiver plotted in red and the inner in black. The bottom two plots are spectra from processing this voltage into inphase and quadrature signals at two different frequencies, 870 and 1590 Hz . A time series was created by convolving the passive voltage with the sine and cosine of the “transmit” frequencies over a sliding $1/30^{\text{th}}$ of a second window. This window was slid in steps of $1/300^{\text{th}}$ of a second. The solid curves are inphase and the dashed curves quadrature. The quadrature output is relatively insensitive to low frequency passive noise, $< 10 \text{ Hz}$. At higher frequencies, inphase and quadrature output are comparable.

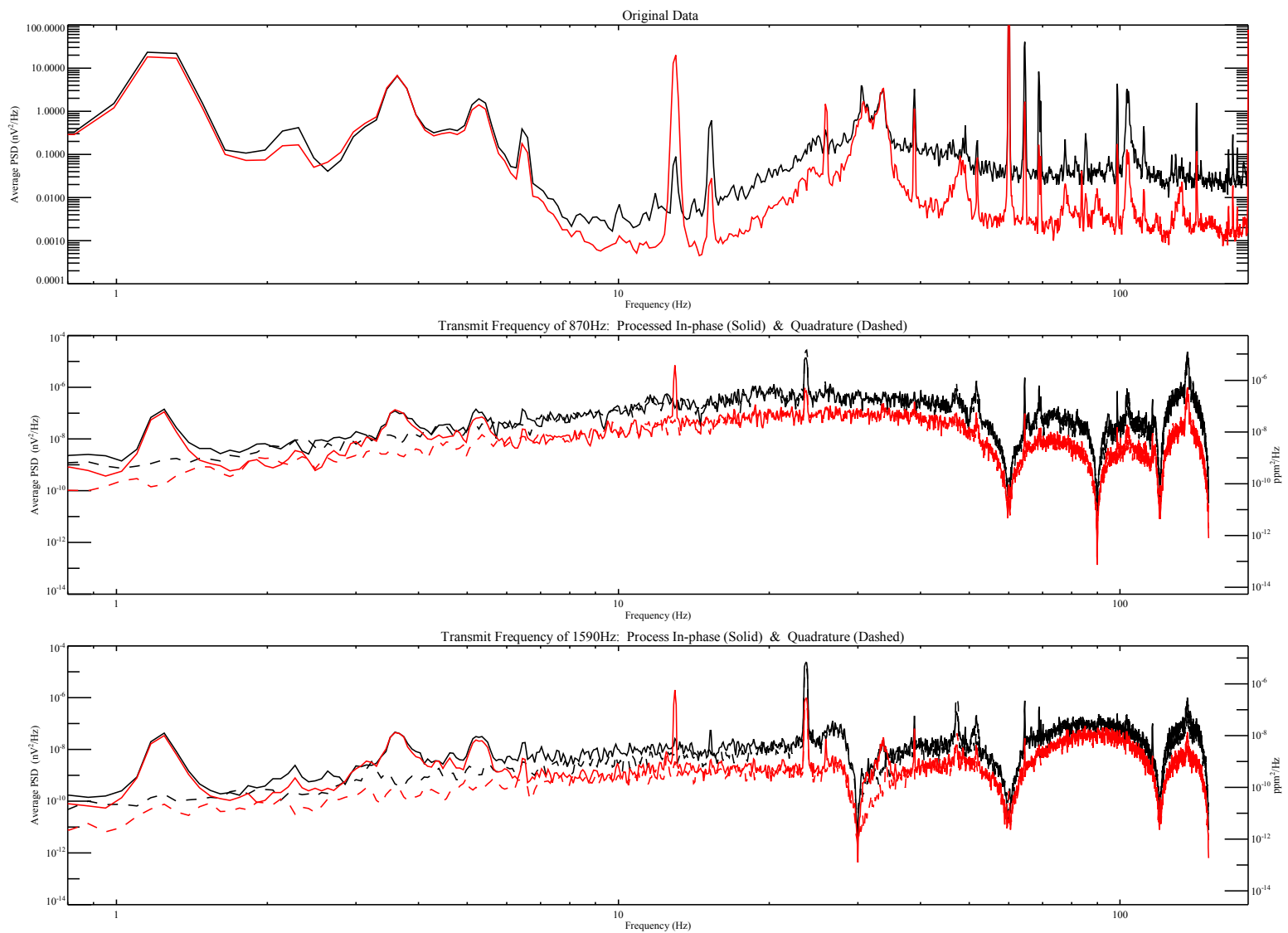


Figure 18. Spectra of passive voltage (top) and processed I,Q at 870 Hz and 1590 Hz.

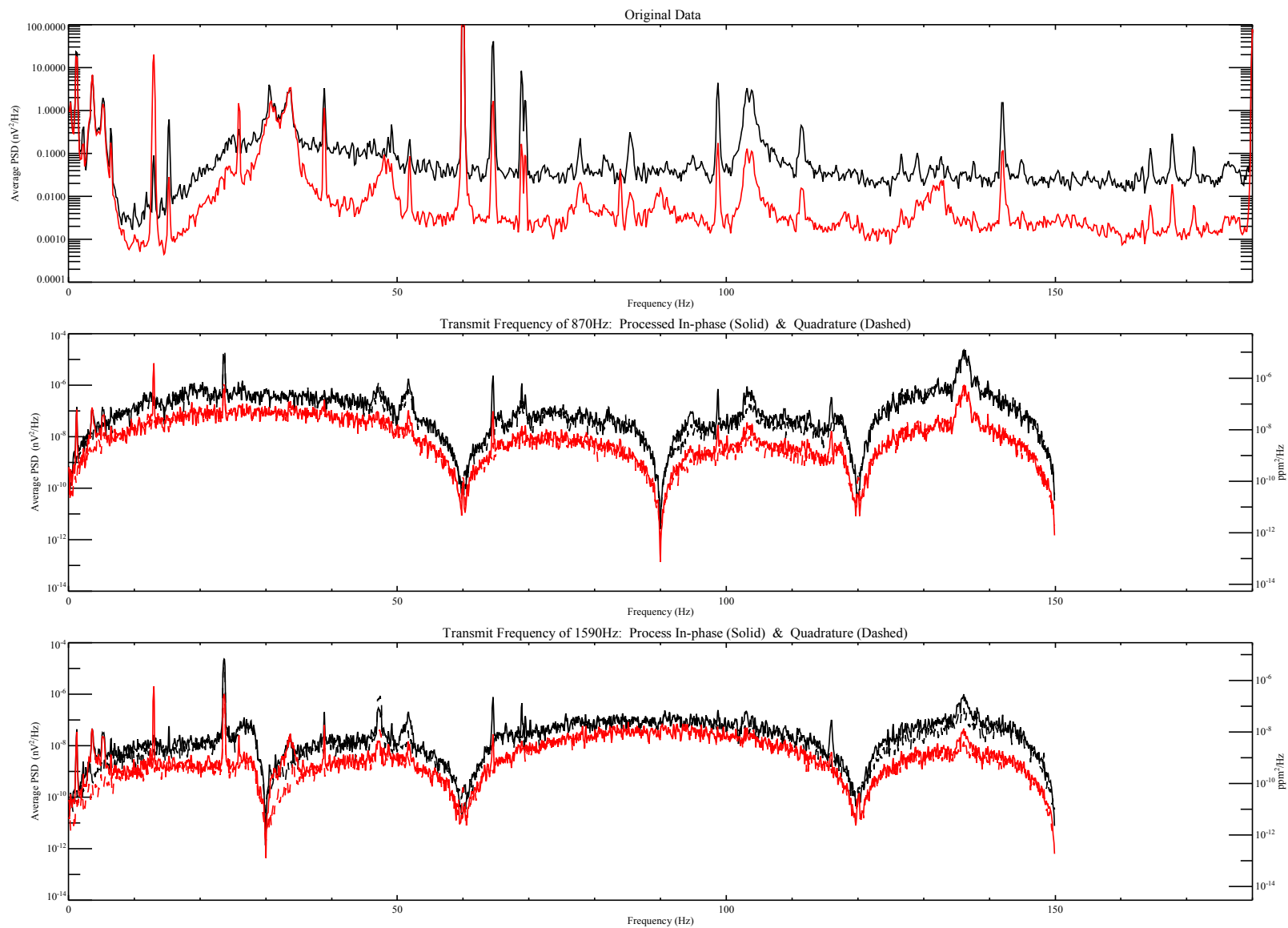


Figure 19. Same as Figure 18, but with linear frequency scale.

3.1.10 Comparison to Time Domain

3.1.10.1 Signal Strength Comparison to Time Domain

Given the transmit current as a function of time, equations (1), (3), and (4) can be modified to calculate the secondary and primary voltages induced in a receive coil for a time domain system. Instead of the $i\omega$ terms in the frequency domain case, one would have the time derivative of the transmit current. For purposes of comparison, we will take a reasonable representation of the current pulse of the TEM-8 helicopter system at a 150 Hz repetition rate and compare it to the frequency domain response at 150 Hz and 1 kHz. The simple, coaxial configuration of CASE 1 will be used with a transmit diameter of 3 m and receive diameter of 1 m. The time decay voltage will be averaged over the TEM-8 time gates. Figure 20 plots the waveform and gates of a 150 Hz, bipolar TEM-8 pulse.

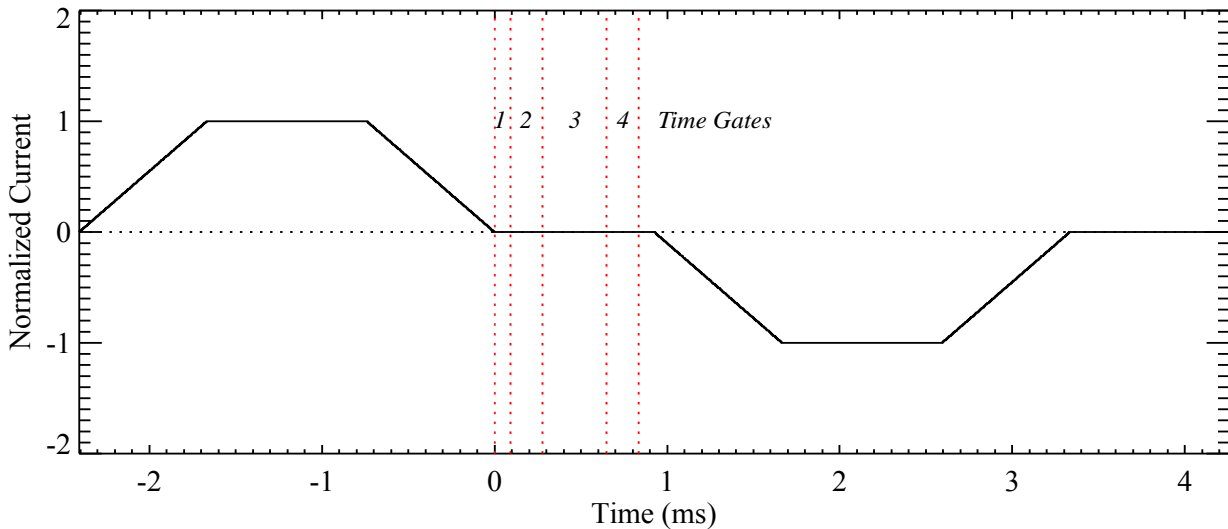


Figure 20. Transmit waveform and time gates of TEM-8 with 150 Hz repetition rate.

In the frequency domain, the transmit current is always on, and the measured signal is usually expressed as the ratio of receive voltage induced from the object to the direct voltage induced from the transmit coil. The ratio is expressed in parts-per-million or ppm. In the time domain, the voltage induced in the receive coil directly from the transmit coil is the time derivative of the transmit pulse and the transmit pulse is off during the receive coil measurement. The largest direct voltage is during the pulse cut-off and can be approximated as a linear ramp. By convention, the time domain signal can be normalized by this voltage and can be expressed in ppm as well. For the TEM-8, this cut-off is on the order of 0.74 milliseconds.

For a given transmit pulse, the magnetic polarizations, $\beta(t)$, would have to be measured or calculated. An analytic solution exists for the response of a conducting permeable sphere to a step response, but a general analytic expression does not exist for general shapes and arbitrary transmit pulses. Numerically, $\beta(t)$ can be calculated by FFT'ing the transmit pulse into the

frequency domain, convolving it with $\beta(\omega)$, and FFT'ing back into the time domain. The time derivative of this would be used in equation (1) to give the receive voltage as a function of time. The frequency domain sphere response, $\beta(\omega)$, can be expressed analytically [Grant and West, 1965] and convolved numerically with the TEM-8 pulse. As an approximation to a 105mm/155mm ordnance item, we have selected an equivalent sphere that closely matches the measured frequency domain polarizations of these ordnance items in the frequency range of 100 to 1000 Hz. The sphere parameters are: 0.25 m diameter, 0.7×10^7 S/m conductivity, and a relative magnetic permeability of 100. The inphase (dashed) and quadrature (solid) components of this sphere's polarization response is plotted in Figure 21 (black curves) and compared to the measured responses of large ordnance (red, green, and blue curves). In particular, it is a close match to a horizontal 155 mm in this frequency range. At the frequencies of 150 Hz and 1 kHz, it is very close to the quadrature responses already used of 0.0075 and 0.005 m³ (plotted as black diamonds in Figure 21).

On close comparison between the frequency domain and time domain expressions for the signal strength in ppm (equation 4), most of the equation is identical in terms of the geometry factors of the transmit and receive coils (size, shape, and relative placement). The FFT convolution, time derivative, and normalization by the linear ramp can all be wrapped into one term and expressed as a time domain equivalent, $\beta_{eq}(t)$, and compared directly to the frequency domain, $\beta(\omega)$. Given the same set of transmit/receive coils, the ppm signal strengths will be equal if $\beta_{eq}(t)$ equals $\beta(\omega)$. Figure 22 plots $\beta_{eq}(t)$ for our comparison sphere parameters and the TEM-8 150 Hz transmit pulse. The red lines indicate the TEM-8 time gates and the symbols indicate the response at the mid-point of the gates. Table 6 compares the response terms between frequency and time domain. The time domain terms are given both as an average across the time gates and as the value at the midpoint (terms in parentheses). The frequency domain responses are comparable in amplitude to the second time gate of the 150 Hz TEM-8 waveform.

	Frequency Domain (Quadrature)		Time Domain – 150 Hz Waveform			
	150Hz	1kHz	Gate 1	Gate 2	Gate 3	Gate 4
$\beta(m^3)$	0.0075	0.005	0.0101 (0.0097)	0.0060 (0.0058)	0.0033 (0.0032)	0.0021 (0.0021)

Table 6. Comparison of frequency domain and time domain β response terms.

Figure 23 plots the signal strength as a function of coil height above ground. The plots are for the CASE 1, coaxial configuration with a transmit diameter of 3 m and a receive diameter of 1 m. The comparison sphere is buried one meter below the surface. The frequency domain results at 150 Hz (dotted) and 1000 Hz (dashed) are shown for comparison. At a coil height of 2 m, the signal strengths are in the 1-5 ppm range for the four time gates and the frequency domain responses are comparable to the second time gate as expected from the β comparison in Table 6. The top plot is the measured voltage in the receive coil. This voltage is a function of transmit frequency and the response is greater at 1000 Hz than at 150 Hz or the time gates. This effect

normalizes out when compared to the primary voltage induced in the receive coil from the transmit coil.

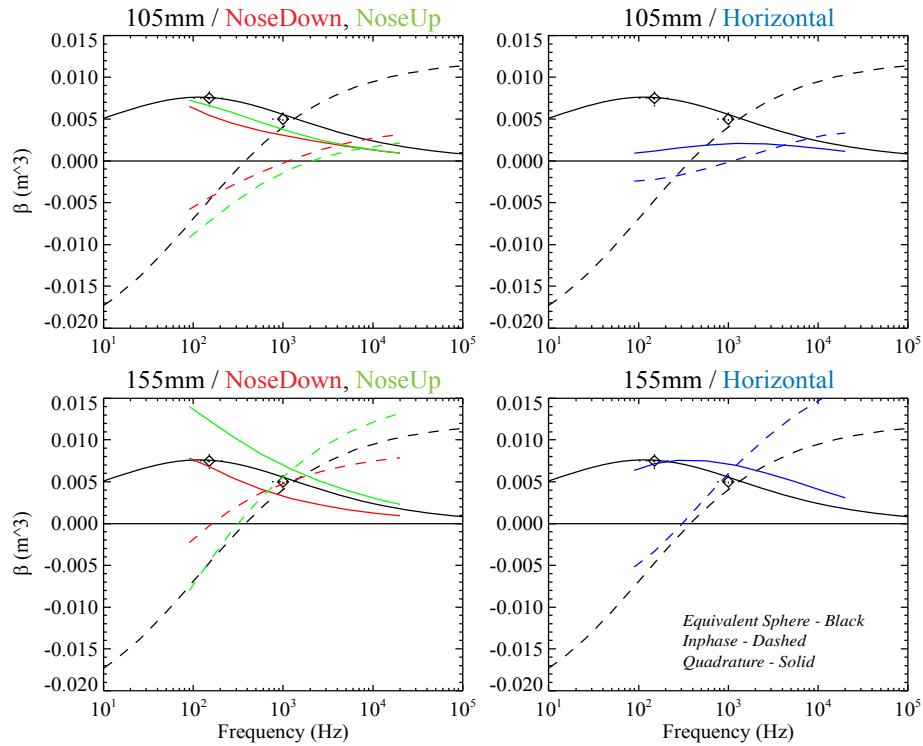


Figure 21. Frequency domain response of comparison sphere (black curves) compared to large ordnance at various orientations (red, green, and blue curves).

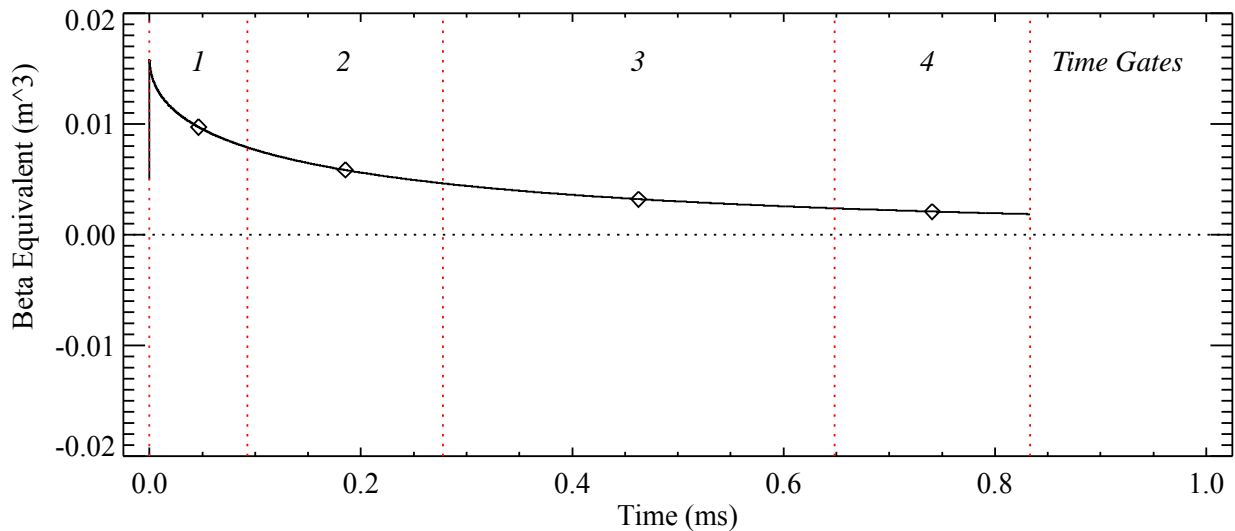


Figure 22. Equivalent β response term of comparison sphere as a function of time for 150 Hz waveform. Symbols indicate values at time gate midpoints. Red lines indicate starts and stops of four time gates.

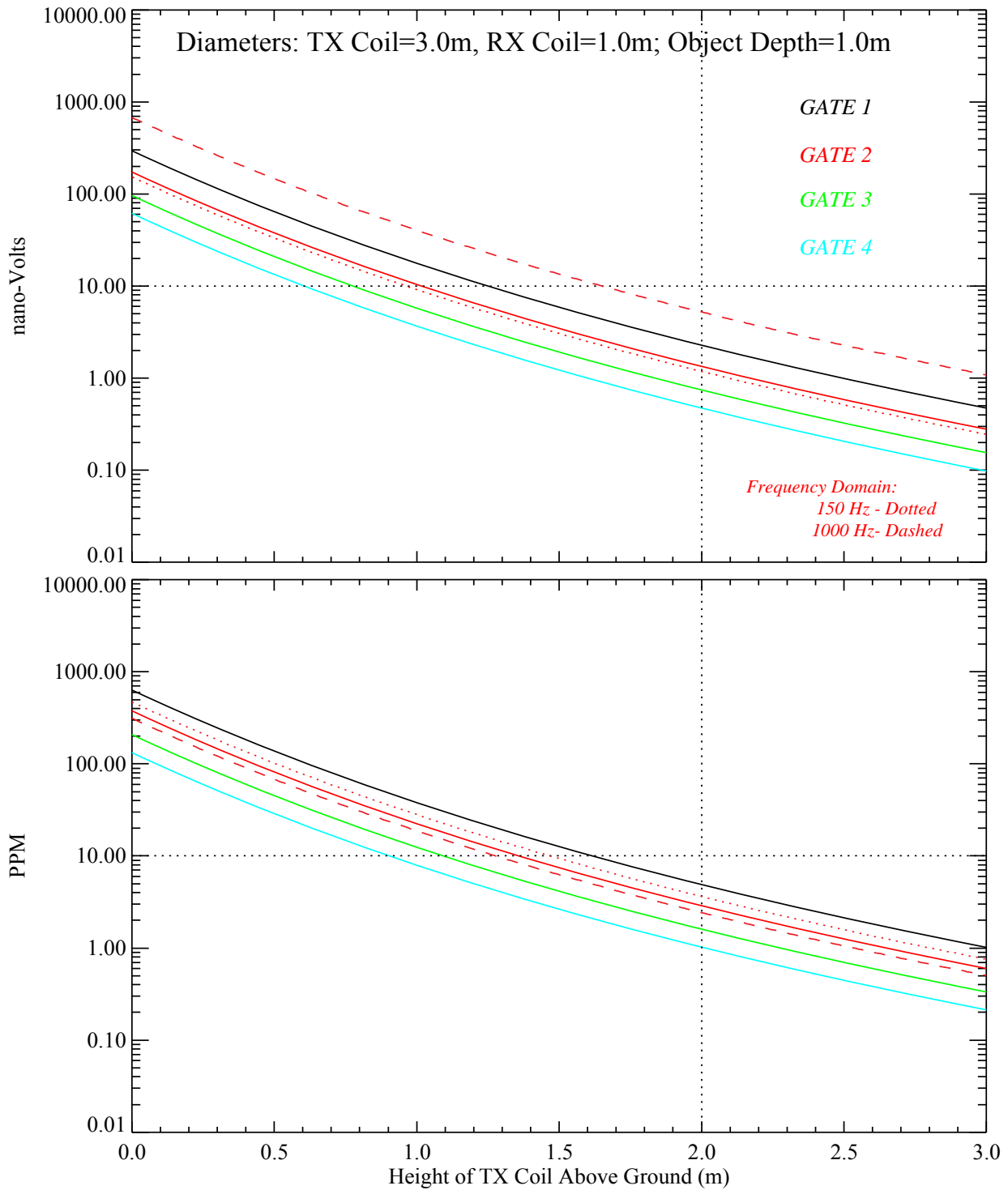


Figure 23. Signal strength as a function of coil height above ground from the comparison sphere buried one meter deep. TX coil is 3 m and RX coil is 1 m. Top plot is response in nano-volts and bottom plot is in ppm. Solid curves are the time domain response for the 150 Hz waveform and dotted/dashed curves are the frequency domain response at 150 Hz and 1000 Hz.

3.1.10.2 Soil Response and SNR Comparison to Time Domain

The response of a time domain system to the ground can be calculated in a similar numerical fashion. In section 3.1.8, the frequency dependence of the ground response was calculated for a fixed conductivity and three levels of a complex, frequency dependent magnetic susceptibility model. This response to the soil can be convolved with the FFT of the transmit pulse and FFT'ed back to calculate the time domain response of the coil system to the ground. The voltage in the receive coil can again be normalized by the direct coupling voltage induced during the current ramp off, i.e., the time domain equivalent of ppm units.

The resulting ppm ground response time decay curves of this calculation are presented in Figure 24. The pulse and time gates used are the ones plotted in Figure 20 and the time decay curves are given as a function of time after the pulse has turned off. The ground parameters are for a conductivity of 0.005 S/m and three levels of magnetic susceptibility (black – 2×10^{-4} , green – 20×10^{-4} , and red – 200×10^{-4}). The diamond symbols indicate the mid-point of the four time gates. The receive coil diameter is 1 meter and the two plots are for a 3 m (left) and 12 m (right) diameter transmit coil. The coil height above ground is 2 m. There was some numerical noise resulting from the calculation of the soil response over a large frequency range and the process of FFT'ing it with the current pulse. This resulted in some roughness of the decay curves and the curves of signal strength as a function of height. Figure 25 plots the average signal over the time gates as a function of sensor height above ground. There is one curve for each of the four time gates. Each set of colored curves corresponds to the four gates at a given level of magnetic susceptibility. The top set of curves plots the signal strength in ppm and the bottom set plots the signal gradient in ppm/cm.

Combining these results with the time domain signal strengths, estimates of signal to ground noise can be made and compared to the frequency domain results in section 3.1.8. The upper plots in Figure 26 show the time domain signal strength in ppm of the comparison sphere shown before in Figure 21. The four solid lines are the time gates and the dashed line is the frequency domain quadrature signal at 150 Hz. The lower plots are the signal strength divided by the expected ground noise if the coil-to-ground height fluctuated on the order of 0.25 m. The three colors again correspond to increasing soil magnetic susceptibility. The pairs of solid curves are the first and second time gate. The dashed curve is the 150 Hz frequency domain SNR. At the lowest magnetic level, the time domain SNR is significantly higher. The frequency domain ground response sees a larger contribution from ground conductivity than the time domain. At higher magnetic levels, the time and frequency domain SNR's are comparable. From the 3 m to the 12 m transmit coil, the signal strength increases for both the time domain and frequency domain cases, but the SNR does not increase as much particularly at greater heights. The gradient in the ground response does not fall off as rapidly for the large coil.

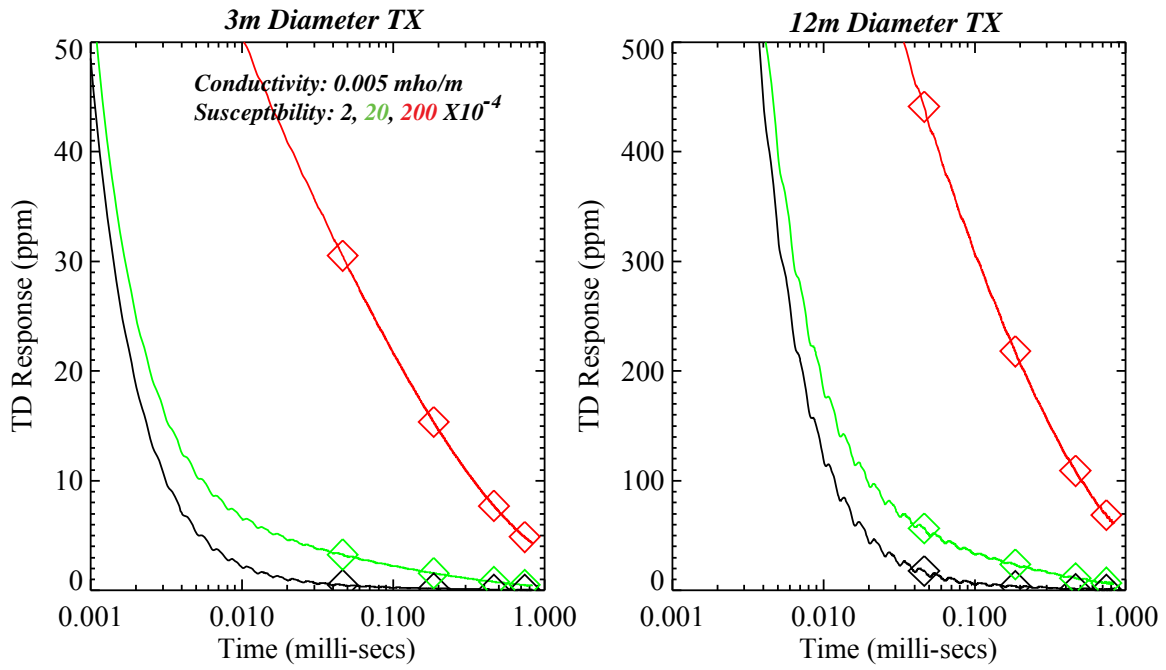


Figure 24. Time domain response to ground.

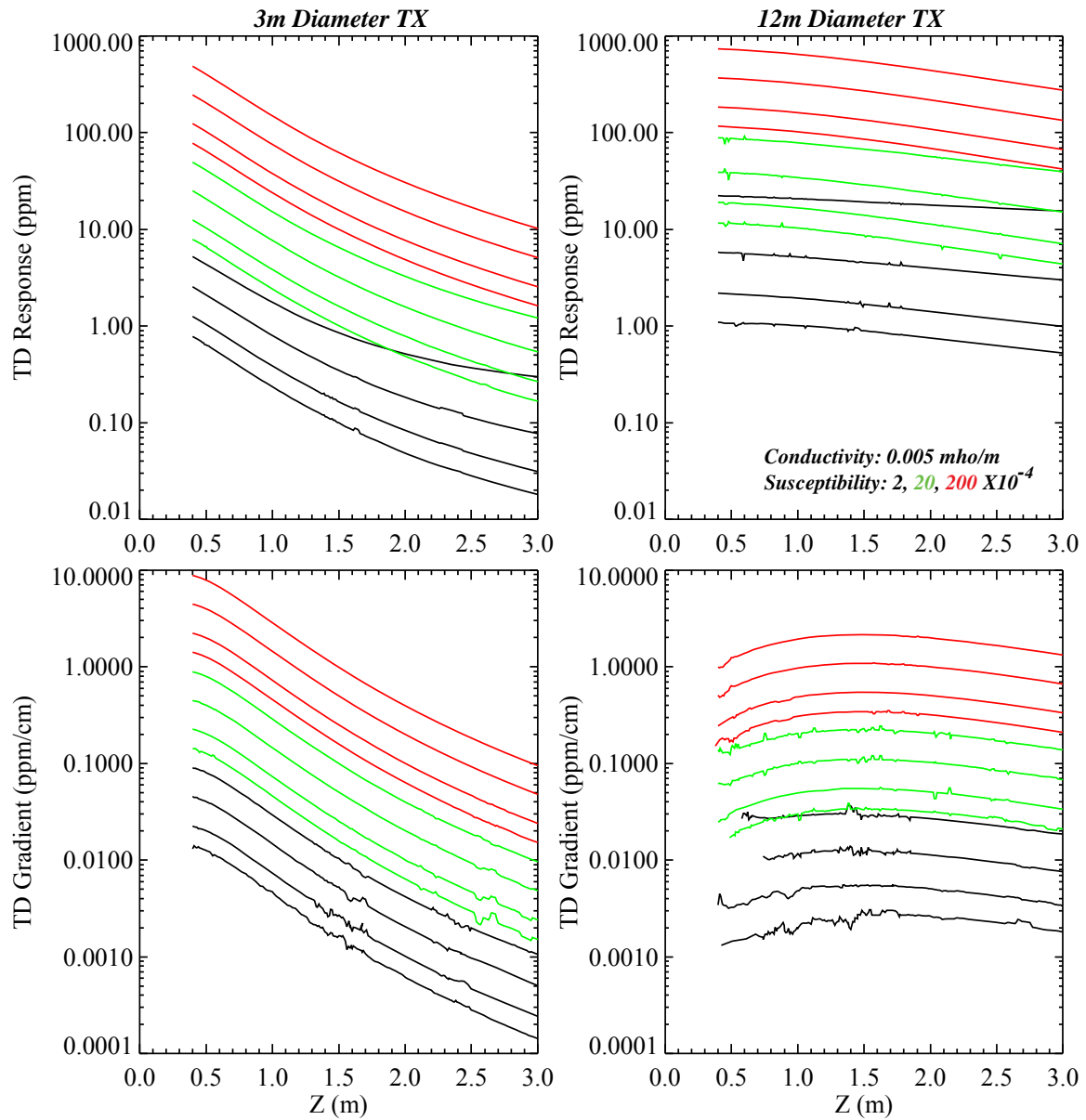


Figure 25. Time domain response to ground as a function of height for the four time gates.

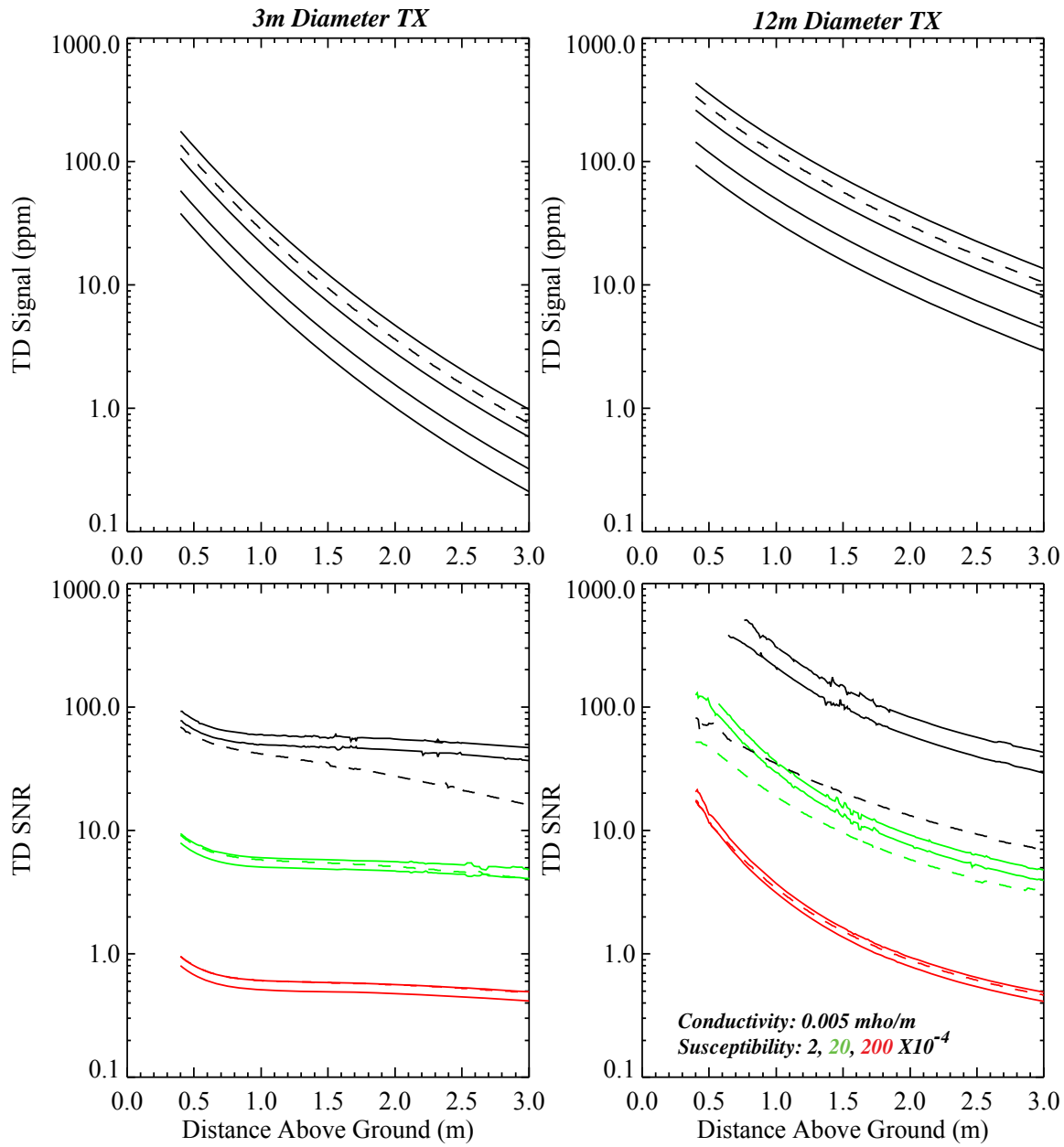


Figure 26. Comparison of time domain response to frequency domain response in terms of ground response SNR.

As observed in an earlier section, these results probably over-estimate noise arising from frequency-dependent susceptibility (FDS) effects, since they assume a uniform halfspace of FDS soil, rather than a relatively thin surface layer.

3.1.11 Ground-based transmit loop

In Section 3.1.6.1, it was noted that a larger transmit coil was the only way to significantly increase signal strength relative to the primary transmit signal. Taking this result to an extreme is the concept of a very large ground based transmitter loop. Figure 27 provides a rough sketch. As a starting point, we have modeled a one square kilometer transmit loop at ground height ($Z = 0$). The object would be below this at a depth of 1 m. The Case 1 configuration is a single circular coil and the Case 2 configuration is a coaxial pair of circular coils. These would fly above the ground at a nominal height of 2 m. Figure 28 plots vertical and horizontal profiles of the field from a 1 by 1 km transmitter with a single turn and 1 ampere of current. The change in the field on meter scale lengths is very small in both directions.

Appendix 2A presents the results of calculating the signal strength in nano-volts and ppm for a 1 km square ground based transmitter and Case 1 / Case 2 circular receive coil(s). The target of interest is one meter below the surface with the transmit coil on the surface. The target is at the center of the transmit coil. A fixed object response of $\beta = 0.005 \text{ m}^3$ is used corresponding to the nominal quadrature response of a 105mm/155mm projectile at a frequency of 1 kHz. Nominal responses would be about 1.5 times stronger at 150 Hz. Vertical and horizontal profiles of signal strength are plotted in the appendix. For Case 2, the signal strength as a function of coil separation is also shown. As an example, Figure 29 plots the signal strength in ppm as a function of vertical height above ground. Case 1 is shown in solid red with a receive coil diameter of 1 m. Case 2 is shown in solid green with a coil separation of 0.5 m and 1 m coil diameters. The dotted red and green lines are Case 1 and 2 for the 12 meter diameter transmit coil for comparison. The dashed red line is Case 1 for the 3 m transmit coil. Because of the uniform transmit field and the weakened primary coupling, the ground based transmit signal strength in ppm is increased over the small, flying transmit coil cases and does not fall off as rapidly with receive coil height. Table 7 presents a quick comparison of signal strengths at a height above ground of 2 m.

Sensor Configuration	3m dia. TX Coil (ppm)	12m dia. TX Coil (ppm)	1 km square Ground TX Coil (ppm)
CASE 1	2.42	20.19	28.3
CASE 2	1.26	10.06	10.3

Table 7. Comparison of signal strengths between TX coil sizes for receive coils 2 m above ground.

The large scale uniform transmit field greatly reduces perturbation noise as well. Plots of various perturbation levels for Case 1 and Case 2 receive coils and a 1 km square transmitter coil are shown in Appendix 2B. The overall results are presented in Table 8 for the sensors flying at a 2 m height above ground. Most of the levels are lower than the flying transmitter cases. The pitch perturbation is about equal to the flying cases for the Case 1 configuration and Case 2 configuration singly perturbed. For the flying transmit coil, the Case 2 jointly perturbed result goes to zero for pitch perturbations because the receive coils are centered about $Z = 0$ of the

transmit coil. However, if the receive coil pairs are slightly off center in X or Z, the pitch perturbation levels grow very large. For the ground based case, the receive coil pair is centered 2 m above the coil center and does not go to zero there. Its level however is very small compared to the off center, flying cases.

Receive Coil Configuration		Change in Primary Coupling (ppm)		
		dZ=1mm	dX=1mm	Pitch= $\frac{1}{2}^\circ$
CASE 1		0.020	2.5×10^{-6}	38.077
CASE 2	Individually perturbed	0.0175	2.5×10^{-6}	38.077
	Jointly perturbed	0.0050	→0	0.0023

Table 8. Perturbation noise levels for a ground based, 1 km square transmit coil and receive coils 2m above ground.

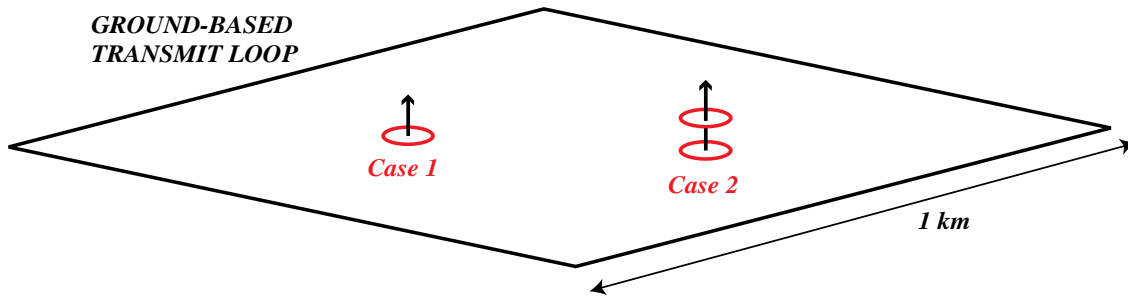


Figure 27. Sketch of ground based transmitter configurations.

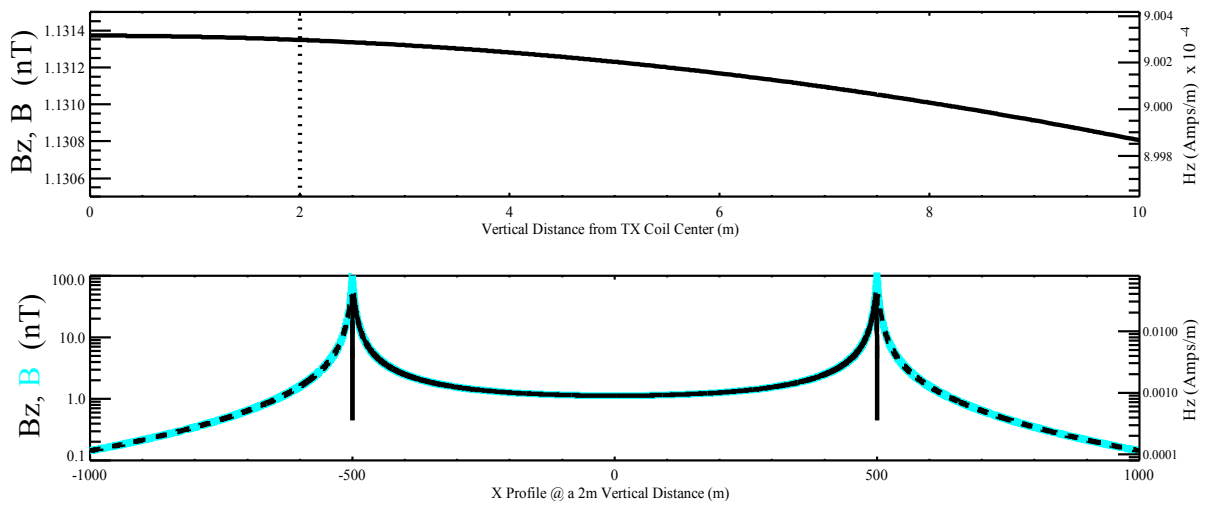


Figure 28. Field from 1 km square, ground based transmitter loop with 1 turn and 1 ampere of current.

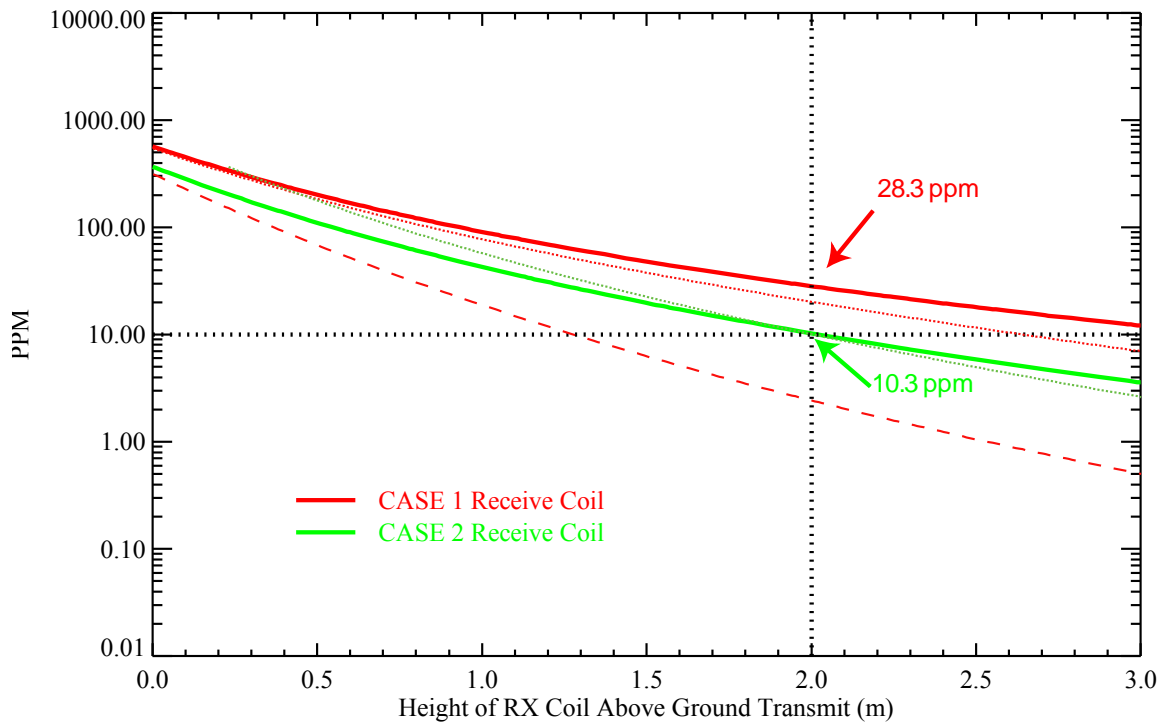


Figure 29. Signal strength from ground based transmitter. Solid lines are from 1 km square ground TX. Dotted lines are from 12 m diameter, flying TX. Dashed is 3 m diameter flying TX.

3.2 Helicopter Noise Measurements

Data were acquired during the warm-up and take-off period for pairs of channels with the TEM-8 system installed. This system was used because of its availability and the opportunity to measure noise at several locations at different offsets from the centerline of the helicopter. The transmitter was not turned on for these tests, and data were acquired at 10 kHz sample rate. The channel numbering is sequential from port to starboard, as shown in Figure 30.

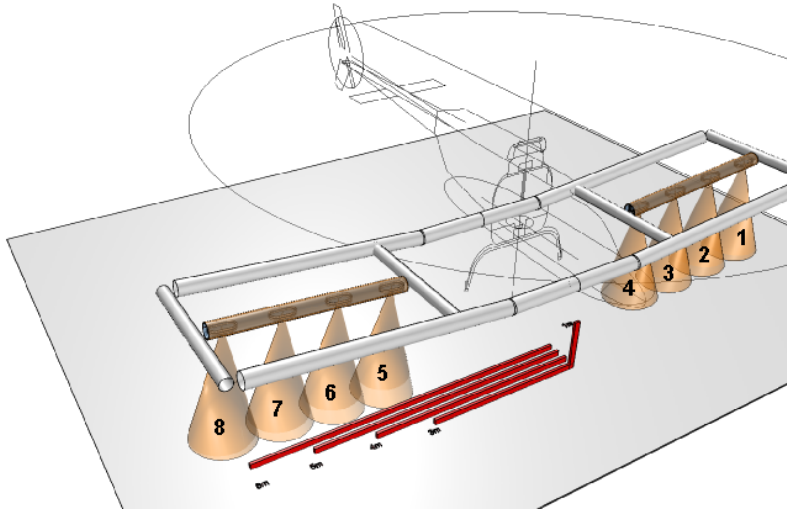


Figure30. Diagram of the TEM-8 system, which was used for acquiring helicopter noise measurements.

3.2.1 Noise Measurements During Takeoff and Landing

Data were acquired in pairs of channels at 10kHz sample rate. Fiducial marks (for the takeoff sequence) were used to bracket 1) system start up, 2) warm up; 3) turn-on for generator; 4) turn on for heli power; 5) run up; 6) skids up; and 7) ascent. Similar events were marked for the landing sequence. A representative sample is shown in Figure 31.

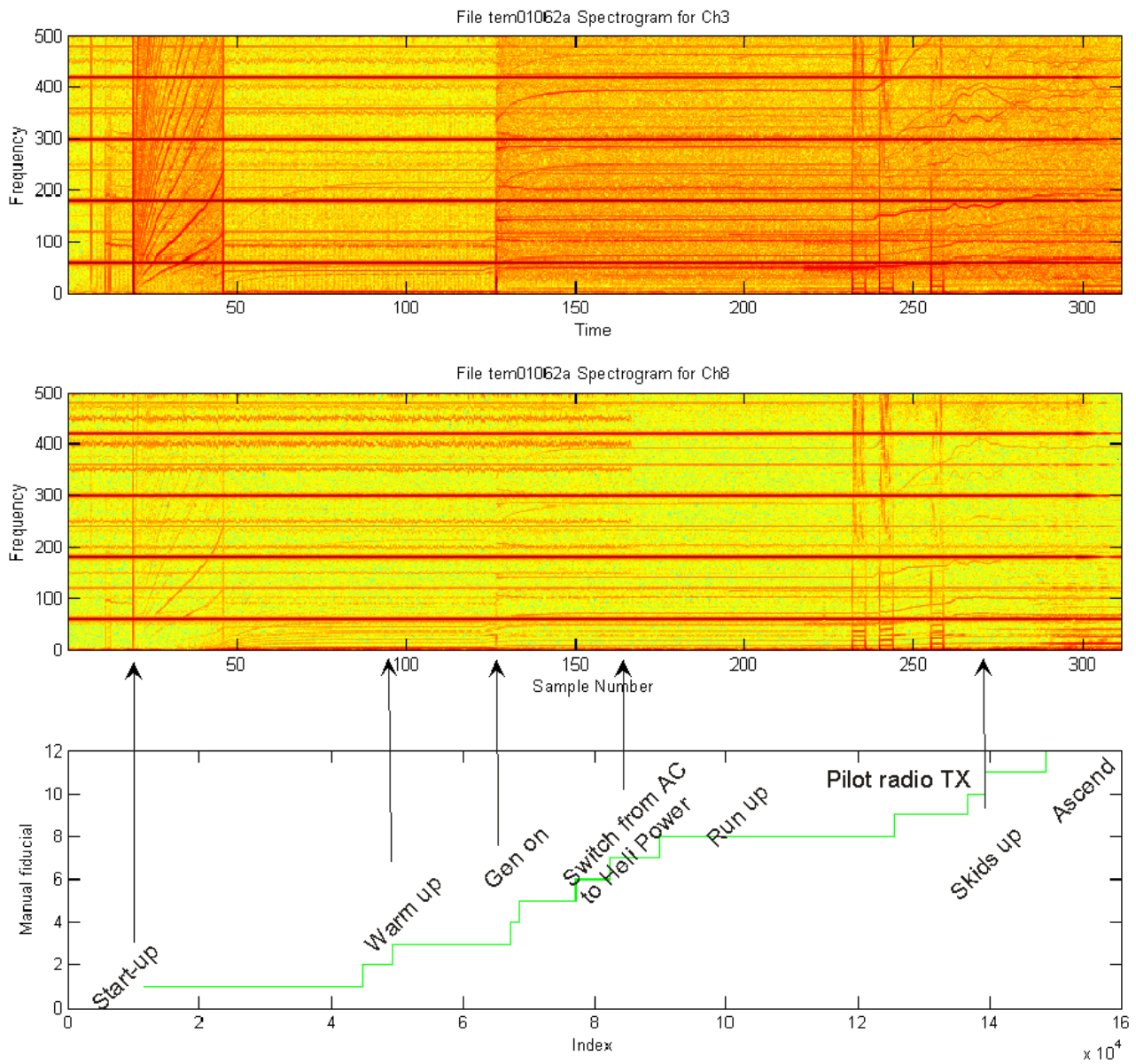


Figure 31. Noise Measurements from take-off sequence for channels 3 and 8. Similar plots were prepared for other pairs of receivers, and for frequencies to 1 kHz.

3.2.2 Noise Spectra, Transmitter off, at 500 ft AGL

Data were also acquired in-flight with pairs of channels. There are eight files with channel 4 always serving as the reference. The spectra for these channels for 0-1200 Hz are plotted in eight separate figures. The upper limit was extended to 1200 Hz because of some interesting features in the spectra above 1000 Hz. Results for channels 1 and 4 are shown in Figure 32 as an example.

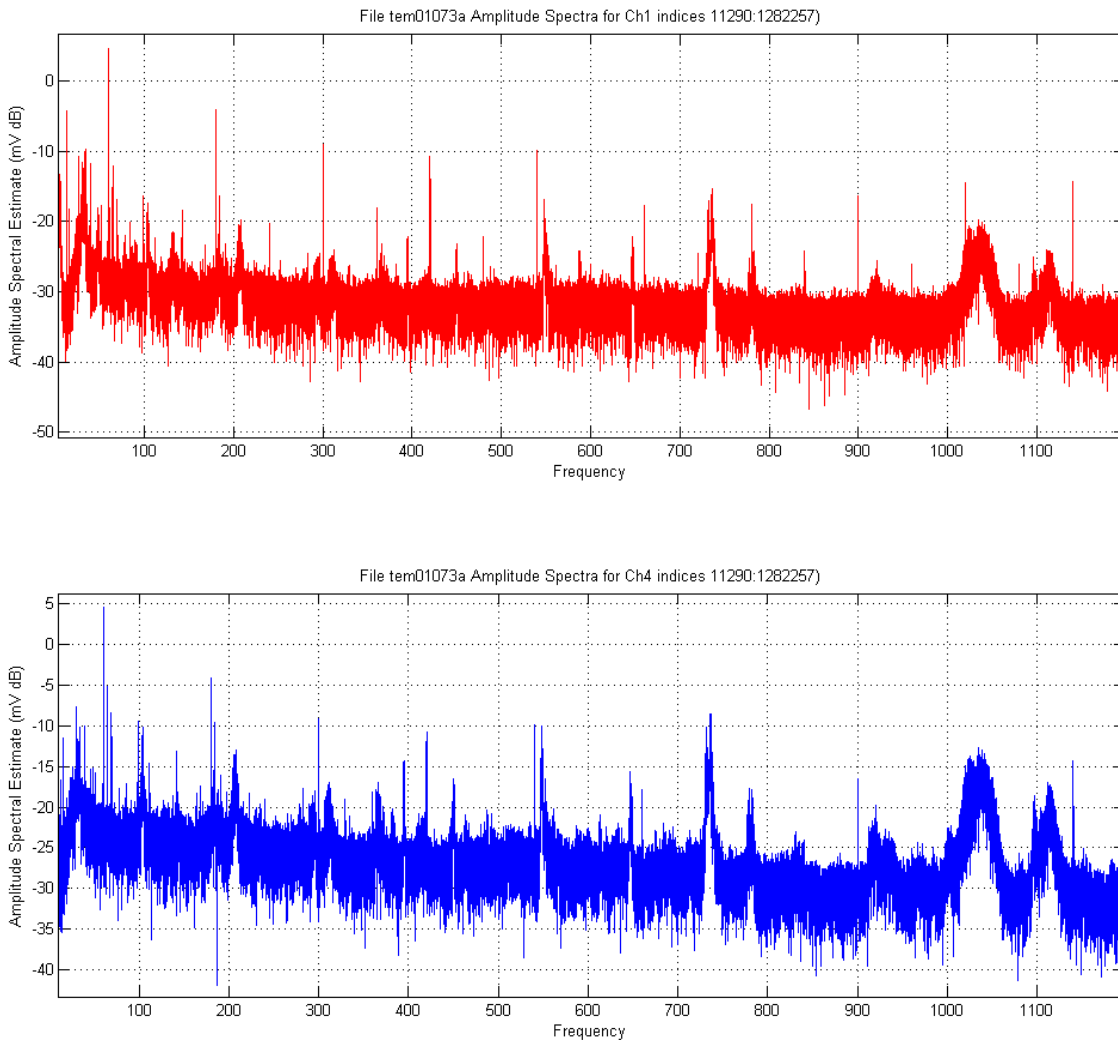


Figure 32. Noise spectra from data acquired at altitude for channels 1 and 4.

3.3 Overview of FDEM and TEM design constraints for nulling and mock-up testing

The following factors governing the practical application of FDEM and TEM technologies should be considered when comparing FDEM and TEM models and results.

Structural differences between FDEM and TEM systems:

One of the reasons why TEM is used exclusively in large-transmitter airborne EM systems (e.g. SkyTEM, MegaTEM, AeroTEM) is that the physical structure linking the transmitter and receiver in TEM has few constraints. It is sufficient that the transmitter position and orientation be reasonably stable and known, and that the receiver orientations and position be stable, low-vibration and known. In contrast, to obtain stable data, an FDEM system has to be very stable in its transmitter-receiver geometry. Any shifts in that geometry will generate inphase errors on the order of ppm per ppm of relative motion. However, noise in the quadrature is limited to (a) the components of vibrational noise that directly generate receiver coil voltages that are out of phase with the transmitter, which from TEM experience will be small for a large structure at frequencies well away from structural resonances, (b) motion of the array or array elements relative to the helicopter, which should be similar or smaller for FDEM implementations compared to TEM due to the greater requirement for structural rigidity, and (c) feed-through of inphase into quadrature via numerical and electronic effects, which is dealt with separately below.

Operating frequency:

A perceived advantage of FDEM over TEM at the outset of the project was the greater degree of freedom in choice of the operating frequency(s). In TEM, base frequency is primarily determined by proximity to powerline frequencies and to harmonics of the rotor frequency, which drives many of the vibrational modes of the Tx and Rx arrays. After further analysis, the same factors are seen to be important for FDEM, removing this as a distinguishing factor between the systems. As a general rule, it is best to avoid odd harmonics of powerline frequencies and of the blade frequency. A convenient way to assess this is to look at the noise spectrum of a given system with the transmitter turned off.

Noise bandwidth of TEM and FDEM systems:

The other perceived advantage of FDEM over TEM at the outset of the project was a narrower noise bandwidth at the operating frequency. In TEM, the system output data are accumulated into multiple time bins during the transmitter's "off time" and ignores data acquired during the "on time." As such, fewer than half of the data being digitized in each cycle of the waveform are used at all, and these data are divided up into a series of bins. In FDEM, data from the entire waveform are correlated against selected sinusoids, so that the values in phase and out of phase for a particular frequency are combined into just two numbers. Depending on the shape of the transmitter waveform, there may be sufficient energy at other frequencies to obtain good EM data at those frequencies.

For a given frequency and continuous input waveform(s), the correlation of the input against sine and cosine functions is a very stable process, becoming progressively more stable as the base frequency decreases due to the larger number of sample points being multiplied. The effective

output bandwidths of TEM and FDEM processing turn out to be similar if the same spatial resolution is required, so there is no strong noise advantage to either FDEM or TEM in this respect.

Motion noise leakage from inphase to quadrature in FDEM acquisition and processing:

This factor is related to the preceding noise bandwidth discussion, but here pertains in particular to the potential for signal or noise in the inphase component to “leak” into the quadrature. “False” quadrature output should only occur when there is a distortion in the transmitter waveform signal that correlates with the quadrature part of the Fourier transform. However, there is another step in our processing that suppresses the effects of changes or distortions in the transmitter signal itself; we acquire both signal and transmitter reference data, and divide the Fourier-transformed signal by its transformed reference counterpart. Thus any “real” feature in the transmitter current waveform is captured in both signal and reference channels and removed during the reference division step. Sampling time jitter would be another possible source of leakage, but since the ADCs operate in lockstep for the signal and reference channels and the sampling rate is very stable already, this should not be an issue.

The most likely way in which crosstalk could occur is therefore via mis-phasing. A small phasing adjustment on FDEM data is generally necessary due to small differential delays in the electronics, with phase angles of about $1 \pm .5$ degree, or about 10 ± 5 parts per thousand. There are thus up to 10 ppt of inphase present in the quadrature portion of the raw reference division output, and less than 1 ppt after phasing. The phase adjustment could be made even more precisely with an improved measurement procedure. Phase adjustments could also be performed in real time at altitude if necessary in an operational system, though this seems unlikely to be required.

If 1 ppt of phasing error is assumed, then quadrature noise from Tx-Rx geometry changes will be 1 ppt of of the inphase noise from the same source. If the target quadrature “noise” level were 0.1 ppm, than inphase noise amplitudes of <100 ppm would be acceptable. 100 ppm of inphase anomaly corresponds to the response of the vertically oriented 105/155 simulant at a sensor-target vertical separation of 1.3m, a very large anomaly.

Table 9 uses data from Table 3 in the numerical modeling section to estimate nominal perturbations in mm required to generate 0.1 ppm of quadrature error assuming 1:1000 phasing accuracy (equivalent to 100 ppm of inphase error). In this table, small values indicate high sensitivity and vice versa.

Sensor Configuration		Motion to generate 0.1 ppm of Quadrature Response, Assuming 1:1000 Phasing Accuracy (mm)		
		dZ	dX	Pitch (deg)
Case 1		-125.00	250.00	-1.32
Case 2	Indiv. perturbed	0.26	322.58	-1.32
	Jointly perturbed	0.13 (insensitive)		-3.92
Case 3		-125.00	-125.00	0.01
Case 4	Indiv. perturbed	-0.48	-104.17	0.01
	Jointly perturbed	-0.24 (insensitive)		4.37
Case 5	Rx perturbed	-5.52	11.03	-649.35
	PFN perturbed	-5.29	10.56	-1.31

Table 9. Spatial perturbations in millimeters and degrees corresponding to 0.1 ppm of quadrature response for 1:1000 phasing accuracy for Cases 1-5 with 3m transmitter diameter

These values are linearized from field gradients and are thus approximate, but they do give a sense of quadrature noise levels that could arise from relative motion of the transmitter and receiver for various configurations. For example, for Case 1, 100 ppm of inphase error (and thus 0.1 ppm of quadrature error) corresponds to 125 mm of vertical motion, 250 mm of horizontal motion or 1.3 degrees of angular motion. These are all very large distortions of the array, indicating that Case 1 quadrature output should be relatively insensitive to such motions. In contrast, Case 2 is very sensitive to vertical displacement of the differential receiver pair but insensitive to horizontal motion or rotation of the coil pair. Case 3 is insensitive to linear motion, but extremely sensitive to rotational motion of the receiver relative to the transmitter. Case 5 is moderately sensitive to motion of the receiver coil or the PFN coil. Table 10 examines the corresponding performance of Case 1 and Case 2 receivers for a large ground-based transmitter.

Sensor Configuration		Motion to generate 0.1 ppm of Quadrature Response, Assuming 1:1000 Phasing Accuracy (m or deg)		
		dZ (m)	dX (m)	Pitch (deg)
Case 1		5.00	(insensitive)	-1.32
Case 2	Indiv. perturbed	5.71	(insensitive)	-1.32
	Jointly perturbed	20.00	(insensitive)	-3.92

Table 10. Spatial perturbations in meters and degrees corresponding to 0.1 ppm of quadrature response for 1:1000 phasing accuracy for receiver Cases 1-2 near center of 1 km square transmitter loop

For the large ground-based transmitter loop, Cases 1 and 2 both yield good to excellent stability with respect to vertical and horizontal motion. In this case, sub-meter positioning accuracy with post-survey corrections would suffice to yield motion-derived quadrature noise levels on the order of 0.02 ppm or better. Receiver orientation error is three or more times more significant for Case 1 than for the jointly perturbed Case 2 result, suggesting that for this class of transmitter-receiver geometries, vertical difference receivers with a very rigid interconnecting structure would yield the lowest motion-related noise levels.

EM Transmitter Size:

Numerical modeling performed during this project shows significant signal benefits from using a larger transmitter. This is equally true for FDEM and TEM systems. Careful thought should be given to deploying as large a transmitter as possible without compromising the safety of the system.

One shortcoming of using larger transmitters is a greater sensitivity to terrain coupling “noise” caused by variations in flight height relative to conductive soils. However, frequency-dependent susceptibility (FDS) effects appear to be substantially weaker with the larger transmitter, which would improve SNR related to this effect.

3.4 Primary Field Removal Assessment

3.4.1 Dynamic Range Issues: FDEM vs TEM

The design of an FDEM system for airborne applications is more challenging in many respects than is the design of a TEM system of comparable sensitivity. One of the principal challenges is the enormous electronic dynamic range required to acquire the full received dB/dt waveform (as compared to the smaller dynamic range required in order to acquire the off-time transient for a TEM system). Strategies used in existing FDEM sensor systems for dealing with this dynamic range issue include:

- Working within the available dynamic range limits imposed by existing A/D technology and software-based dynamic range extension methods (structurally simple, but limits the sensitivity of the sensor)
- Passive bucking of the primary field received signal to permit acquisition of the much smaller secondary field (this is the approach used in conventional helicopter EM systems);
- Primary field nulling (PFN) at the receiver for the same purpose (used in the Geophex GEM-3 sensor and the prototype Geonics EM-73),
- Measuring magnetic field B (or a band-limited version of B) rather than dB/dt (the quantity normally measured with coils), to compress the signal’s dynamic range

3.4.2 Transmitter-Receiver Configurations

As part of the evaluation of FDEM methods under the SERDP project, mock-ups were constructed to assess practical performance of the system concepts outlined in the SERDP proposal. To keep the test diversity and timeframe manageable, a single 3m diameter hexagonal transmitter coil was constructed, using a fiberglass form and a copper transmitter cable. This was used to test a variety of receiver configurations and dynamic range compression methods. The ORAGS-EMP console (from the two-channel prototype system, developed by the project team while at ORNL), comprising x2 gain and dual 24-bit ADCs, was used to acquire data: this receiver arrangement yields good data to approximately 20 bits. The ORAGS-EMP preamplifier and coil configurations were adjusted and used as necessary. The transmitter waveform was

adjusted to reduce peak dB/dt by lengthening the on/off ramps and minimizing the off-time, as well as by using a relatively high-inductance transmitter coil configuration.

A variety of transmitter and receiver configurations were evaluated through modeling and/or bench tests. Prototype components were prepared to evaluate the selected approaches. The resulting mock-up FDEM system used and further modified these prototypes and other components from the ORAGS-EMP system as appropriate.

Multiple approaches have been considered and compared for bucking or nulling of the primary field, in order to decrease the dynamic range requirements of the system as a whole, as described in the previous section. In traditional frequency-domain systems, passive bucking coils substantially offset from the transmitter have been used for this purpose, but the concentric system geometry being studied with the mock-up is not directly compatible with this approach. Alternatives considered include the following:

- Using small bucking coils for each receiver, mounted adjacent to the transmitter coil, adjusting their positions relative to the transmitter coil windings for optimal bucking. This alternative requires a very high degree of mechanical “stiffness” in the transmitter-bucking-receiver coil array, but does not add significantly to the weight of the array as a whole.
- Primary Field Nulling (PFN) coils. This approach is more mechanically complex than the passive bucking method. The PFN coils would probably need to be physically integrated with the receiver coils on a rigid substrate to ensure minimal vibrational noise generation through differential motion of the PFN and receiver coils. For the purposes of this project, a single PFN coil with a single receiver was tested.
- Vertical difference coils disposed symmetrically about the transmitter plane. As has been shown in the previous sections, this approach yields good nulling performance, at some cost to signal levels and with increased sensitivity to certain motions. A virtue of this approach is that it can aid in rejection of ambient noise from power lines and sferics.

In general, it should be noted that it is sufficient, though not optimal, to null or buck out 99.0% of the primary field, because ADC’s that are currently available are capable of acquiring signals with a dynamic range of approximately 1 part in 10^6 with good linearity and noise properties, to bring the ADC’s effective one-bit level down to the 0.01 ppm range. Nulling beyond 1 part in 100 yields improved noise performance in cases where noise from ambient sources in the operating frequency bands is smaller than 0.01 ppm—this might happen in exceedingly quiet areas, or if the primary field amplitudes are made unusually large.

3.4.3 Dynamic Range Compression Methods Testing

Five approaches to dynamic range compression were implemented and tested in conjunction with the mock-up evaluation described in the next subsection, including:

1. **Simple passive bucking using a matched receiver coil**, in which a 25 m², 0.4m diameter bucking coil having the same effective area and physical dimensions as the receiver was connected in opposition to the primary receiver coil located at the center of the transmitter. The bucking coil was located just outside the transmitter coil. Because the receiver and bucking coil had the same areas and winding sense, this approach

increased rather than decreased ambient noise pickup. While this approach was not practical for a survey system because the bucking coil would pick up spurious responses from strong UXO targets, it served as a useful initial step.

2. **Passive bucking using a small-diameter bucking coil**, located adjacent to the inside edge of the transmitter coil. The amplitude of the bucking signal was initially adjusted through the effective area of this coil, followed by adjustments to its radial position relative to the transmitter cable. This configuration avoided the worst defects of the simple passive bucking arrangement described above because the bucking coil had a substantially smaller effective area and was mounted in the zone of strong magnetic field adjacent to the transmitter cable, so the bucking signal is less sensitive to secondary fields from UXO targets.
3. **Vertical difference measurements using matched receiver coils**, in which two identical receiver coils were mounted in a wired vertical difference configuration, located symmetrically above and below the transmitter plane. This configuration strongly rejects ambient noise fields that are nearly identical at the two receivers, but does have increased fall-off in received signal strength with respect to height compared to single-coil receivers.
4. **Primary field nulling (PFN)**. A PFN coil was constructed and adjusted to null out the primary field pickup of the receiver coil at the center of the transmitter coil by routing the transmitter current through its turns. This approach minimizes receiver complexity at the cost of the additional weight and space required for the PFN coil. In the context of this project, PFN coil(s) for multiple receivers were not required.
5. **Pseudo-B data acquisition** was also examined using an integrating preamp adapted from earlier TEM system tests and the vertical difference configuration. This device yields a band-limited waveform that approximates that of the B field, as opposed to the dB/dt waveforms normally recorded with coil based receivers.

A sixth approach was also considered, **Enhanced analog-digital converters**. A search was conducted for newly-available ADC's that could provide dynamic ranges of more than 24 bits during continuous sampling. The minimum working dynamic range required to permit direct digitization of FDEM waveforms with no bucking or nulling requirement is 28 bits, though signal headroom considerations would make 30 or 32 bits more attractive. While progress is being made in this field, such converters are still not commercially available. However, the market continues to move slowly in the direction of higher dynamic range, so it is anticipated that this approach may be prototyped within the next decade, and perhaps within the next few years.

3.5 Mock-up Tests

3.5.1 Mock-up Apparatus

FDEM data acquisition tests were performed with the four PFN configurations described above. The apparatus was intended for ground tests only, and was therefore not designed for airborne operations. These preliminary tests primarily focused on verifying that each configuration was working as expected, and were not intended to be "final," since the project plan called for mock-up equipment to be moved to Oak Ridge for FDEM data acquisition with a suite of inert UXO objects in Year 2 of the project.

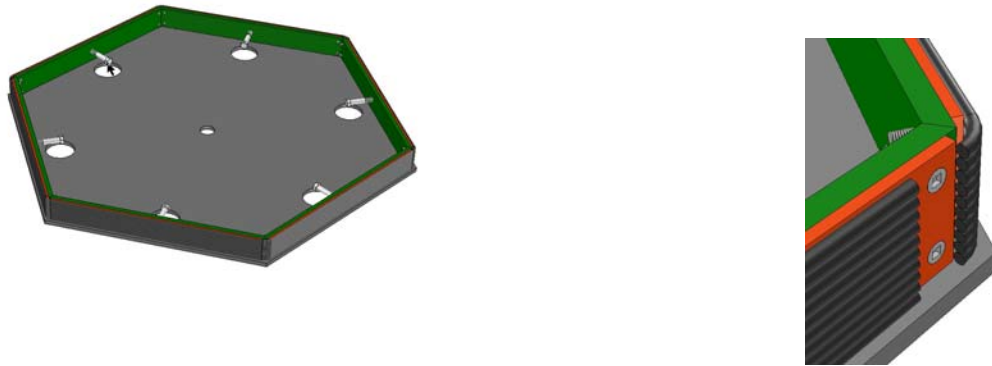


Figure 33. CAD model of PFN test coil form.

One element of the mock-up apparatus prepared under this task was a target track that would allow the operator to move the targets up and down relative to the transmitter plane above the receiver coil located at the center of the transmitter. One detailed data set was acquired using this track and the PFN coil configuration, which will be presented later in this section.

The transmitter consisted of 7 layers of flat 4-conductor copper cable. These were tightly wound onto a form constructed from fiberglass U-channel with corner stiffeners, with the leads brought out to the ORAGS-EMP junction box. While the coil as a whole is relatively heavy and displays some flexibility at its vertices, it was found to be very stable when firmly supported at its vertices.

The receiver coils were 25 m^2 , 0.4m diameter wideband coils originally used in the ORAGS-EMP system.

A small reference receiver coil of effective area 0.385 m^2 was mounted just outside the transmitter loop to monitor transmitter output. Its output was monitored by a preamplifier identical to that used for the receiver.

A small bucking coil was used in one of the mock-up configurations, and was mounted adjacent to the inner edge of the transmitter coil. Its effective area was 3.9 m^2 , and its position relative to the transmitter coil was adjusted to buck out the primary signal in the receiver.

A primary field nulling coil was wound onto a five-turn hexagonal form described below, using AWG 8 copper wire. The inscribed radius of the vertices of the coil used for testing was 0.58m. The coil's effective area was adjustable by a set of nylon bolts located at the centers of each side for the purposes of fine tuning.

In Figure 33, one vertex of the PFN coil form is shown in the detail image on the right. Stainless screws and nylon deflection bolts were used to minimize inductive effects. The orange color represents an adjustable ply panel, while green is an 11mm ply rigid frame, and gray is a bottom hex sheet. The top is not shown. Deflection bolts permitted increases in PFN area in small increments to tune nulling efficiency. The receiver coil was located at the centre of the PFN coil.

A target track was constructed to facilitate accurate and repeatable measurements at a series of heights above the transmitter plane. The structure breaks down into a set of 16 foot or shorter sections for transport. Target heights of 0.5 to 3.5m above the transmitter plane could be accommodated by this track.

As was done during testing of the ORAGS-EMP and TEM-8 systems, a set of three aluminum plates were used as standard targets. For this project, in order to obtain a closer correspondence between the test measurements and those numerically modeled for this report, as well as with projectile responses measured by Battelle with the TEM-8 system, components were procured for a "projectile simulant" having approximately the same dimensions and mass as a 105/155 class projectile. The simulant consists of a 0.46m (18") length of 0.11m(4.5") diameter steel pipe, wall thickness 0.009m (.337"), with threaded ends and heavy steel caps. Total length was 0.53m (21"). The cap diameter was 0.14m (5.5"), with 0.05m (2") height. The simulant weighs approximately 10 kg.

To summarize, three sets of test targets were used during the course of these preliminary mock-up tests. The first was a 40 cm ferrite bar that was used exclusively for phase measurements for the system, the second included three aluminum sheets of increasing size, as described below, and the third was the 105/155mm projectile simulant.

Planar Test Targets (all aluminum):

9 x 9 x 1/8"	Small
11.5 x 11.5 x 3/32"	Medium
17-3/4 x 17-3/4 x 1/8"	Large

Simulant for 105/155mm projectile:

4.5" (0.11m) OD steel pipe
Length 18" (0.46m)
Cap diameter 5.5" (0.14m) and height 2" (0.05m)
Total length with caps 21" (0.53m)
Total weight 10 kg



Figure 34. Photo of assembled PFN configuration (white hexagon at center of red and black transmitter coil), showing target track and 105/155mm target simulant in its horizontal orientation. Transmitter-receiver separations were measured between the transmitter plane and the closest point of the EM target, in this case its lower edge.

3.5.2 Results from Preliminary Mock-up Tests

A series of tests were performed as each of the trial configurations was implemented. These became increasingly detailed and comprehensive as the configurations progressed from simple bucking to the vertical difference (VD) and Primary Field Nulling (PFN) configurations. FDEM response in ppm was measured as a function of distance between the transmitter plane and the lower edge of the target. Signal and SNR results for each test are presented in the tables below. The noise measure used was one standard deviation in all cases.

	Height (m)	0.5	1	1.5	2
Item		QD1 Amplitude (ppm)			
Small Al Sheet	800	78	15		4.2
Horiz Simulant	700	90	17		4.3
		QD1 SNR			
Small Al Sheet	18182	1773	341		95
Horiz Simulant	15909	2045	386		98

Table 11. Bucking configuration Signal and SNR results, QD1 noise 0.044 ppm

The bucked configuration (Table 11), corresponding approximately to Case 1 in the numerical modeling, displays higher noise than the vertical difference case (Table 12), at least partially due to its lower ambient noise rejection. Ambient noise levels were observed to fluctuate somewhat from test to test. Noise was estimated from the standard deviation of the signal obtained near the end of each set of test measurements. The bucking coil used to obtain the results above had an effective area of 16% of the receiver coil, and was positioned approximately 1.45 m from the center of the receiver coil, near a vertex of the transmitter coil. Up to 16% signal attenuation due to the anomaly pickup by the bucking coil would therefore be expected at higher sensor-target altitudes as the anomaly broadens. Vertical positional accuracy in this test was lower ($\pm .05\text{m}$) than for later vertical test track results.

	Height (m)	1	1.5	2	2.5
Item		QD1 Amplitude (ppm)			
Large Al Sheet	1600	170	34		7
Medium Al Sheet	800	100	18		5
Small Al Sheet	350	33	7		1.4
		QD1 SNR			
Large Al Sheet	61538	6538	1308		269
Medium Al Sheet	30769	3846	692		192
Small Al Sheet	13462	1269	269		54

Table 12. Vertical difference (VD) configuration results, QD1 noise 0.026 ppm

The noise level in the vertical difference (VD) configuration (Table 12), corresponding to Case 2 in the numerical modeling, was lower than the other configurations tested, presumably due to ambient noise cancellation in the vertical difference coils. A departure from (height)⁻⁶ behavior was observed at 2.5m, as expected. As for the bucked configuration test, vertical positional accuracy was limited compared to vertical test track results. The enhanced signal levels for

heights of 2m and lower relative to the bucked and PFN configurations are due to the increased proximity (by 0.2m) of the closer of the two difference receivers.

Item	Height (m)	QD1 Amplitude (ppm)			
		0.5	1	1.5	2
Small Al Sheet	800	78	15		4.2
Horiz Simulant	700	90	17		4.3
		QD1 SNR			
Small Al Sheet	7273	709	136		38
Horiz Simulant	6364	818	155		39

Table 13. Integrator test in vertical difference configuration, QD1 noise .11 ppm

Comparing QD1 integrating preamplifier SNR (Table 13) to the conventional preamplifier results at 2m, integrated signals are lower and noise higher, so that the overall integrator SNR of 38 is much lower than the SNR of 192 obtained with the standard preamplifier. Some improvement to this result might be possible through optimization of the integrating preamplifier parameters.

For the primary field nulling configuration corresponding to Case 5 in the numerical modeling, simulant responses were acquired with the vertical test track, which permitted more repeatable data acquisition for a range of heights of from 0.5 to 3.5m above the receiver plane. For reference, responses for the small aluminum plate target in a vertical-axis configuration were also acquired. A ferrite bar test conducted at the time yielded a phasing accuracy of 1 part in 1800. Earlier tests conducted without the vertical test track yielded results for the larger aluminum plate targets at heights up to 2.5m. The combined results are shown in Table 14. A subset of these results is plotted in Figure 35.

Item	Height (m)	QD1 Amplitude (ppm)					
		1	1.5	2	2.5	3	3.5
Large Al Sheet	1500	230	40	16			
Medium Al Sheet	580	105	20	7.8			
Small Al Sheet	210	35	8	2.8	1	0.45	
Vert Simulant	400	90	27	9	3.8	1.6	
Horiz Simulant	104	31	9	3	1	0.4	
		QD1 SNR					
Large Al Sheet	38462	5897	1026	410			
Medium Al Sheet	14872	2692	513	200			
Small Al Sheet	5385	897	205	72	26	12	
Vert Simulant	10256	2308	692	231	97	41	
Horiz Simulant	2667	795	231	77	26	10	

Table 14. Primary Field Nulling (PFN) configuration, QD1 noise 0.039 ppm

The noise level was slightly lower at 0.039 ppm for this test than for the bucked configuration. The amplitude and SNR results for the small aluminum plate and two orientations of the simulant are plotted in Figures 35-37.

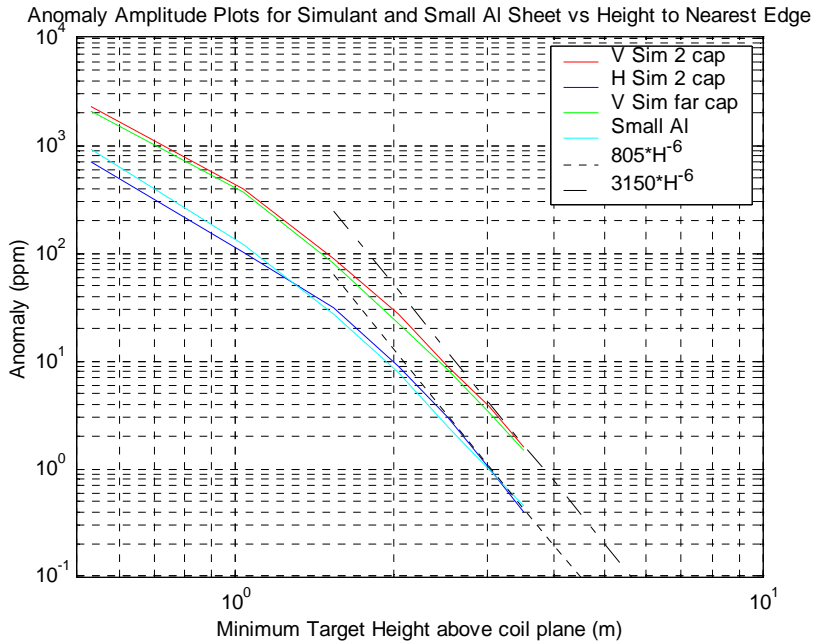


Figure 35. Log-log plot of simulant and small aluminum plate amplitudes in ppm vs height in meters.

The quadrature responses of the vertically-oriented simulant with and without the endcap closest to the coil array were similar, and the response of the horizontally oriented simulant was similar to that of the small aluminum plate. This format clearly shows the (height)⁻⁶ asymptotic behavior of the responses.

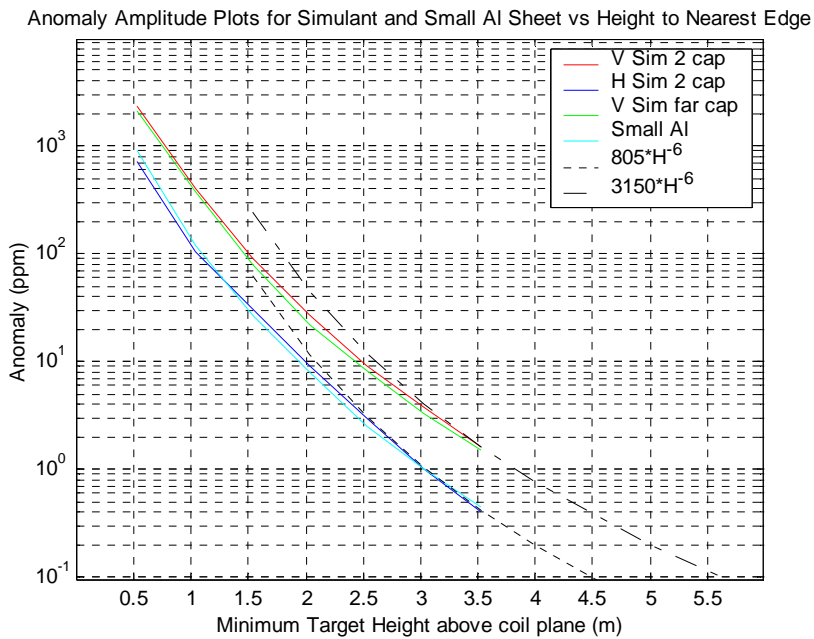


Figure 36. Amplitude data shown in previous plot, displayed in linear-log format.

A signal/noise ratio plot was constructed for this dataset, using the 0.039 ppm noise level estimated during the test.

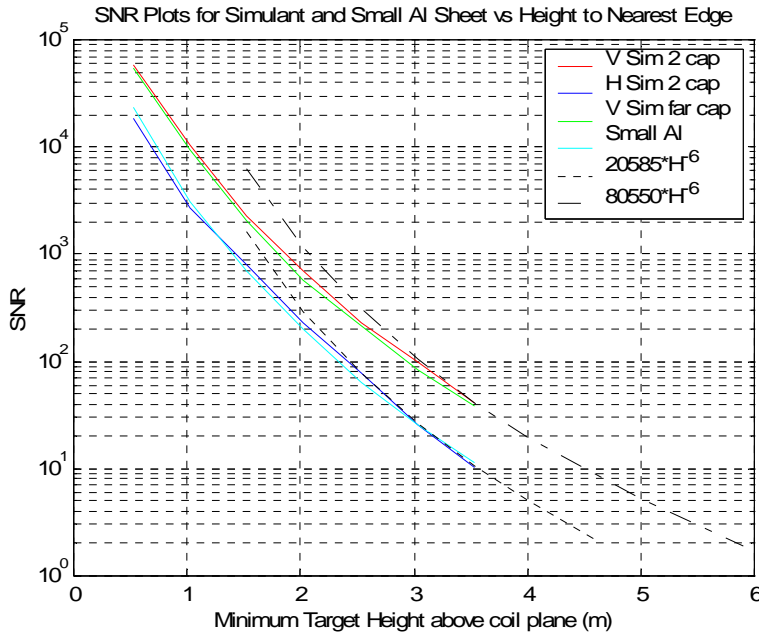


Figure 37. SNR plot for amplitude data shown in previous plot, displayed in linear-log format.

The SNR results indicate that the simulant in horizontal orientation under comparable noise conditions should be detectable (with SNR of 2 or higher) to about 4.6m, while in its vertical orientation it should be visible to 5.9m. As expected, the SNR appears to fall off as the sixth power of height above the transmitter plane for heights above the 3m transmitter coil diameter.

3.6 Discussion

3.6.1 Preferred model configurations

Modeling suggested that the three most promising configurations are the Case 1 concentric vertically oriented planar transmitter and receiver loop, the Case 5 version of Case 1 that includes a PFN coil, and Case 2, which substitutes a vertical difference receiver for the Case 1 loop receiver. These configurations were all briefly assessed during the preparation of the mock-up. This section compares the application of these configurations, differences and similarities between FDEM and TEM, and observed performance for FDEM.

3.6.2 Comparison of Observed and Modeled FDEM and TEM Performance

3.6.2.1 Modeled and Measured Responses:

While comparing measured mock-up quadrature amplitudes at 135 Hz (Fig 35-36 above) for particular targets to those computed for the numerical reference target (Fig 7 above), recall that

1m altitude on the model plots is equivalent to 2m on the mock-up data plots due to differing plotting conventions. The vertically oriented mock-up simulant target response at 2m total separation between sensor and the nearest point on the target was on the order of 30 ppm for the PFN and bucked configurations, while the horizontal simulant response was approximately 10 ppm. At 3m total separation, the corresponding responses are 4 and 1 ppm.

The corresponding (1 kHz) quadrature anomalies from the SAIC model study were 18 ppm at 1m nominal altitude (2m total height above target) and 2.2 ppm at 2m nominal altitude (3m total). In the absence of 135 Hz model data, we can approximate 135 Hz responses by assuming that the amplitude ratios seen in Fig. 2 are applicable: these are approximately 1.5:1 when comparing 135 Hz to 1000 Hz data, yielding amplitudes of 27 and 3.3 ppm at 2m and 3m sensor-target separation.

The following plot shows the Case 5 model data multiplied by 1.5 (X symbols), plotted with the observed PFN data amplitudes (red and blue solid lines for vertical and horizontal simulant orientations). The correspondence between the modeled and vertical simulant responses is good.

The same plot shows TEM model data (+ symbols) obtained for a 0.25m diameter sphere with properties approximating those of steel. These data were plotted with position offset by the radius of the sphere, in order to be consistent with the convention of plotting data at the distance from the sensor to the closest point on the target. TEM data obtained during ground tests of the TEM-8 system using vertically and horizontally oriented 155mm inert projectiles are also plotted as solid and dashed green traces. These responses are about 3-4 times weaker than the vertical FDEM simulant response and match the horizontal simulant response fairly well.

Finally, power-law extrapolations of the FDEM vertical simulant and TEM responses are shown as black dotted and dashed traces.

Vertical Difference data were not included on this plot. SNR for VD was enhanced at low sensor-target distances due to the enhanced ambient noise suppression of the VD array, but at altitudes above 2.2m, this benefit is lost due to the H^{-7} VD signal fall-off rate.

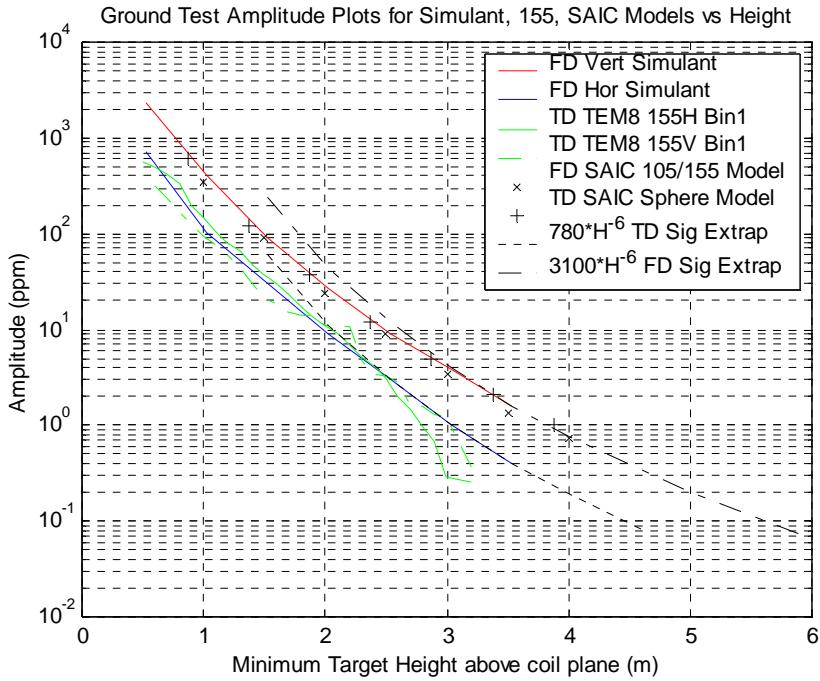


Figure 38. Response amplitudes for the Case 5 mock-up data, plotted with sample data from Battelle TEM-8 tests and modeled FDEM and TEM responses.

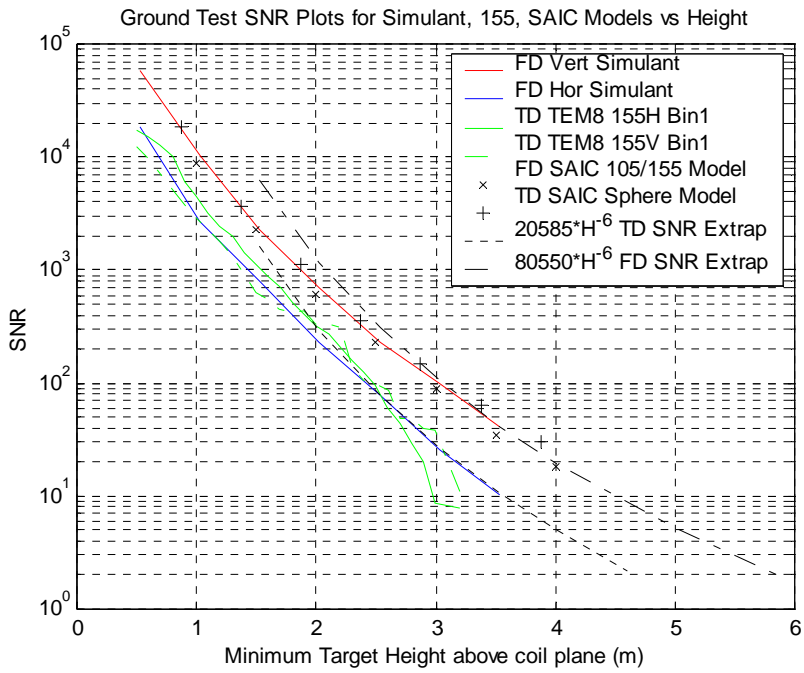


Figure 39. Comparison of FDEM (Case 5 type array) and TEM SNR's for synthetic and actual measurements.

3.6.2.2 Ground Test SNR Comparison:

The Signal/Noise Ratio (SNR) estimates listed in Tables 11-14, a subset of which were plotted in Fig. 39, used noise levels measured for each configuration to provide estimates of the ground-based, static target detection performance of these configurations.

Expressed as ratios to the PFN SNR values, SNR values for the small aluminum test target at 2m sensor-target distance were 1.3 for VD, .46 for pseudo-B VD, and .46 for the bucked configuration (though the bucked configuration data were probably compromised by other issues that would be eliminated in a more thorough test; they would normally be expected to yield SNR values very similar to the PFN configuration). The benefit seen for VD relative to the PFN configuration is reversed at 2.5m sensor-target distances by the higher fall-off rate of the VD response with respect to height. These ratios should be comparable to those for a TEM system of the same configuration.

Comparing SNR for the FDEM and TEM results based on the modeled and observed ground-based data summarized in Fig. 39, it appears that FDEM has a 3:1 to 4:1 advantage over TEM. The fact that SNR is only three to four times higher for FDEM compared to TEM is not surprising in view of the comparable noise levels seen for ground-based FDEM quadrature and TEM off-time data with similar operating frequencies, which ranged from 0.026 to 0.044 ppm for various FDEM mock-up configurations and 0.03 ppm for TEM ground data, corrected for noise bandwidth and transmitter moment

3.6.2.3 Airborne SNR Comparison:

Anticipated airborne noise levels will be higher than observed during ground tests, due to noise sources associated with the helicopter and with vibration of the receiver coils. Observed TEM-8 noise levels with a noise bandwidth of 30 Hz were approximately 0.3 ppm. Computing the corresponding FDEM noise level from the PSD plot shown in Figure 15 (constructed from TEM-8 transmitter-off data for the same 30 Hz noise bandwidth) yielded 0.33 ppm, approximately an order of magnitude larger than the static noise levels, and comparable to the observed airborne TEM-8 noise levels.

Given that this FDEM airborne noise prediction is based on transmitter-off TEM-8 data that employs specialized noise reduction techniques it is possible that airborne FDEM noise levels could exceed comparable TEM noise levels for practically realizable airborne systems. Part of the original project plan for Year 2 was intended to investigate this issue through further tests with the mock-up system.

3.6.2.4 Conclusions for helicopter-mounted transmitter cases

To summarize, computational modeling of system Cases 1-5 has resulted in the following conclusions:

- Cases 1 and 5 yield the best signal levels and perturbation noise for the concentric transmitter-receiver geometry studied;

- Case 2 displays reduced noise due to lower ambient noise pickup, but signal levels are lower than for Case 1. Case 2 is also quite sensitive to vertical motion of the receiver array relative to the transmitter;
- Uniformity of primary magnetic field is a key factor in improving signal amplitudes and therefore signal/noise;
- Quadrature is the best measurement parameter, but actual performance would depend on the accuracy and stability of the inphase/quadrature separation;
- Noise spectral amplitude varies over about 2-3 orders of magnitude, depending on frequency. Proper selection of operating frequency yields similar benefits in FDEM compared to TDEM.

Mock-up static test and comparison to TEM-8 ground and airborne data have yielded the following conclusions:

- Case 1, 2 and 5 signal levels are consistent with model predictions
- Case 2 vertical difference signal levels fall off as seventh power of height rather than sixth power for transmitter-target heights equal to transmitter diameter or higher
- SNR for FDEM in static tests appears to be approximately 3-4 times that of TEM for comparable configurations and transmitter moments. It is important to note that FDEM and TEM data sets have not yet been acquired at one test site under matched noise conditions.
- The extent of in-phase crosstalk into quadrature is low in a properly phased system: an accuracy of 1 part in 1000 was readily achieved in mock-up ground tests.
- Observed static noise levels for transmitter moments of 2400 A-m² were on the order of 0.025 to 0.045 ppm for a 30 Hz noise bandwidth, depending on configuration and ambient noise level variations.
- Airborne noise levels are expected to be 0.3 ppm, comparable to observed TEM noise levels, based on reprocessing of TEM-8 transmitter-off data.
- High mechanical rigidity requirements for FDEM systems could increase achievable airborne FDEM noise levels

3.6.3 Semi-Airborne Configuration (ground-based transmitter)

Although the merits and theoretical benefits of a ground-based transmitter were presented at the Spring 2009 In-Progress Review, the presentation was lacking in details, particularly with regard to the practical aspects associated with implementation. This lack of detail led the review panel to conclude that the design would not be practical, and to direct the project team to abandon assessment of this approach. In this section, therefore, we provide a more substantive description and historical background for the approach in hope that the Project Office will reverse this directive.

Earlier sections demonstrated the value of a transmitter coil that is substantially larger in its lateral dimensions than the survey flight height by comparing responses for 12m and 3m diameter circular transmitter coils. Increased transmitter sizes are beneficial because the transmitted field is more nearly uniform with respect to height variations, so that the received signal fall-off rate for small conductive targets approaches the r^{-3} amplitude dependence of small

confined conductors in a uniform magnetic field. This effect reduces altitude sensitivity, although it does increase anomaly width.

Substantially increasing transmitter size for a fully helicopter-borne system is very difficult. The natural progression from present technology, which would be to mount a 10 or 12m diameter transmitter directly onto the helicopter, could potentially impair helicopter flight performance through weight and moment of inertia increases and would require considerable effort, time and cost to achieve. Another approach would be to fly the transmitter-receiver system as a towed array, but we consider such systems to be untenable due to the extreme difficulty of flying such sensor packages safely at offsets of a few meters above the earth surface, while maintaining lateral position and ground clearance. . The remaining airborne option is to deploy the large transmitter on the ground, and to fly an array of receivers over the area energized by the transmitter. Separating the transmitter from the receiver would also reduce the weight of the airborne system, increase its maneuverability, and might permit acquisition of a full swath of receiver data rather than the split swath presently acquired by the TEM-8 system.

From numerical modeling described earlier, the observed signal for a 1A, one-kilometer square transmitter laid on the ground and a receiver flown at 2m altitude over a standard target buried at 1m below the transmitter plane was 28.3 ppm for a Case 1 vertically oriented, 1m diameter receiver coil, and 10.3 ppm for the Case 2 1 m diameter, 0.5m separation vertical difference coil. These signal levels are considerably higher than the 2.4 and 20.2 ppm Case 1 amplitudes obtained for 3m and 12m diameter transmitters; the corresponding Case 2 amplitudes were 1.3 and 10.2 ppm. Inphase perturbation noise with the ground based transmitter was four times lower for vertical displacements of the Case 2 vertical difference coil than for the Case 1 receiver coil, and over three times lower for small pitch errors. Ambient noise pickup would also be reduced for vertical difference measurements, although further study is required to determine the potential degree of such noise cancellation. These considerations suggests that using vertical difference coils of suitable sensitivity would be a good starting point for receiver design using the ground-based transmitter approach.

The anomaly width for the modeled standard target with a Case 1 receiver, as measured at 1/3 peak amplitude, is approximately 4m (see p. A2A-2 in Appendix 2A.) Smaller receiver coil diameters yield slightly higher peak amplitudes, while the largest diameter (2m) yielded higher amplitudes on the flanks. Anomaly widths are somewhat wider for this approach than with a moving source because of reduced signal attenuation with distance from the target. While this effect may slightly decrease lateral resolution, it should improve detection capability for a given system noise level by increasing the number of sample points within the strongest part of the anomaly.

Frequency-dependent susceptibility (FDS) effects were not directly assessed for the ground-based transmitter. However, the fact that modeling indicated a weaker FDS effect for the 12m transmitter loop compared to the 3m loop is a positive indication. It is also consistent with survey experience in areas of superparamagnetic soil in Australia (Buselli, 1982), where coincident-loop (in which transmitter and receiver loops are laid as one cable) ground TEM surveys were found to be strongly affected by FDS effects, while central-loop surveys (in which the receiver is located near the center of a large loop) are much less strongly affected, owing to

the separation between transmitter and receiver. FDS effects should thus be attenuated for a large ground loop relative to the 3m transmitter configuration.

In concept, a semi-airborne system would consist of a boom-mounted array of receiver coils, similar to those in the Battelle TEM-8 system, a ground-airborne synchronization system, and a ground-based transmitter wire loop with associated power supply and transmitter console. A significant benefit of this configuration is that the mass and moment of inertia of booms and boom-mounted hardware would be considerably less than in the current TEM-8 system. The receivers could be mounted in a pair of single lateral boom and in a forward array much as in the Arrowhead or VG magnetometer systems. This would reduce the support structure mass relative to the TEM-8 boom structure while enabling data to be acquired in a full 12m swath without interleaving, making the system efficiency during airborne operations equivalent to that of magnetometer systems.

We would anticipate using a transmitter loop of 1-5 km² area, enclosing between 250 and 1250 acres. Thus in many cases, the entire project survey area could be enclosed in a single transmitter loop. Even if flying at 10-20% coverage, such a loop size would be compatible with daily acquisition rates for airborne systems. The wire could be deployed by helicopter or by all-terrain vehicle. The latter approach is preferred where site conditions and explosive safety allows.

There is a precedent for this approach in earlier “semi-airborne” systems that were deployed by the mineral prospecting industry. Two of these are discussed in the literature: the TURAIR system, an adaptation of the totally ground-based TURAM system, and the FLAIRTEM system. The TURAIR and TURAM systems both used large ground-based transmitter loops (9-15 km²) with a frequency-domain transmitter. The TURAIR system was developed for the specific purpose of increasing the depth of exploration for airborne EM exploration. The FLAIRTEM system employed a time-domain transmitter with airborne receivers. Emplacing the transmitter coil for these systems was straightforward:

“Under average conditions a primary field loop of 3 x 5 km can be laid down by helicopter and the transmitter positioned within little more than one hour. By vehicle or by hand more time is required.”

-Siegel Associates Australasia Pty Ltd., ASEG Bulletin v. 2, no. 3, 1971, p. 42

Elliott (1995) provides a photograph of a suspended device used with a helicopter and achieving a reported rate of 15-20km/hour for laying the transmitter cable. Transmitter loops in this size range are also used for ground-based deep-penetration mineral surveying.

At most DoD sites, it is safe to drive an ATV around the perimeter of the survey area. This would assure precise positioning of the transmitter, since the loop perimeter could be mapped during layout; it would avoid above-ground emplacement of the wire (in trees, shrubs, etc) which could endanger animals; and it would reduce any risk that might be associated with deployment of the wire from the air.

In the TURAIR system, a transmitter current of 2-4 amperes was used to transmit at frequencies between 100 and 800 Hz. As a starting point, we would anticipate using frequencies of 150 and 1000 Hz, and somewhat higher transmitter currents to accommodate increased sampling rates. Currents in this range can be driven through suitable wire at modest transmitter power levels: for example, using a 10A waveform, power dissipation in 4 km of AWG 10 copper wire is on the order of 1 kW. When used with reasonable electronic and procedural precautions, such currents should not present significant fire or shock hazards. For example, careful monitoring of current and voltage by the transmitter electronics and control software could detect breaks or current leakage and shut down the transmitter instantaneously. Procedurally, the transmitter wire could be inspected before starting operations each morning before starting the survey to detect insulation damage caused by chewing, cutting, or otherwise breaking or weakening the wire.

In the past, some have questioned the suitability of using an active source for detecting UXO, fearing that it might cause detonation of ordnance that would endanger the crew or facilities. These concerns are generally shown to be negligible due to the weakness of the transmitted signal. By using a ground-based transmitter, such concerns would be reduced further because the transmitter would be activated over a large area in advance of flight operations, so that any detonations (though highly improbable) would be most likely to occur before the helicopter becomes airborne, and would be independent of the position of the aircraft.

Suitable transmitters and generators are available from commercial sources, while existing electronics and mounting hardware could be used for ground and airborne tests. The most complicated aspect of operating a semi-airborne UXO detection system would be in synchronizing the transmitter and receiver. For the low-frequency system that is under consideration, the most practical method for synchronization would be to use oven-stabilized high-precision quartz timebases, synchronized at the outset of each day and “disciplined” using GPS time signals to maintain their synchronization during the day. Such devices are commercially available, but would need to be integrated and tested with the transmitter and receiver hardware.

In summary, the semi-airborne approach has a precedent in the TURAIR and FLAIRTEM systems, demonstrating that it should be practical for field operations. It has additional safety benefits in reducing the mass and moment of inertia of the boom/sensor structure on the helicopter and further reducing the already-negligible risk of detonation. This design would be more operationally efficient than the TEM-8 system because it could acquire data in a full 12m swath. Calculations described in earlier sections of this report of semi-airborne system response indicate similar or enhanced ppm anomaly amplitudes to those of the two airborne-transmitter FDEM systems discussed in this report.

4. Conclusions to Date and Recommendations for Priorities for Remainder of this Project

A key objective of the project at its inception was to predict whether or not FDEM can provide higher airborne SNR than TEM methods. Other objectives were to examine and assess the options for dynamic range compression in EM methods, to measure FDEM responses using mock-up hardware for a variety of UXO targets, and to assess a ground-based transmitter

approach with a roving receiver as an alternative to more conventional moving-source EM methods for UXO detection.

Through model and mock-up measurements using multiple configurations, FDEM has been demonstrated to yield signal levels on the order of three to four times higher than TEM, for comparable transmitter-receiver geometries. The Battelle TEM-8 system has been used as a basis for calculating TEM capability because it is the only available TEM system for the UXO application, and thus the only available benchmark. Noise levels were assessed in order to estimate SNR for these methods. Preliminary ground-based noise estimates from the FDEM mock-up in a relatively noisy location suggest noise levels at 135 Hz of about .03 ppm for a 30 Hz output bandwidth, compared to TEM noise levels (in a different but comparable location) of about .08 ppm for 90 Hz in Bin 1, corresponding to .03 ppm at the standard TEM-8 Tx current amplitude. SAIC reprocessing of TEM-8 airborne transmitter-off noise as pseudo-FDEM data suggests airborne FDEM noise levels of 0.33 ppm, compared to observed TEM airborne noise estimates of 0.3 ppm. These ground and airborne noise estimates are essentially identical, and their consistency suggests that while FDEM may offer an SNR advantage of up to 4 times due to higher signal levels, it is unlikely to yield an order of magnitude or more increase in SNR relative to TEM using similar transmitter-receiver geometries and base frequencies.

It should be noted that the greater difficulty (and potentially increased weight and complexity) of constructing a rigid array suitable for FDEM measurements could offset or negate the modest SNR advantage observed with FDEM in this study.

Increasing the 3m transmitter size by a factor of four while maintaining the same transmitter current increases the anomaly (as measured in ppm) of a standard target by almost an order of magnitude for transmitter-target vertical separations of 3m or more and reduces the sensitivity of the response amplitude to height. Larger airborne transmitters increase the conductivity response of soils, but decrease frequency-dependent susceptibility effects. Practical difficulties are likely in safe field deployment of such a large transmitter.

In contrast, as summarized in the previous section, a ground-based transmitter (semi-airborne configuration) seems to be worthy of further consideration at this stage. The key benefit of using a very large ground-based transmitter, rather than a helicopter-mounted transmitter, is that it maximizes the uniformity of the primary field while removing the weight, moment of inertia and complexity of the transmitter support structure and electronics from the helicopter, and would permit acquisition of full swaths of EM data. Deployment of very large transmitter loops for ground and semi-airborne surveys is a routine operation in the mining exploration industry, which uses them to increase the depth of exploration

In summary, analysis to date indicates that a 3-4 times improvement in SNR is possible for FDEM systems over the existing TEM-8 system. This is not a ‘hard and fast’ figure, and the actual SNR improvement of an FDEM system could range from none to about an order of magnitude. An improvement of four times in SNR could enable data acquisition at 1m greater height than current capability, and this would be a valuable improvement in the technology. Further mock-up and airborne testing would be required to refine this estimate.

If the SERDP Program Office were to so direct, we believe that there would be value in dedicating additional effort to improving this estimate.

However, based on the modeling presented in this report, we find the calculated performance of a semi-airborne (ground-based transmitter) configuration to be much more compelling, with the potential to yield a breakthrough in airborne UXO mapping and detection capability. Calculations that have been conducted to date are preliminary and additional computational modeling and physical testing is required to validate and refine the current result. Testing with ground-based transmitters and receivers would further confirm the approach. This configuration could be beneficial for both airborne and ground-based receiver arrays. The approach would differ from the sub-audio magnetic (SAM) approach because it would not aim toward integrated magnetometer – EM measurements, with its inevitable compromises in terms of EM sensitivity, and could operate at higher frequencies than are optimal for SAM.

It is therefore our recommendation that plans to focus the second year effort toward more exhaustive evaluations of the performance of selected Case 1-5 configurations be preempted by a more detailed examination of the semi-airborne configuration. This is in keeping with the original intent of the project, in which selected configurations from Year 1 would be assessed in more detail in Year 2.

We propose that the following tasks become the focus of effort in Year 2, all related to the semi-airborne approach:

1. Detailed assessment of anticipated signal and noise arising from various sources for Case 2 and Case 4 style receiver configurations (with ground-based transmitter):
 - a. Model variable ground response as a function of height for these configurations. We propose to extend the current SAIC codes to address this need, and to perform additional modeling using codes that are available within the EM research community
 - b. Model frequency-dependent susceptibility response as a function of height for a realistic source layer thickness (this should be compared with the halfspace response)
 - c. Measure ambient noise amplitudes as a function of receiver height for these receiver configurations
 - d. Measure helicopter noise emissions for these receiver configurations. We plan to measure noise using a ground-based transmitter with the existing receivers on the TEM-8 system. Additional airborne measurements will be made with Cases 2 and 4 receiver configurations to assess degree of noise cancellation obtained with these arrays.
 - e. Model and measure vibration effects in ground-based transmitter field for these receiver configurations
 - f. Model and measure the above effects as a function of horizontal position relative to ground-based transmitter. Determine effective useful area.
2. Although modeling indicates a significant signal performance improvement for a FDEM semi-airborne system over a fully airborne TEM configuration, it does not address comparison with a semi-airborne TEM configuration. As part of the above measurements, we will compare the benefits of TEM and FDEM systems which both use a ground-based transmitter.

3. Consider operational constraints on system viability:
 - a. Analyze Case 2 and Case 4 receiver coil array requirements for ambient noise rejection performance under airborne conditions, effective area, rigidity, weight, thermal noise and electrical characteristics, and build mock-up for bench and ground-based testing
 - b. Assess required transmitter capabilities (current, voltage, timebase stability)
 - c. Assess transmitter cable diameter and weight for the likely range of transmitter size and currents
 - d. Consider practical cable deployment and retrieval procedures
 - e. Assess available transmitter safety mechanisms and related operating procedures
 - f. Analyze modifications to TEM-8 console required to accommodate a high-stability, GPS-disciplined timebase.
4. Conduct simple ground-based signal and noise measurements using frequencies that would be operationally suitable for airborne deployment, using the Battelle airborne UXO test grid near Columbus, Ohio

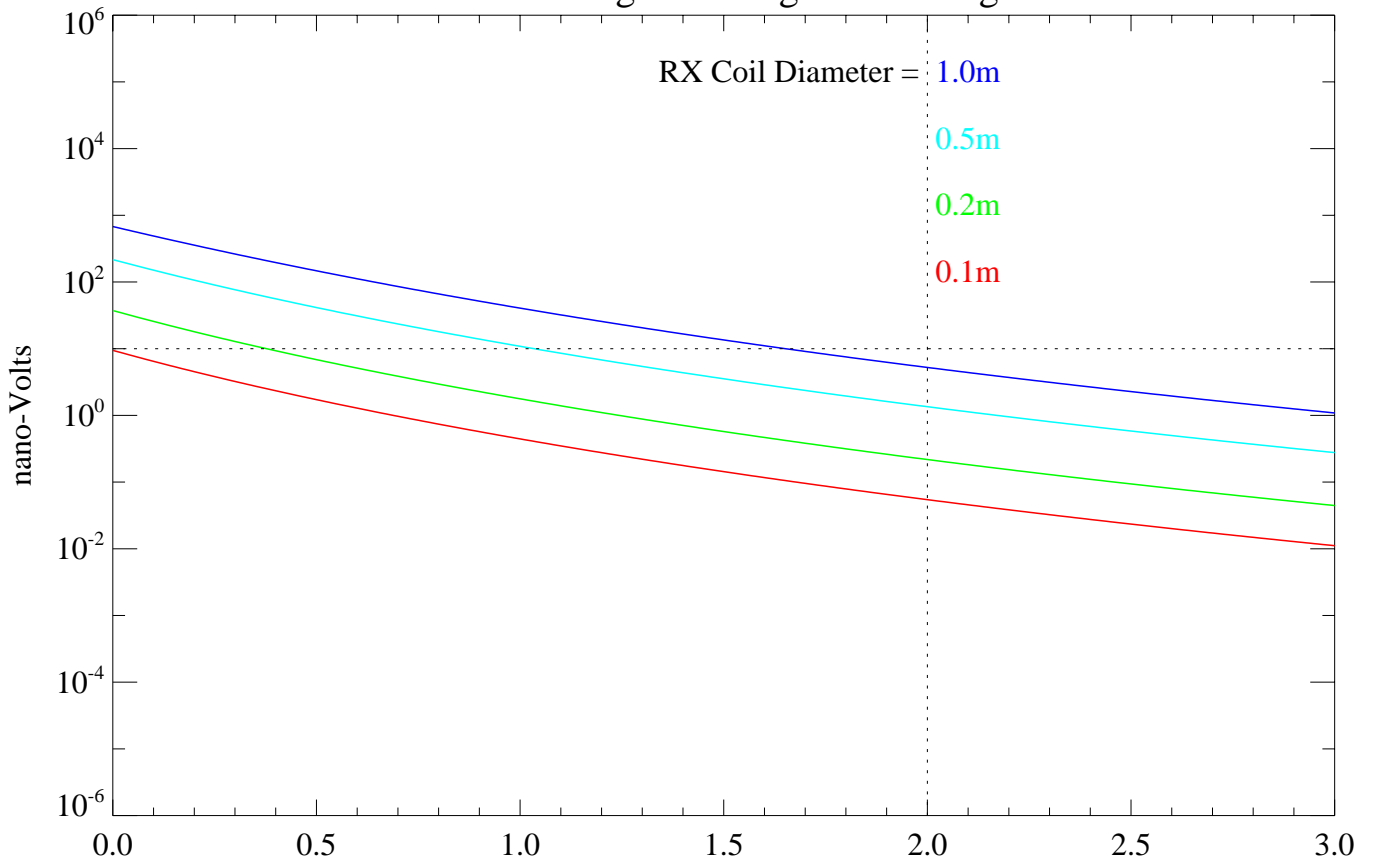
5. Literature Cited

- Buselli, G, 1982, The effect of near-surface superparamagnetic material on electromagnetic measurements, *Geophysics* V47, No 9, September 1982, p. 1315-1321.
- Das, Y., 2004, "A preliminary investigation of the effects of soil electromagnetic properties on metal detectors," *Proc. SPIE*, vol. 5415, pp. 677-690, Apr. 2004.
- Das, Y. , 2006, "Effects of Soil Electromagnetic Properties on Metal Detectors," *IEEE Trans. Geosci. Remote Sens.*, vol. 44, no. 6, pg. 1444-1453, June 2006.
- Elliott, P., 1995, FLAIRTEM – A deep exploration airborne electromagnetic method, *Preview*, n.55, 21-24.
- Elliott, P., *The Principles and Practice of FLAIRTEM*, 1998, *Exploration Geophysics*, v. 29, p. 58-60.
- ESTCP MM-0508, 2006, *Technology Demonstration Report: Quantification of Noise Sources in EMI Surveys*, Army Research Laboratory Blossom Point Facility, Maryland July - September, 2006.
- Grant, F. S., and G. F. West, 1965, *Interpretation theory in Applied Geophysics*, McGraw-Hill, 584pp.
- Nelson, H. H., B. Barrow, T. Bell, R. S. Jones, B. San Filipino, and I. J. Won, 2002, "Frequency Domain Electromagnetic Sensors for the Multi-sensor Towed Array Detection System," NRL/MR/6110--02-8650 (November 27, 2002).
- Pasion, L.R., S. D. Billings and D. W. Oldenburg, 2002, "Evaluating the effects of magnetic soils on TEM measurements for UXO detection," *Proceedings of 2002 UXO/Countermine Forum*.
- Seigel Associates Australasia Pty. Ltd., 1971, TURAIR, A recent development in semi-airborne electromagnetic prospecting, *ASEG Bull.*, v. 2, n. 3, p. 25-45.
- Simms, Janet E., Robert J. Larson, William L. Murphy and Dwain K. Butler, 2004, "Guidelines for Planning Unexploded Ordnance (UXO) Detection Surveys," USAEC/ERDC Technical Report ERDC/GSL TR-04-8, August 2004
- West, G. F., 2009, Audio Frequency Magnetic Induction in Soils, Extended abstract, presented at SAGEEP 2009, p. 527-540.

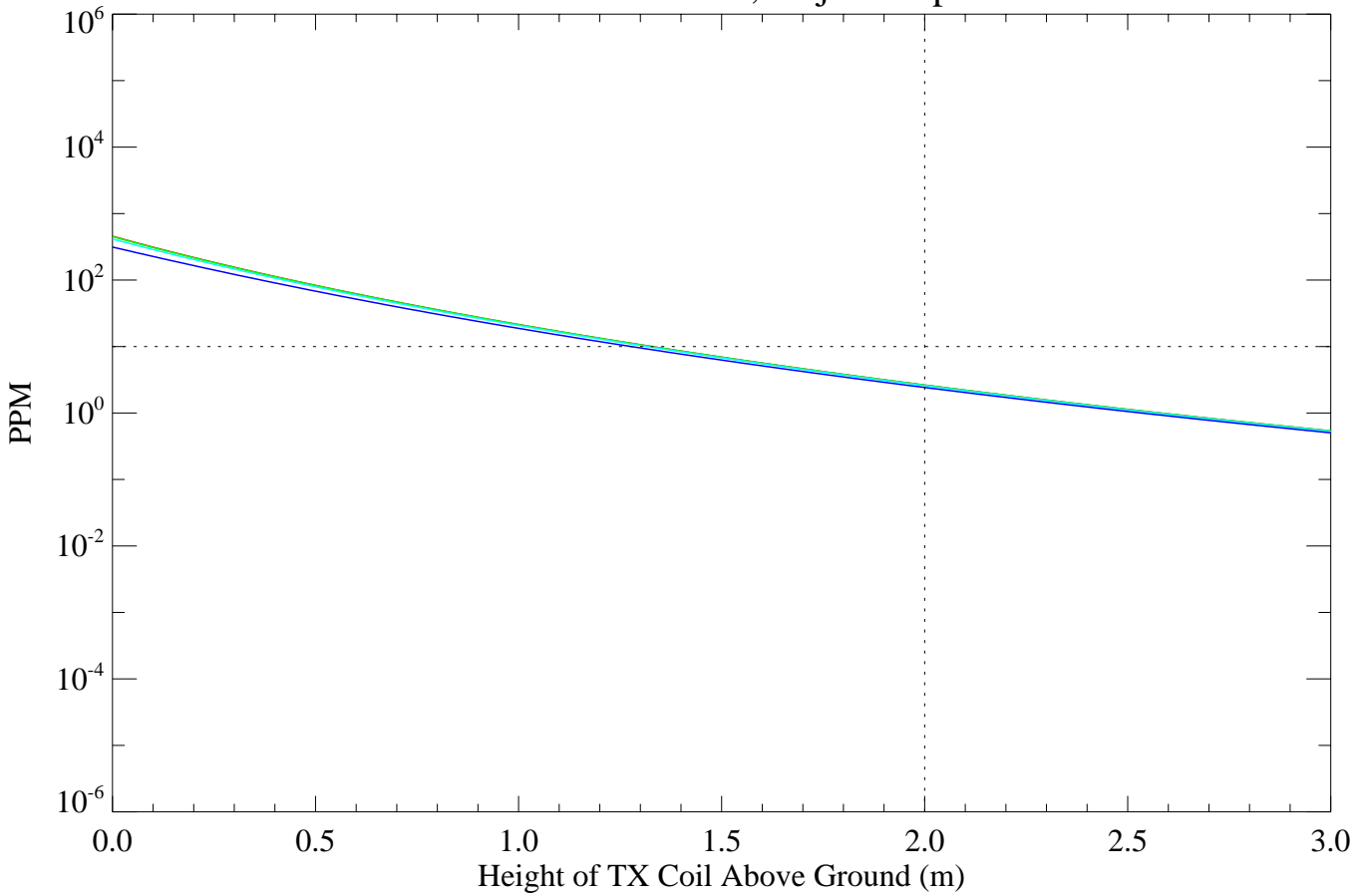
Appendix 1A

Plots of the signal strength modeling results for the sensor configurations of Figure 3.

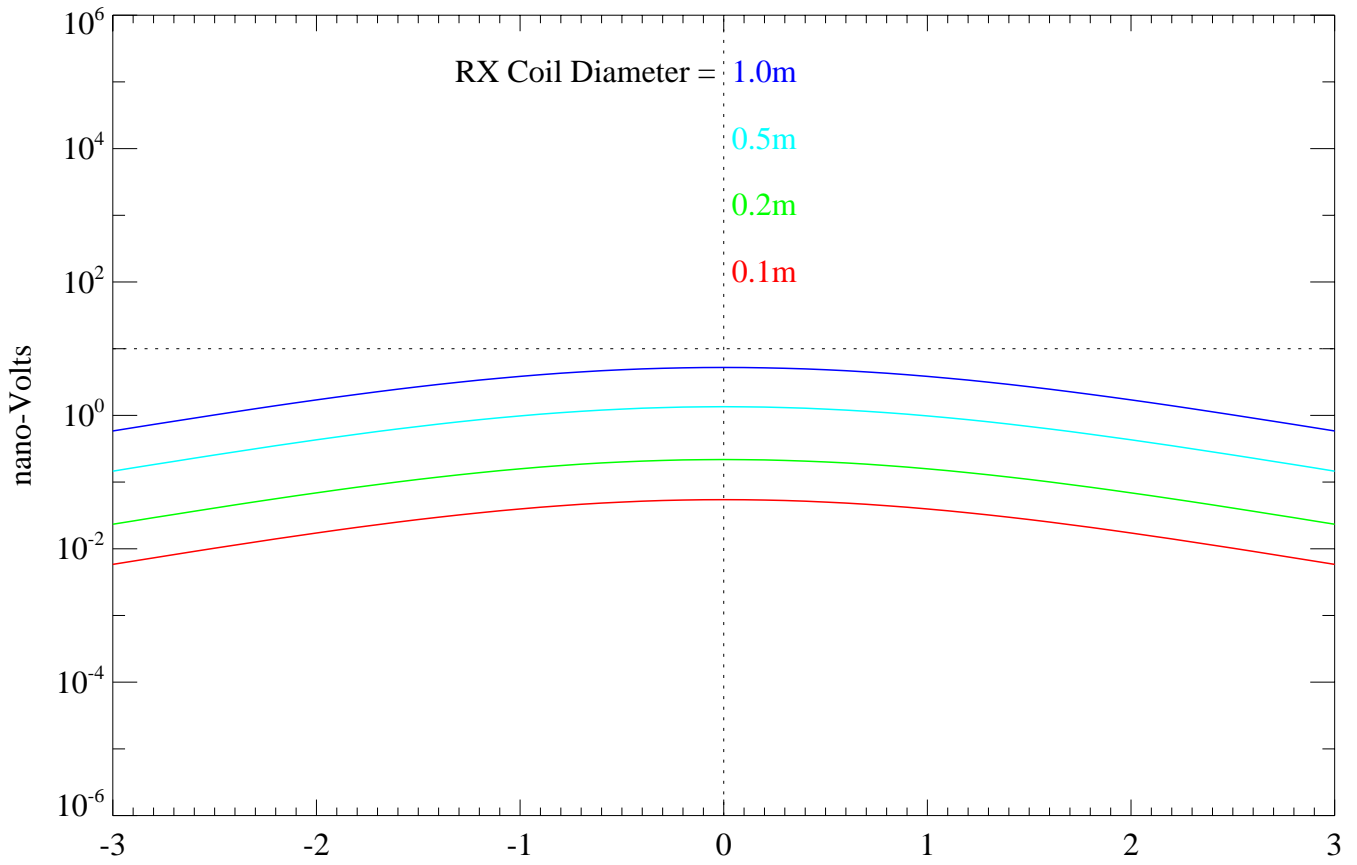
CASE 1 - Signal Strength with Height



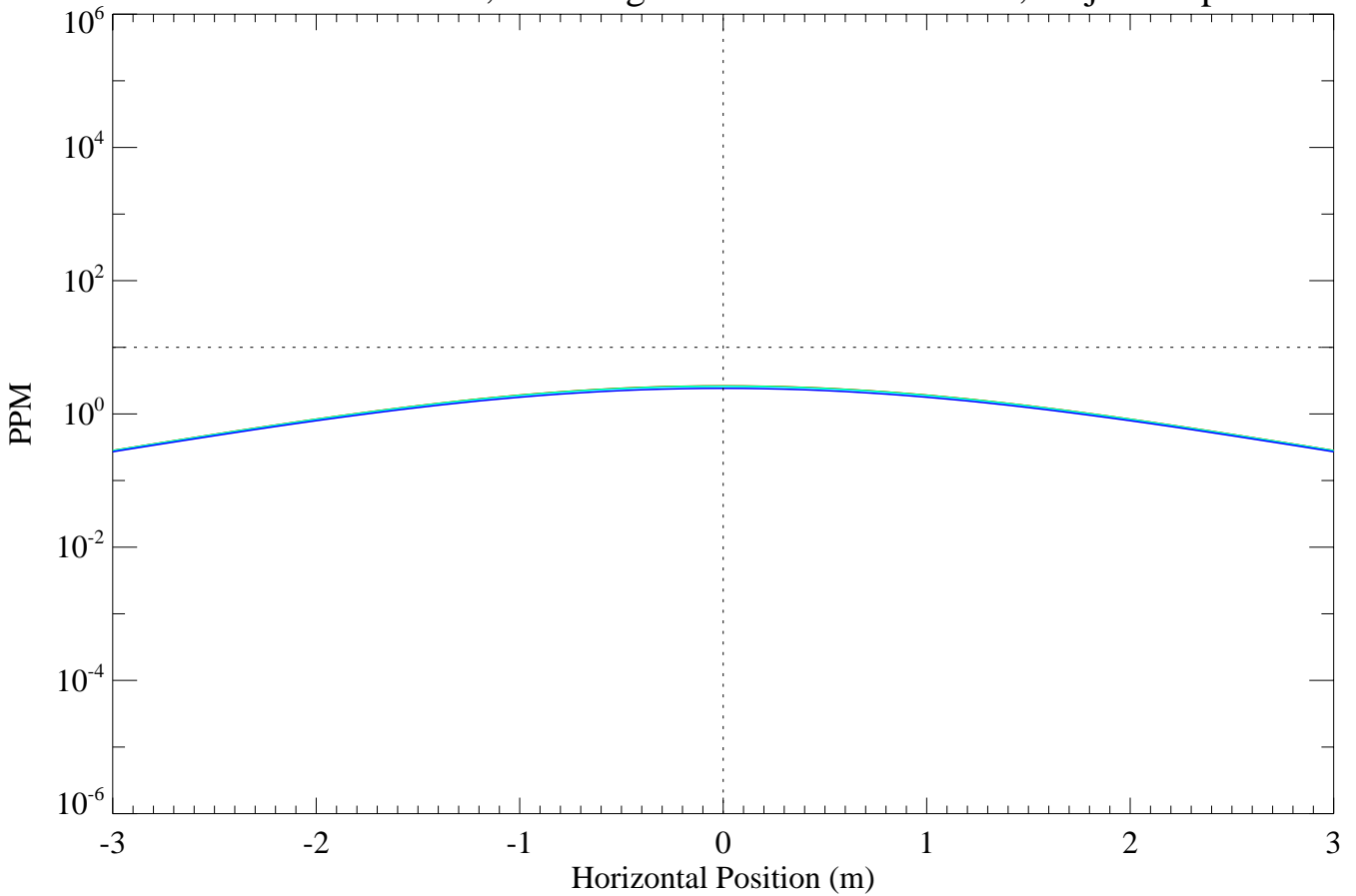
TX Coil Diameter=3.0m, Object Depth=1.0m



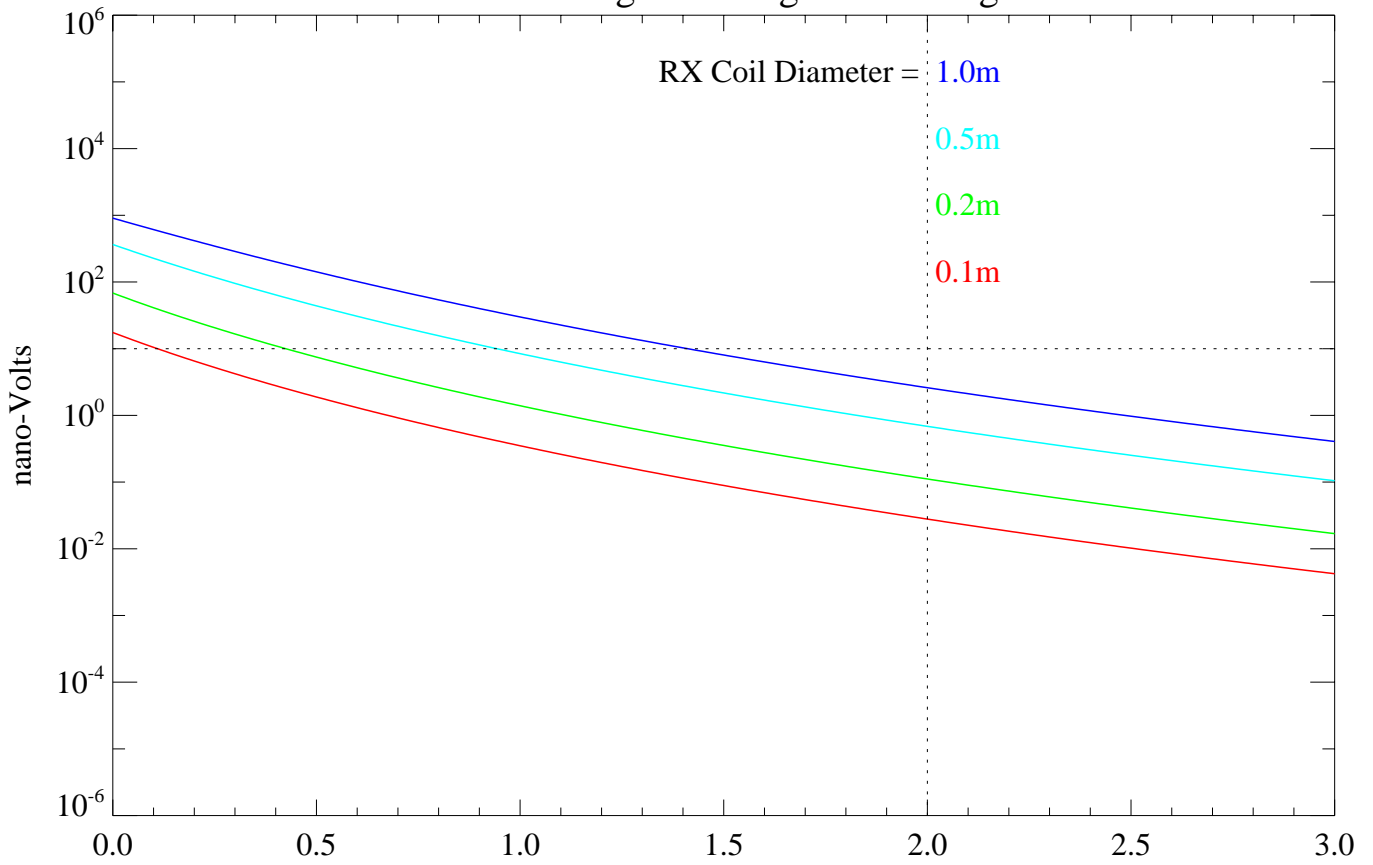
CASE 1 - Horizontal Profile



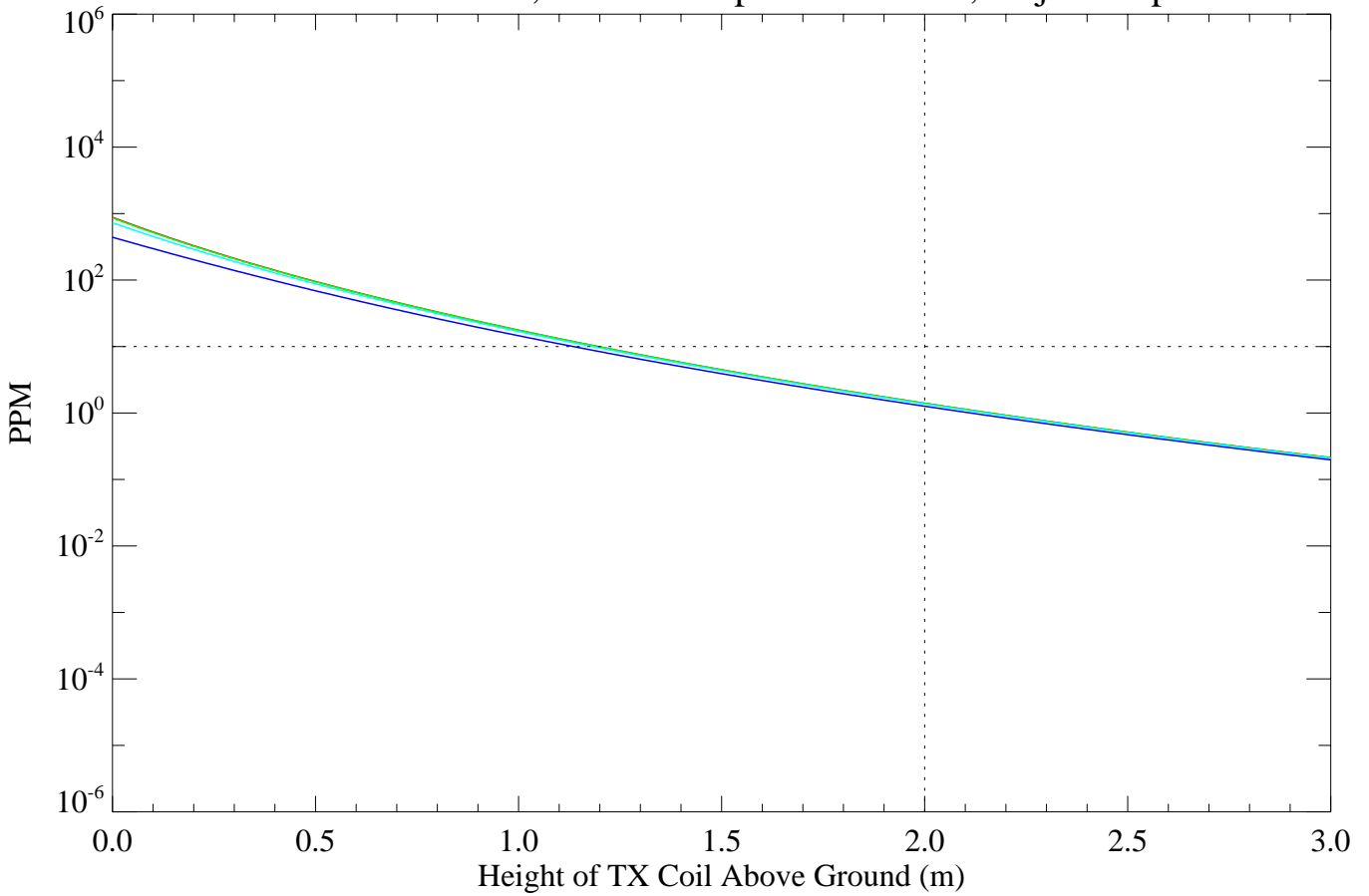
TX Coil Diameter=3.0m, TX Height above Ground=2.0m, Object Depth=1.0m



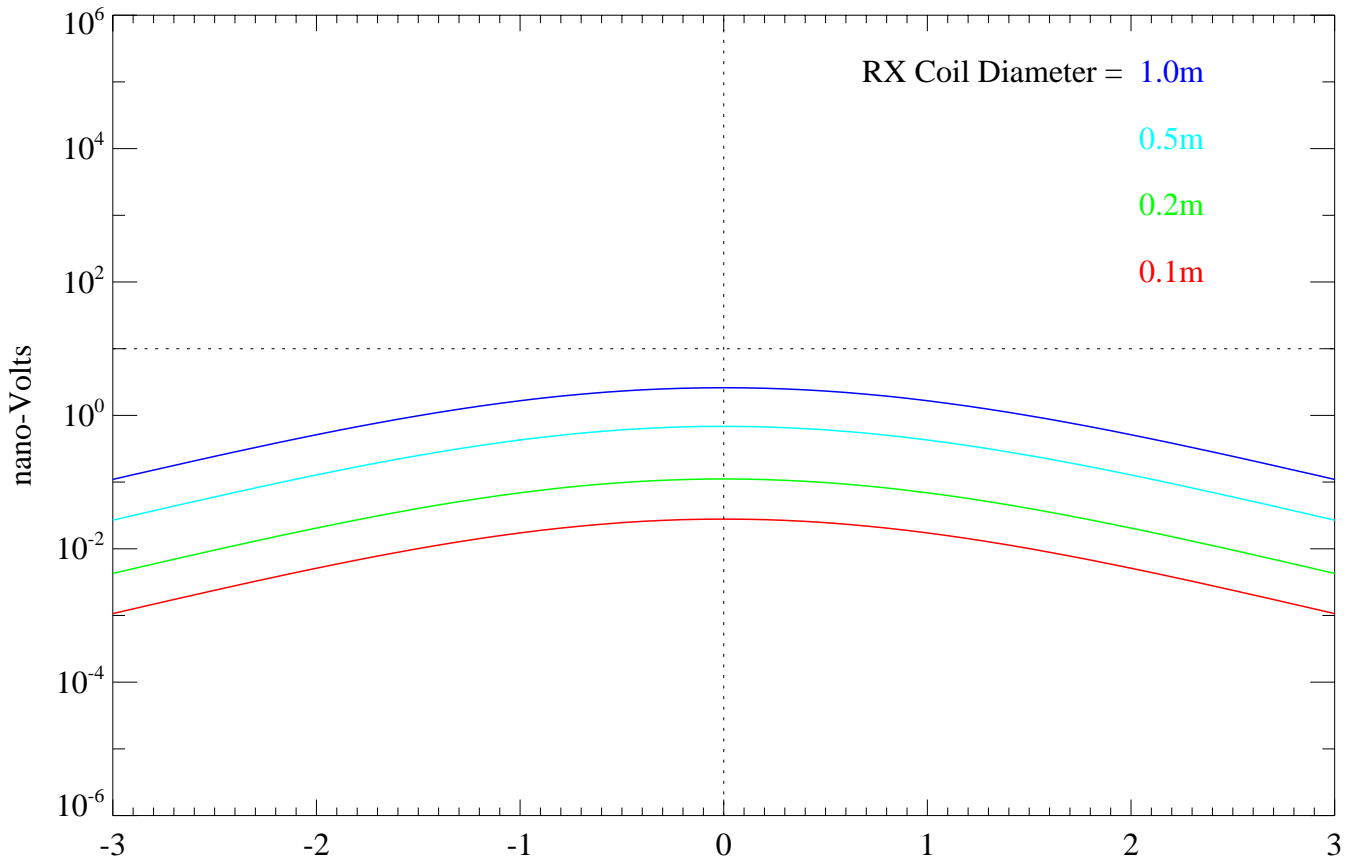
CASE 2 - Signal Strength with Height



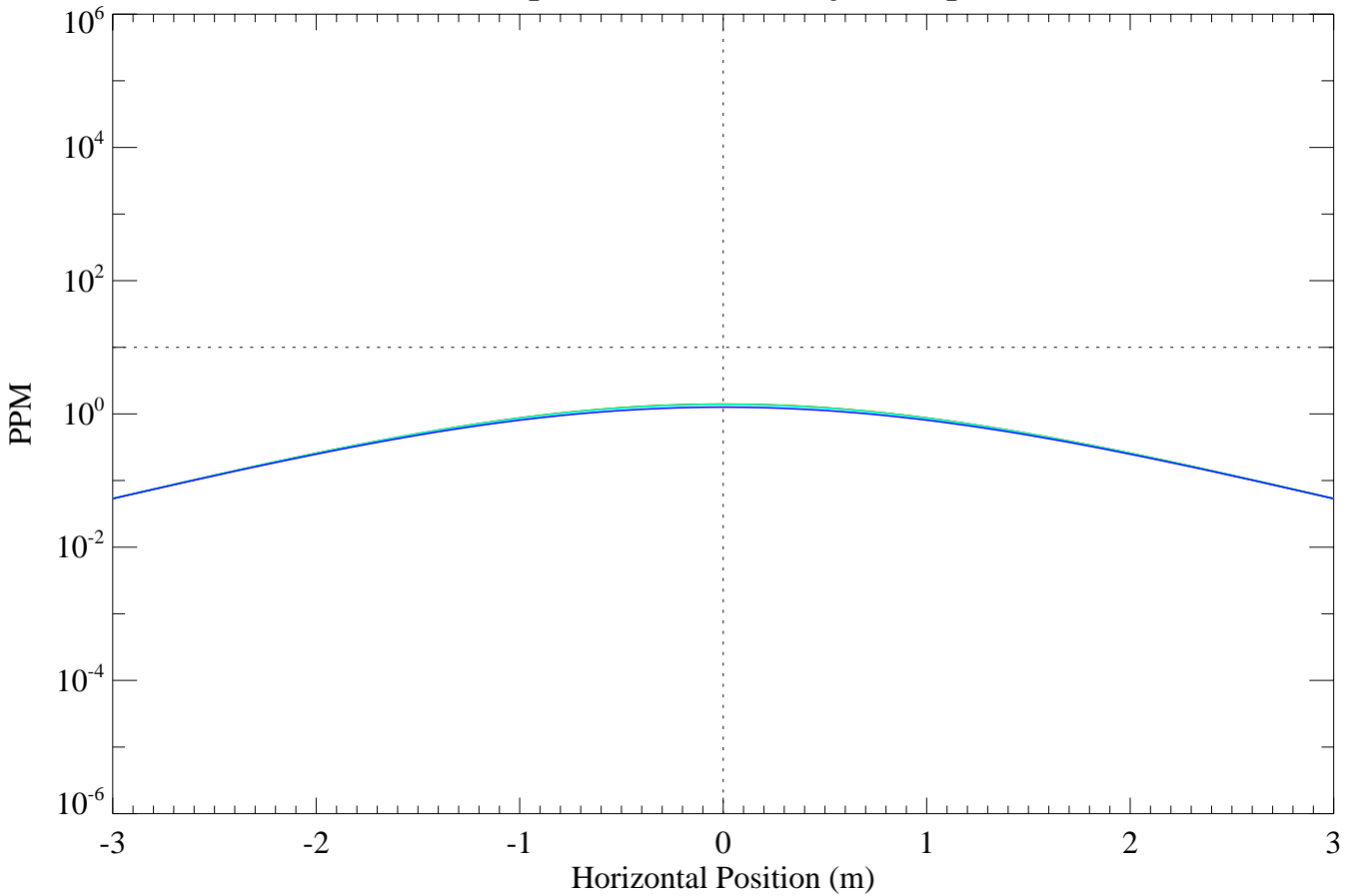
TX Coil Diameter=3.0m, RX Coil Separation=0.5m, Object Depth=1.0m



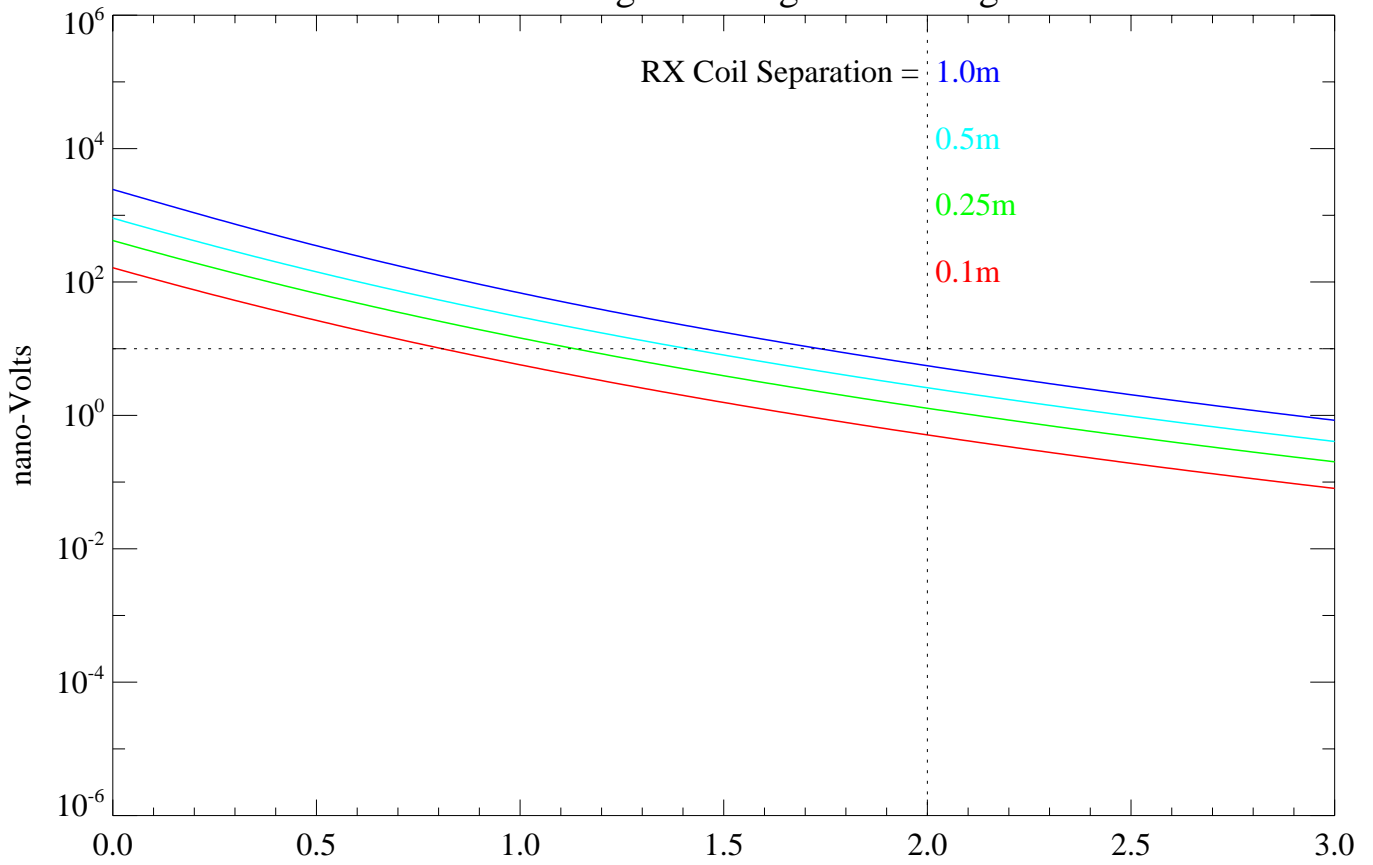
CASE 2 - Horizontal Profile



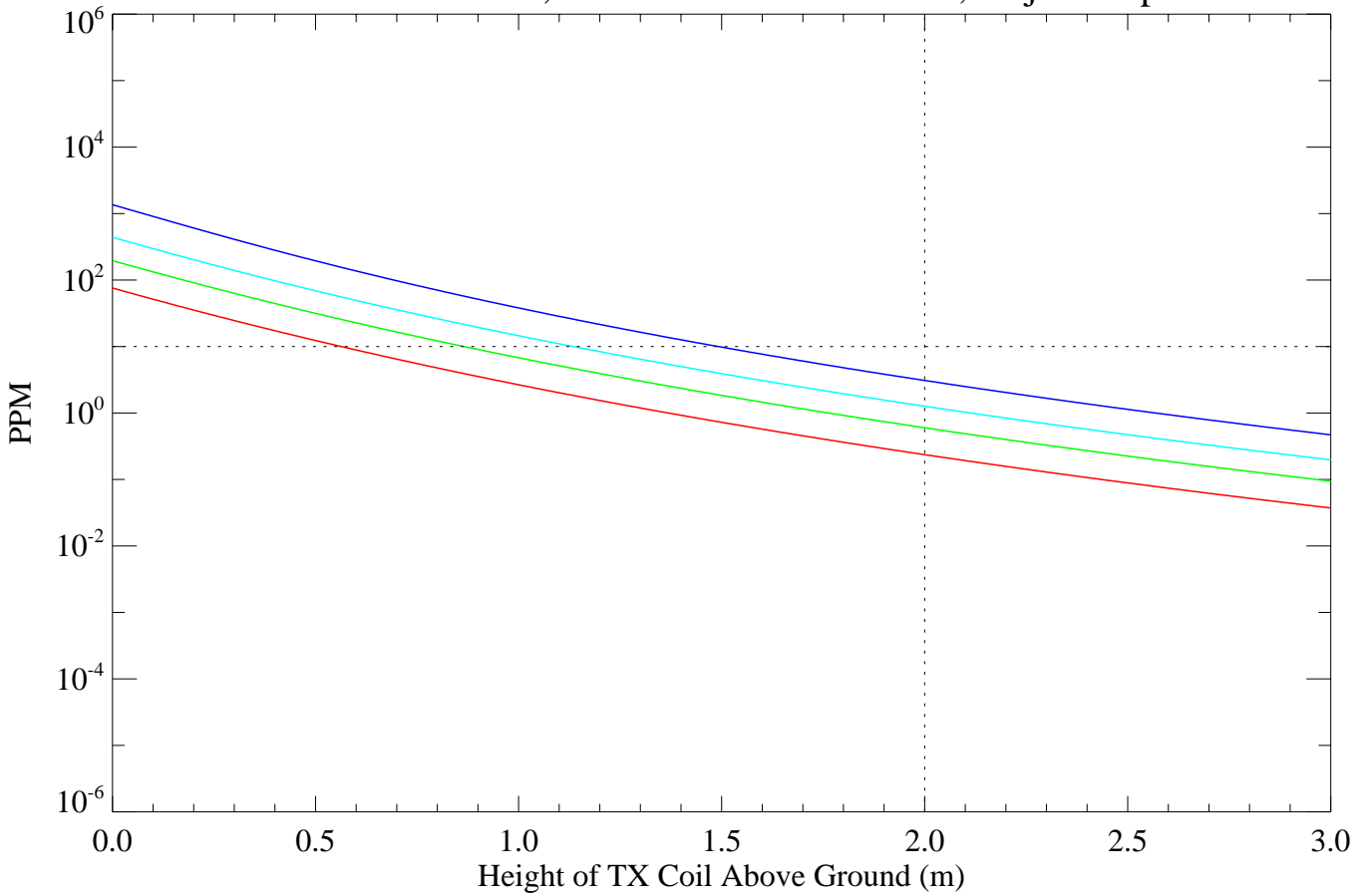
TX Coil Diameter=3.0m, TX Height above Ground=2.0m
RX Coil Separation=0.5m, Object Depth=1.0m



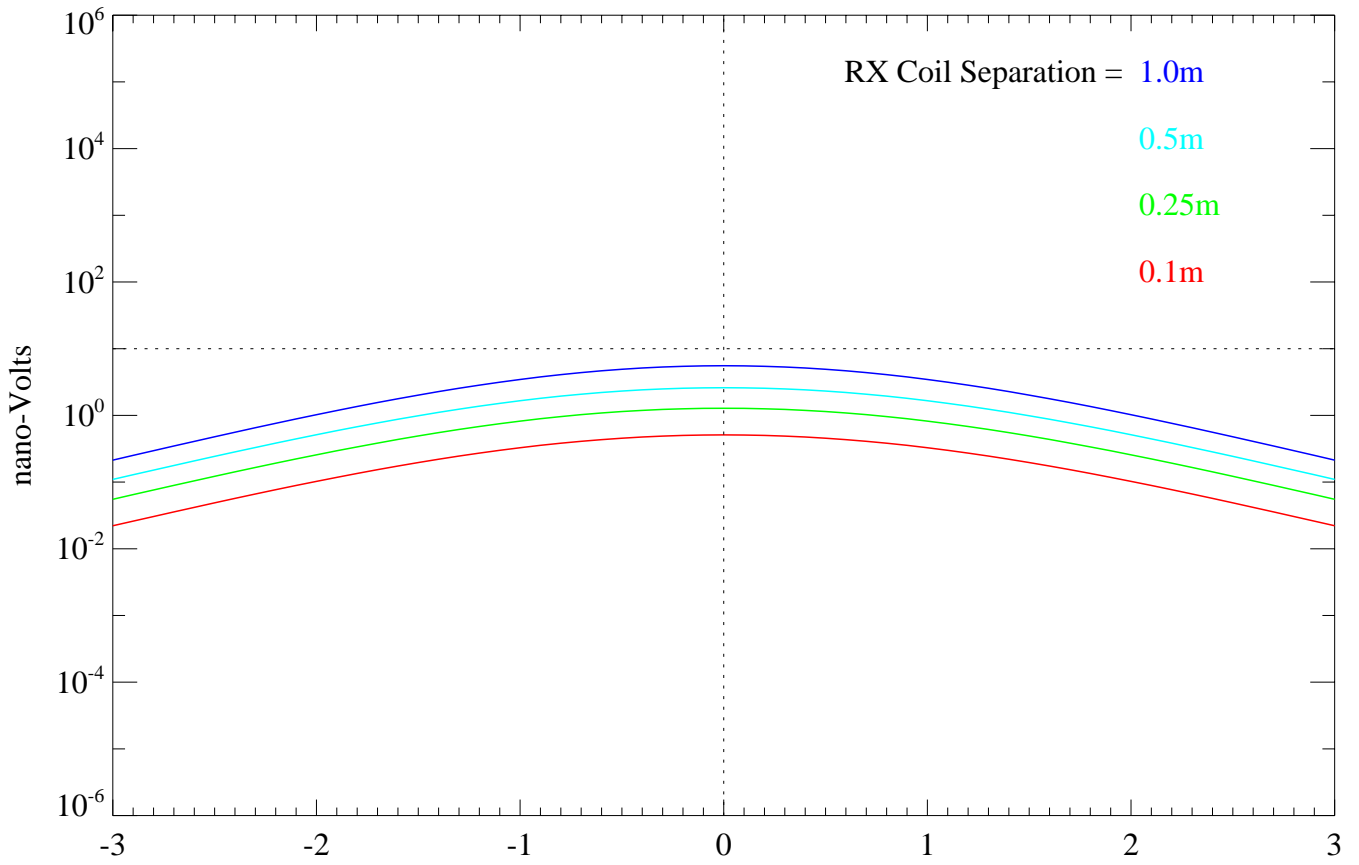
CASE 2 - Signal Strength with Height



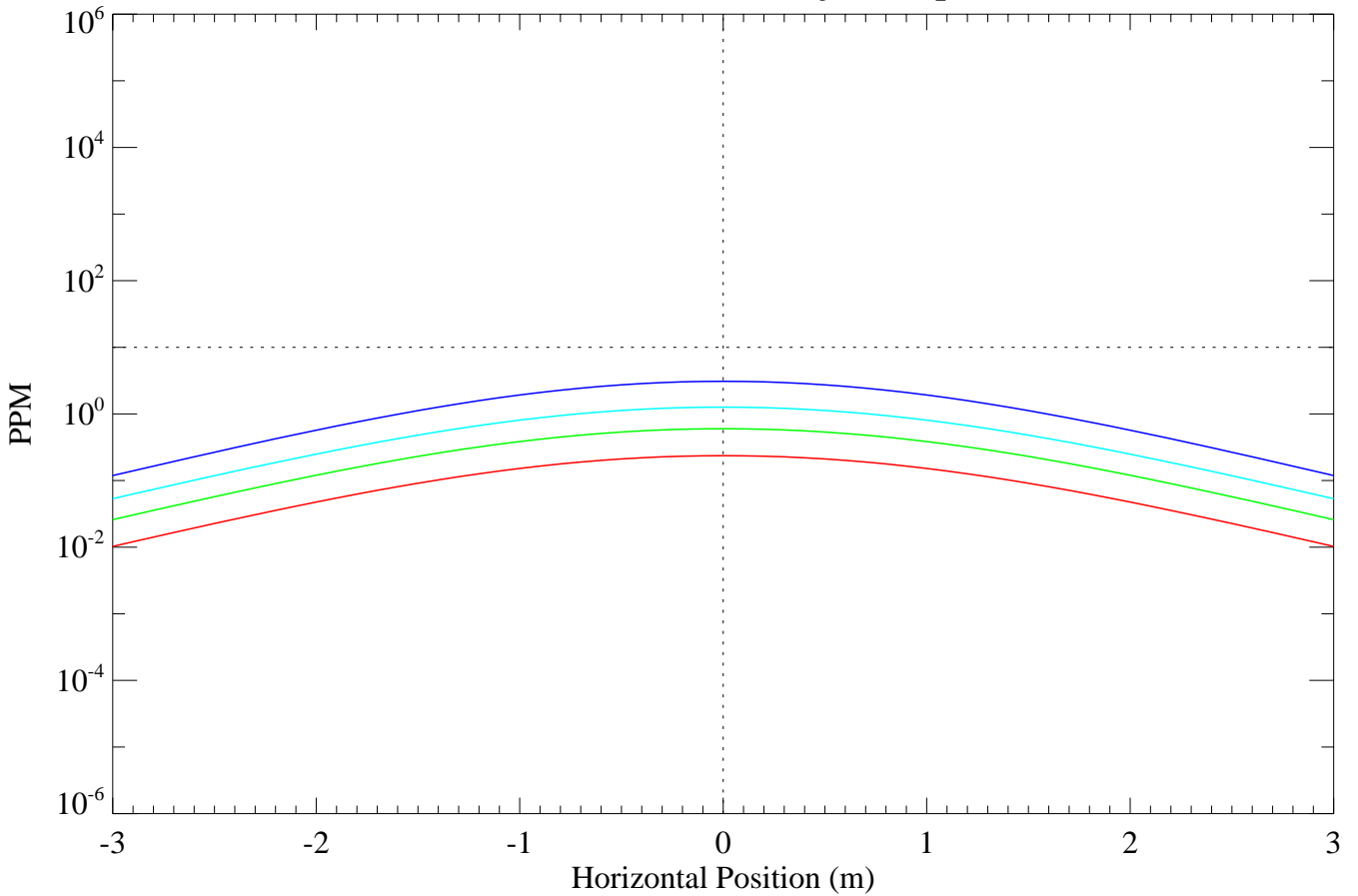
TX Coil Diameter=3.0m, RX Coil Diameter=1.0m, Object Depth=1.0m



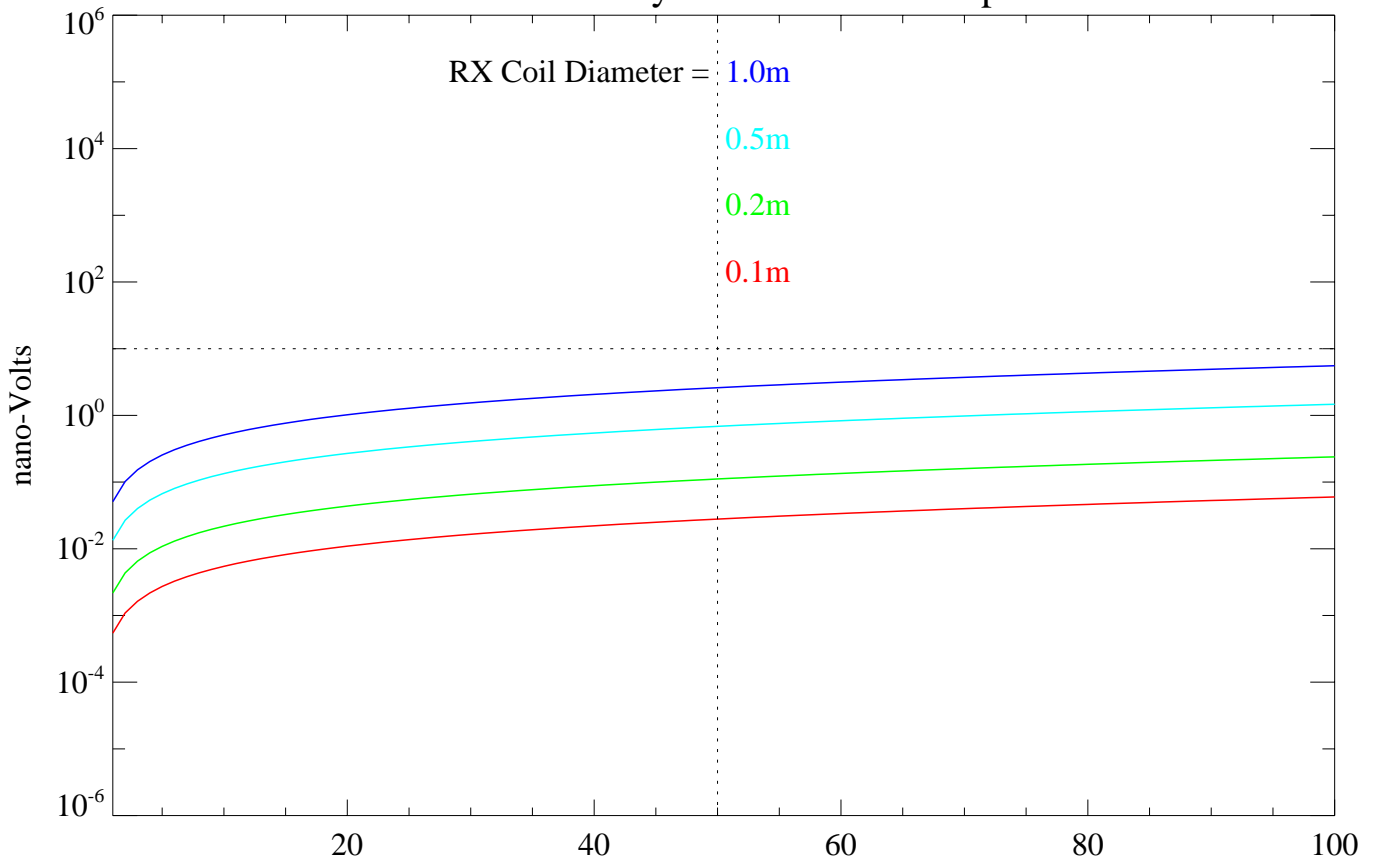
CASE 2 - Horizontal Profile



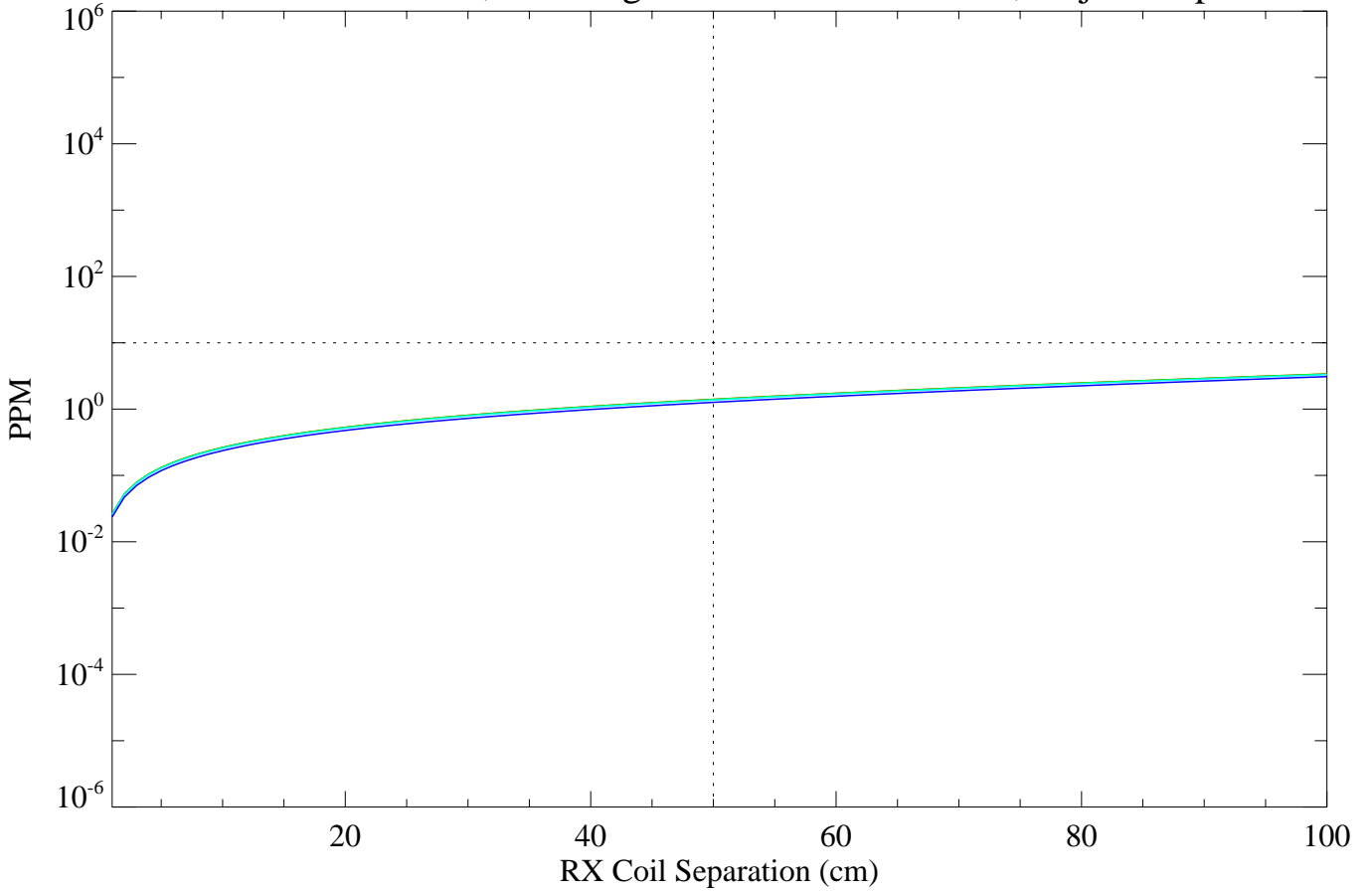
TX Coil Diameter=3.0m, TX Height above Ground=2.0m
RX Coil Diameter=1.0m, Object Depth=1.0m



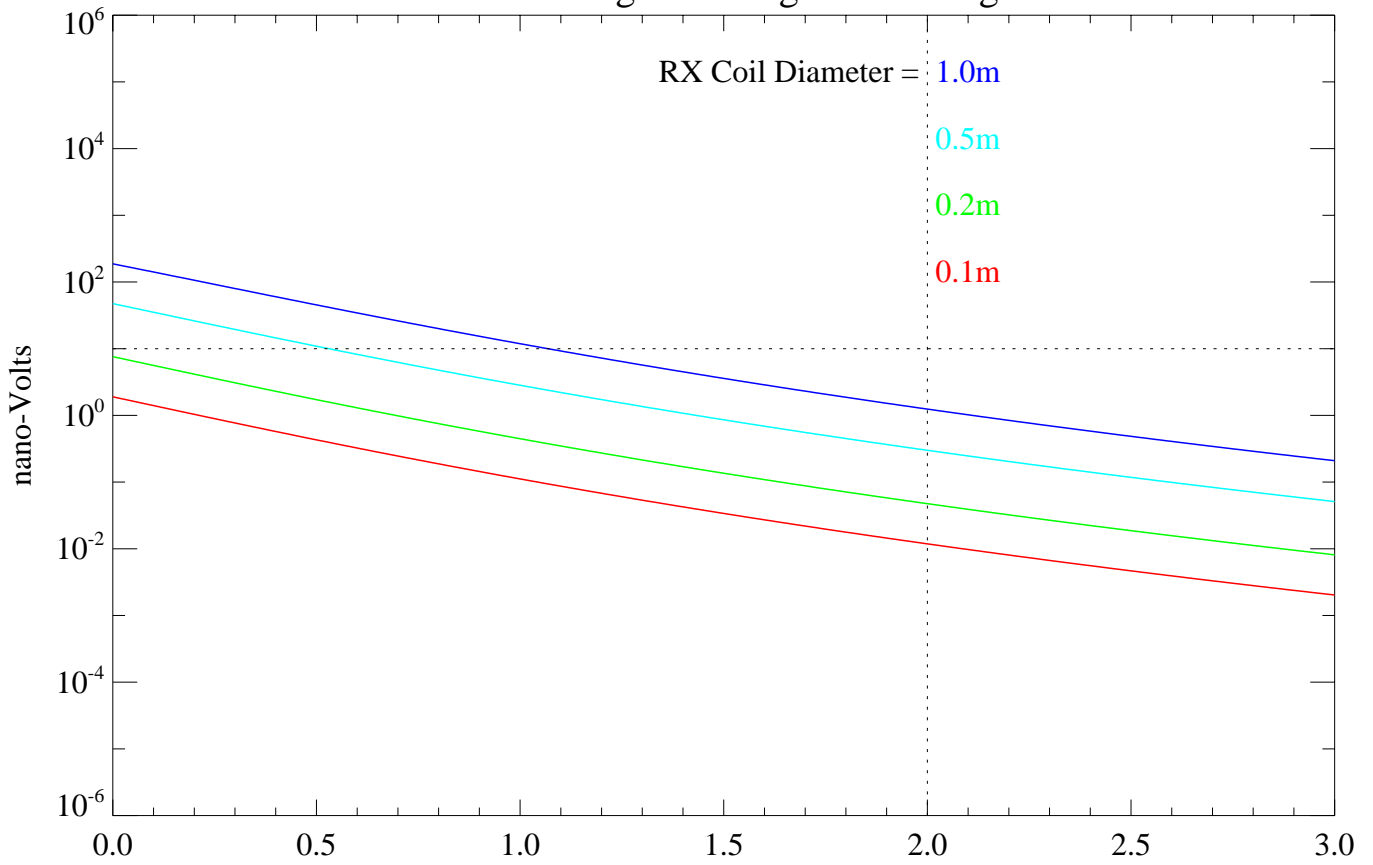
CASE 2 - Sensitivity to RX Pair Coil Separation



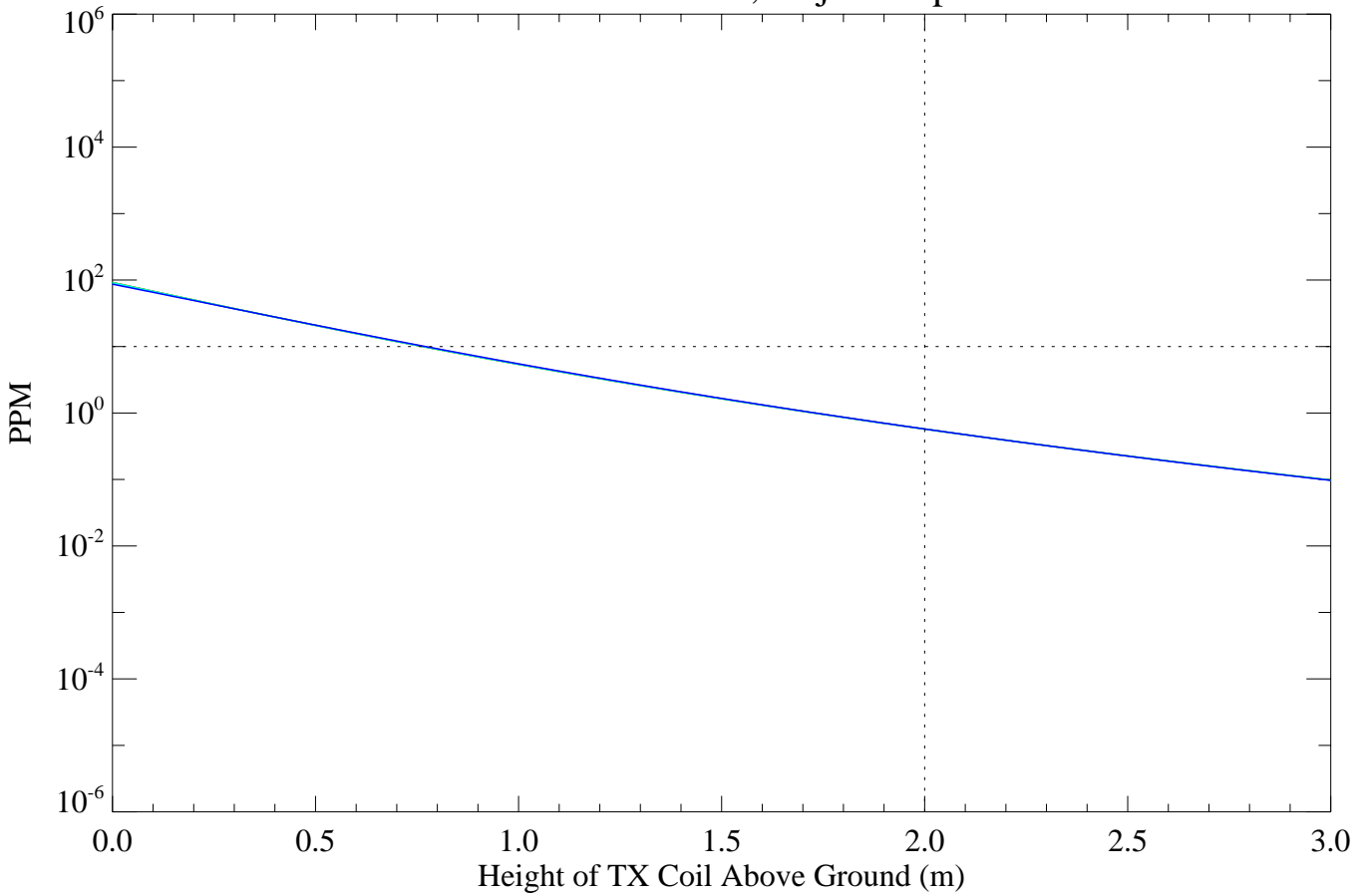
TX Coil Diameter=3.0m, TX Height above Ground=2.0m, Object Depth=1.0m



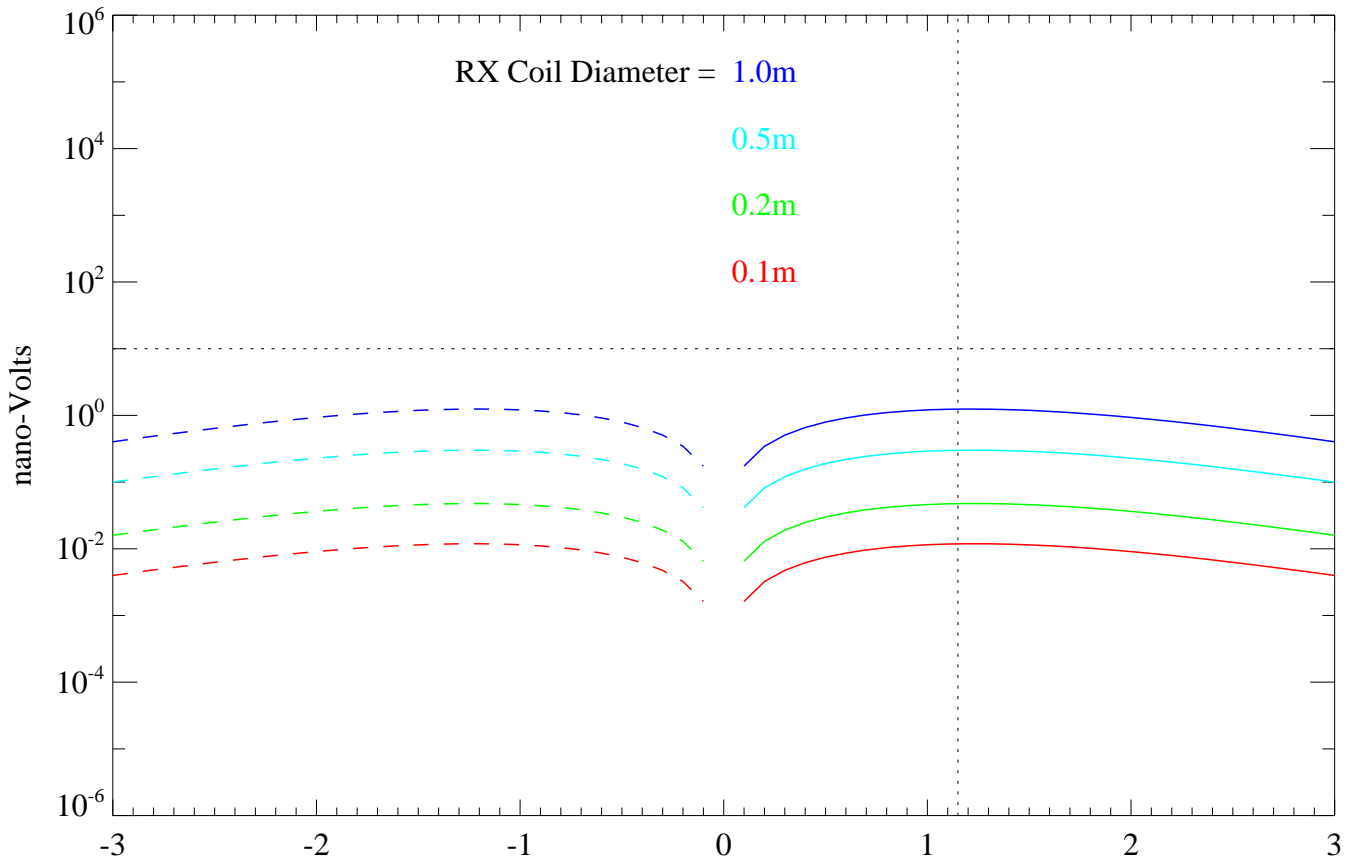
CASE 3 - Signal Strength with Height



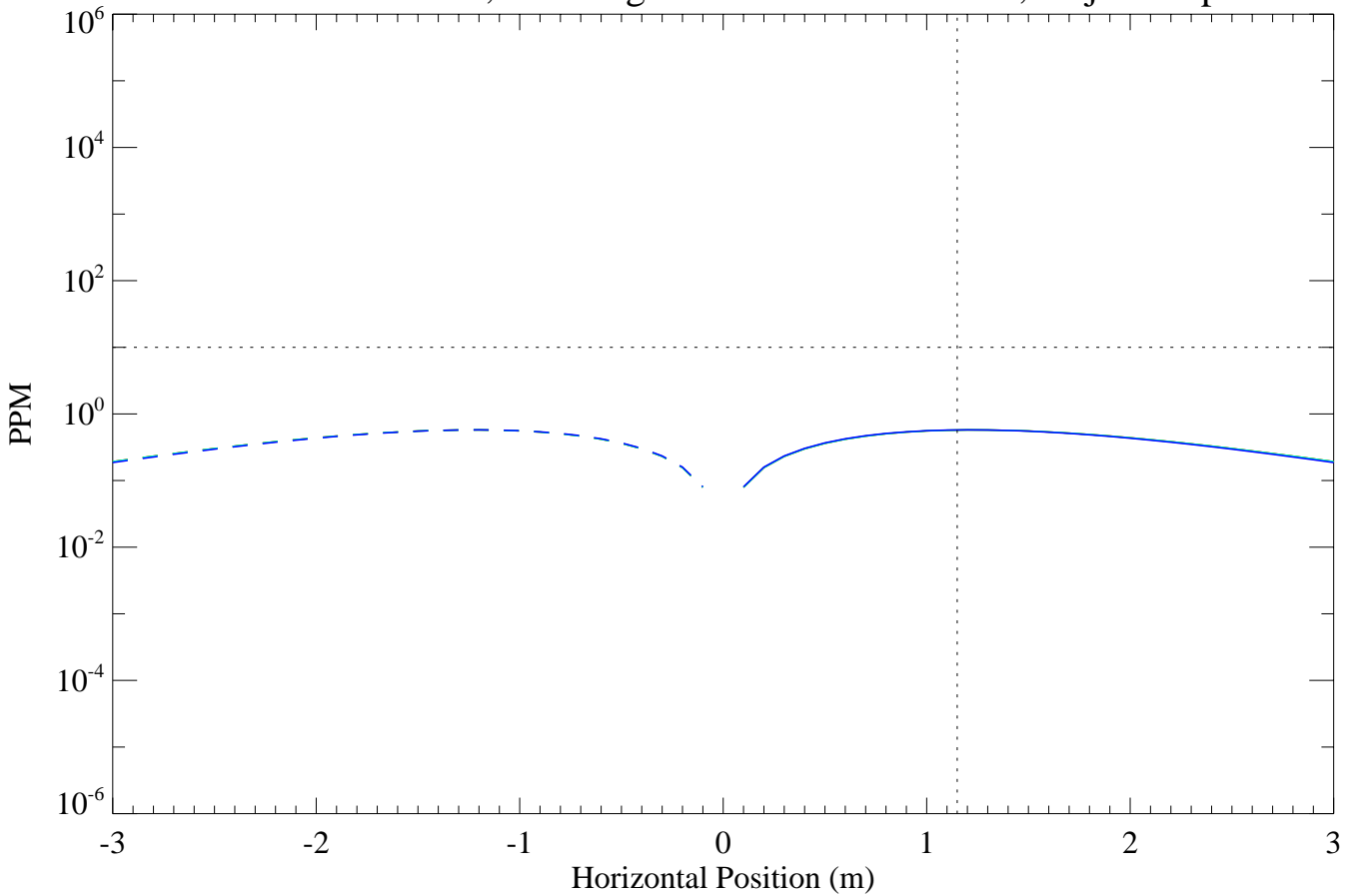
TX Coil Diameter=3.0m, Object Depth=1.0m



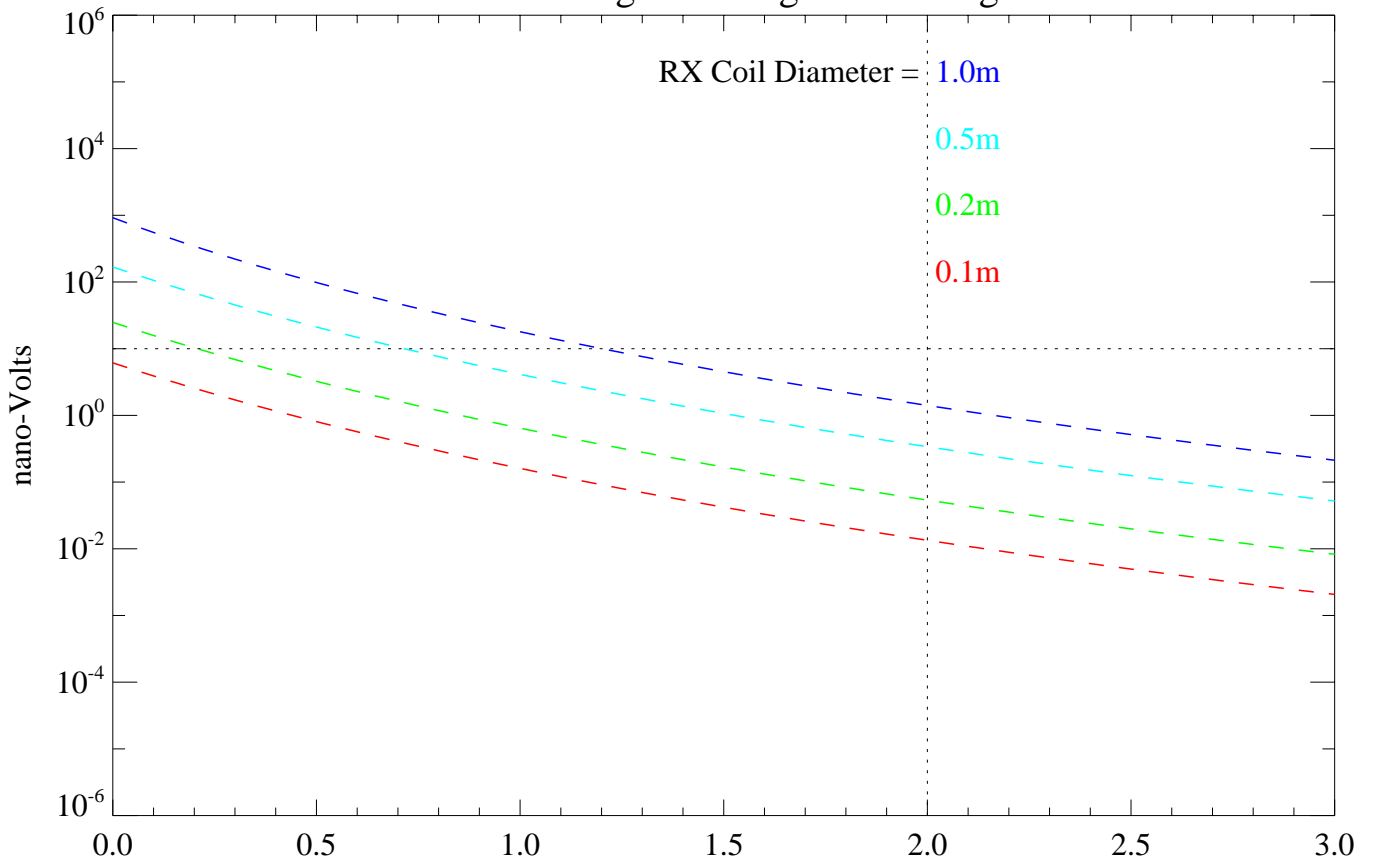
CASE 3 - Horizontal Profile



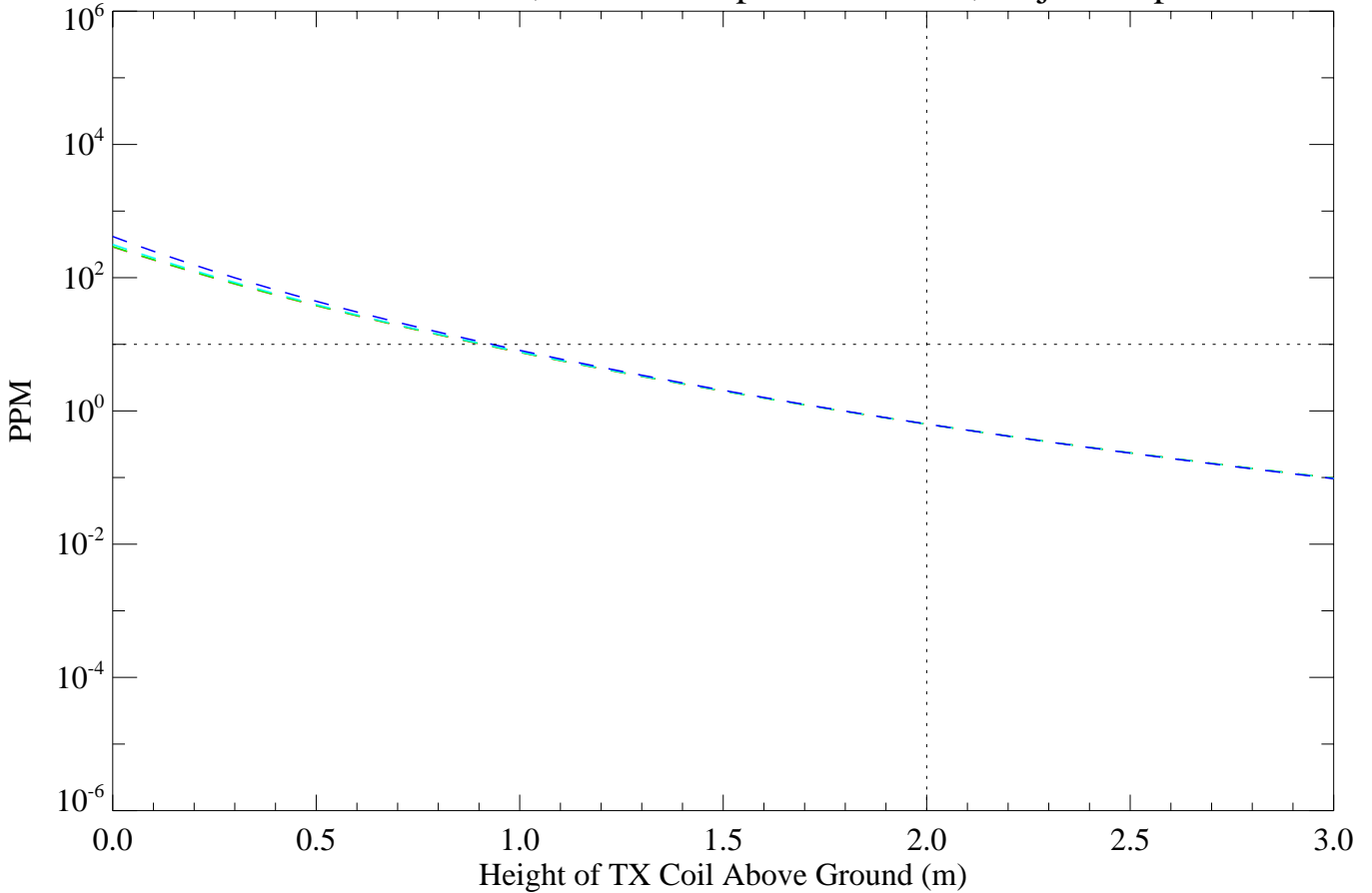
TX Coil Diameter=3.0m, TX Height above Ground=2.0m, Object Depth=1.0m



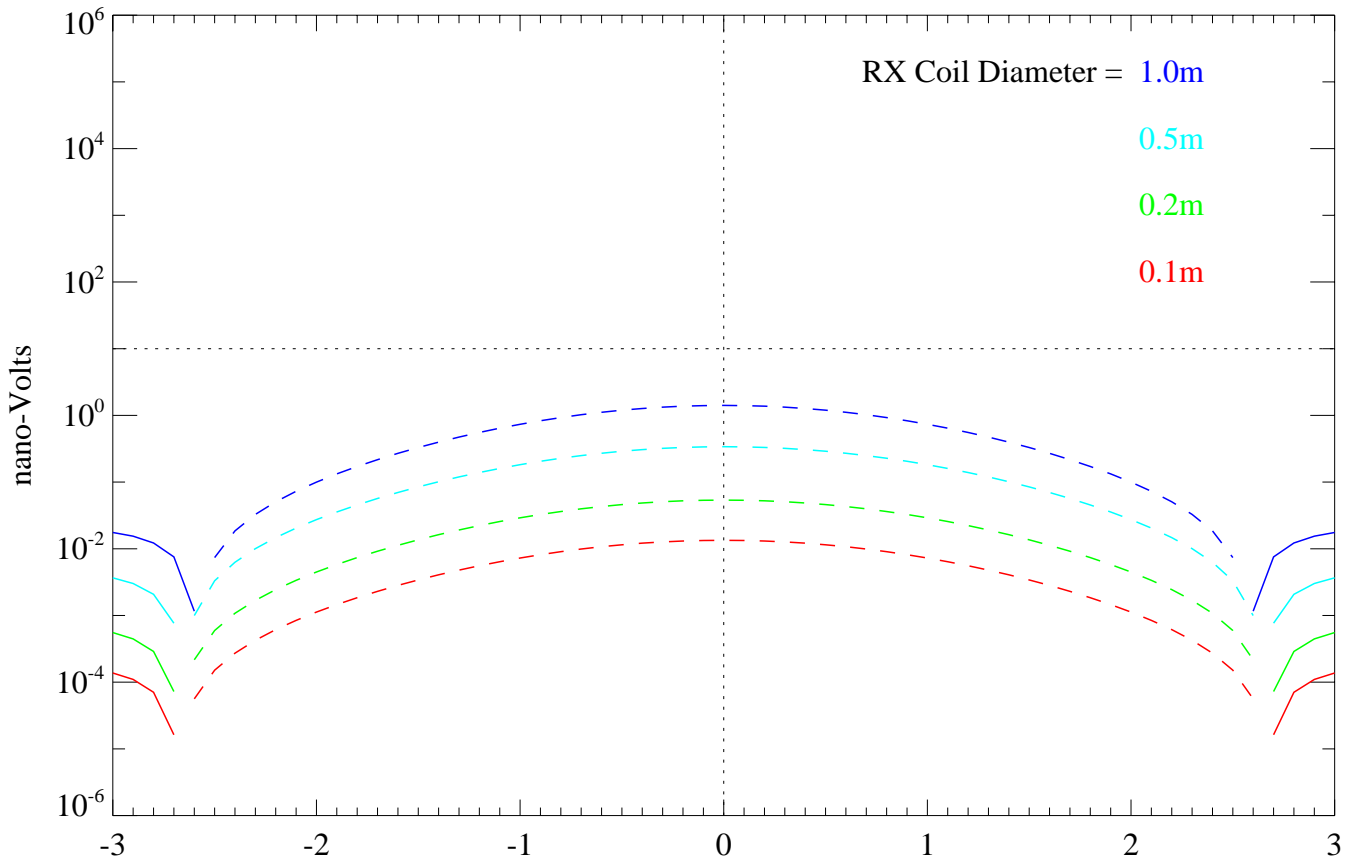
CASE 4 - Signal Strength with Height



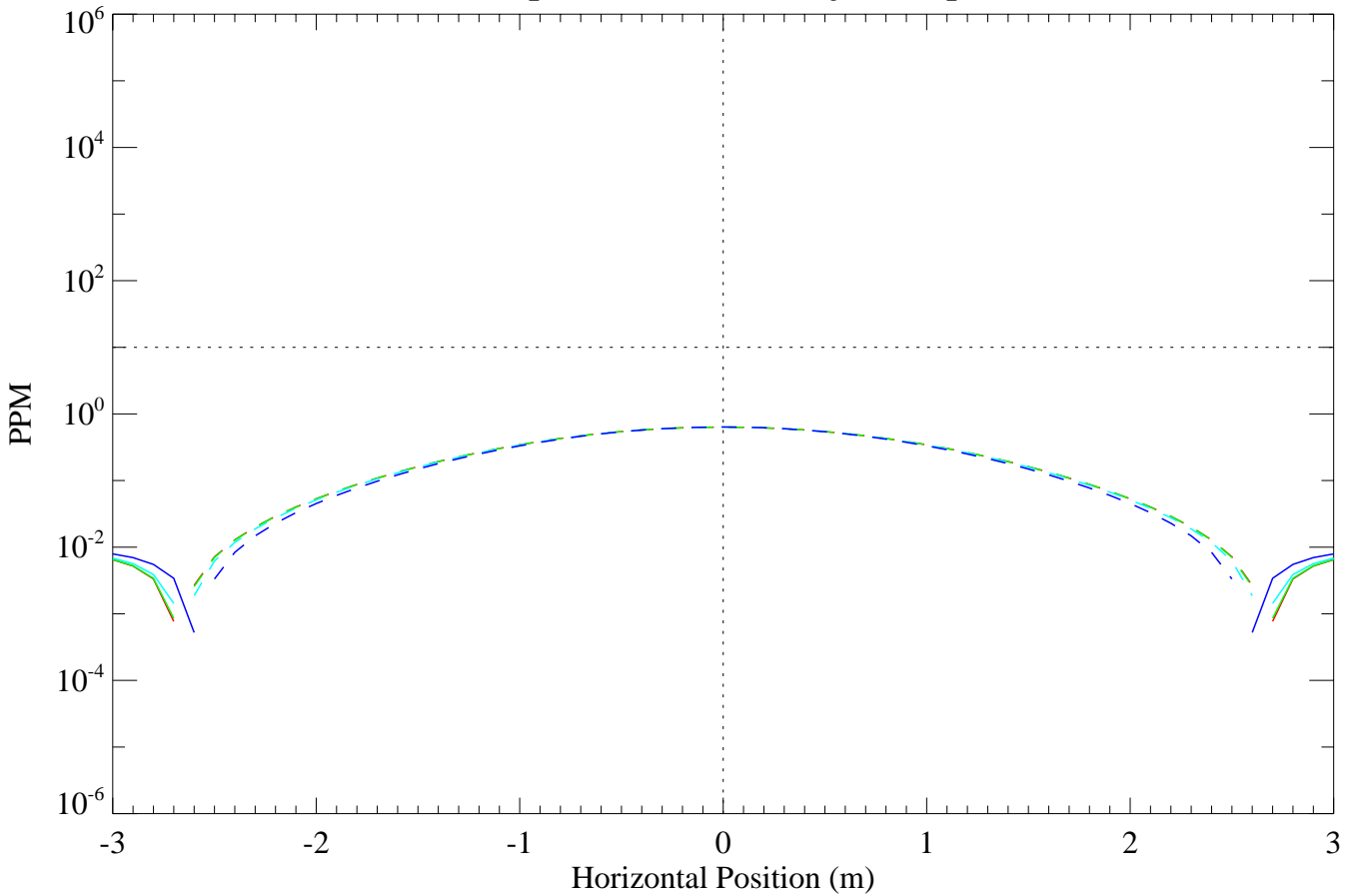
TX Coil Diameter=3.0m, RX Coil Separation=0.5m, Object Depth=1.0m



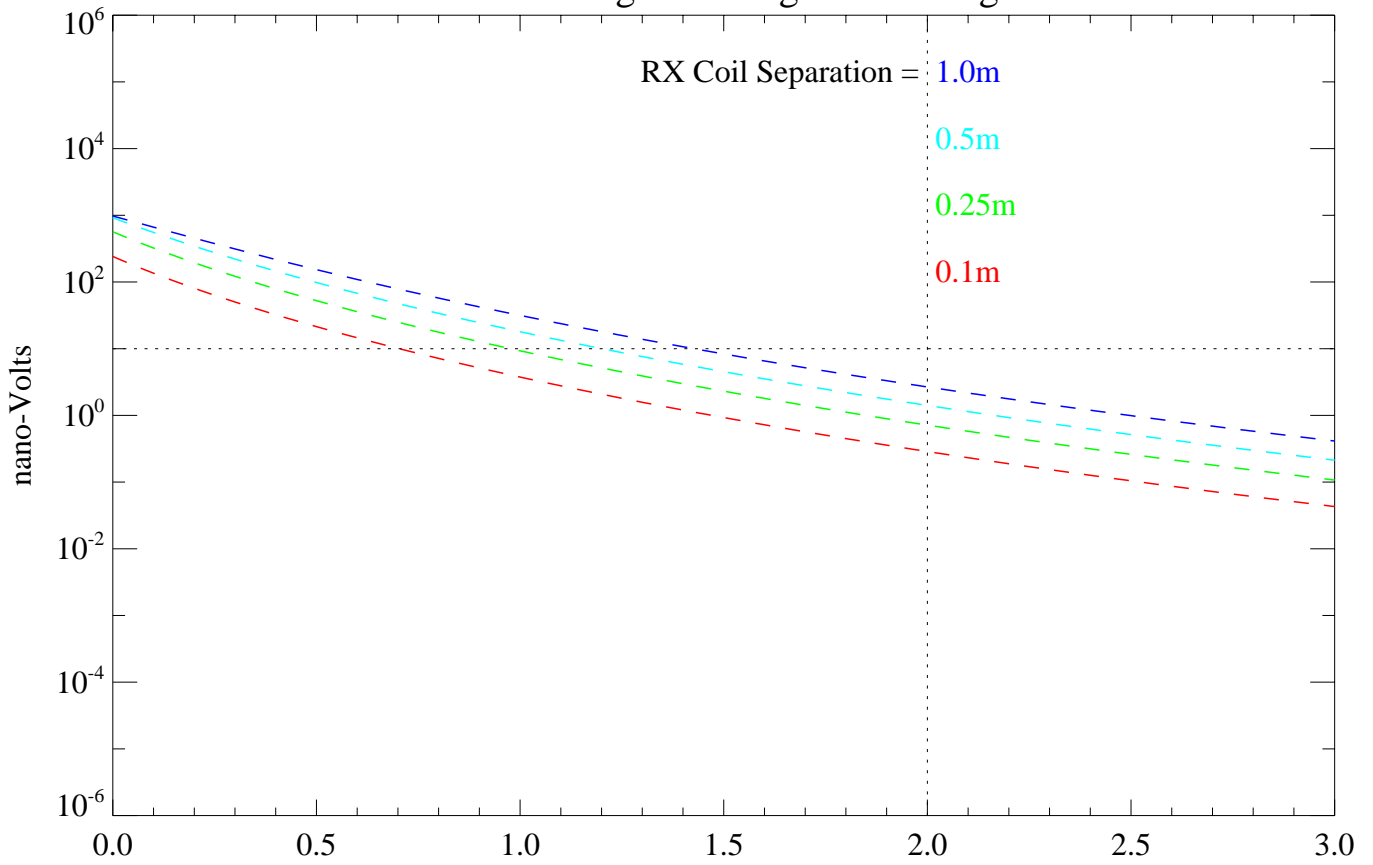
CASE 4 - Horizontal Profile



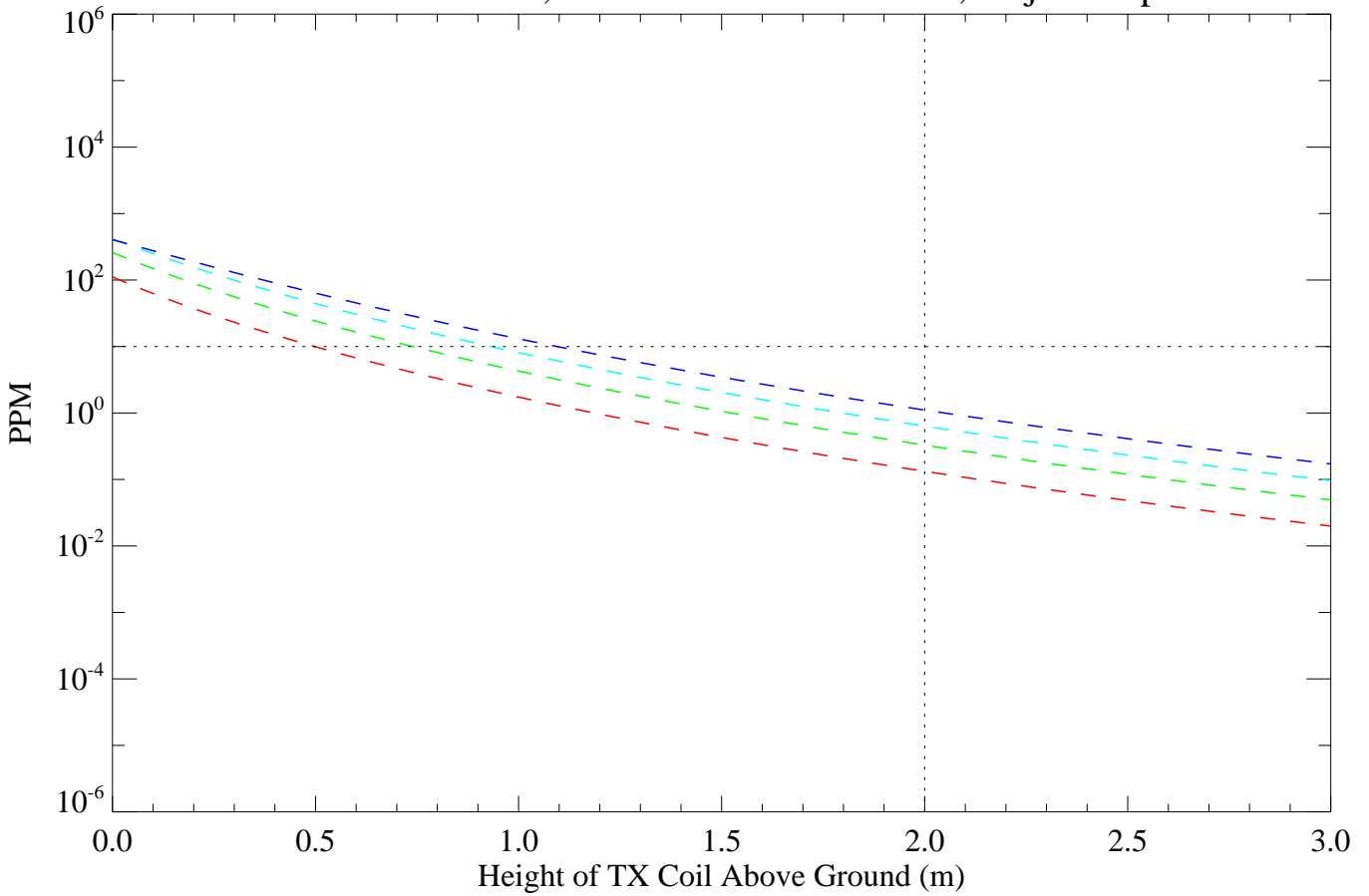
TX Coil Diameter=3.0m, TX Height above Ground=2.0m
RX Coil Separation=0.5m, Object Depth=1.0m



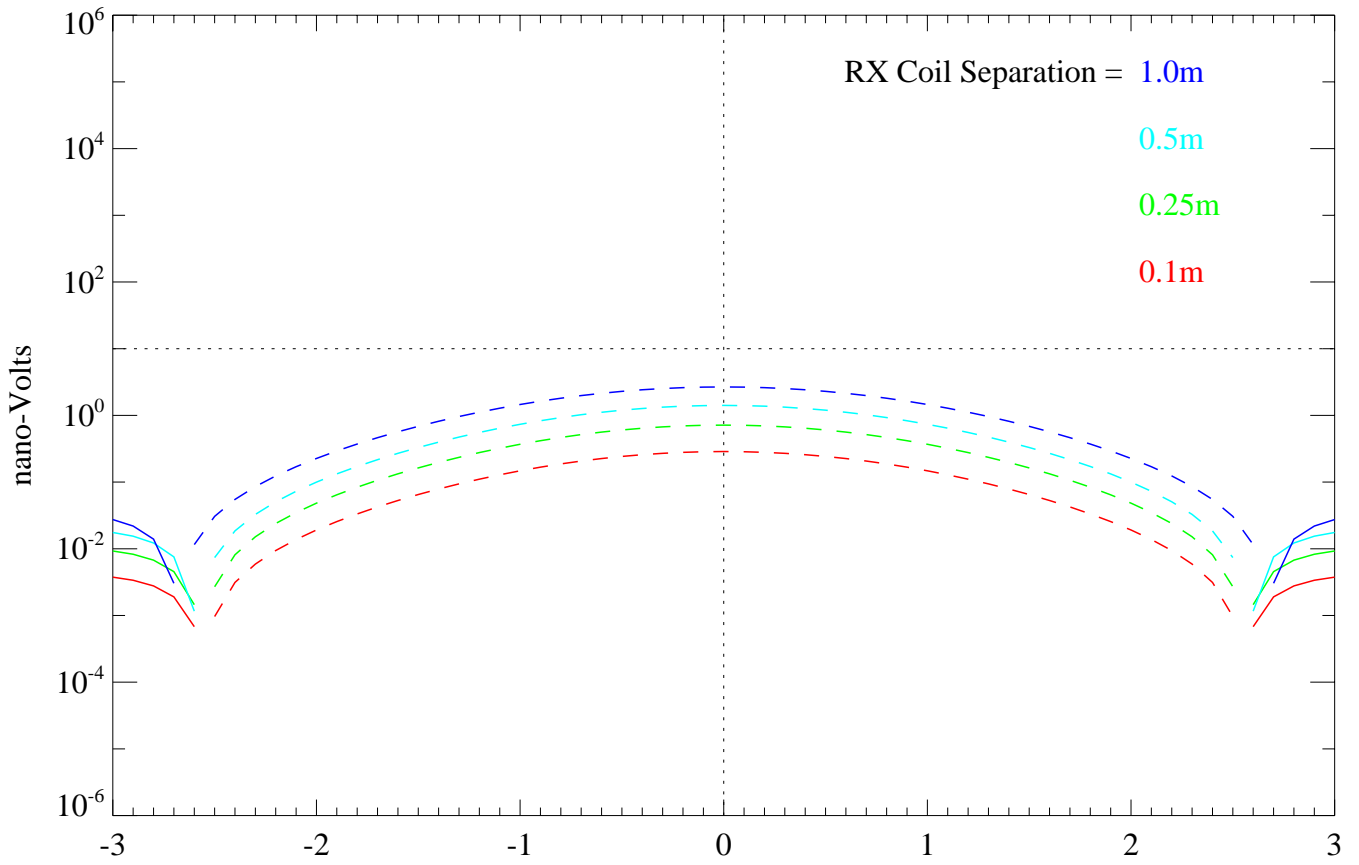
CASE 4 - Signal Strength with Height



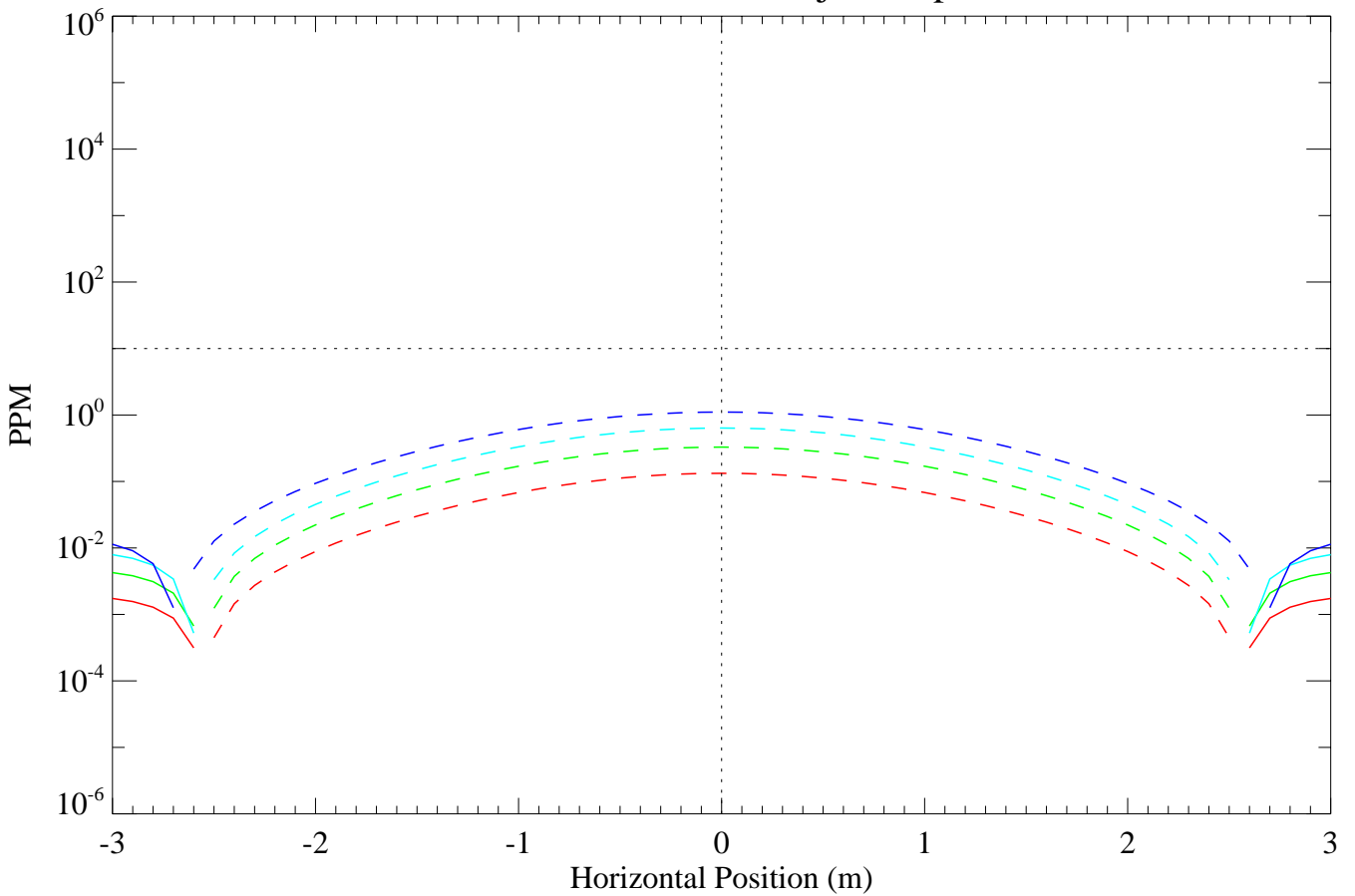
TX Coil Diameter=3.0m, RX Coil Diameter=1.0m, Object Depth=1.0m



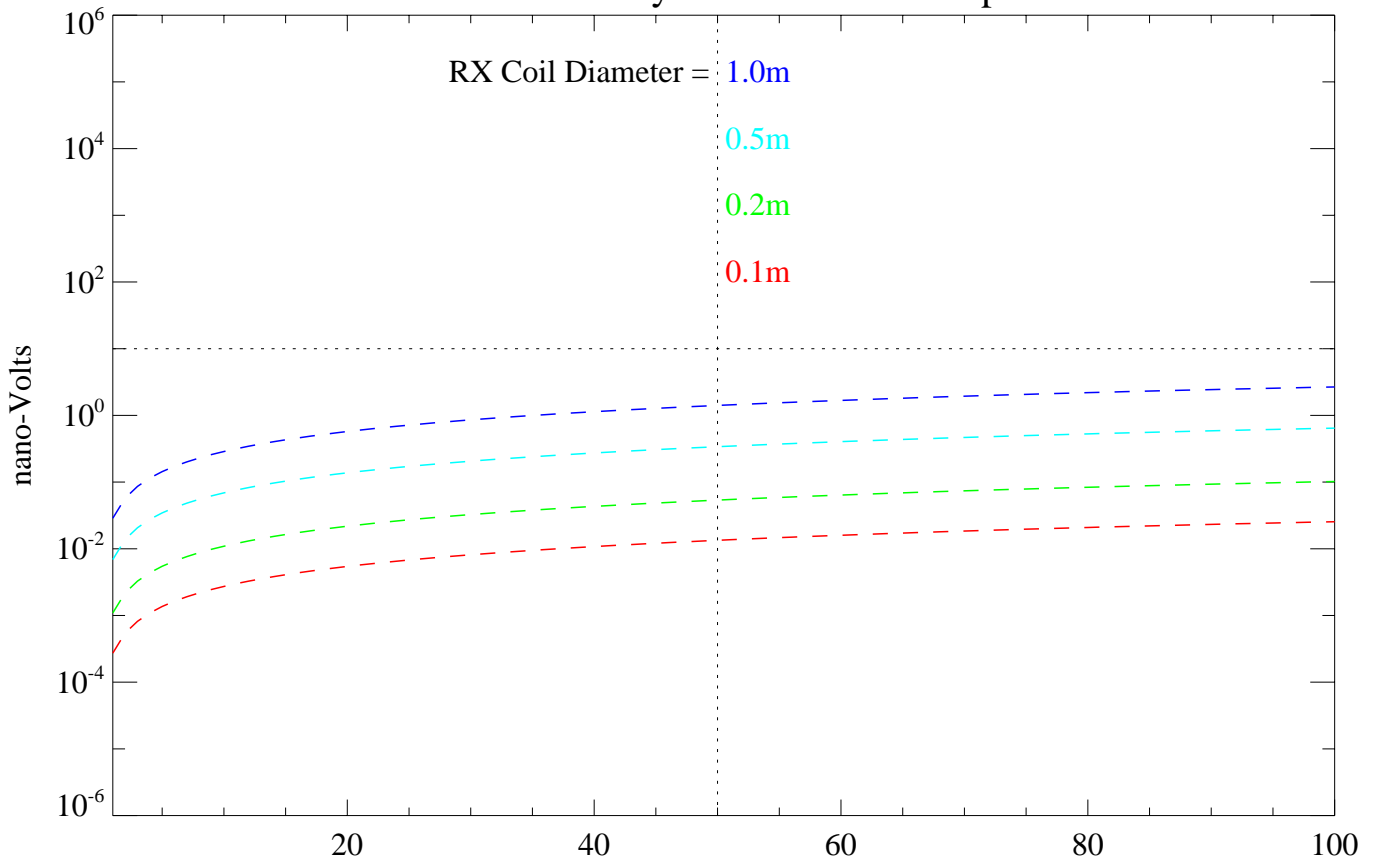
CASE 4 - Horizontal Profile



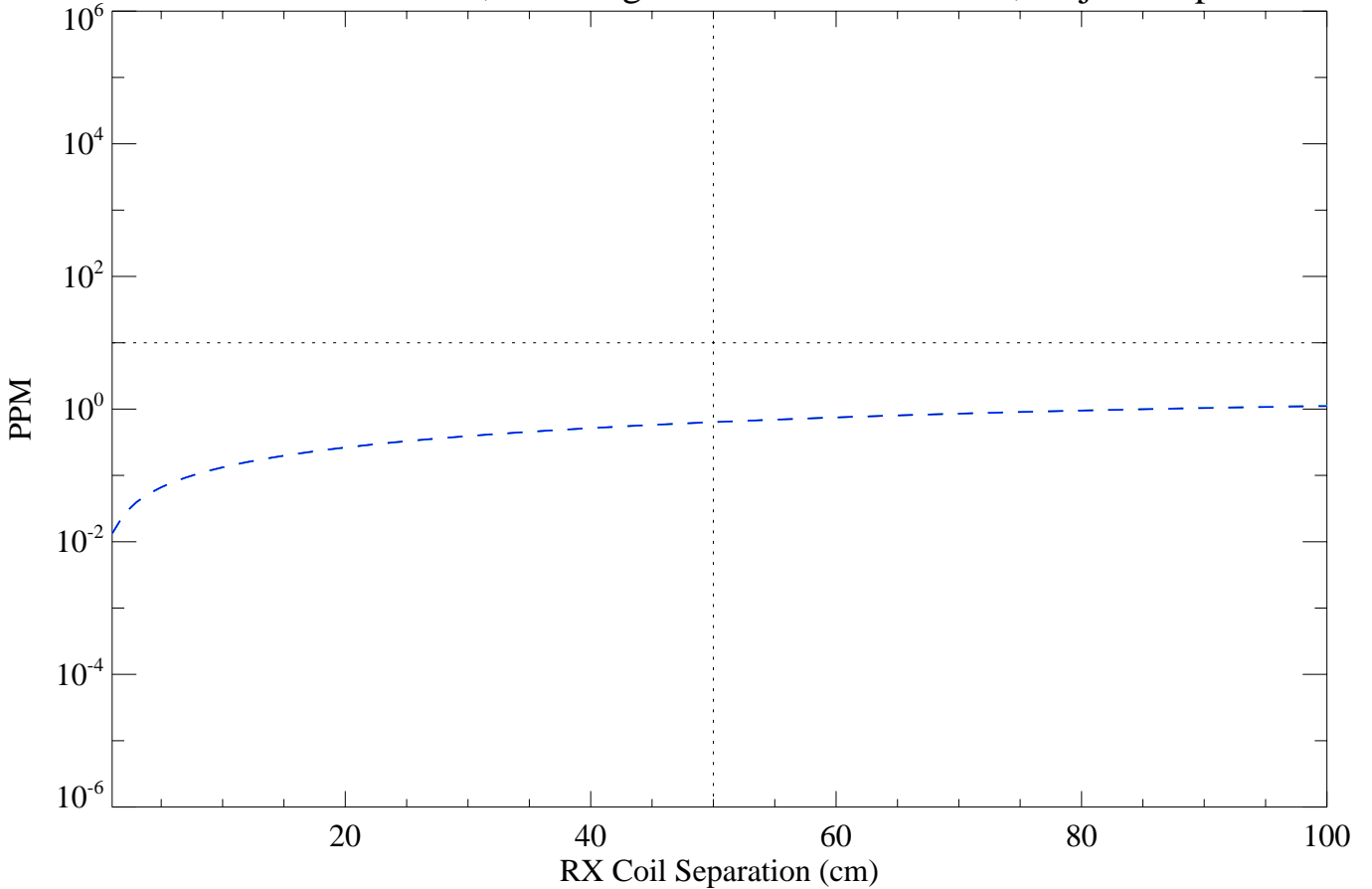
TX Coil Diameter=3.0m, TX Height above Ground=2.0m
RX Coil Diameter=1.0m, Object Depth=1.0m



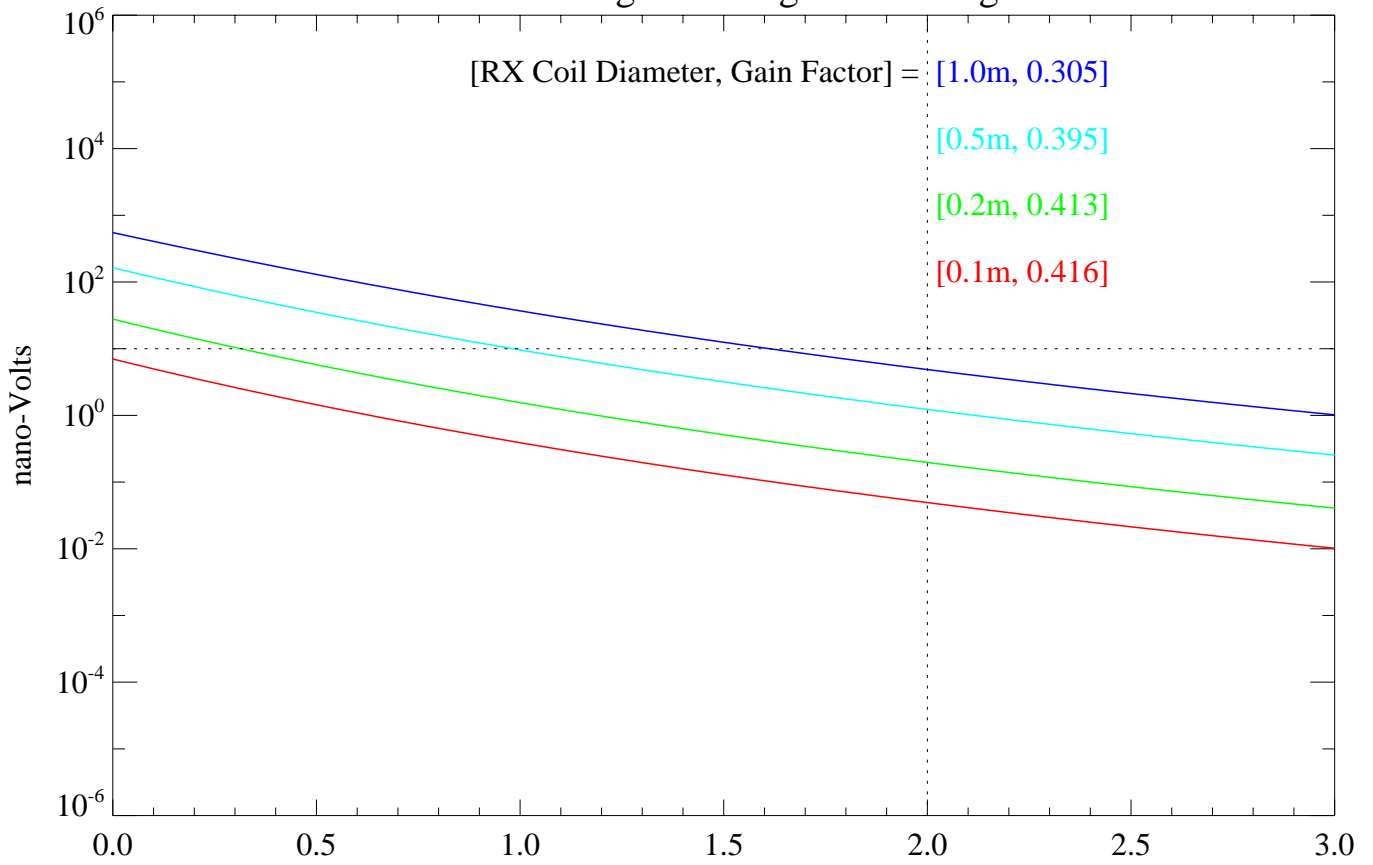
CASE 4 - Sensitivity to RX Pair Coil Separation



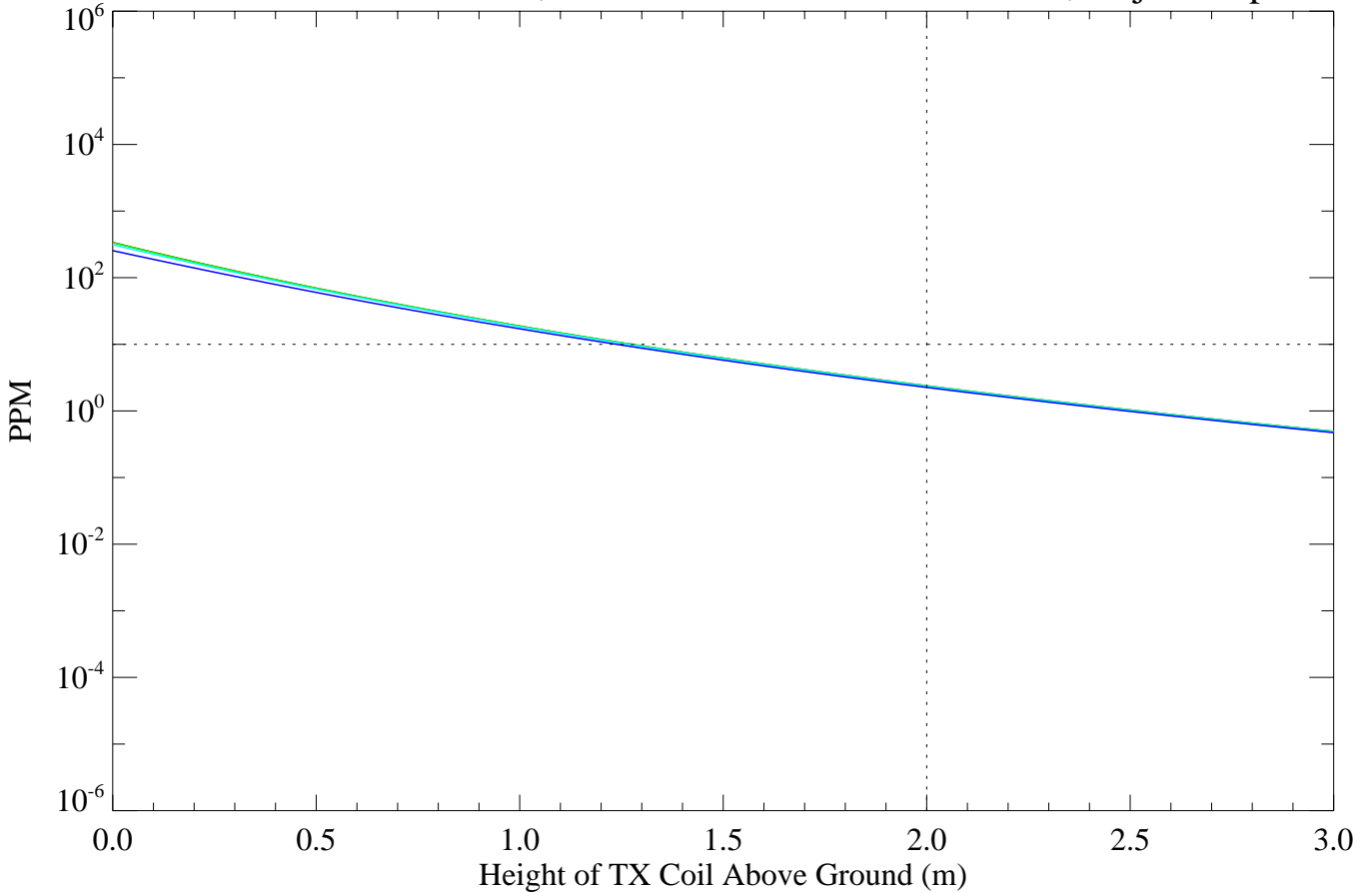
TX Coil Diameter=3.0m, TX Height above Ground=2.0m, Object Depth=1.0m



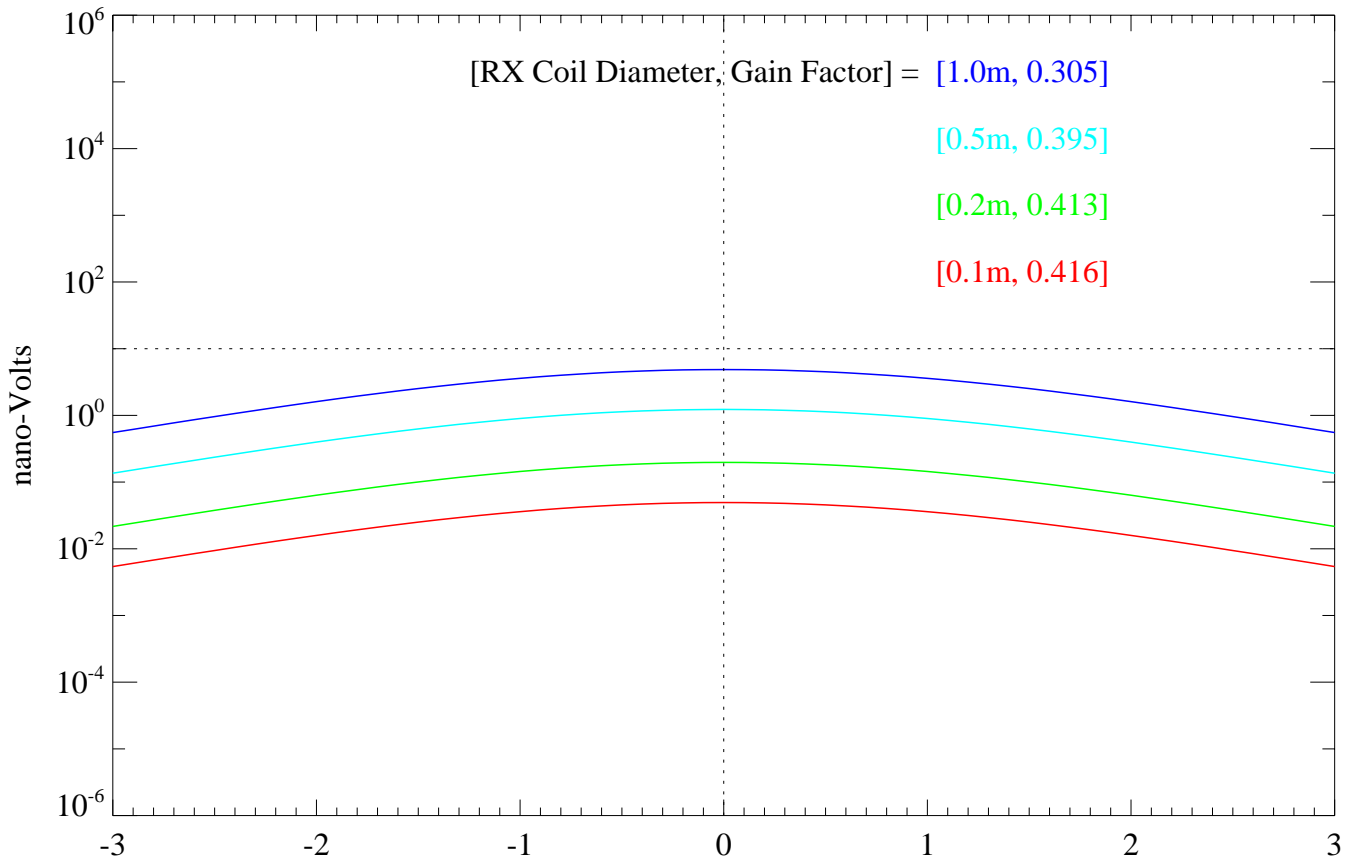
CASE 5 - Signal Strength with Height



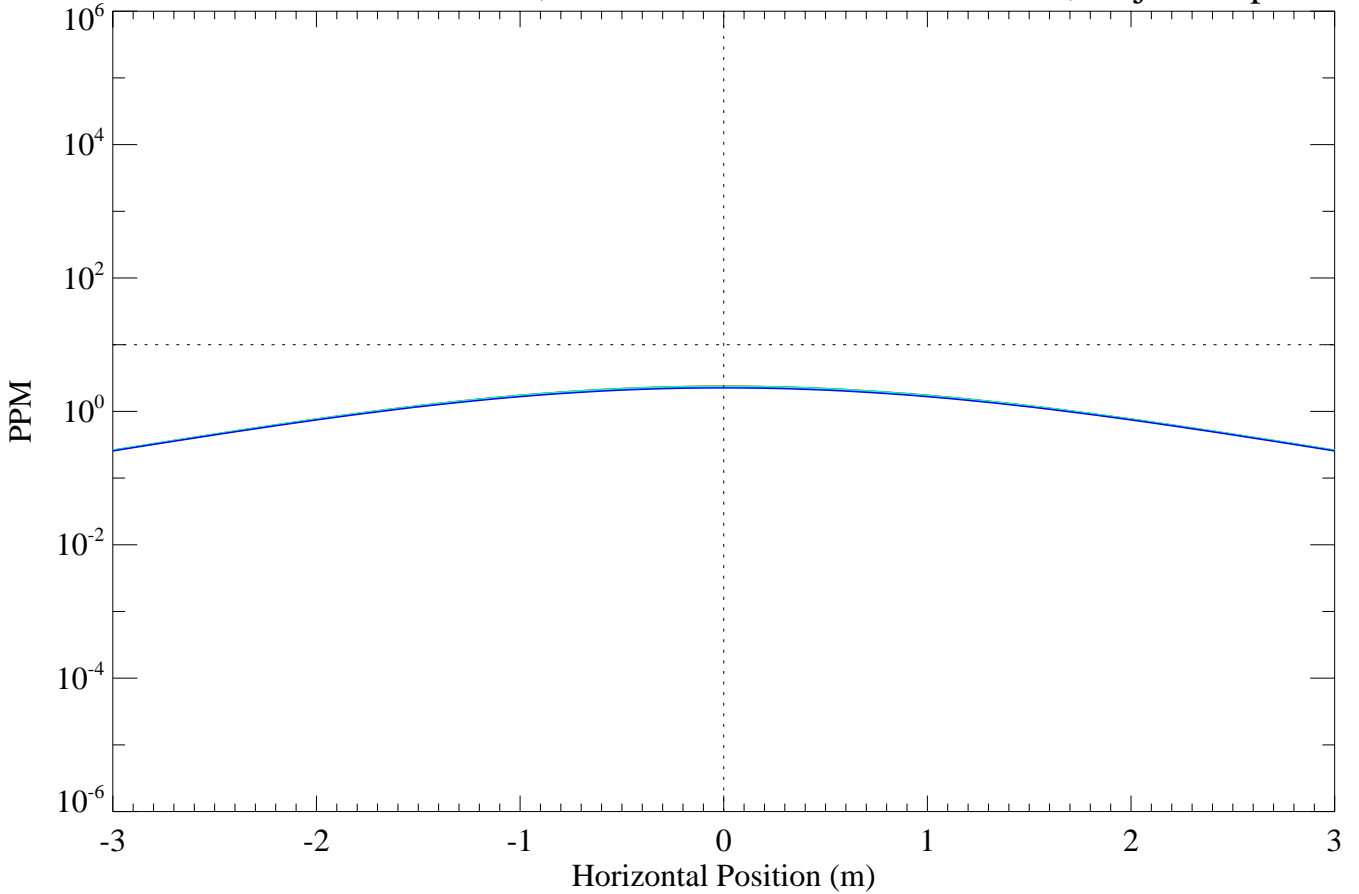
Outer TX Coil Diameter=3.0m, Inner TX Coil Diameter=1.25m, Object Depth=1.0m



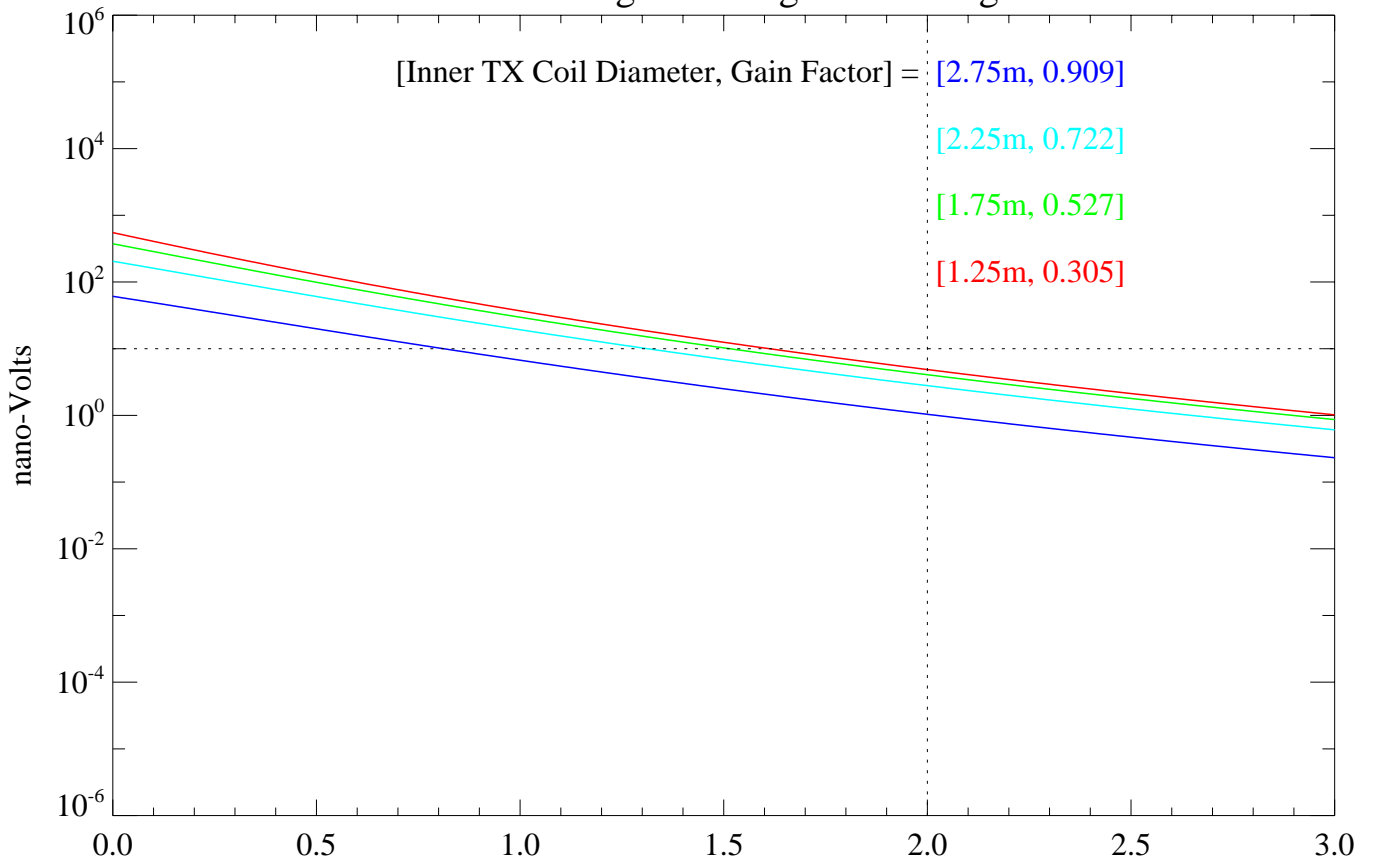
CASE 5 - Horizontal Profile



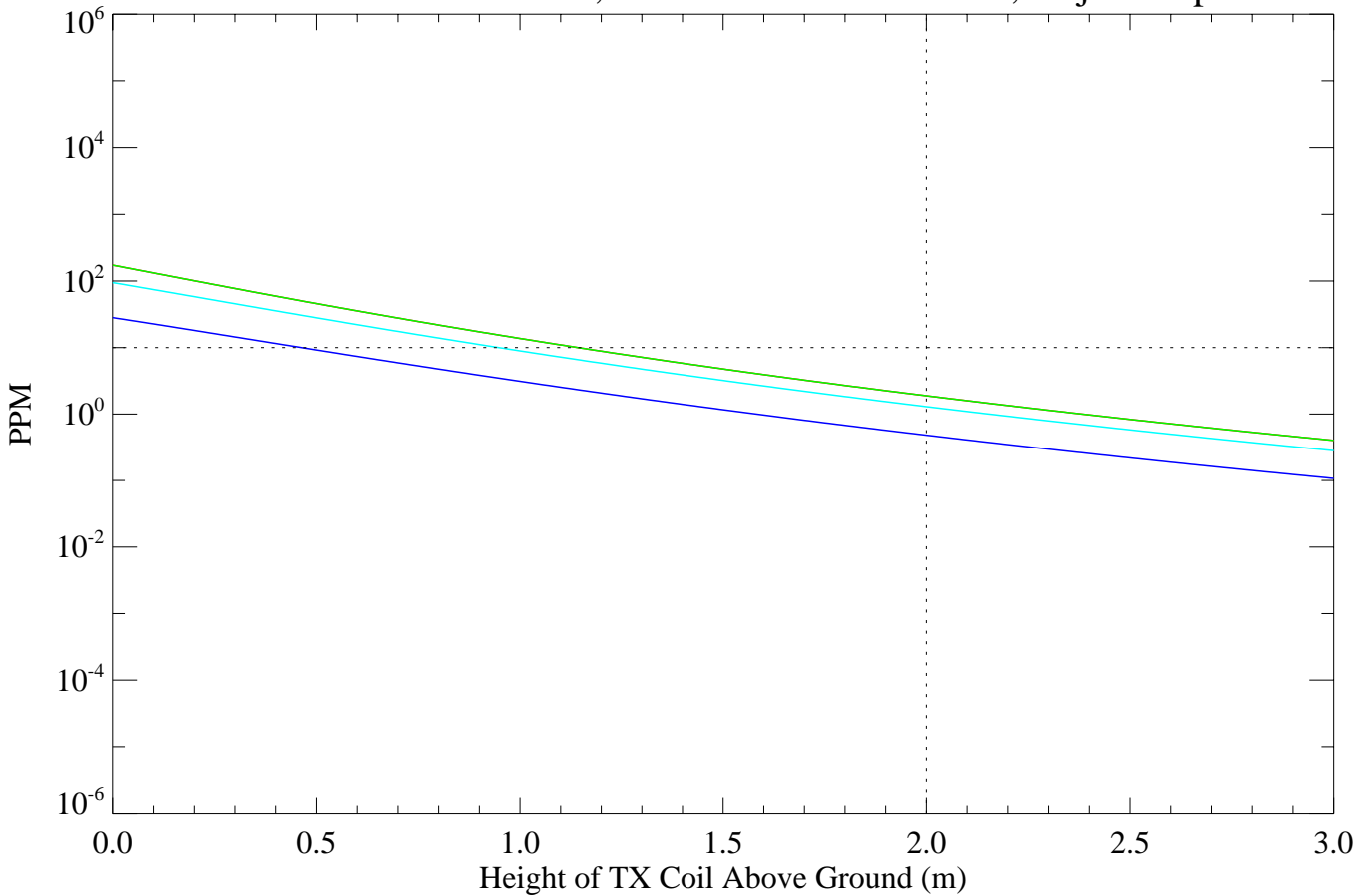
Outer TX Coil Diameter=3.0m, Inner TX Coil Diameter=1.25m, Object Depth=1.0m



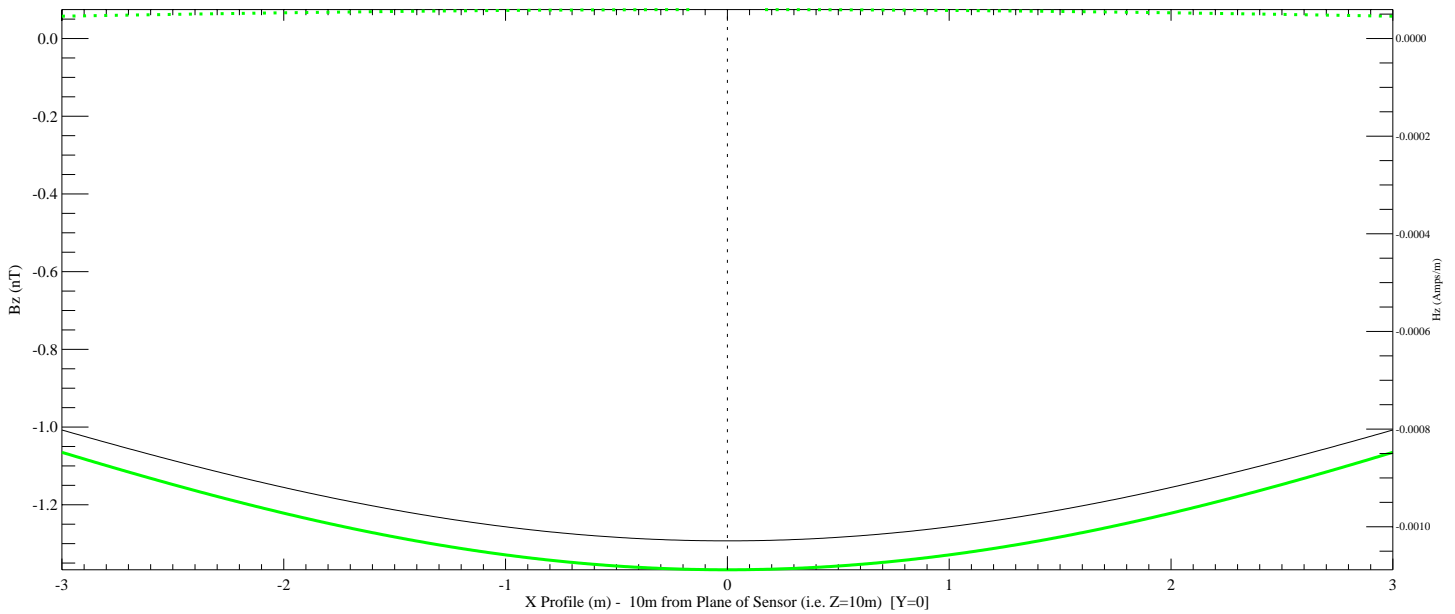
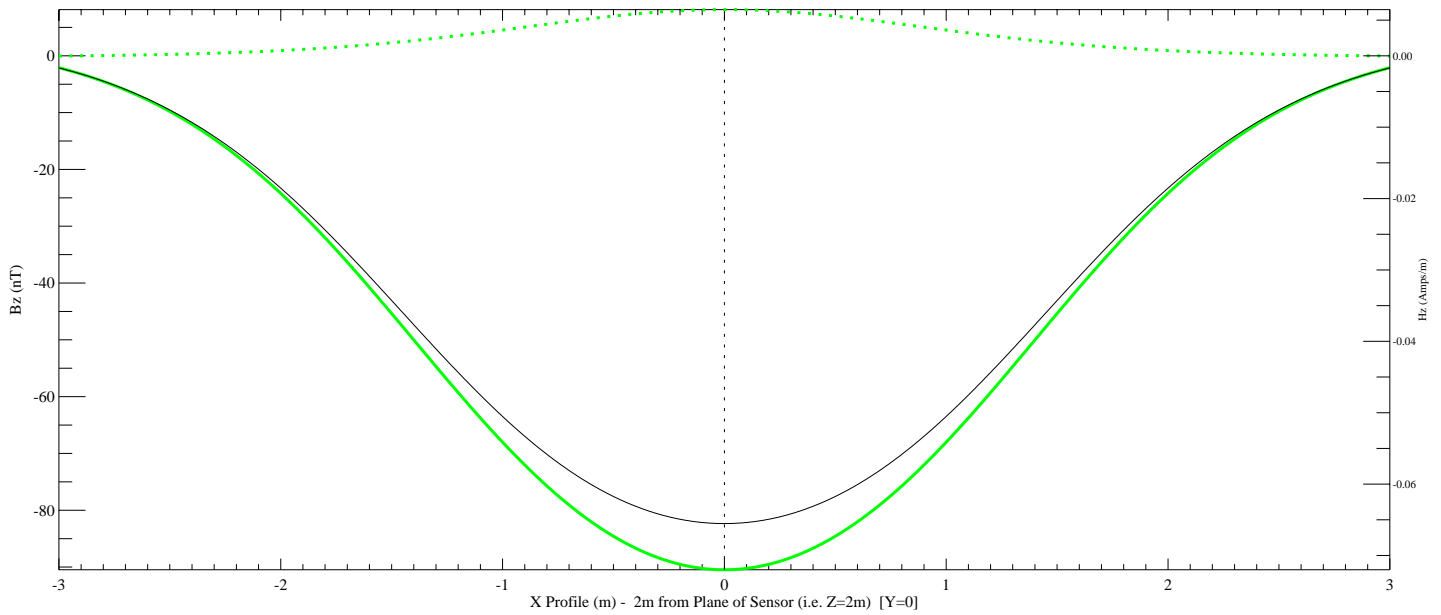
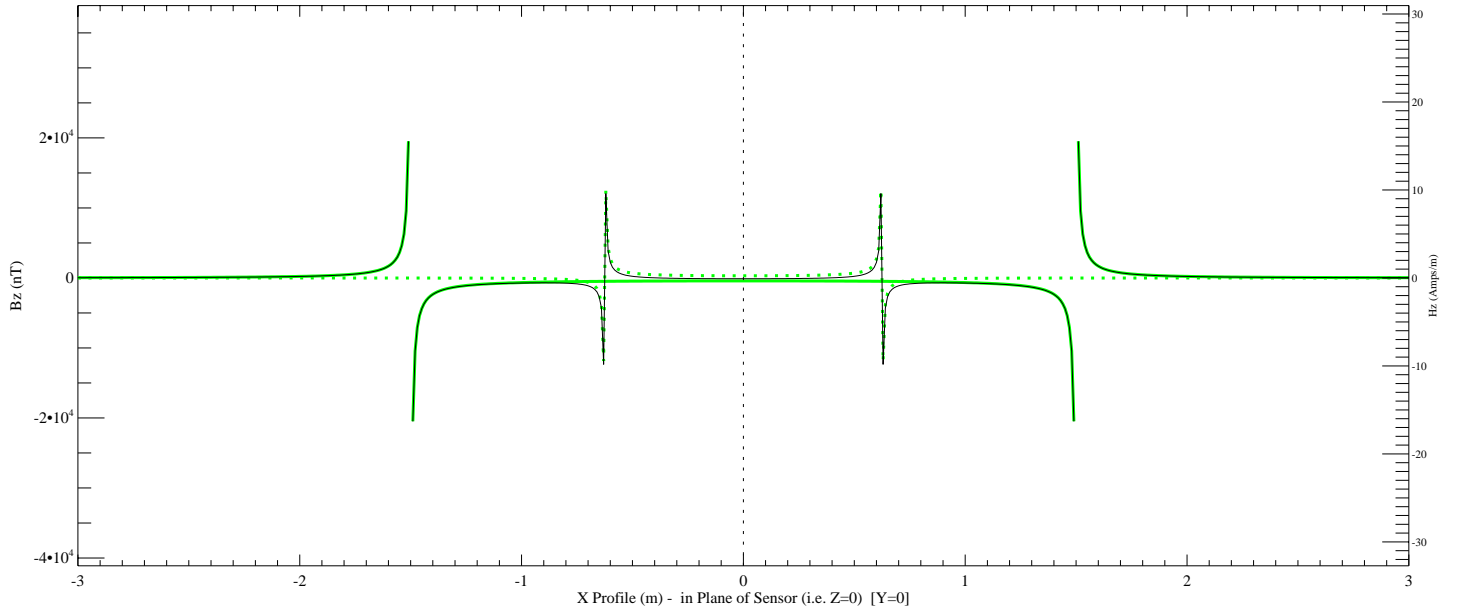
CASE 5 - Signal Strength with Height



Outer TX Coil Diameter=3.0m, RX Coil Diameter=1.0m, Object Depth=1.0m



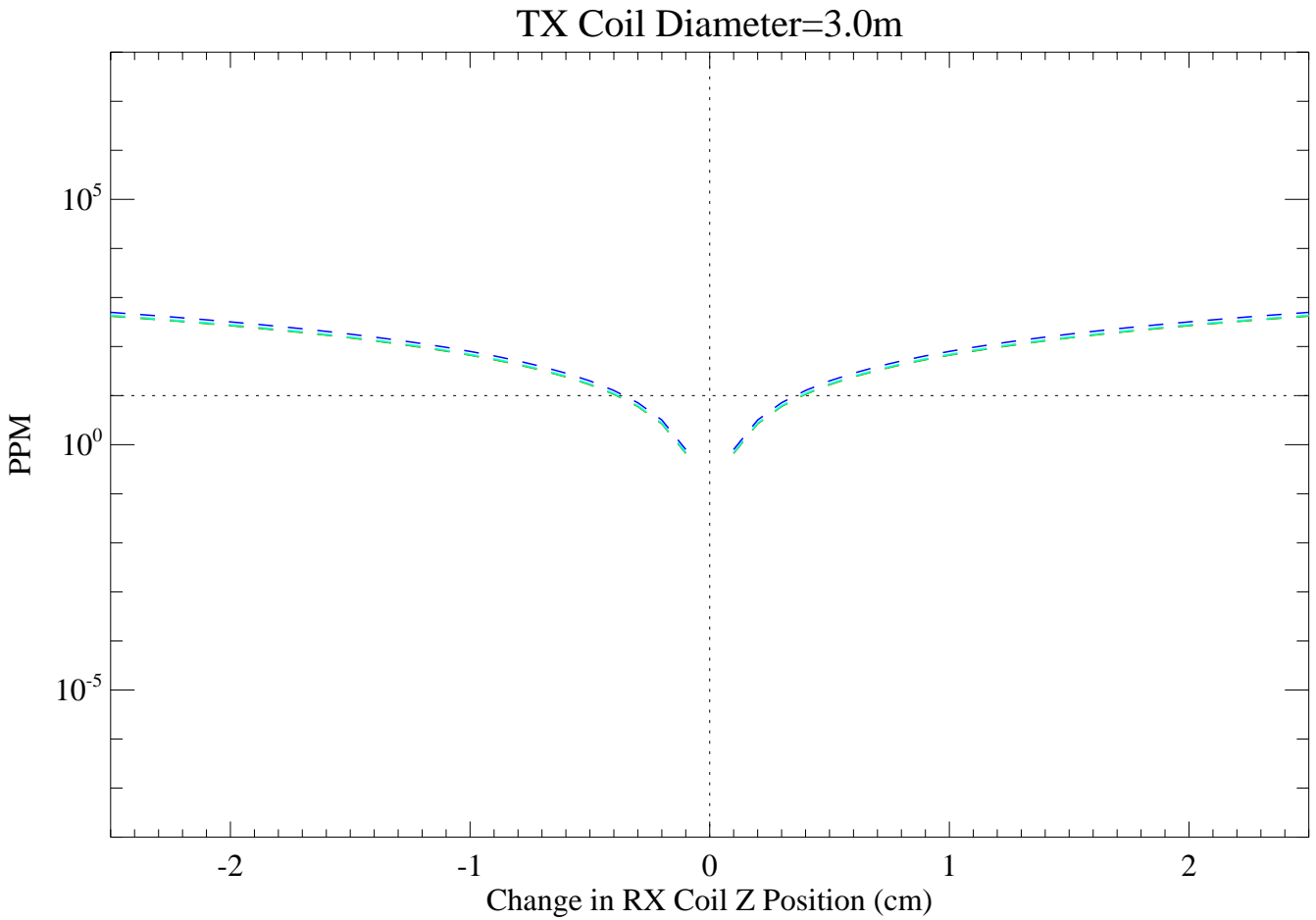
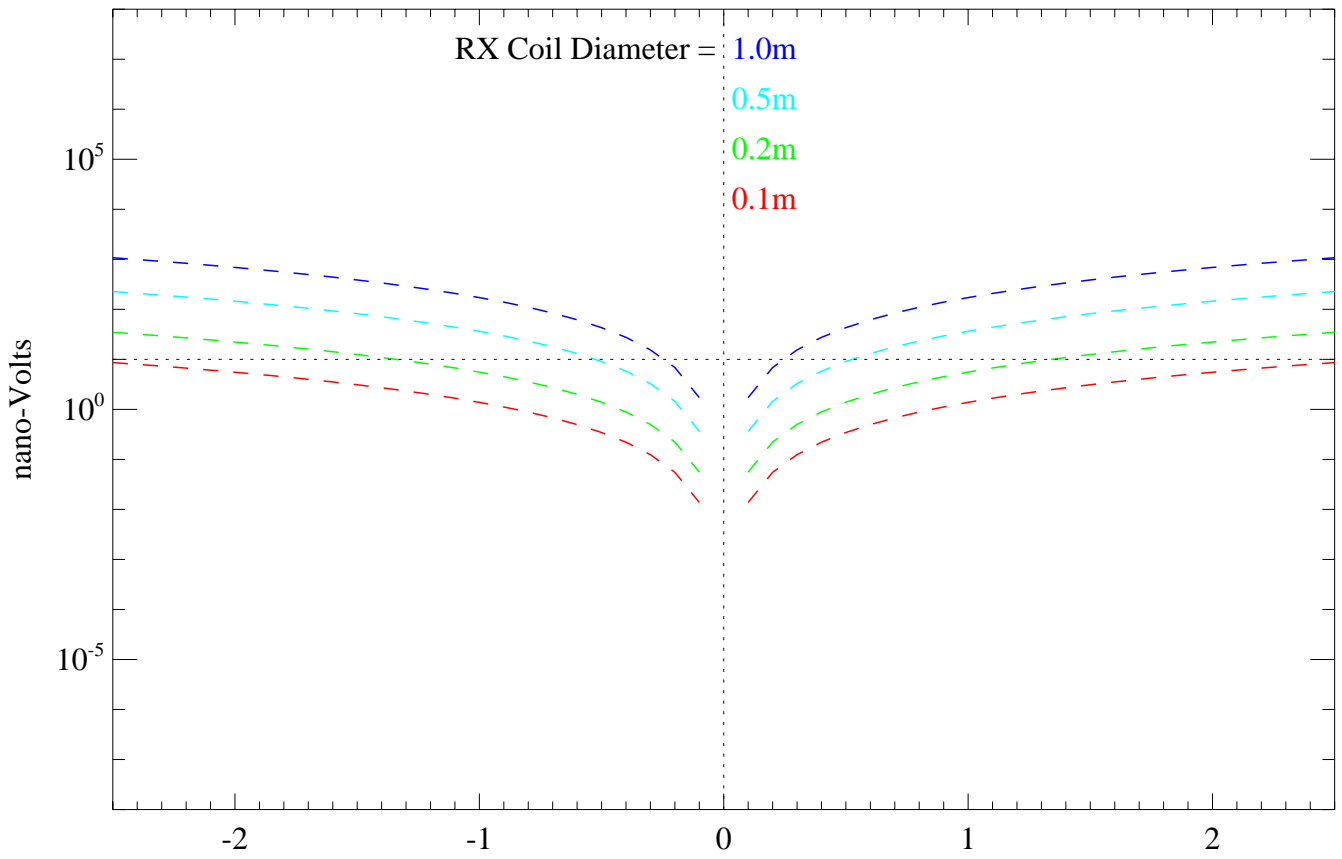
CASE 5 - Outer TX Coil Diameter=3.00m, Inner TX Coil Diameter=1.25m with Gain Factor=0.305, and RX Coil Diameter=1.00m
 [SOLID GREEN - OUTER TX COIL ONLY; DOTTED GREEN - INNER TX COIL ONLY]



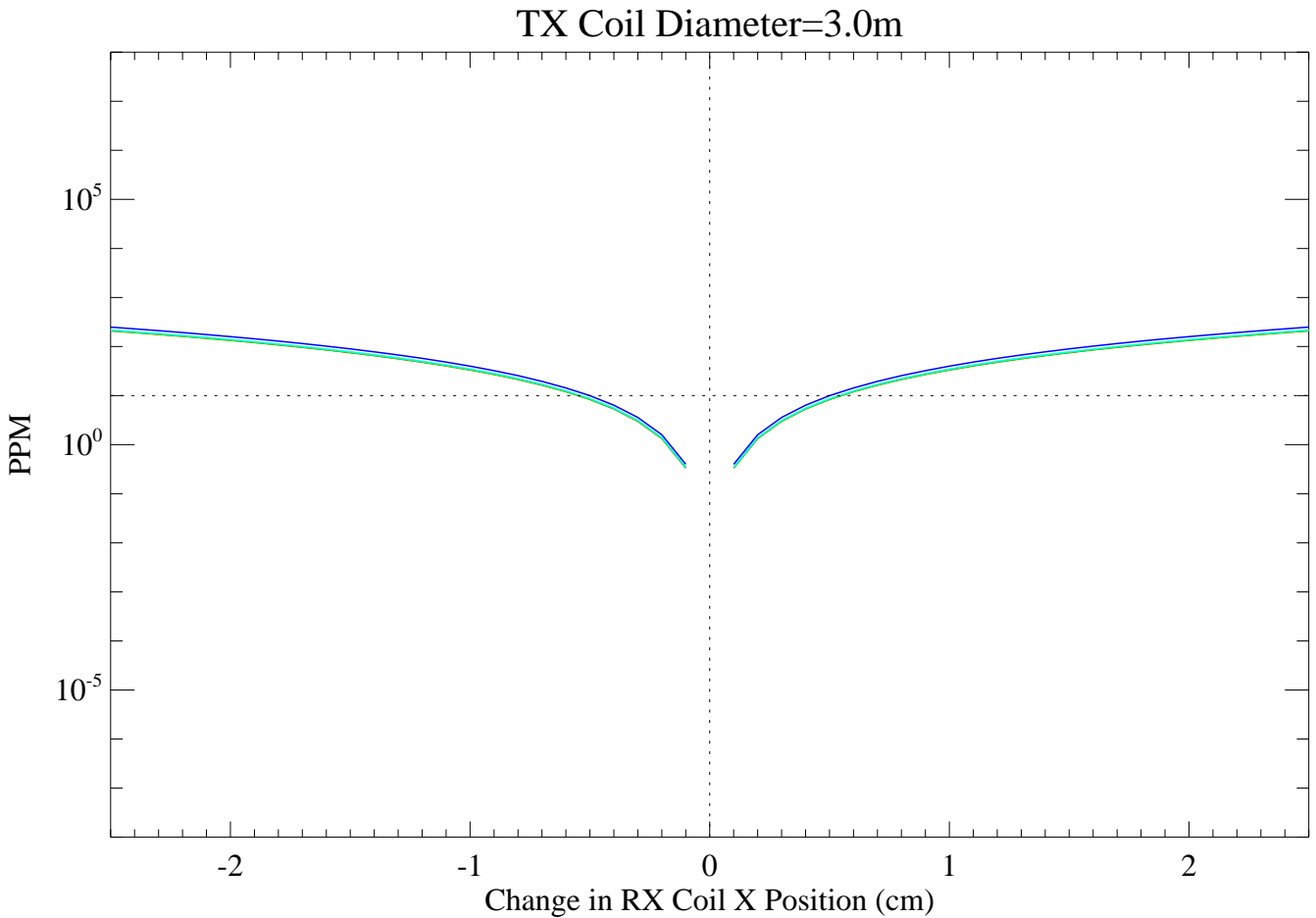
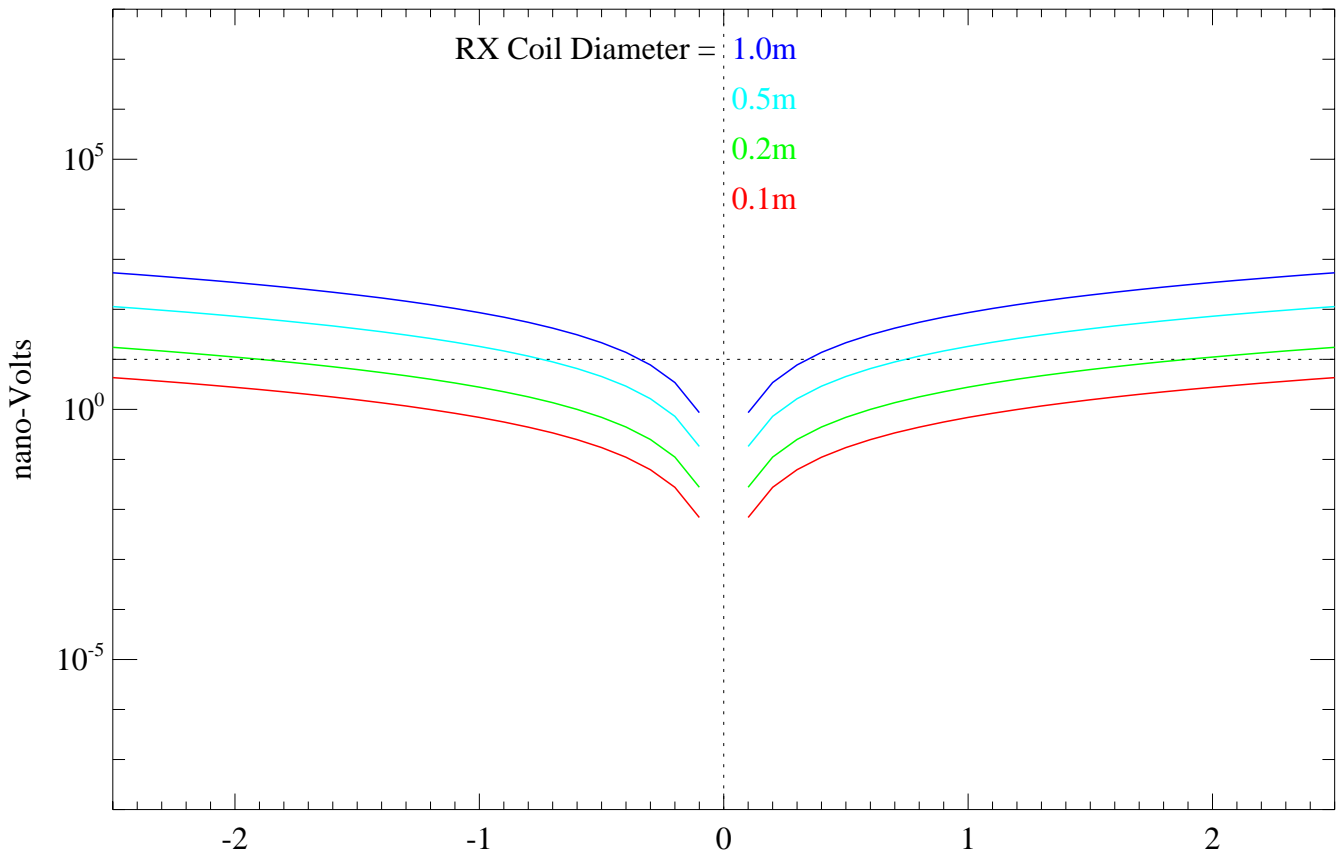
Appendix 1B

Plots showing modeling results of the change in primary (i.e. transmit) field coupling due to perturbations

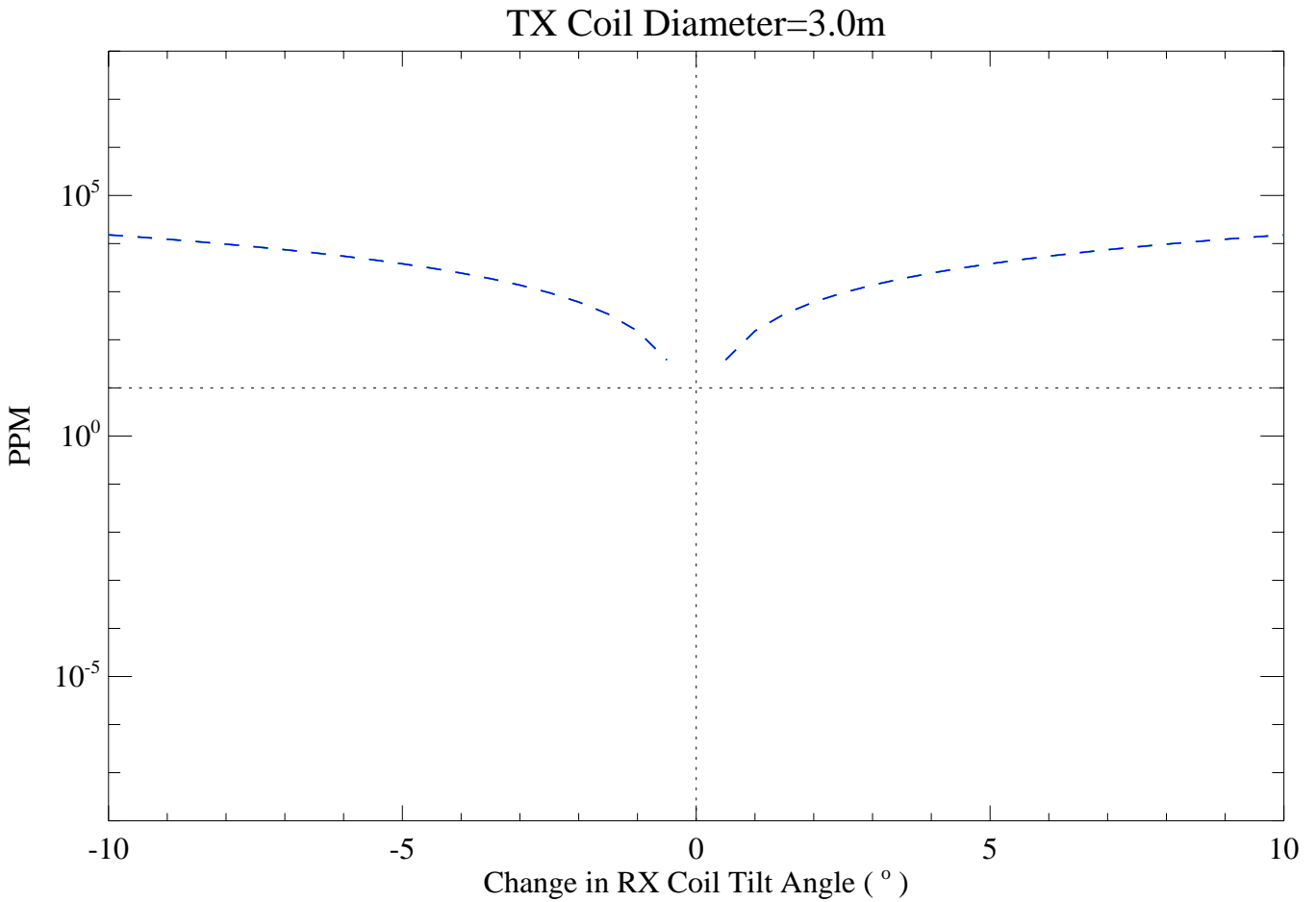
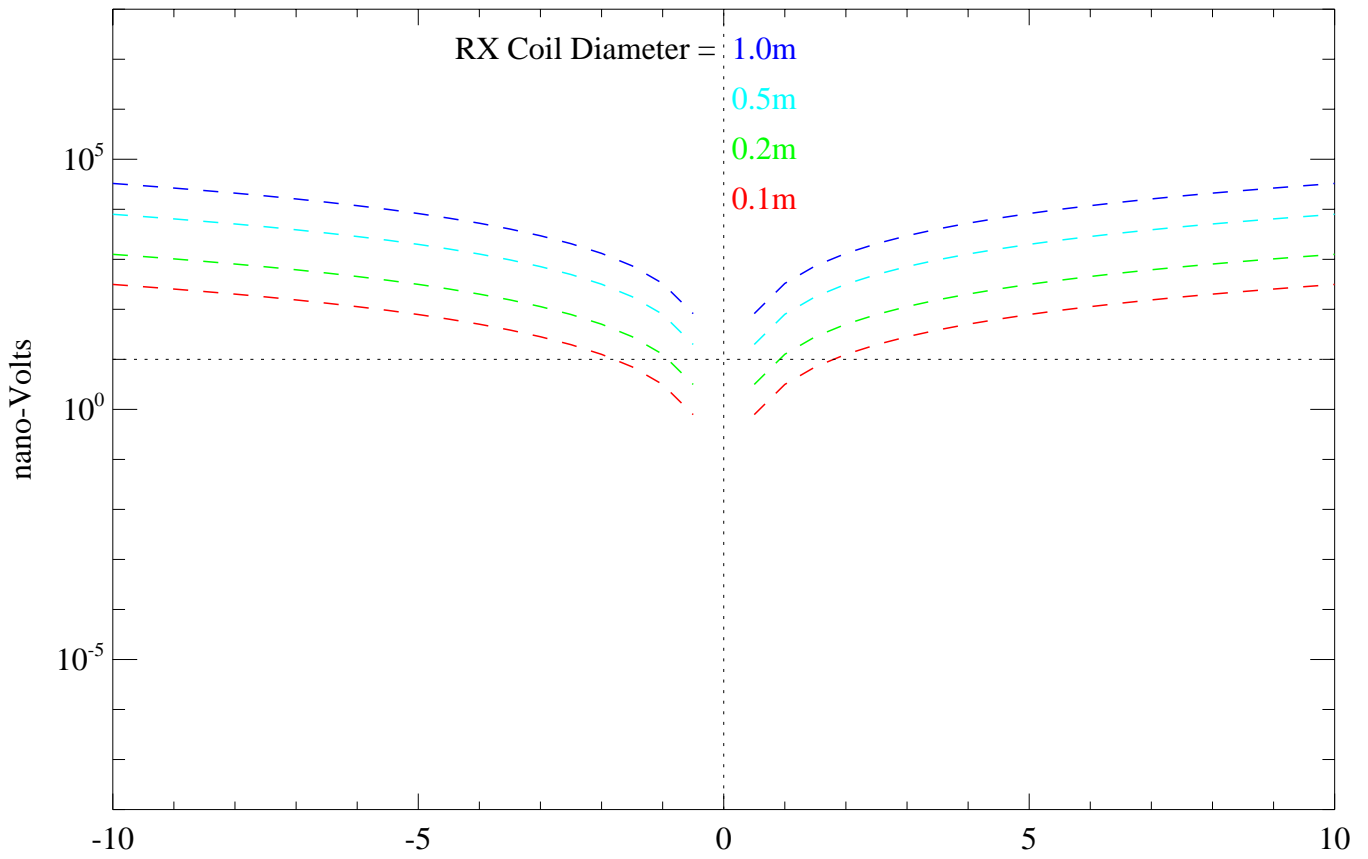
CASE 1 - Change in Primary Field Coupling due to dZ Perturbations on RX Coil



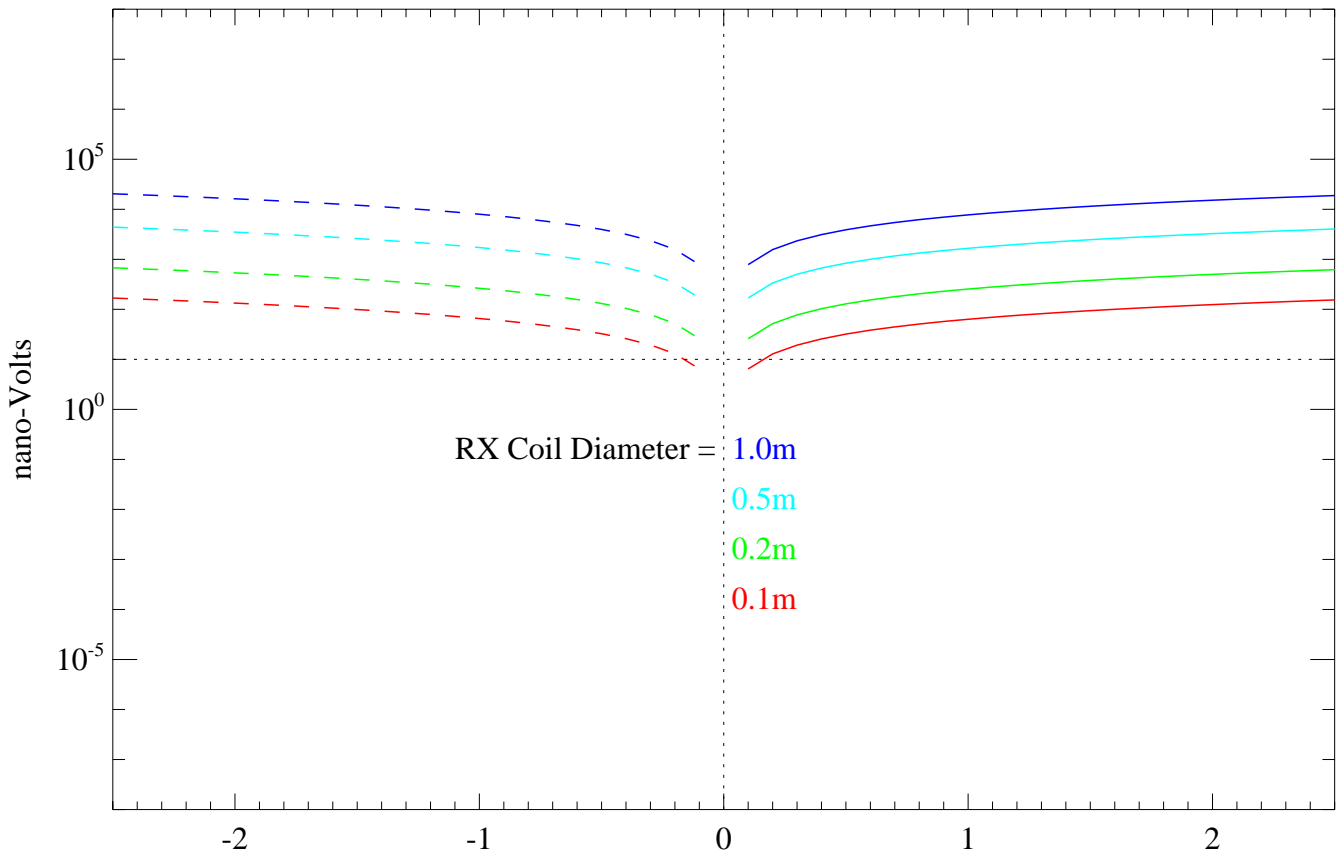
CASE 1 - Change in Primary Field Coupling due to dX Perturbations on RX Coil



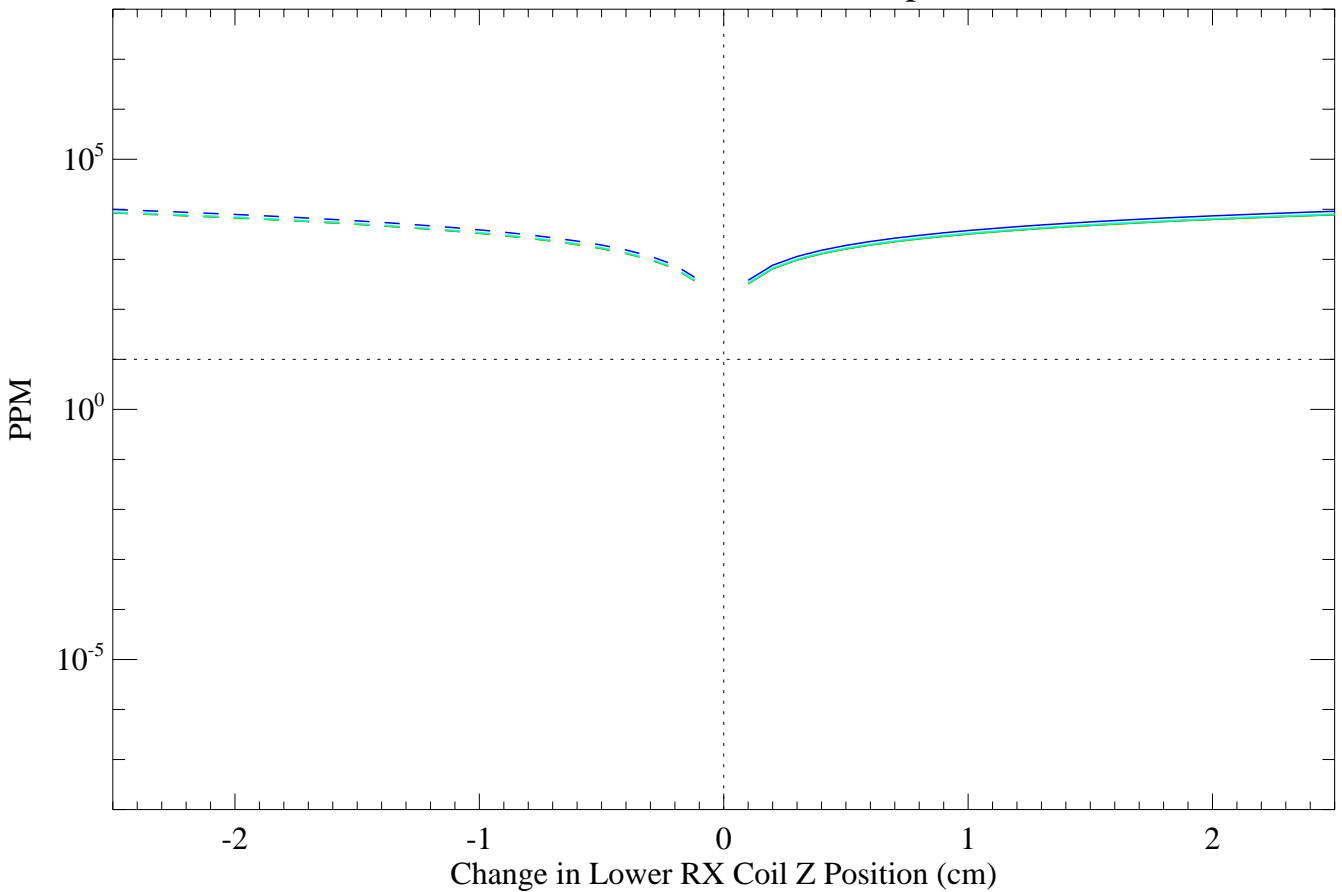
CASE 1 - Change in Primary Field Coupling due to Pitch Perturbations on RX Coil



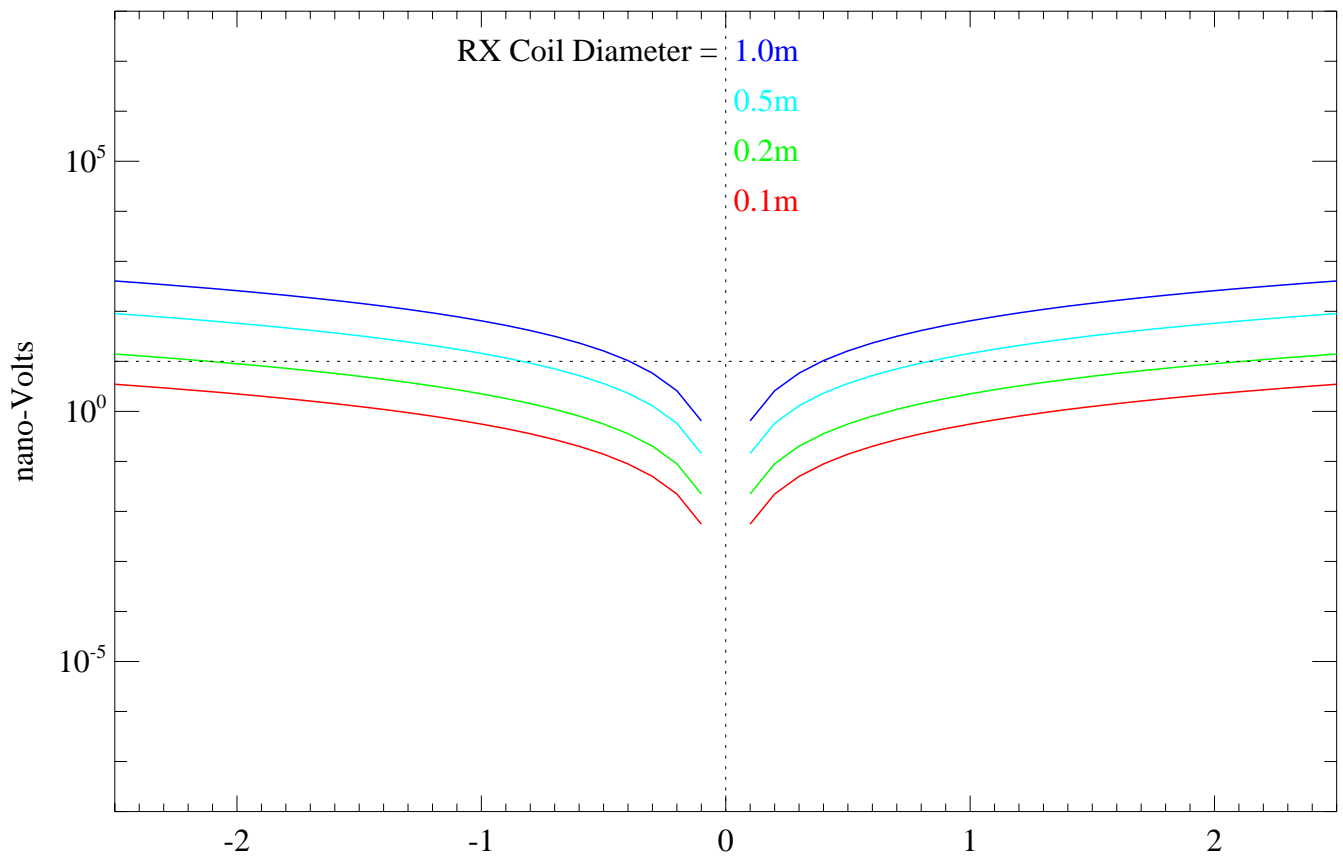
CASE 2 - Change in Primary Field Coupling due to dZ Perturbations on a single RX Coil in a Gradient Pair



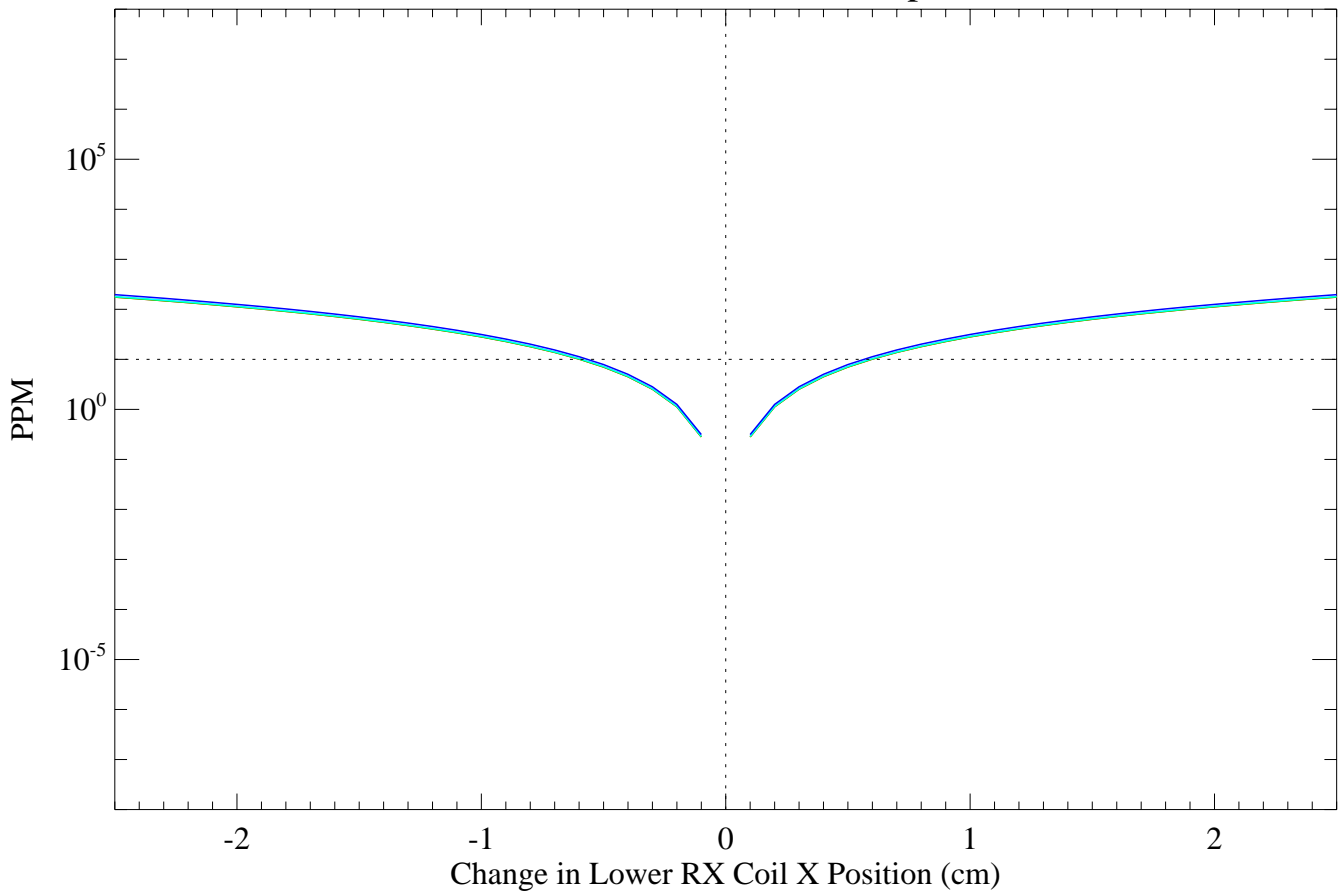
TX Coil Diameter=3.0m, RX Coil Separation=0.5m



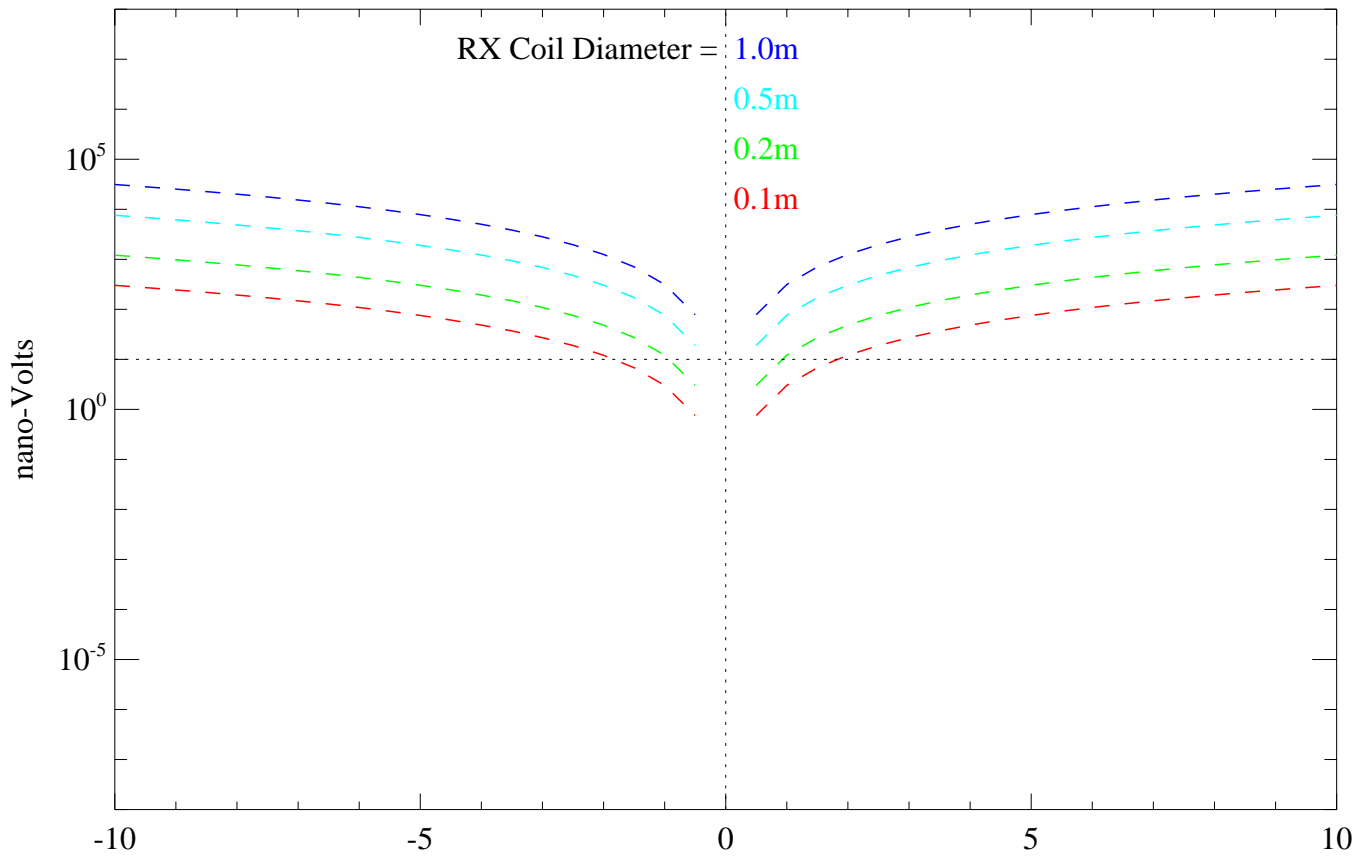
CASE 2 - Change in Primary Field Coupling due to dX Perturbations on a single RX Coil in a Gradient Pair



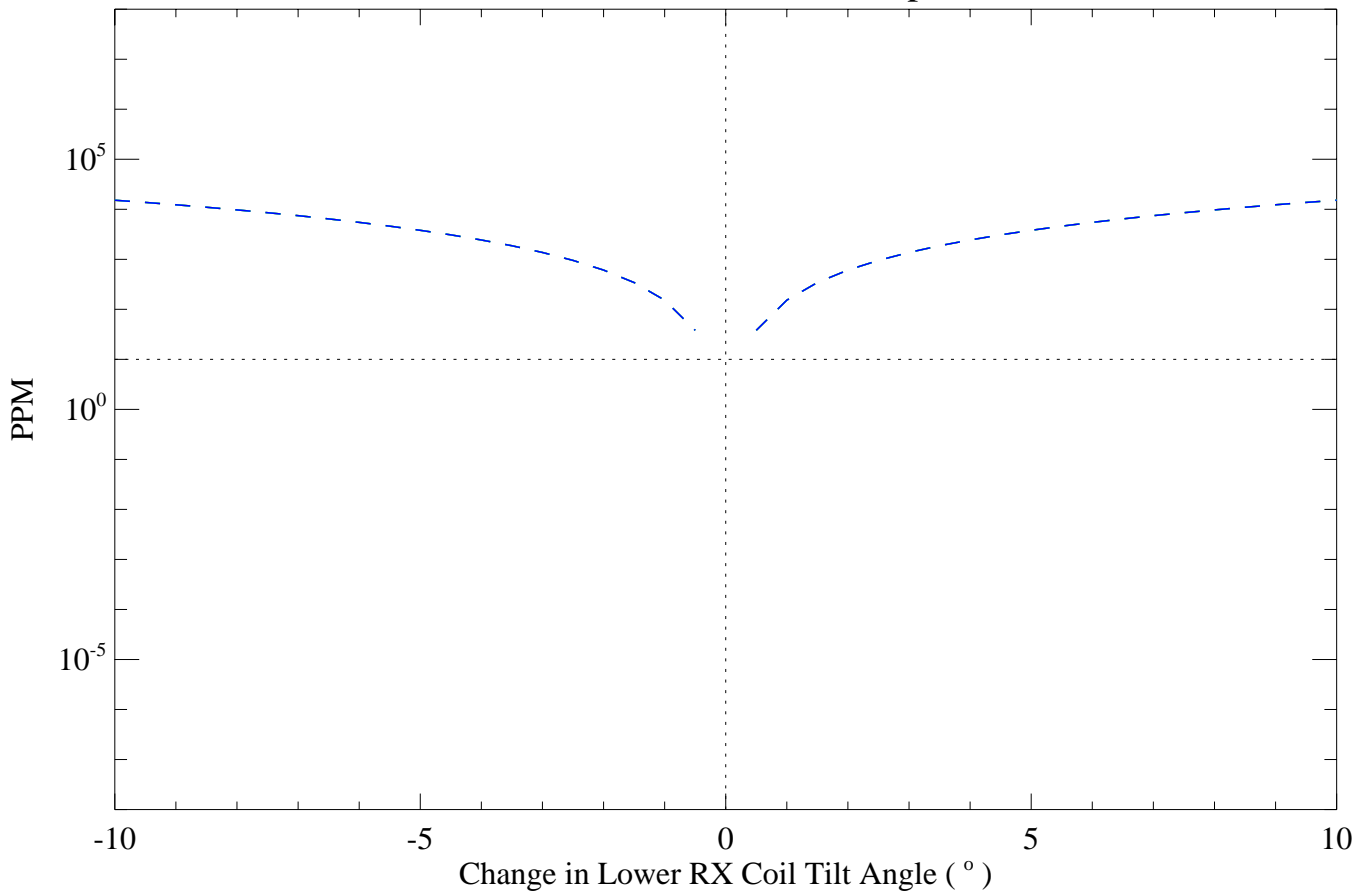
TX Coil Diameter=3.0m, RX Coil Separation=0.5m



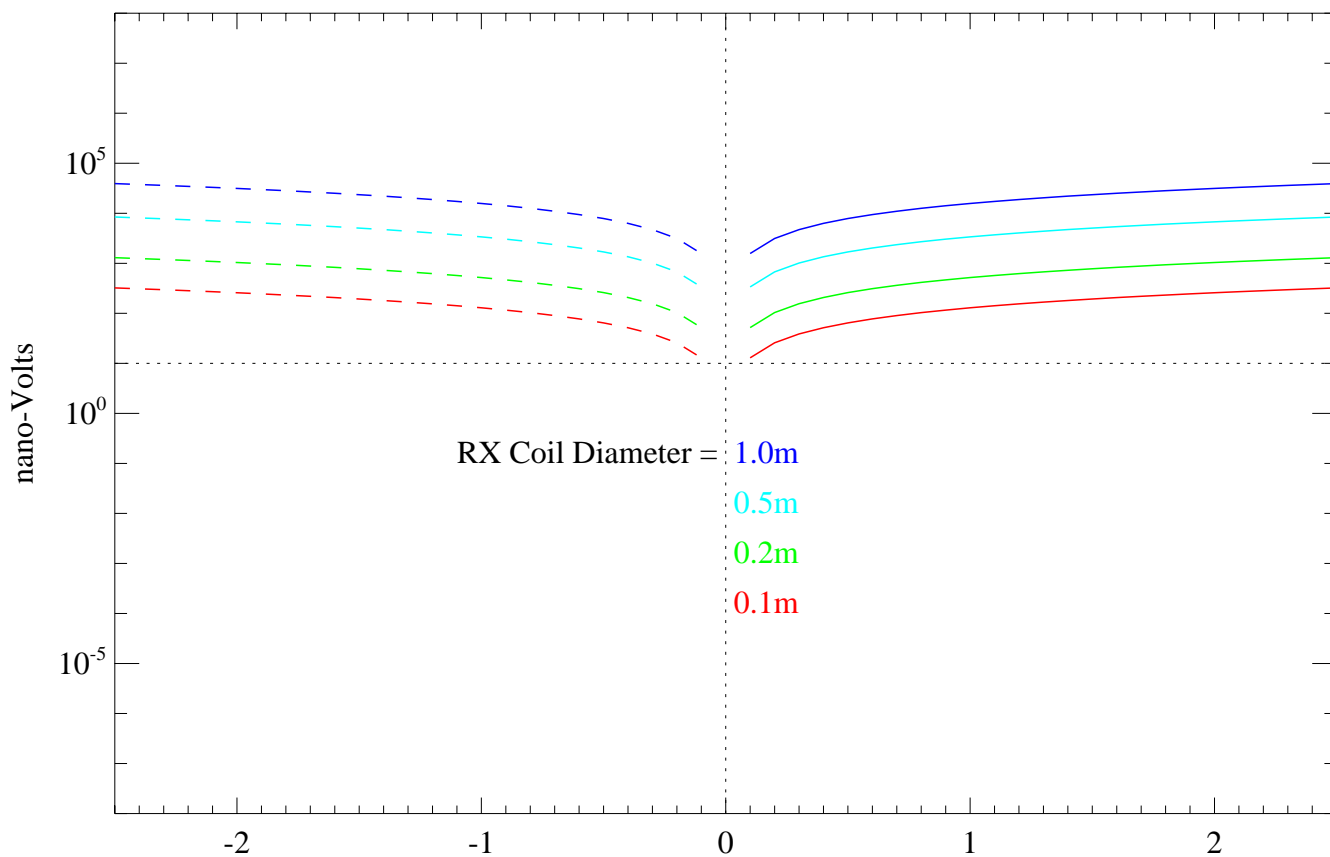
CASE 2 - Change in Primary Field Coupling due to Pitch Perturbations on a single RX Coil in a Gradient Pair



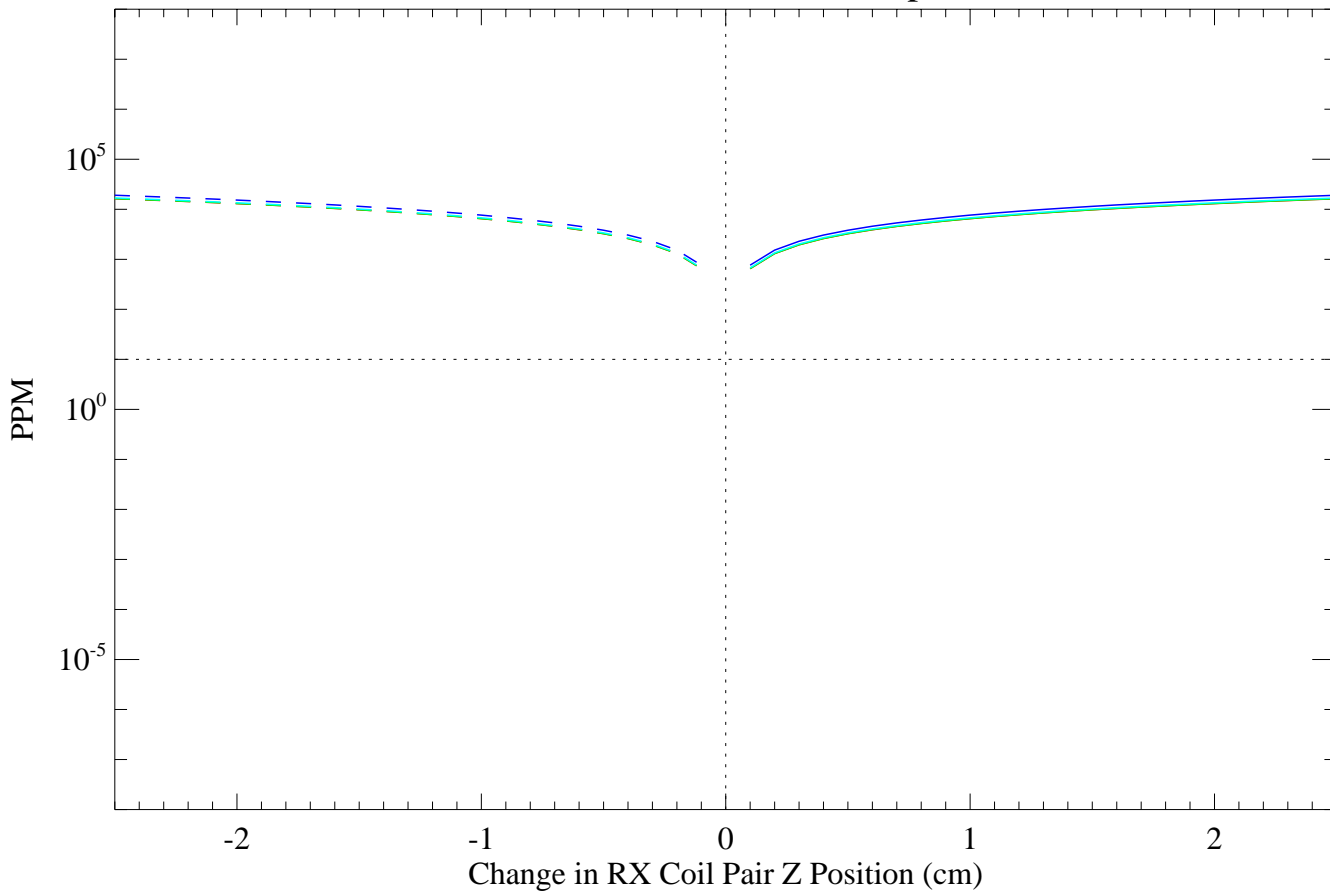
TX Coil Diameter=3.0m, RX Coil Separation=0.5m



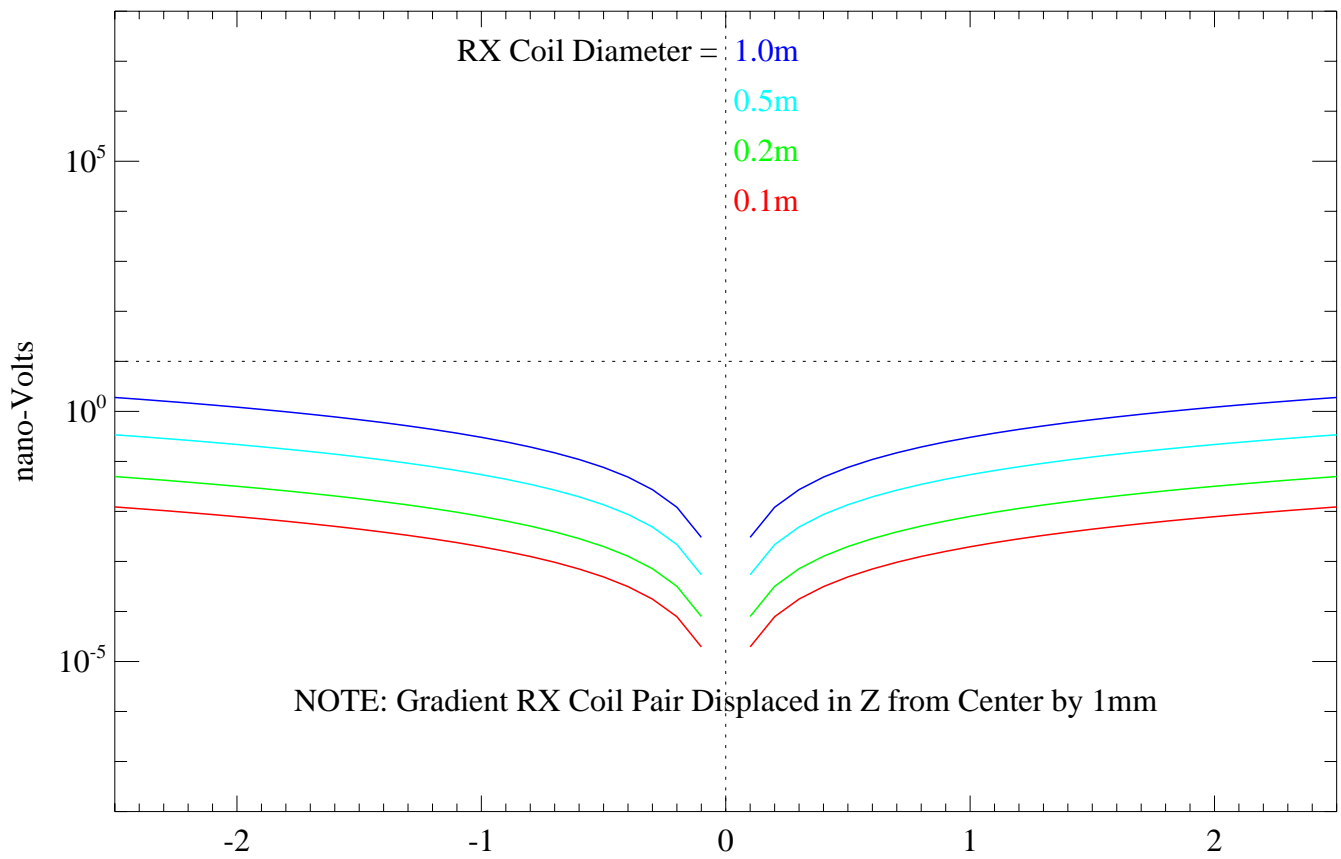
CASE 2 - Change in Primary Field Coupling due to dZ Perturbations on a rigid Gradient RX Coil Pair



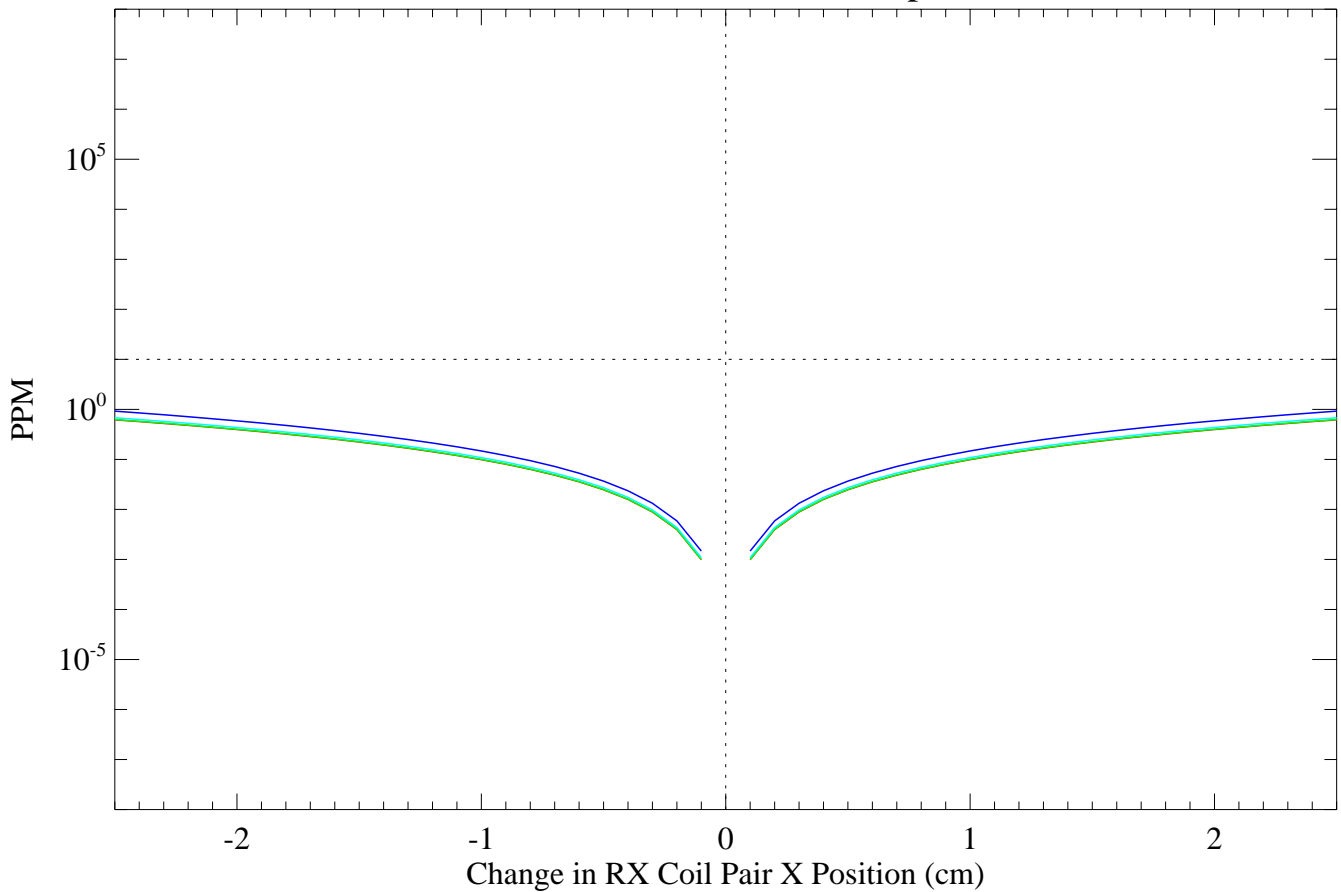
TX Coil Diameter=3.0m, RX Coil Separation=0.5m



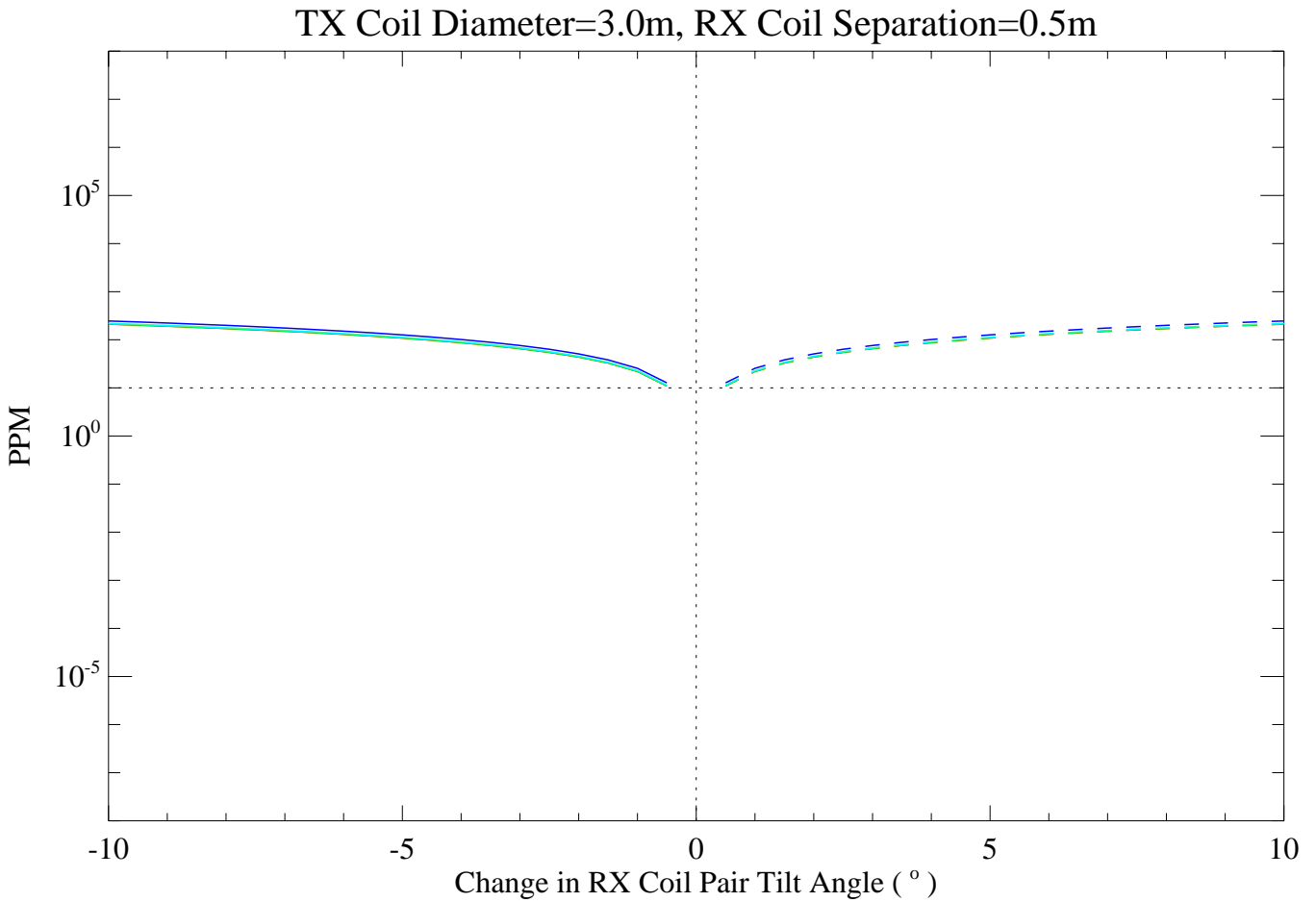
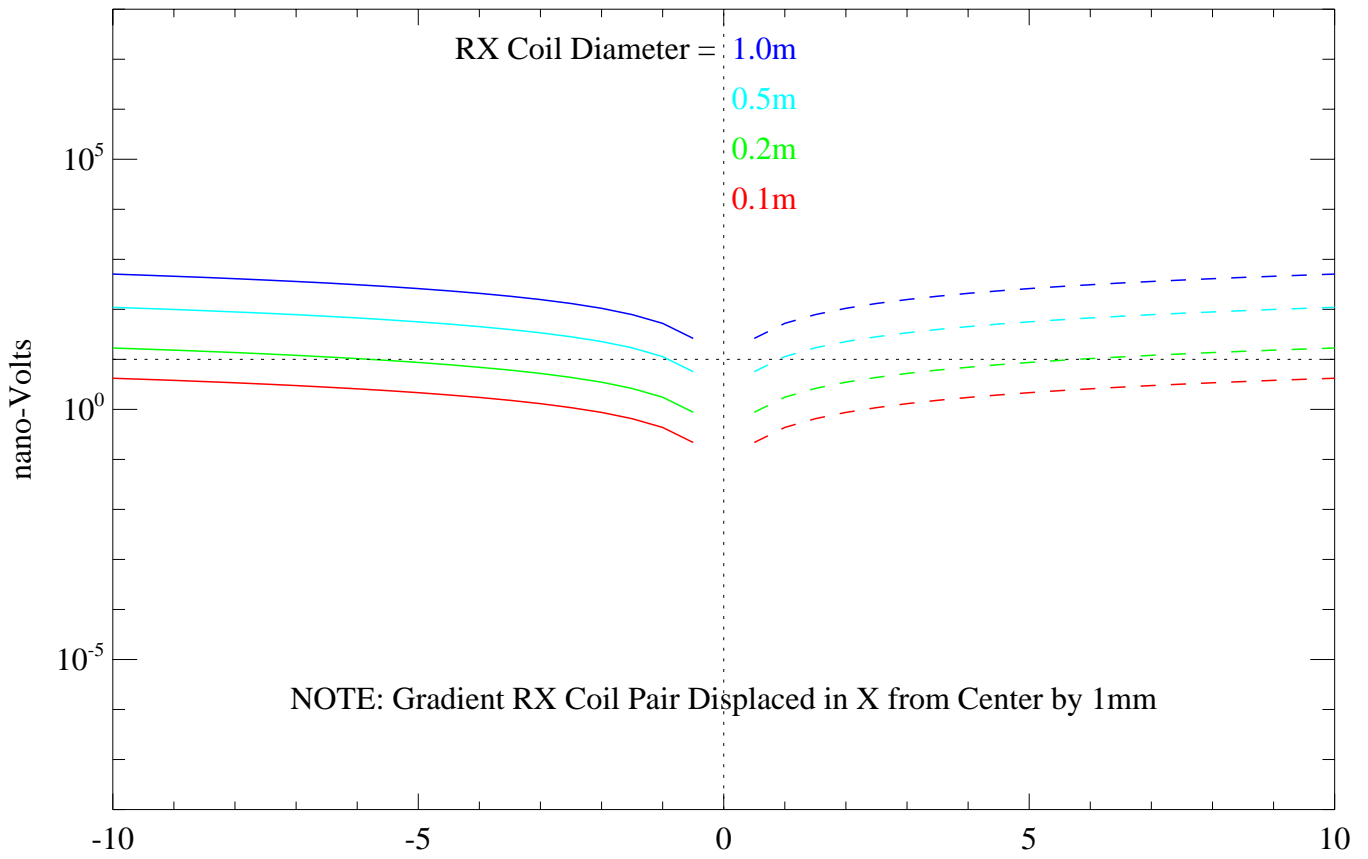
CASE 2 - Change in Primary Field Coupling due to dX Perturbations on a rigid Gradient RX Coil Pair



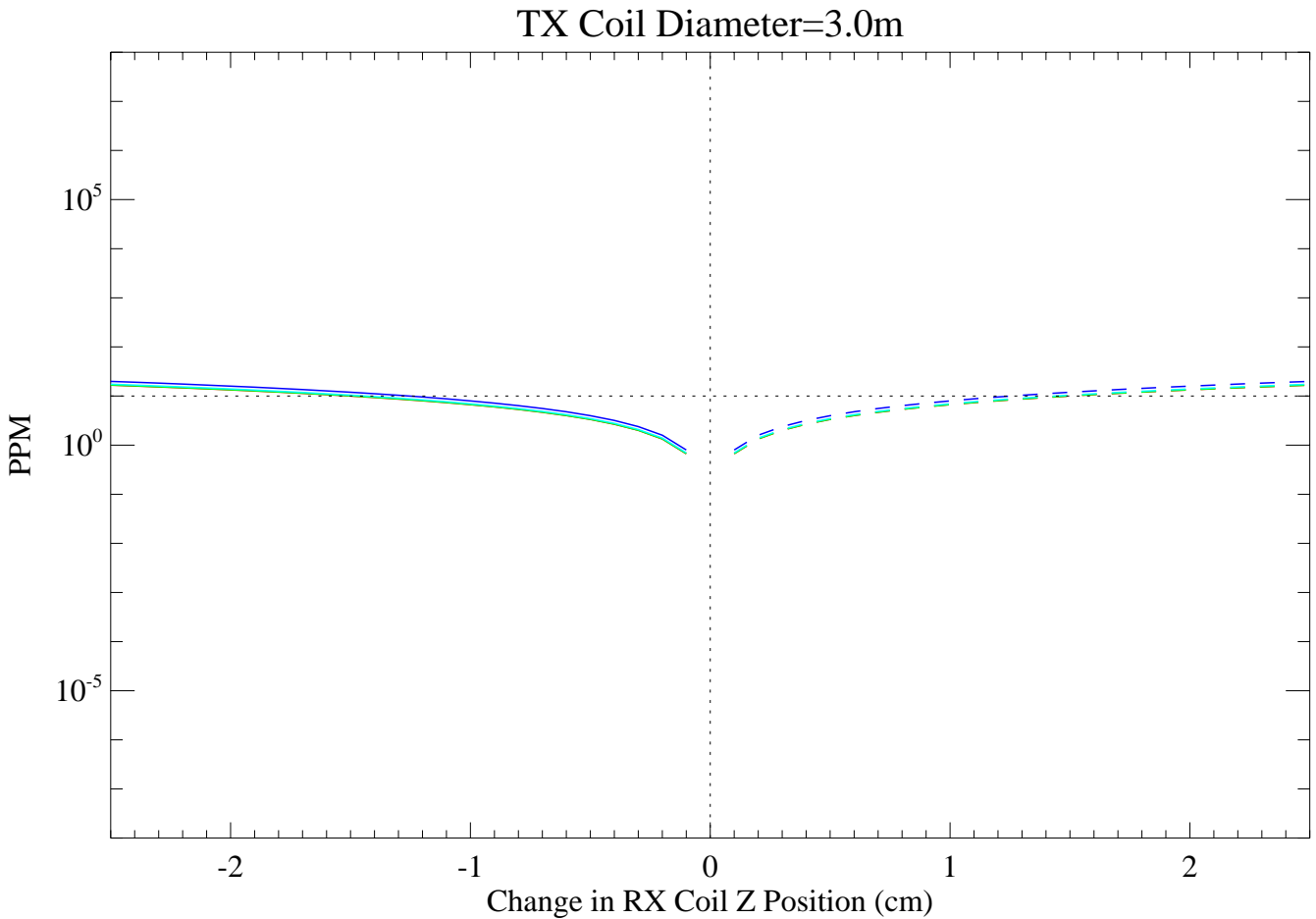
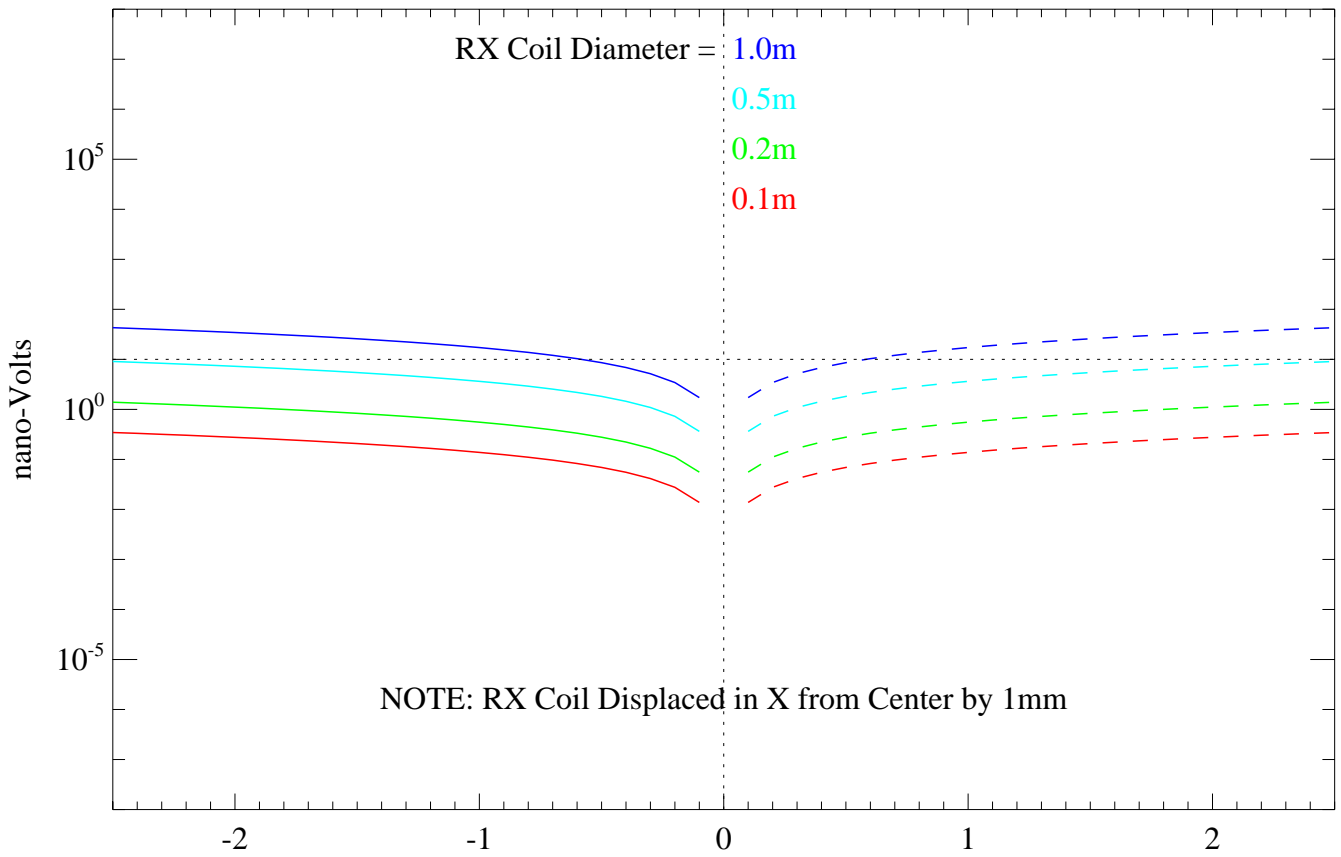
TX Coil Diameter=3.0m, RX Coil Separation=0.5m



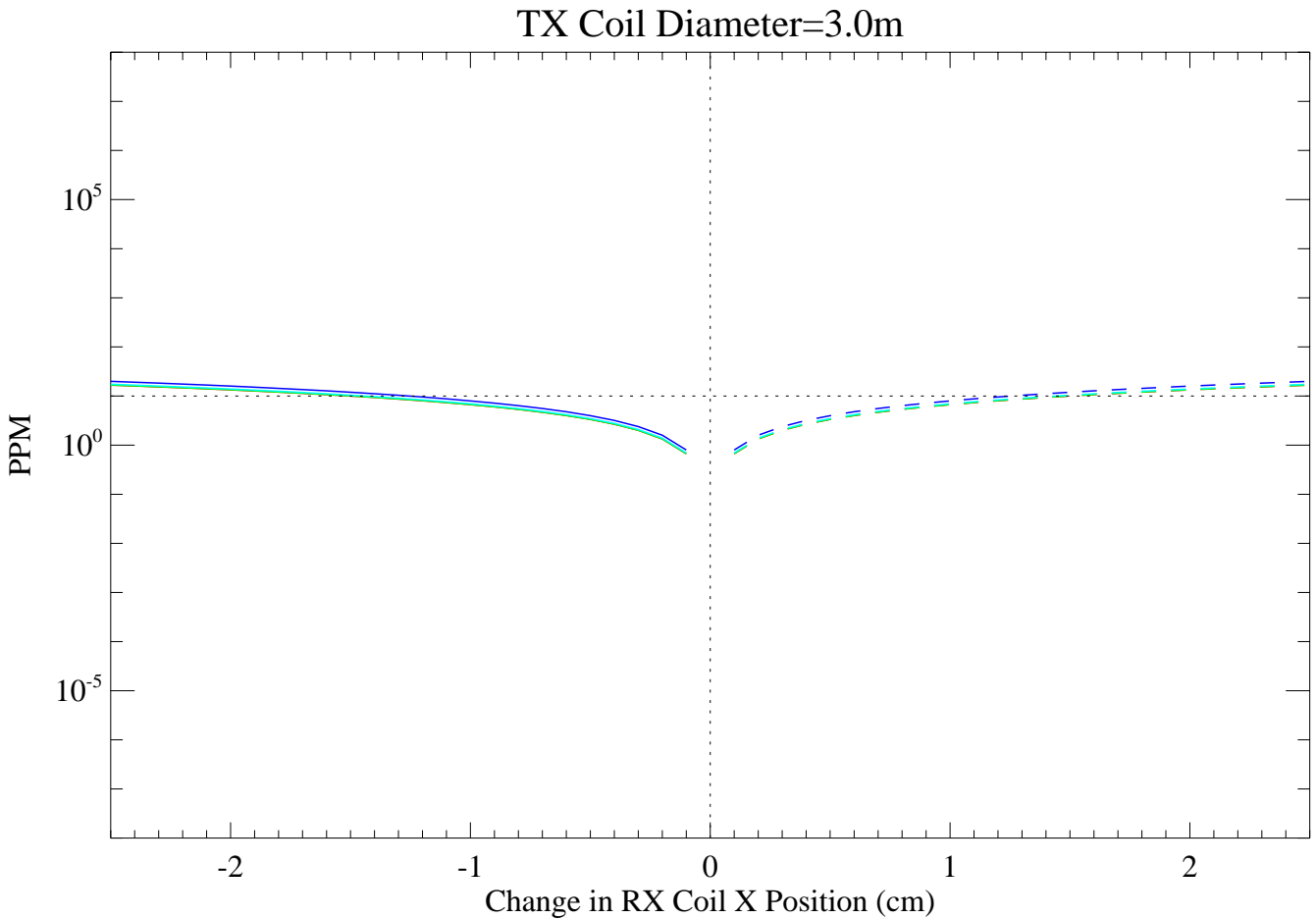
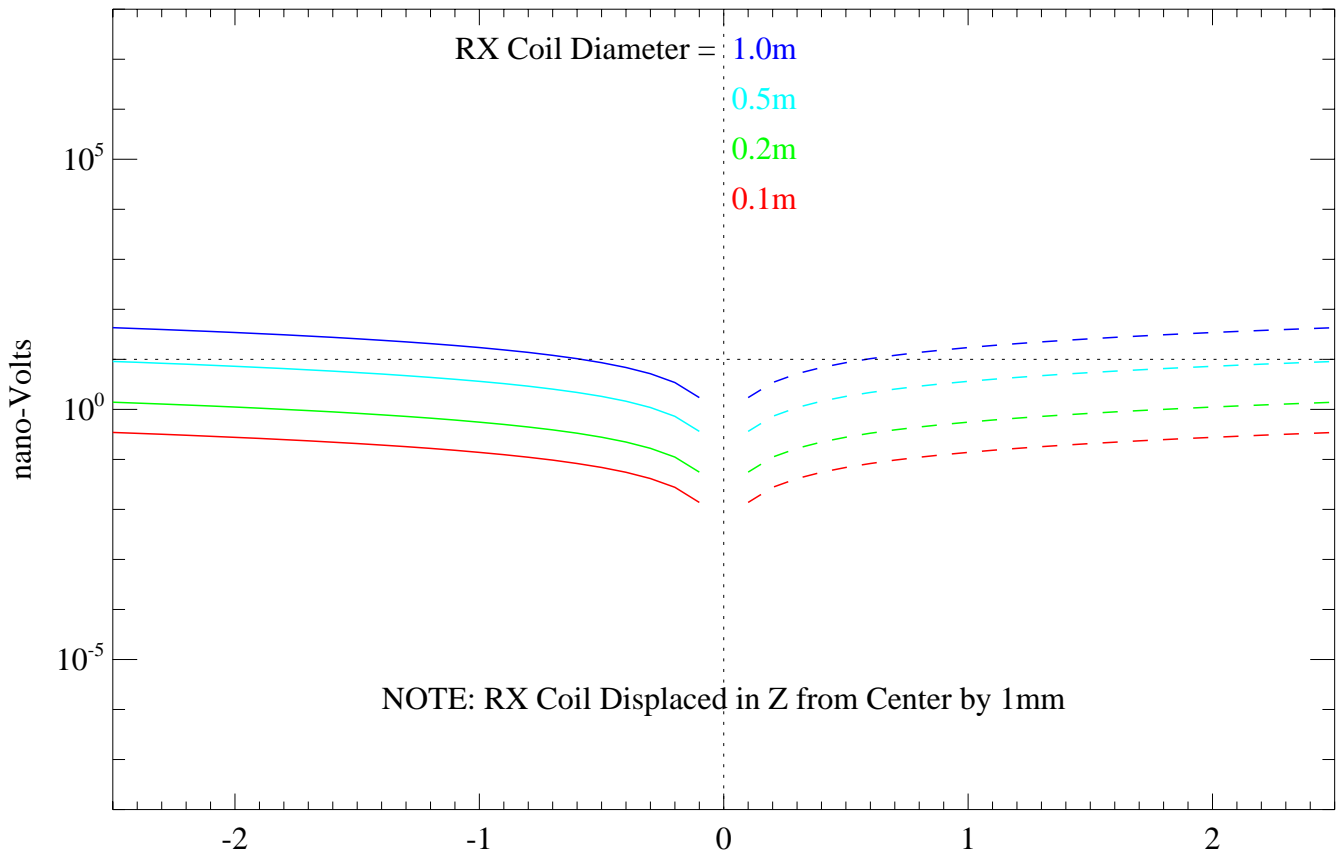
CASE 2 - Change in Primary Field Coupling due to Pitch Perturbations on a rigid Gradient RX Coil Pair



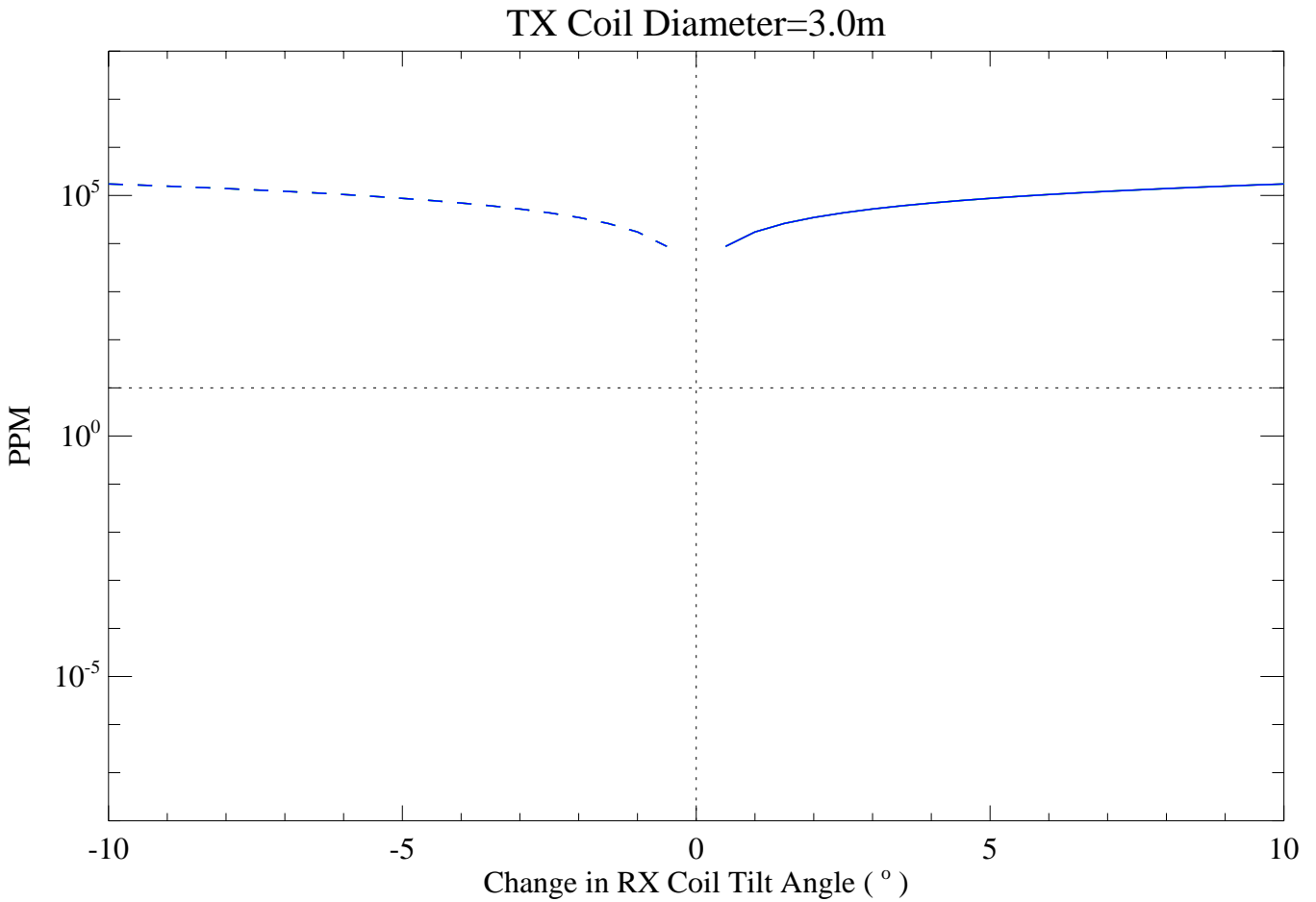
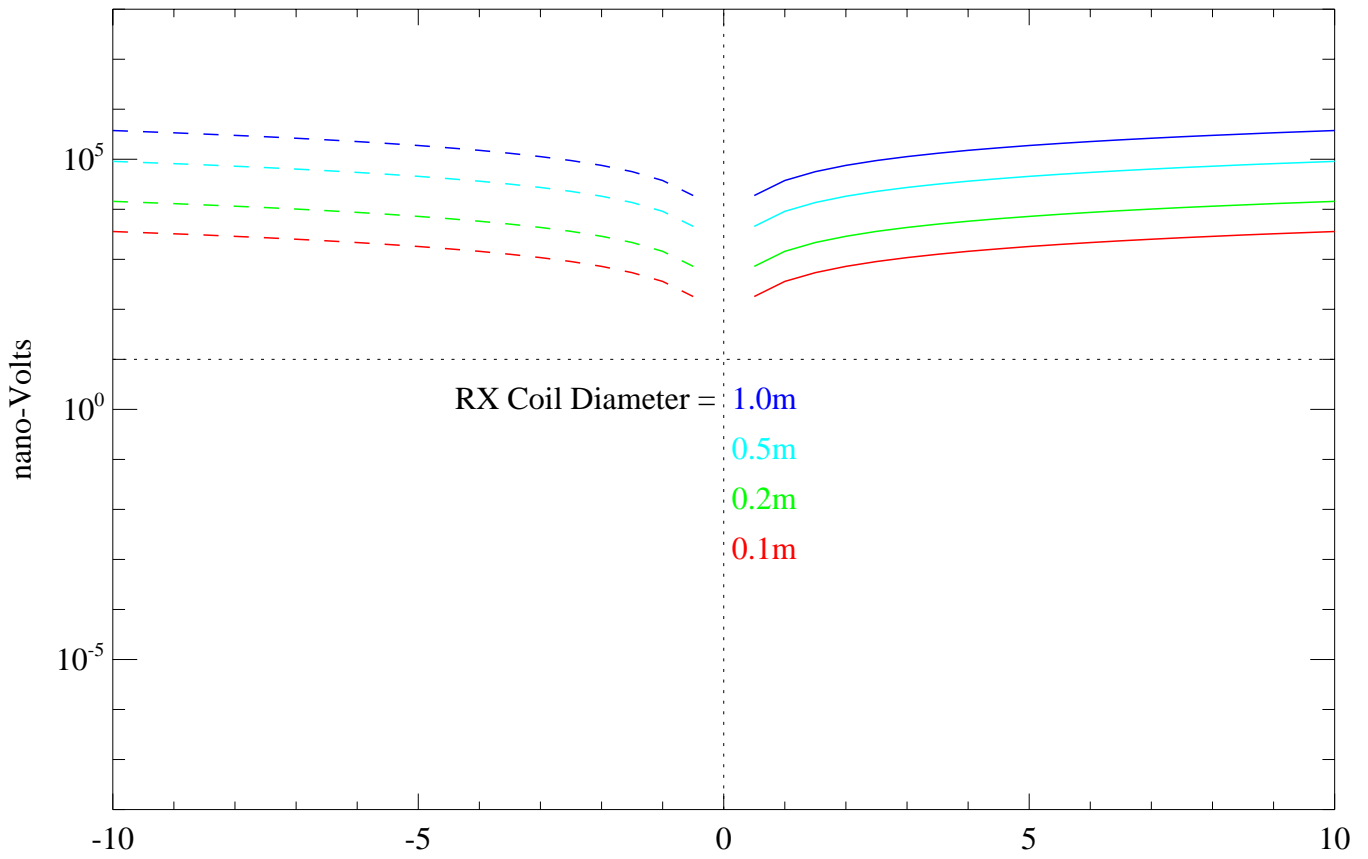
CASE 3 - Change in Primary Field Coupling due to dZ Perturbations on RX Coil



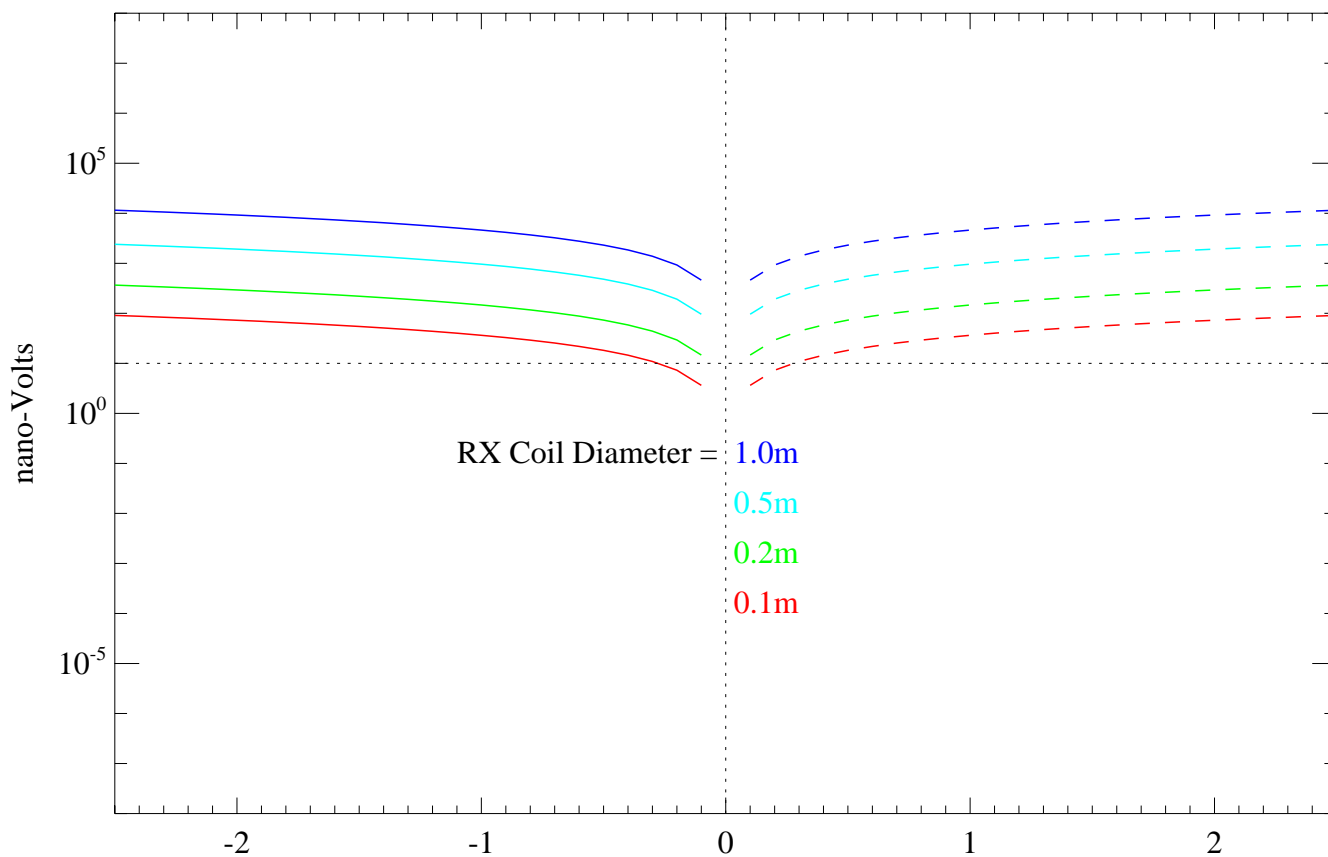
CASE 3 - Change in Primary Field Coupling due to dX Perturbations on RX Coil



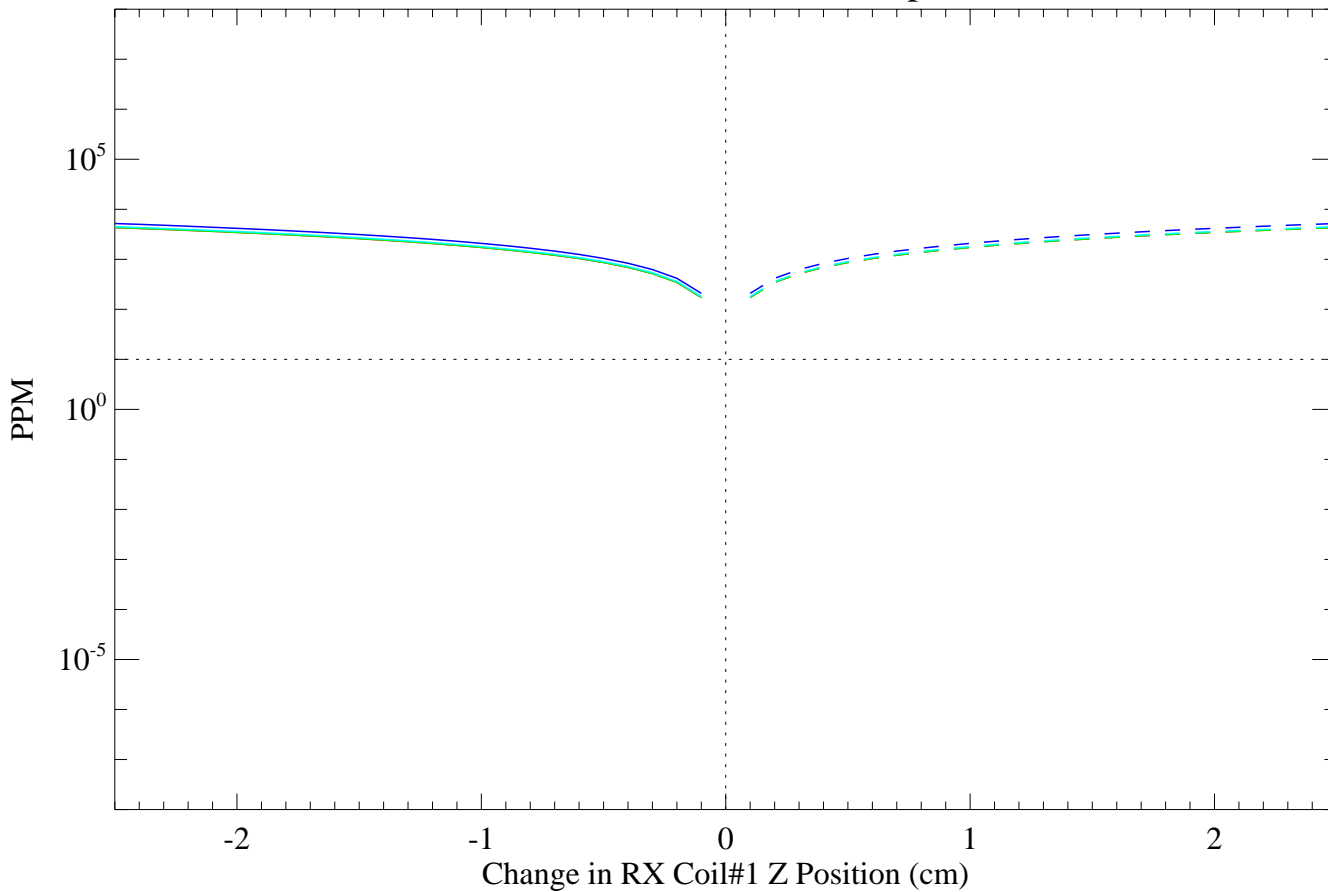
CASE 3 - Change in Primary Field Coupling due to Pitch Perturbations on RX Coil



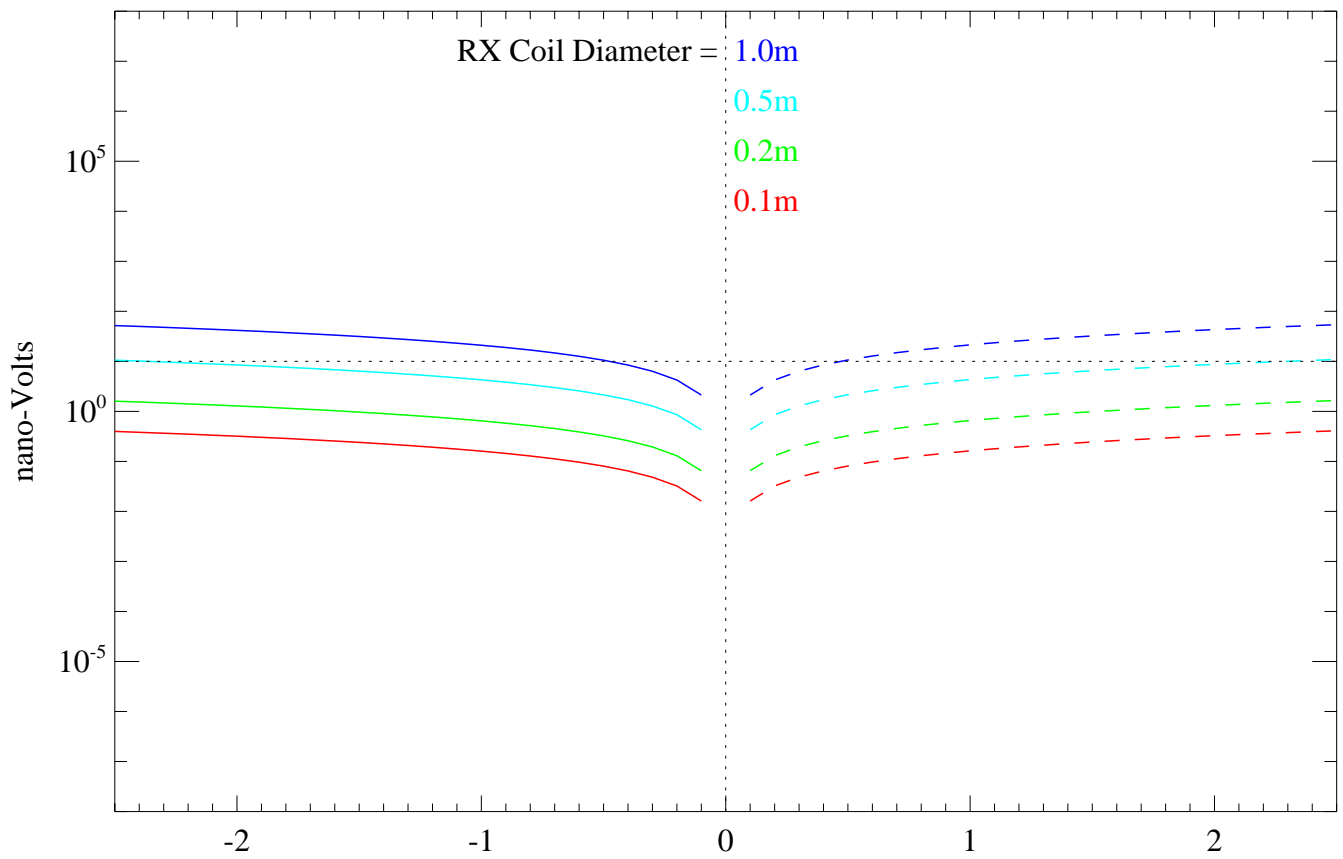
CASE 4 - Change in Primary Field Coupling due to dZ Perturbations on a single RX Coil in a Gradient Pair



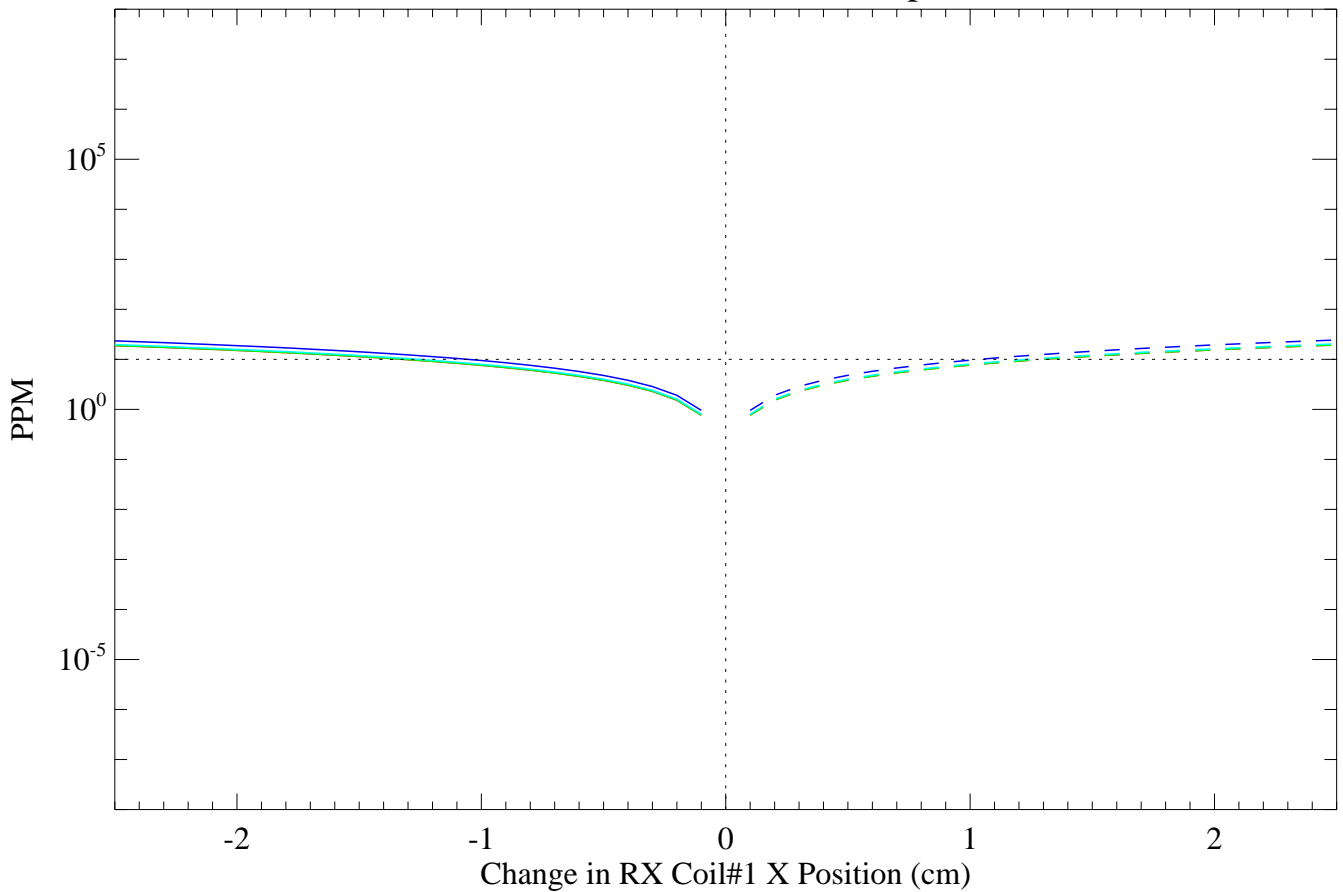
TX Coil Diameter=3.0m, RX Coil Separation=0.5m



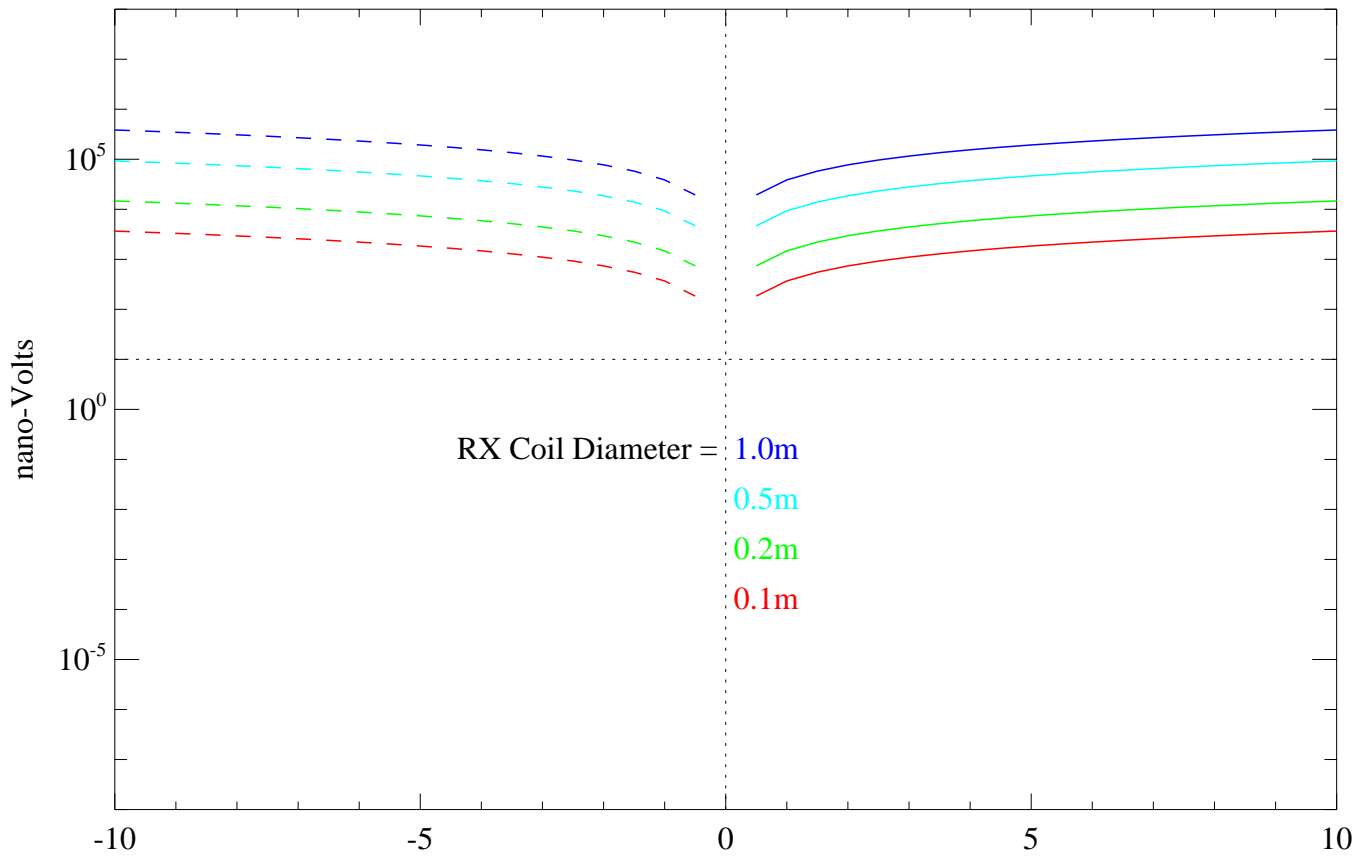
CASE 4 - Change in Primary Field Coupling due to dX Perturbations on a single RX Coil in a Gradient Pair



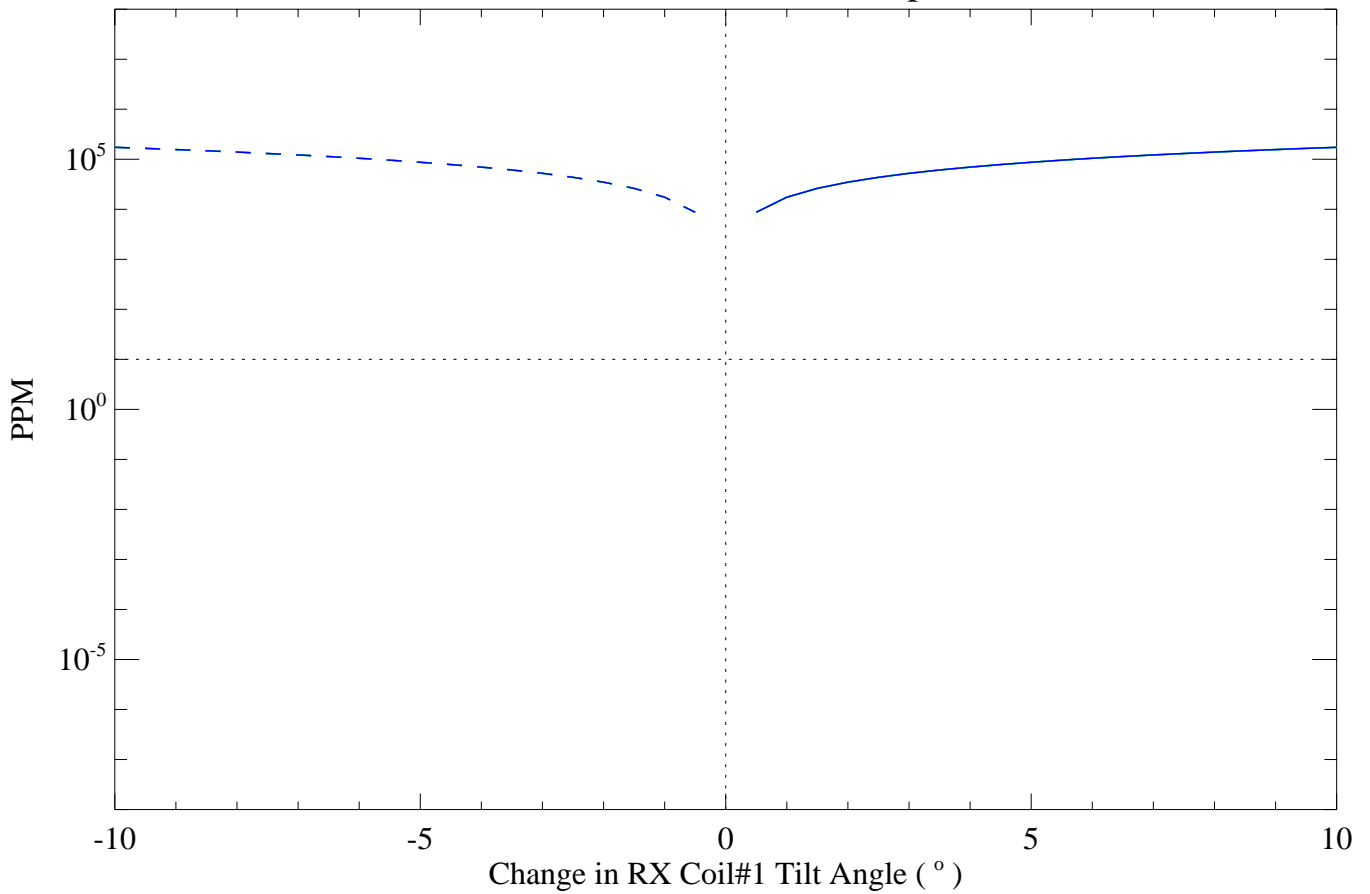
TX Coil Diameter=3.0m, RX Coil Separation=0.5m



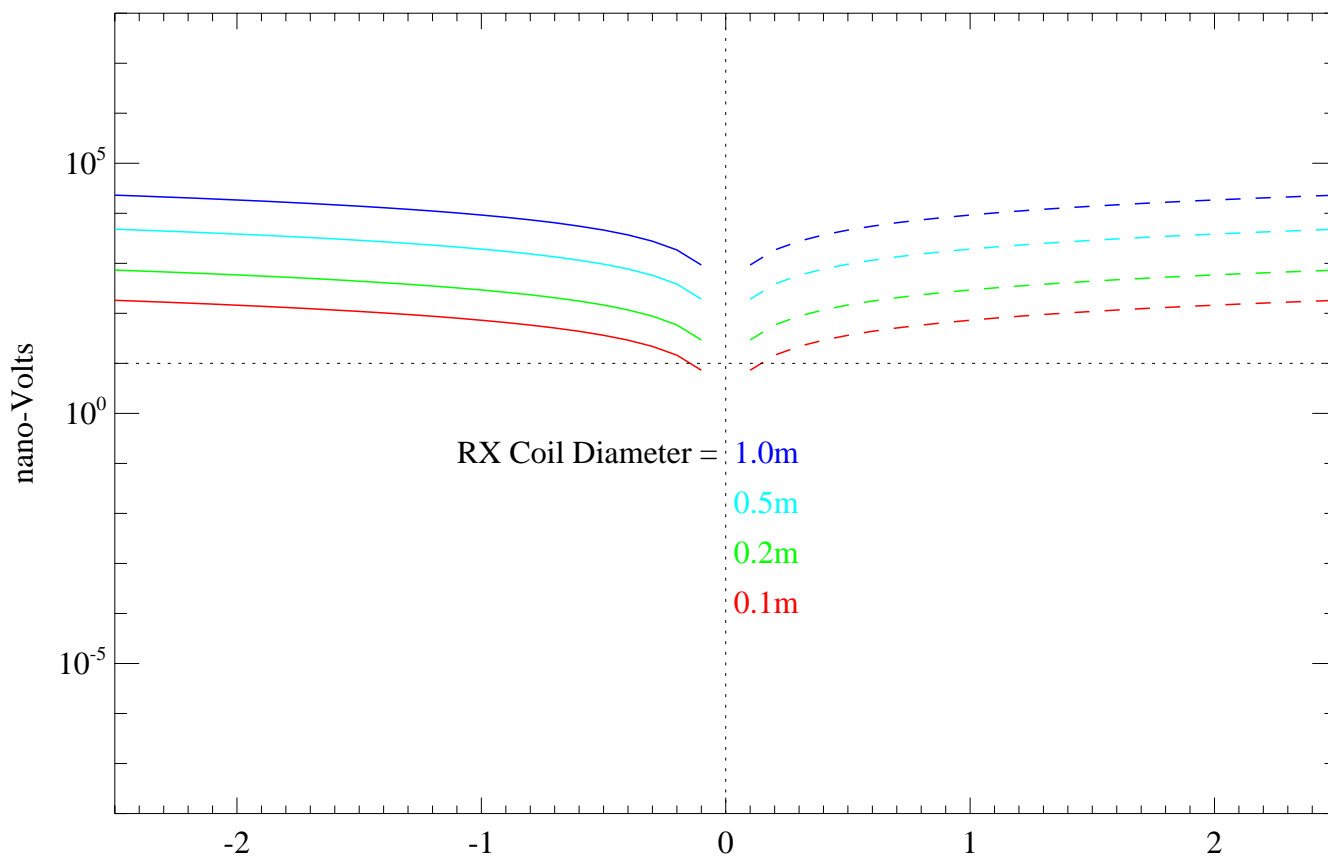
CASE 4 - Change in Primary Field Coupling due to Pitch Perturbations on a single RX Coil in a Gradient Pair



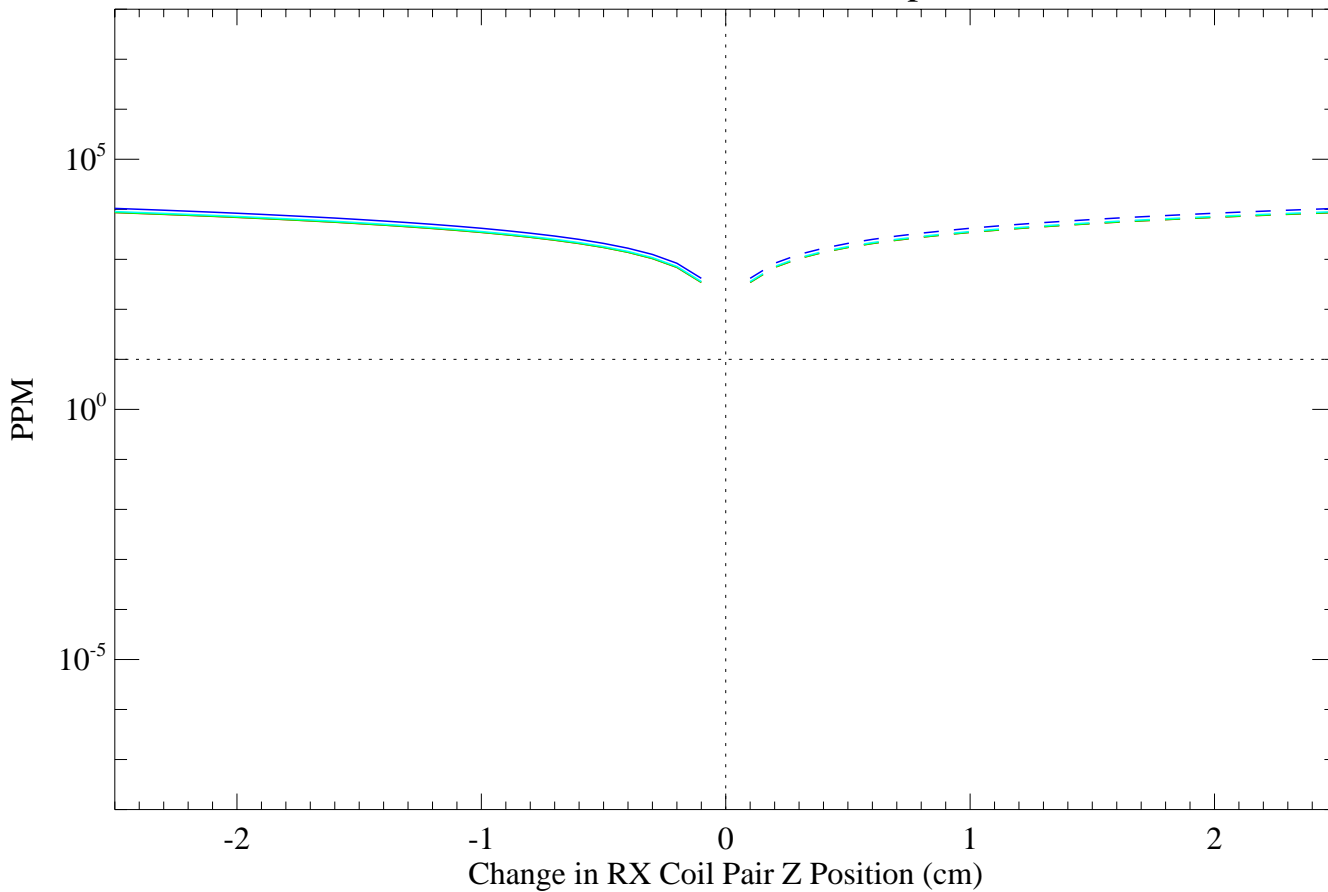
TX Coil Diameter=3.0m, RX Coil Separation=0.5m



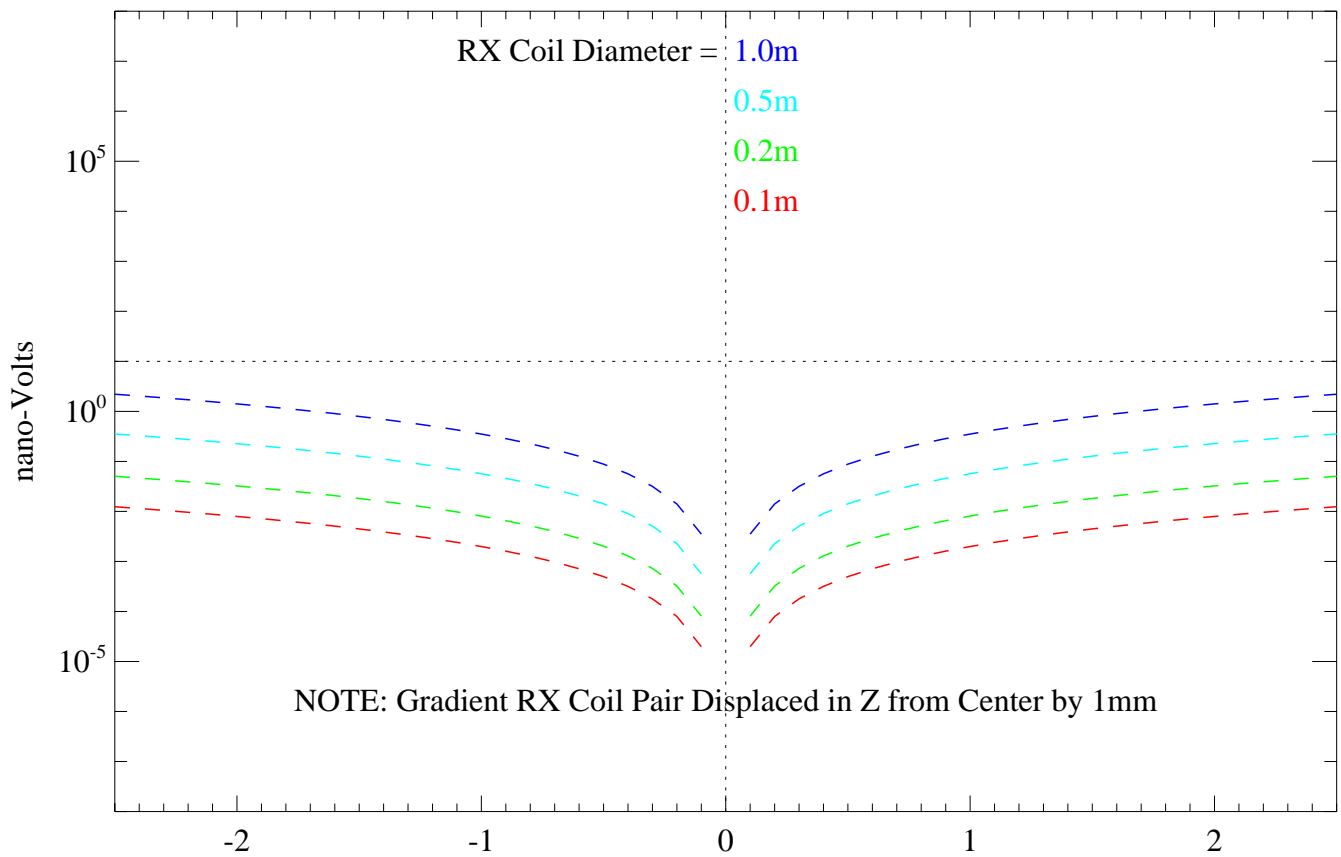
CASE 4 - Change in Primary Field Coupling due to dZ Perturbations on a rigid Gradient RX Coil Pair



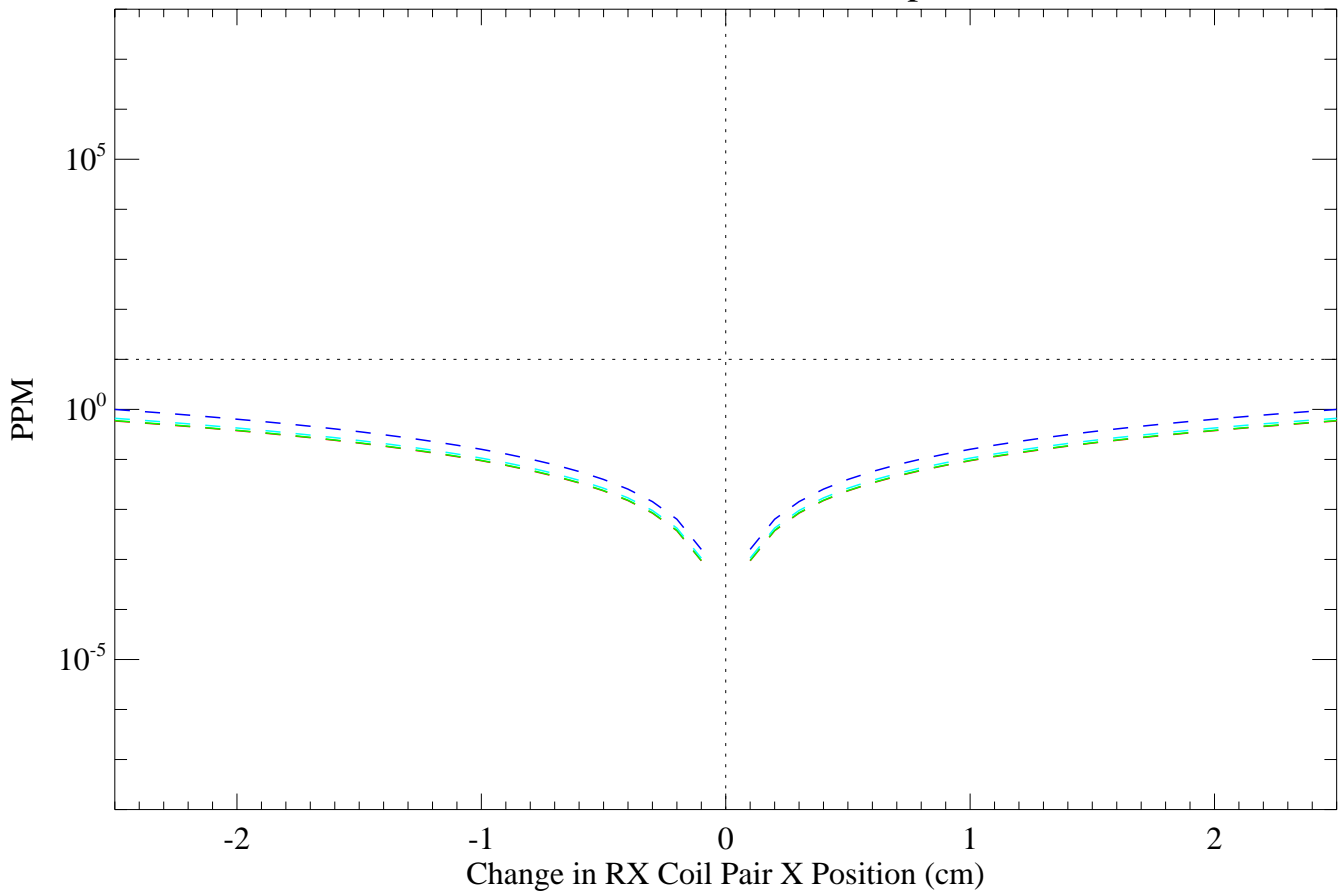
TX Coil Diameter=3.0m, RX Coil Separation=0.5m



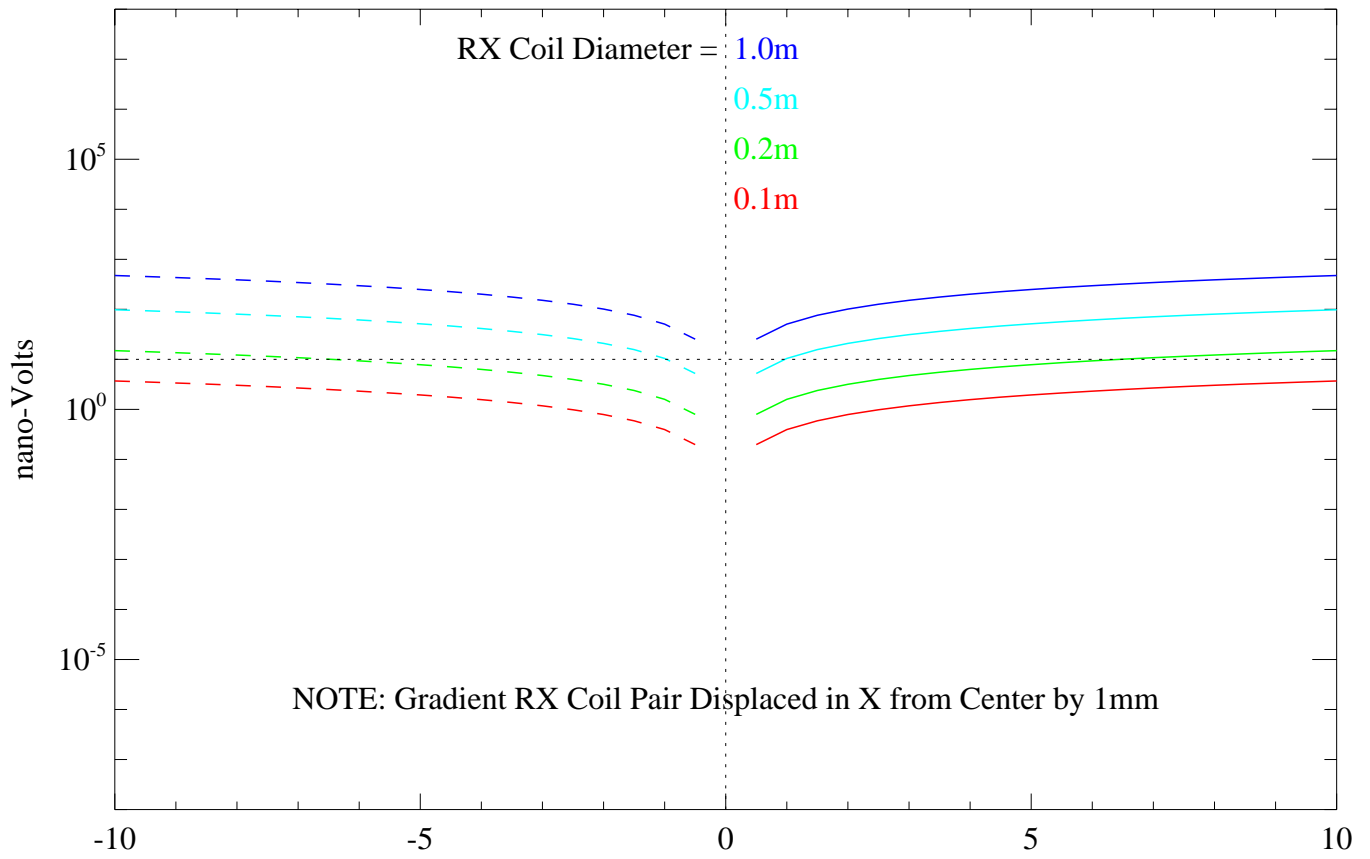
CASE 4 - Change in Primary Field Coupling due to dX Perturbations on a rigid Gradient RX Coil Pair



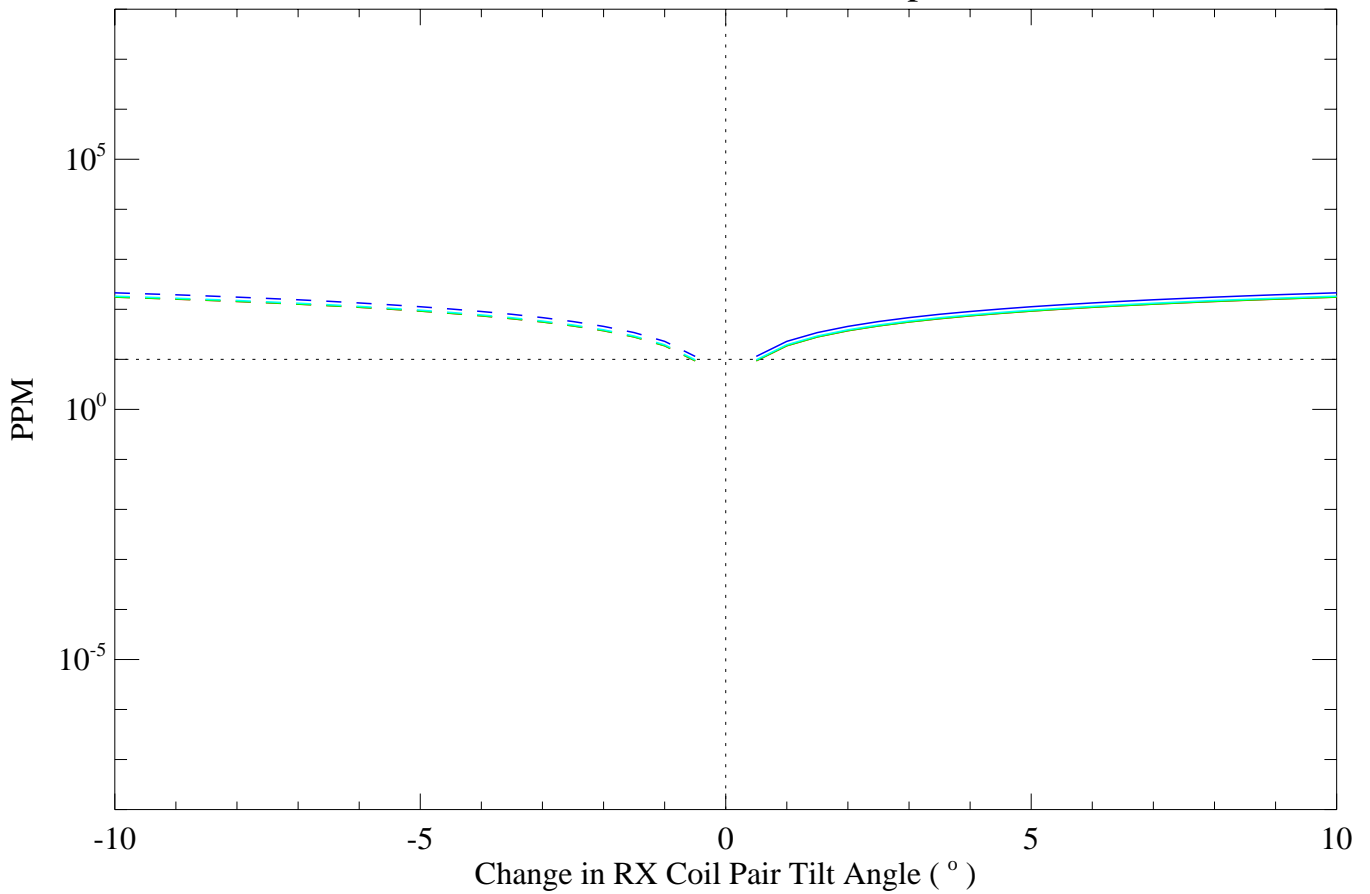
TX Coil Diameter=3.0m, RX Coil Separation=0.5m



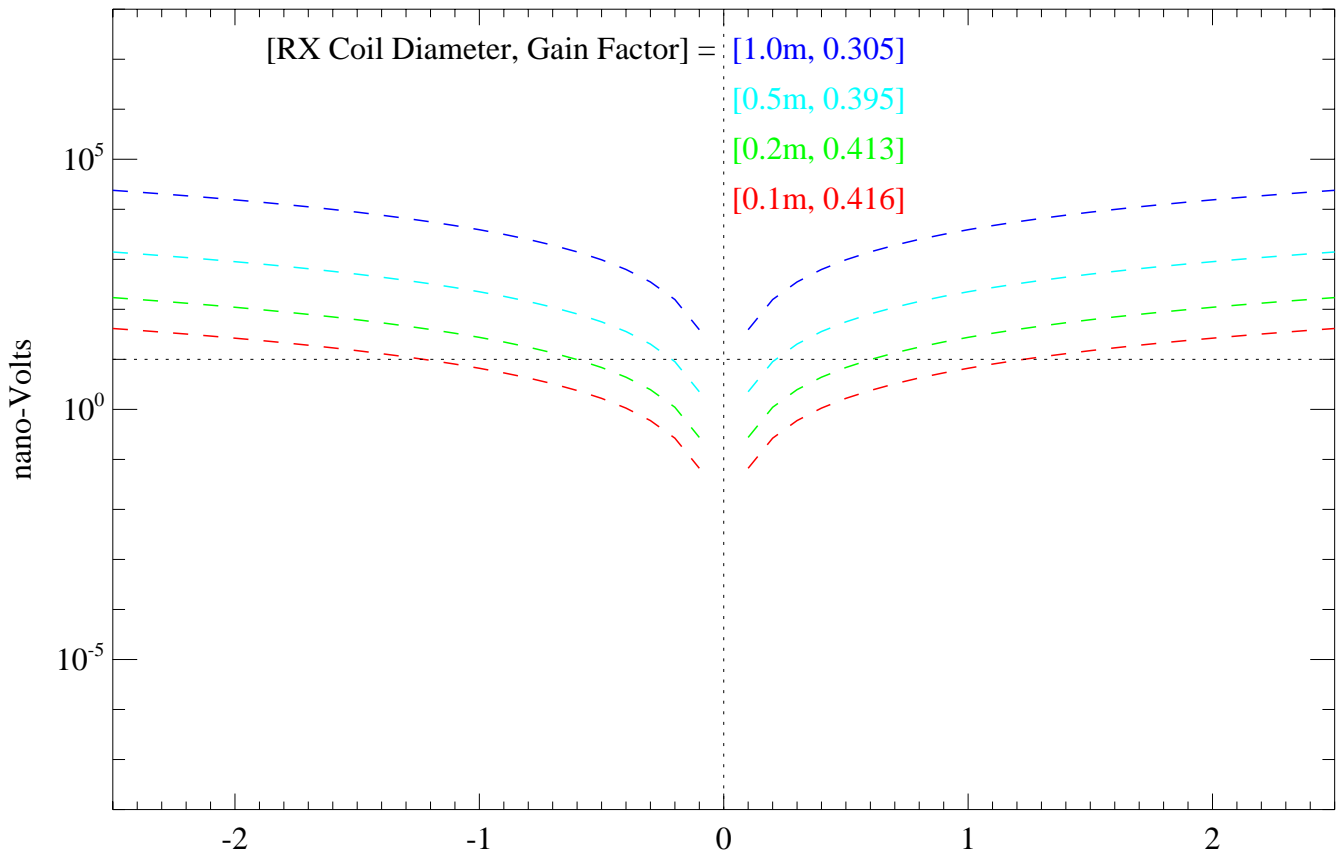
CASE 4 - Change in Primary Field Coupling due to Pitch Perturbations on a rigid Gradient RX Coil Pair



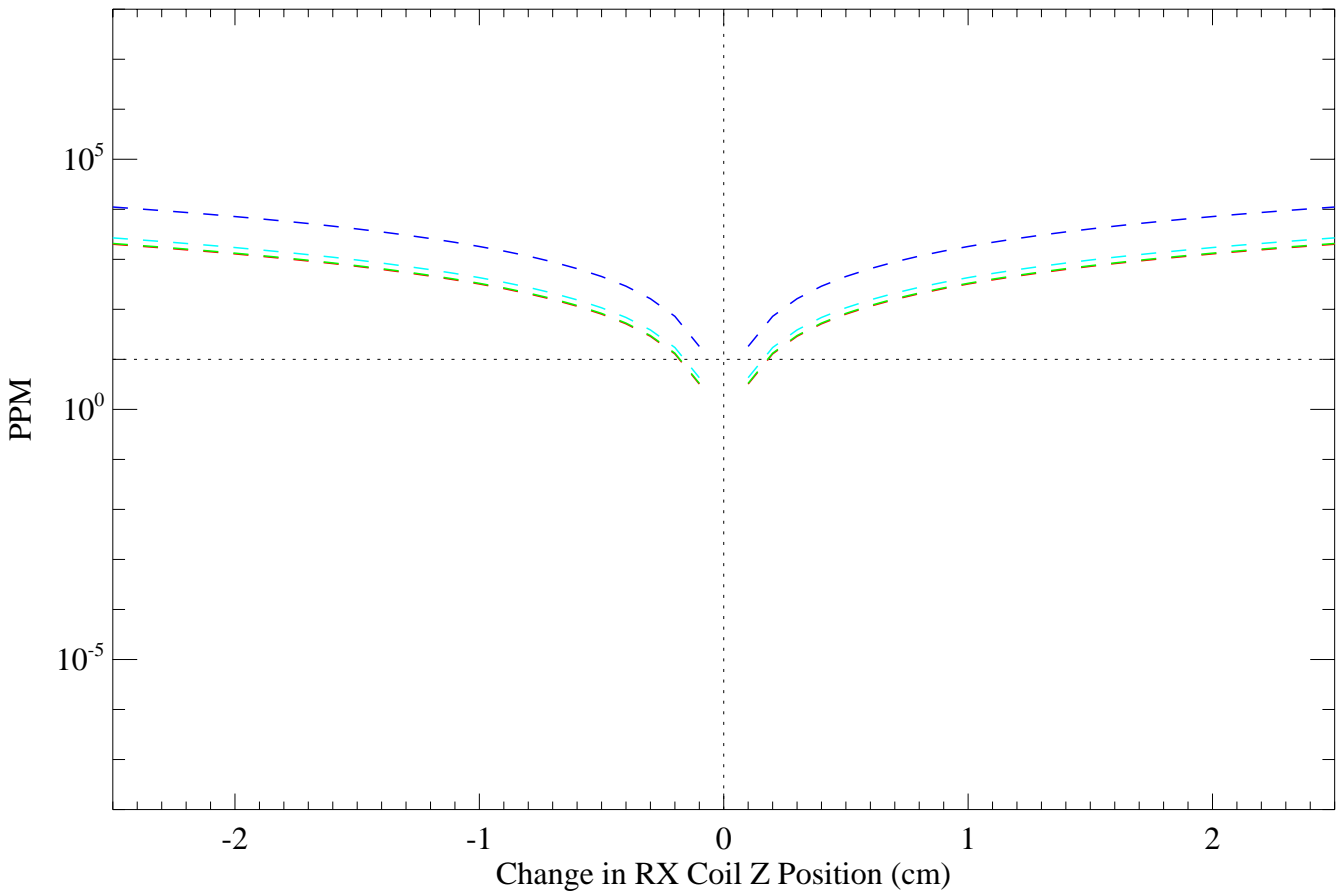
TX Coil Diameter=3.0m, RX Coil Separation=0.5m



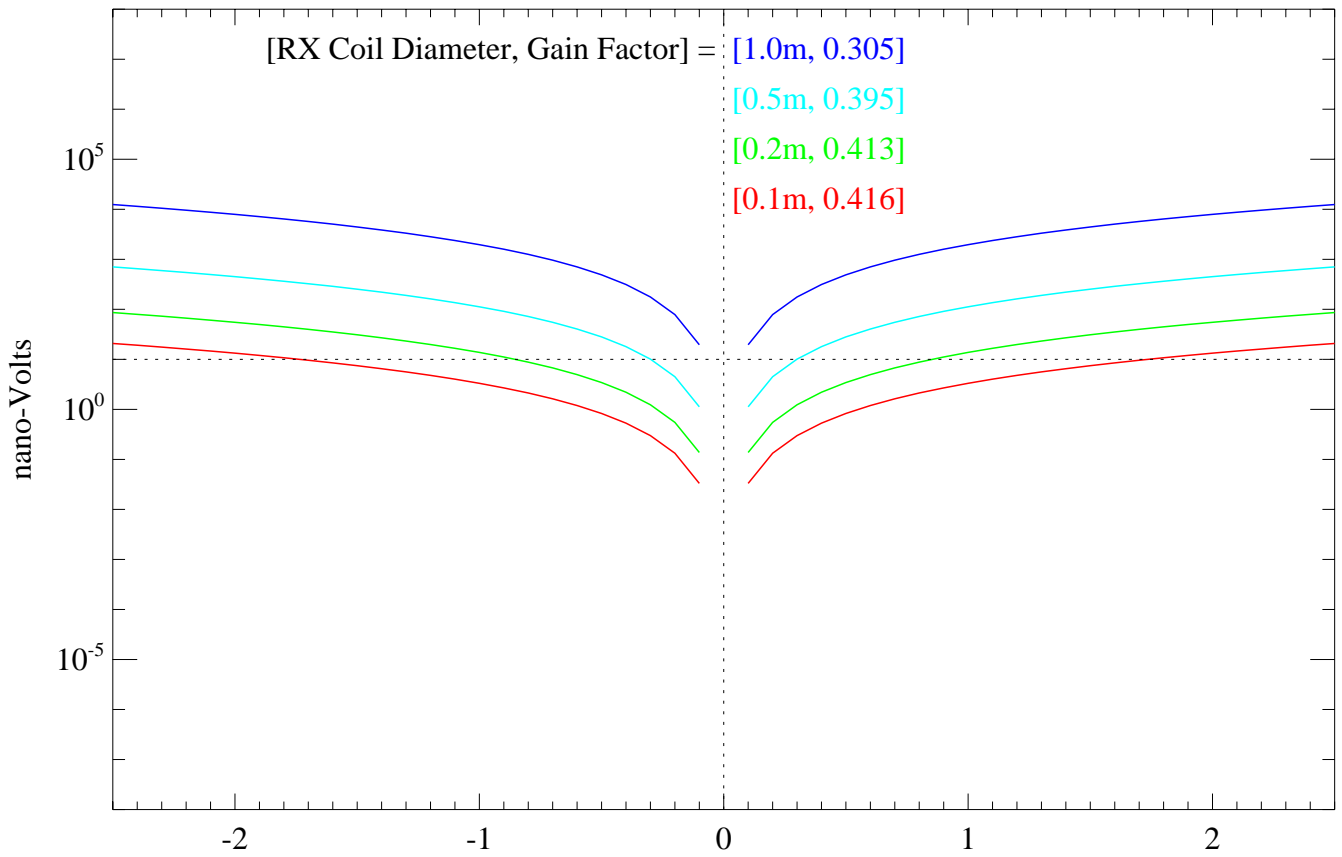
CASE 5 - Change in Primary Field Coupling due to dZ Perturbations on RX Coil



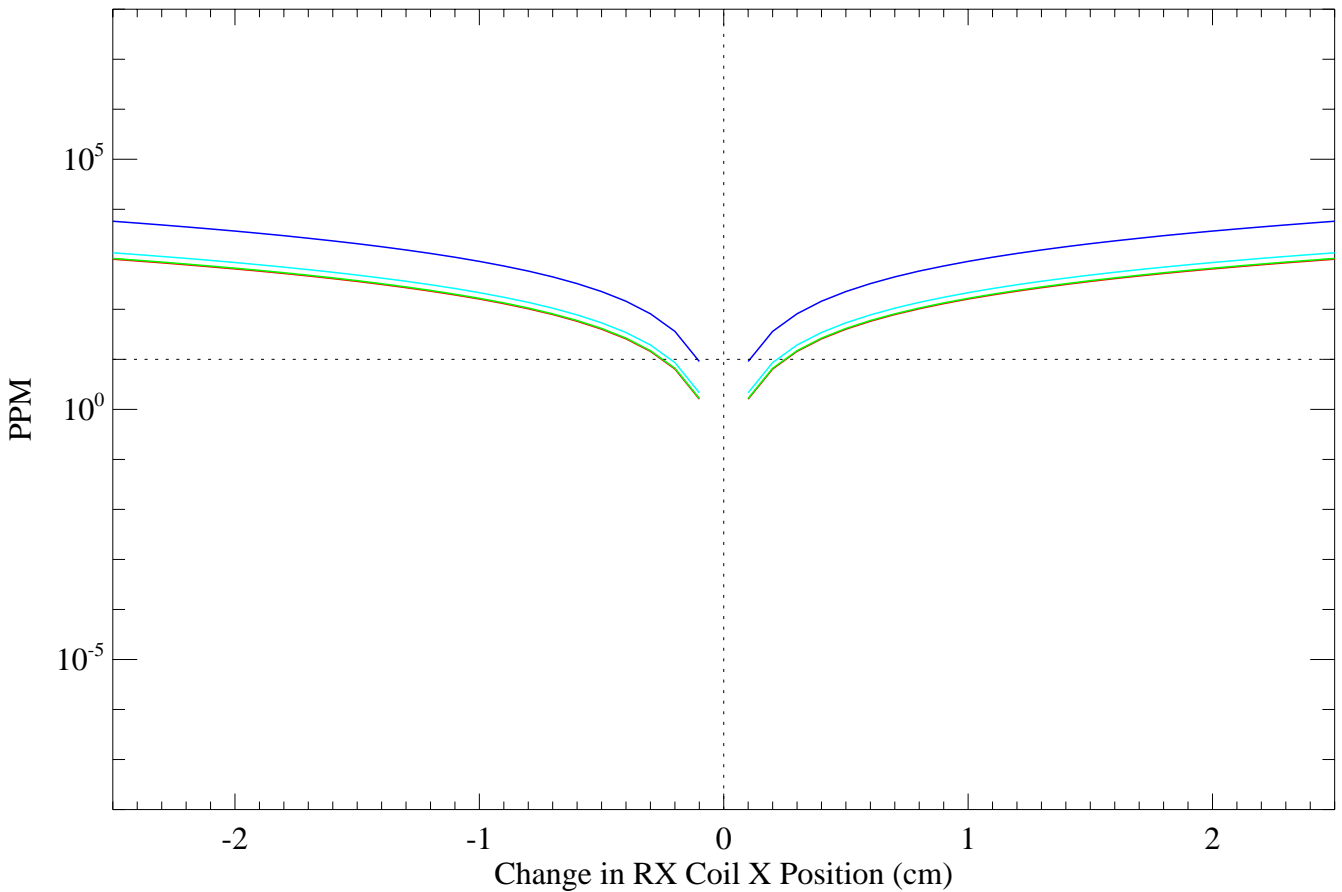
Outer TX Coil Diameter=3.0m, Inner TX Coil Diameter=1.25m



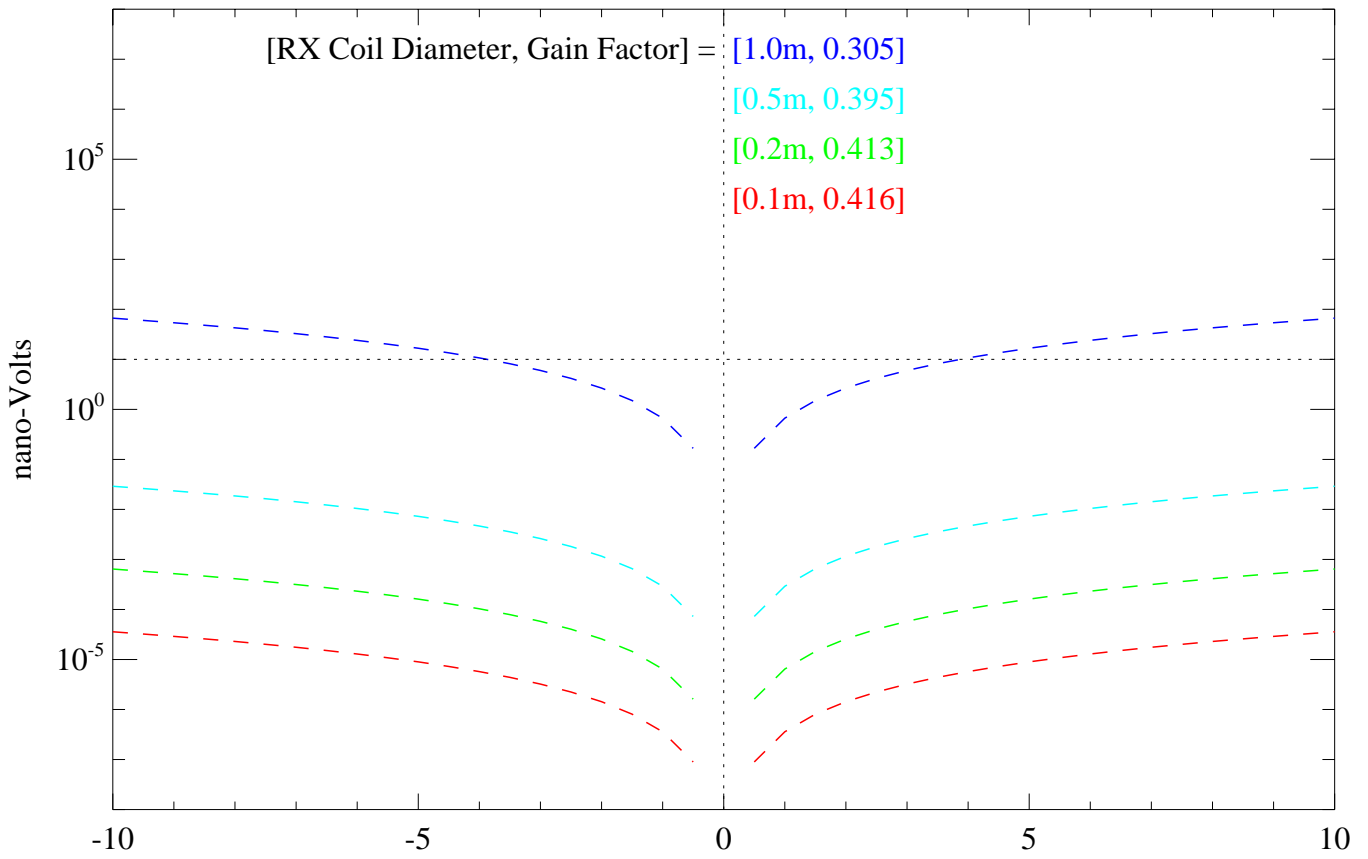
CASE 5 - Change in Primary Field Coupling due to dX Perturbations on RX Coil



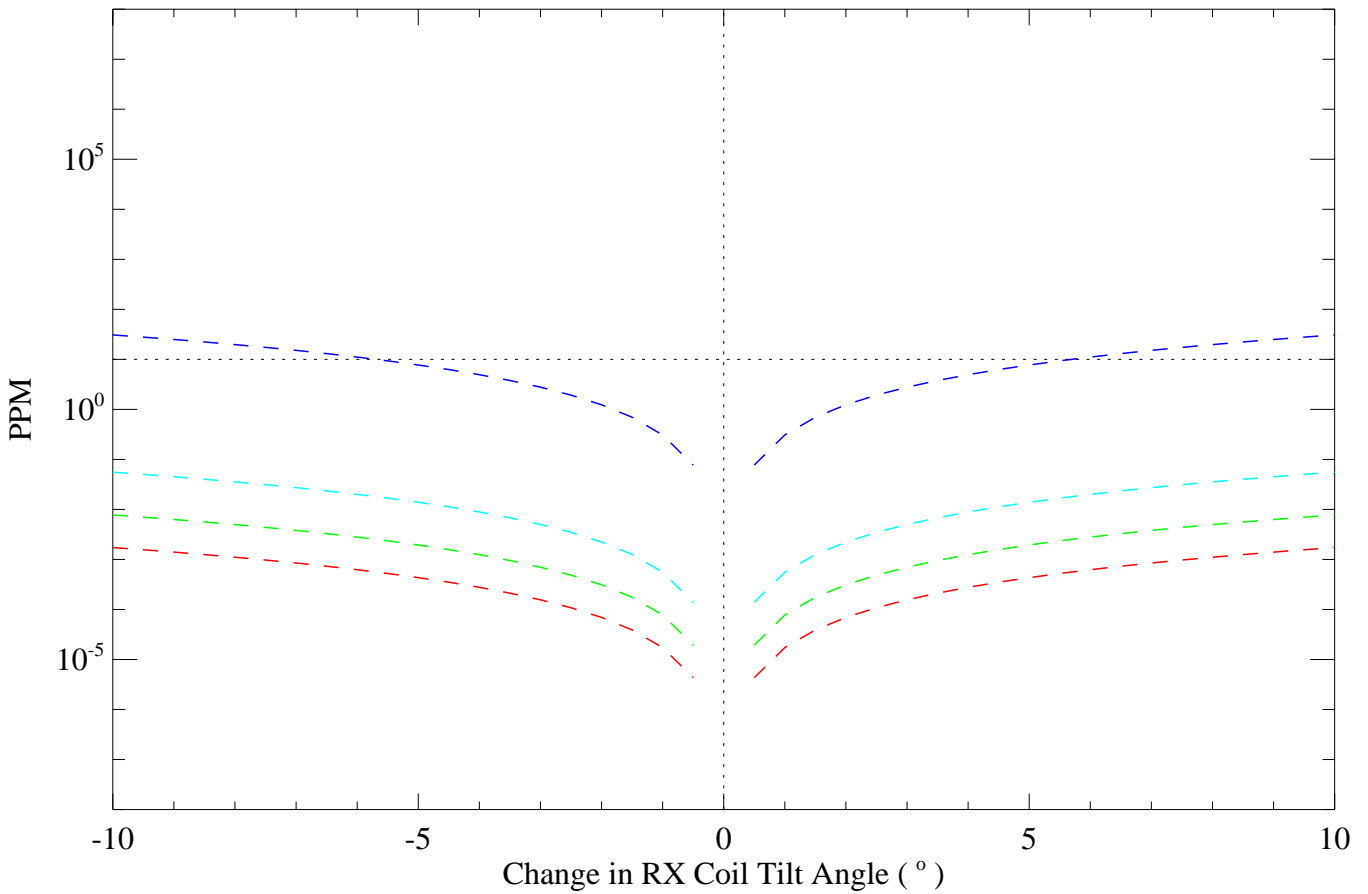
Outer TX Coil Diameter=3.0m, Inner TX Coil Diameter=1.25m



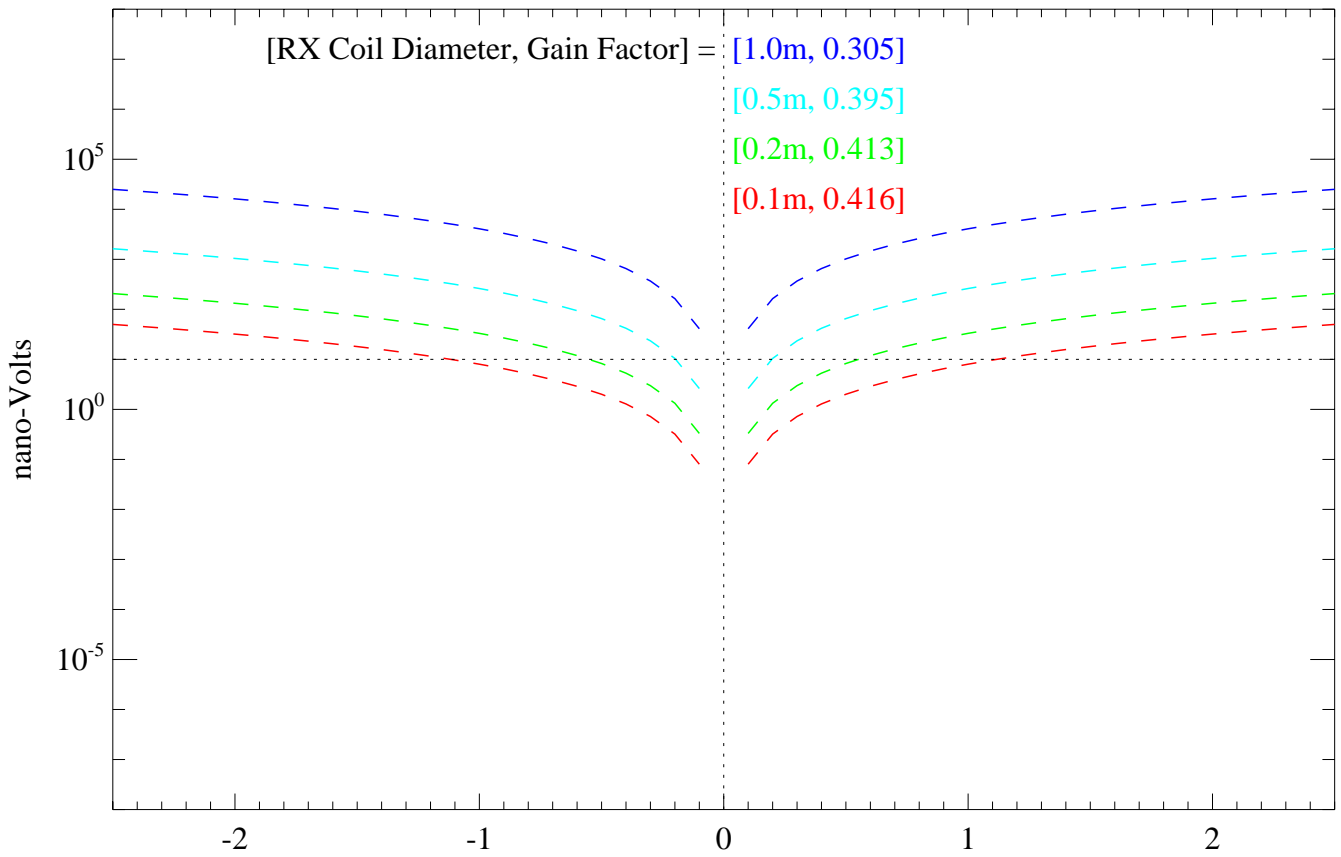
CASE 5 - Change in Primary Field Coupling due to Pitch Perturbations on RX Coil



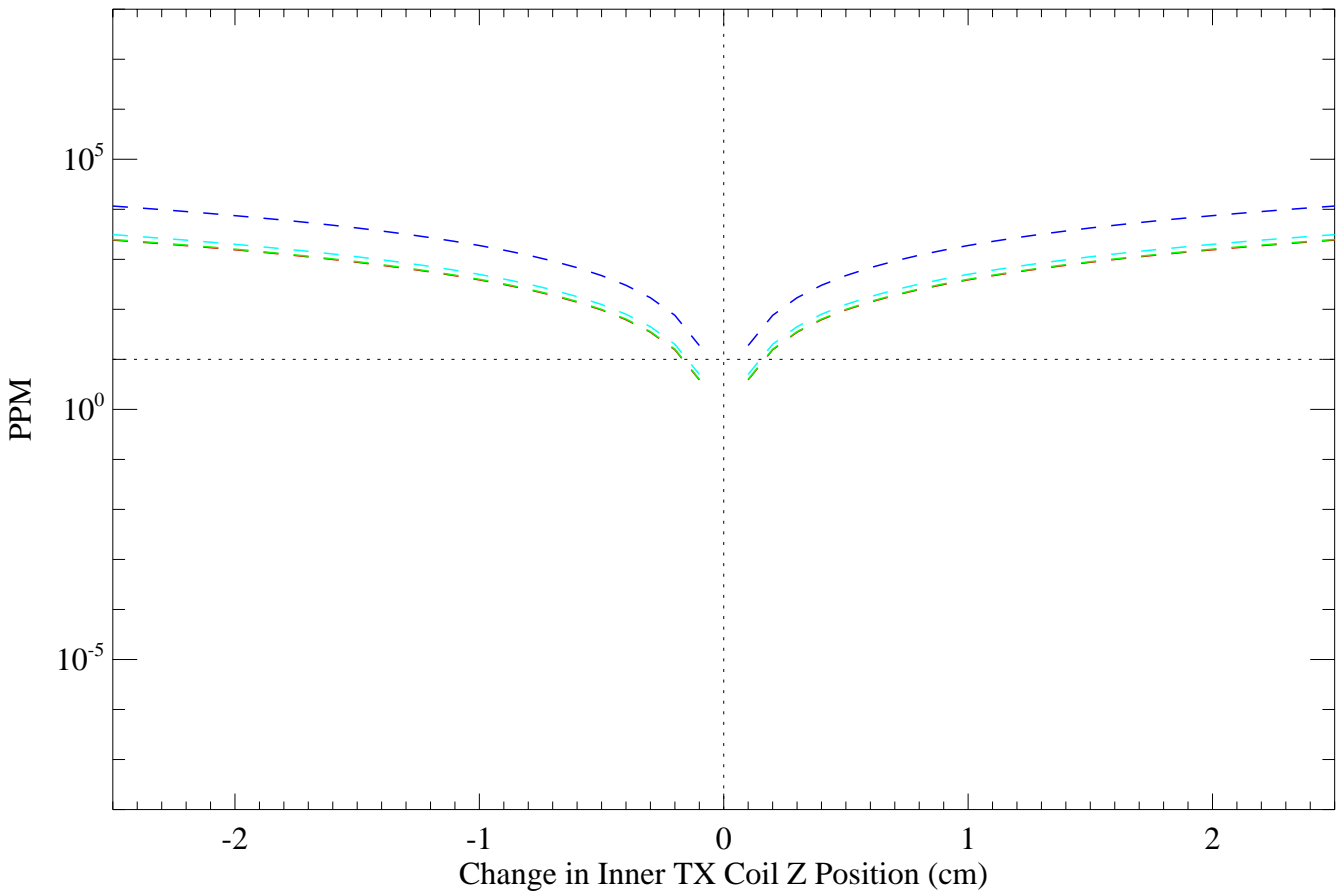
Outer TX Coil Diameter=3.0m, Inner TX Coil Diameter=1.25m



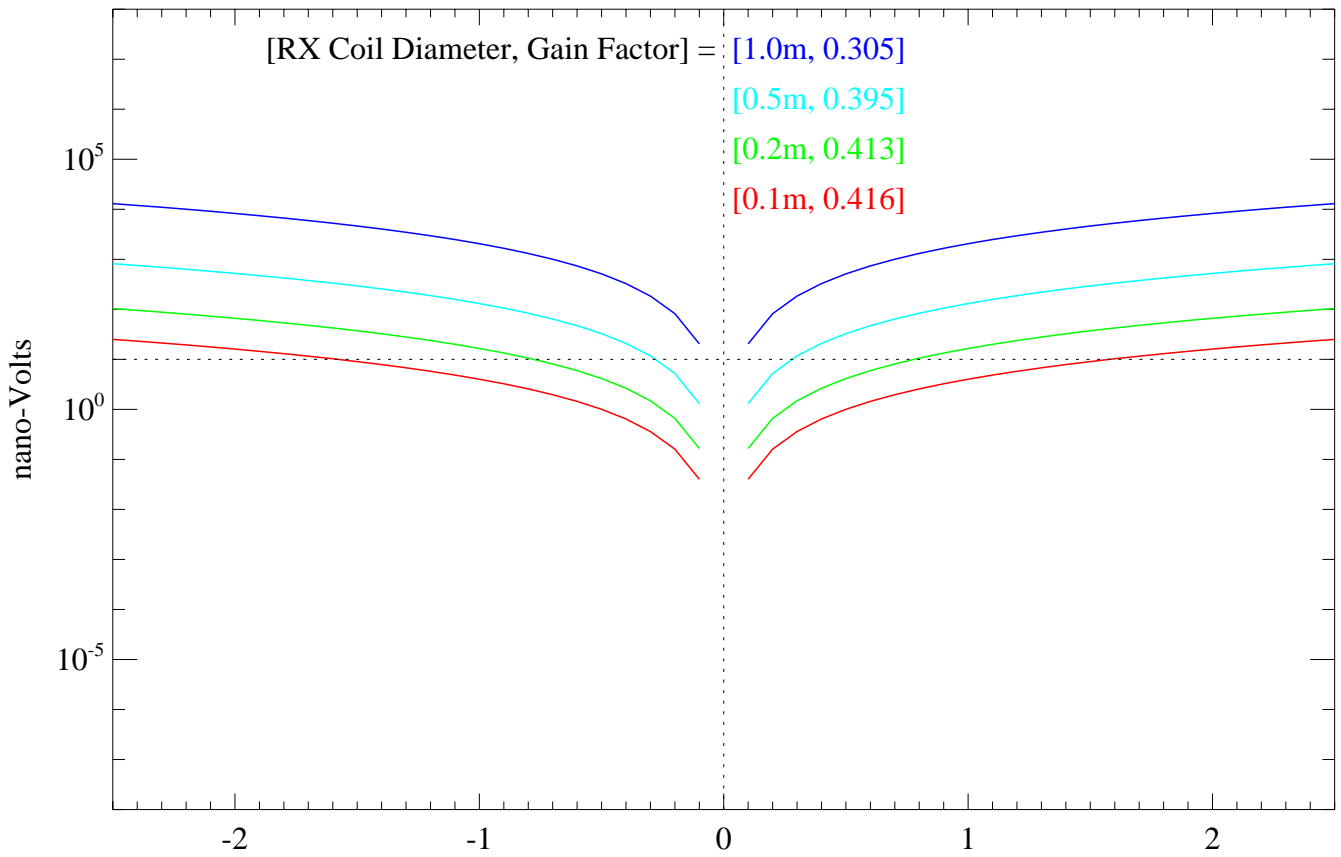
CASE 5 - Change in Primary Field Coupling due to dZ Perturbations on Inner TX Coil



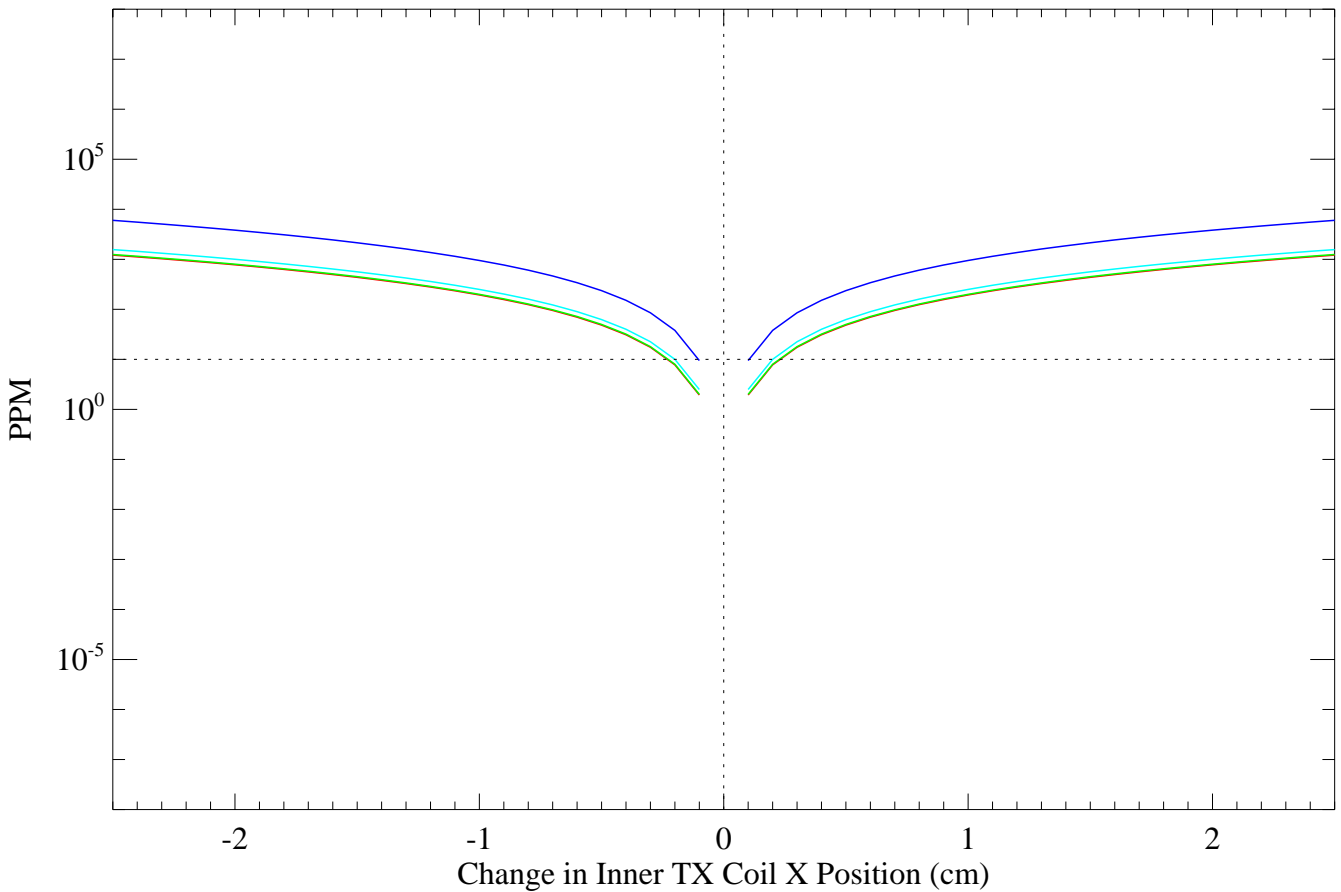
Outer TX Coil Diameter=3.0m, Inner TX Coil Diameter=1.25m



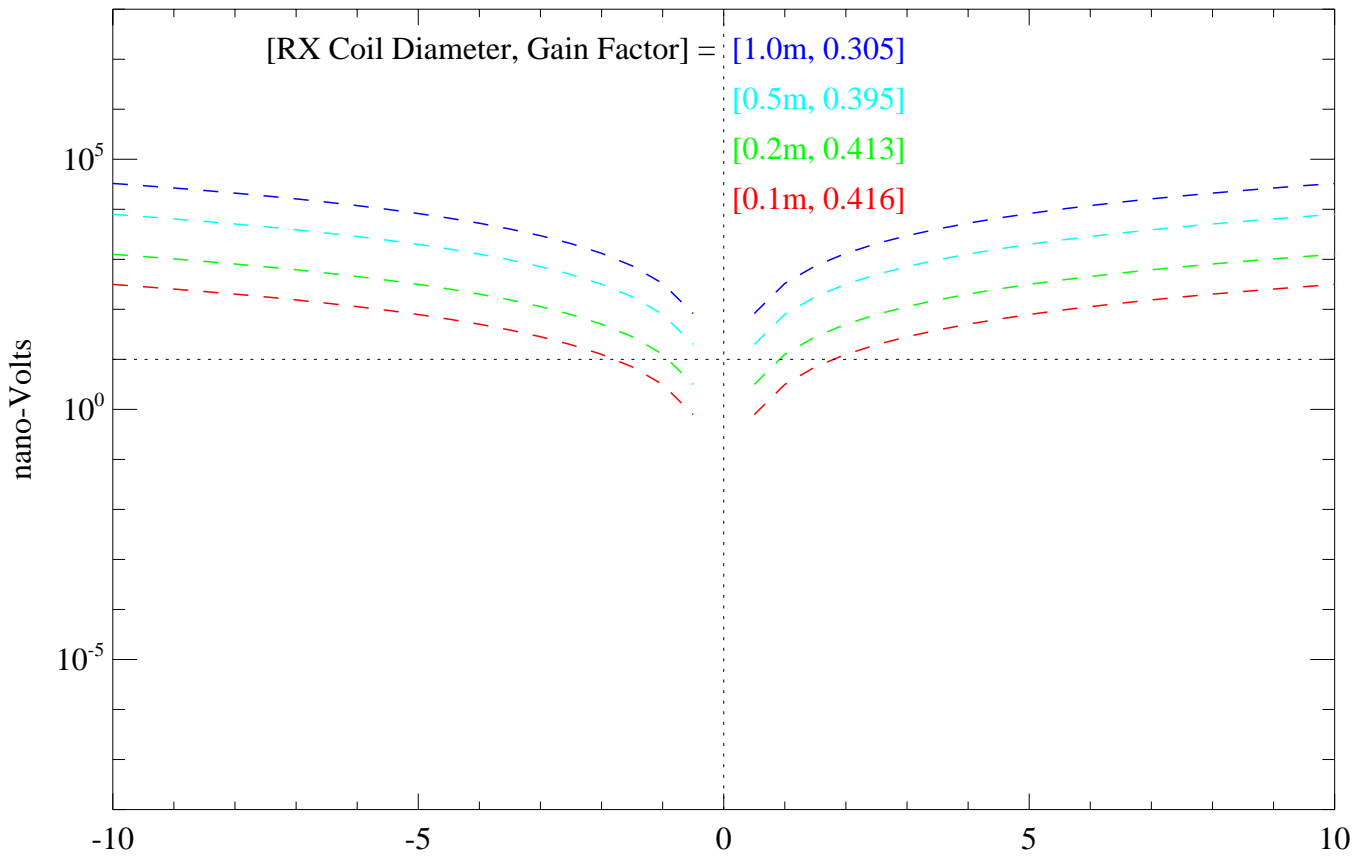
CASE 5 - Change in Primary Field Coupling due to dX Perturbations on Inner TX Coil



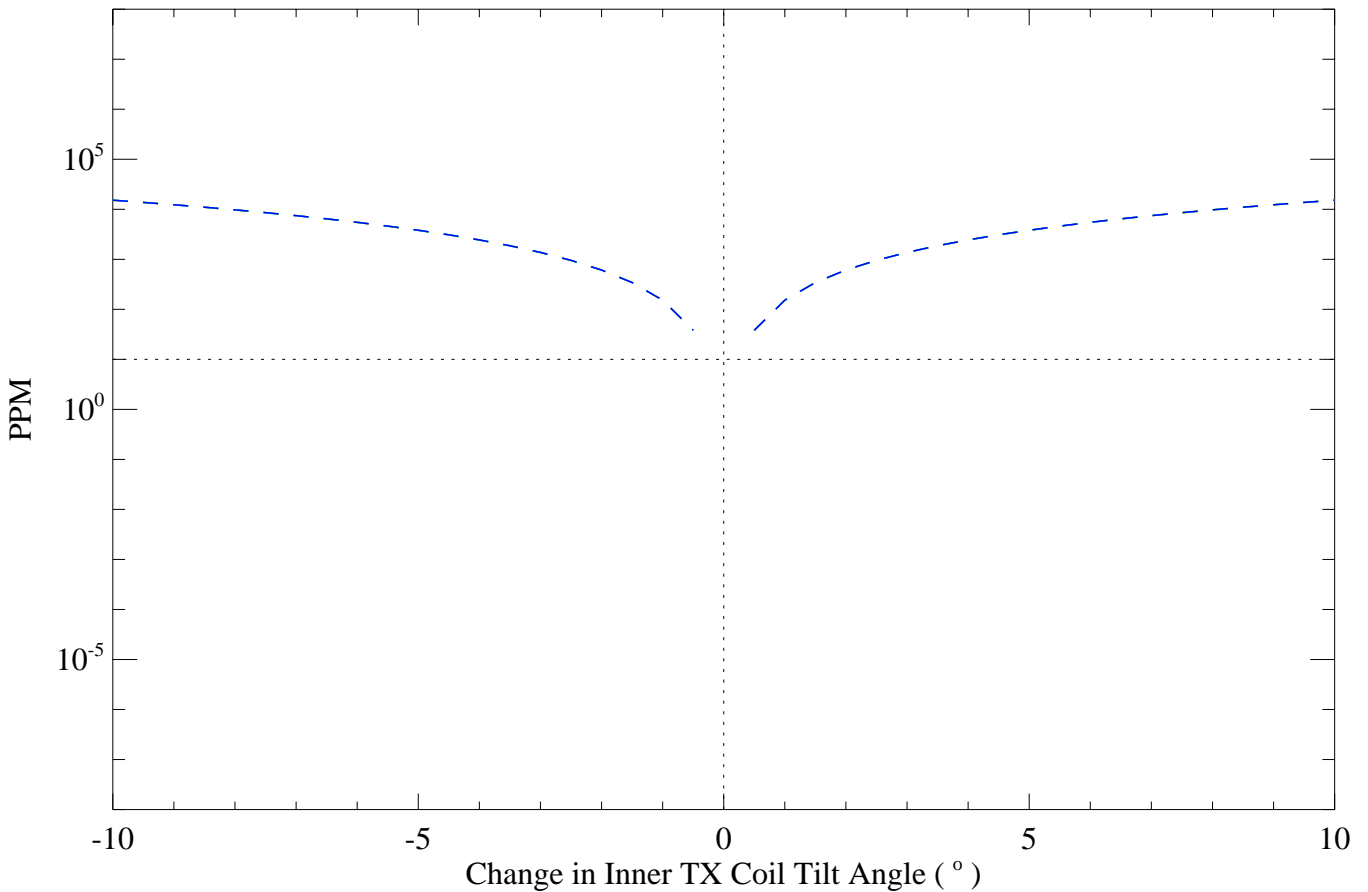
Outer TX Coil Diameter=3.0m, Inner TX Coil Diameter=1.25m



CASE 5 - Change in Primary Field Coupling due to Pitch Perturbations on Inner TX Coil



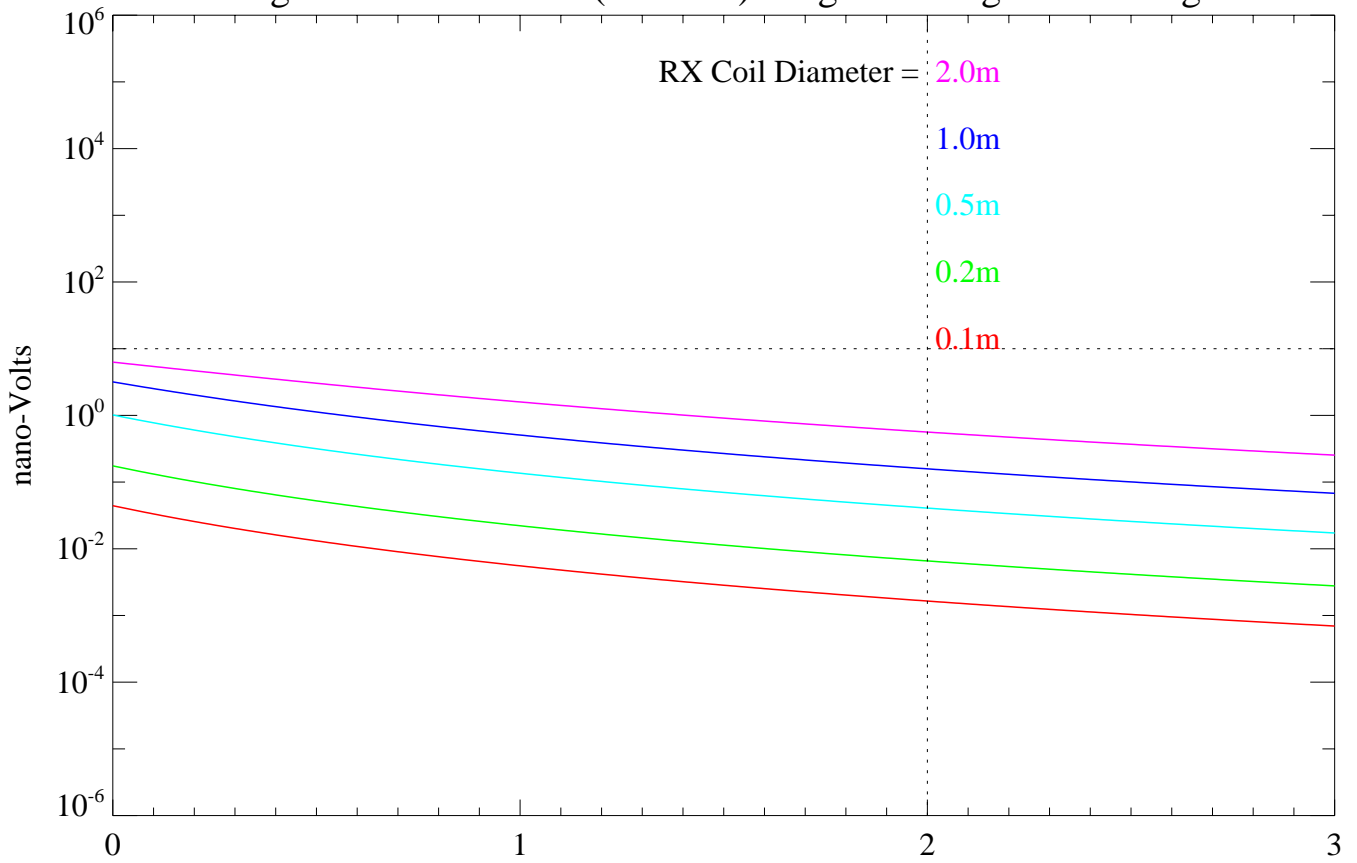
Outer TX Coil Diameter=3.0m, Inner TX Coil Diameter=1.25m



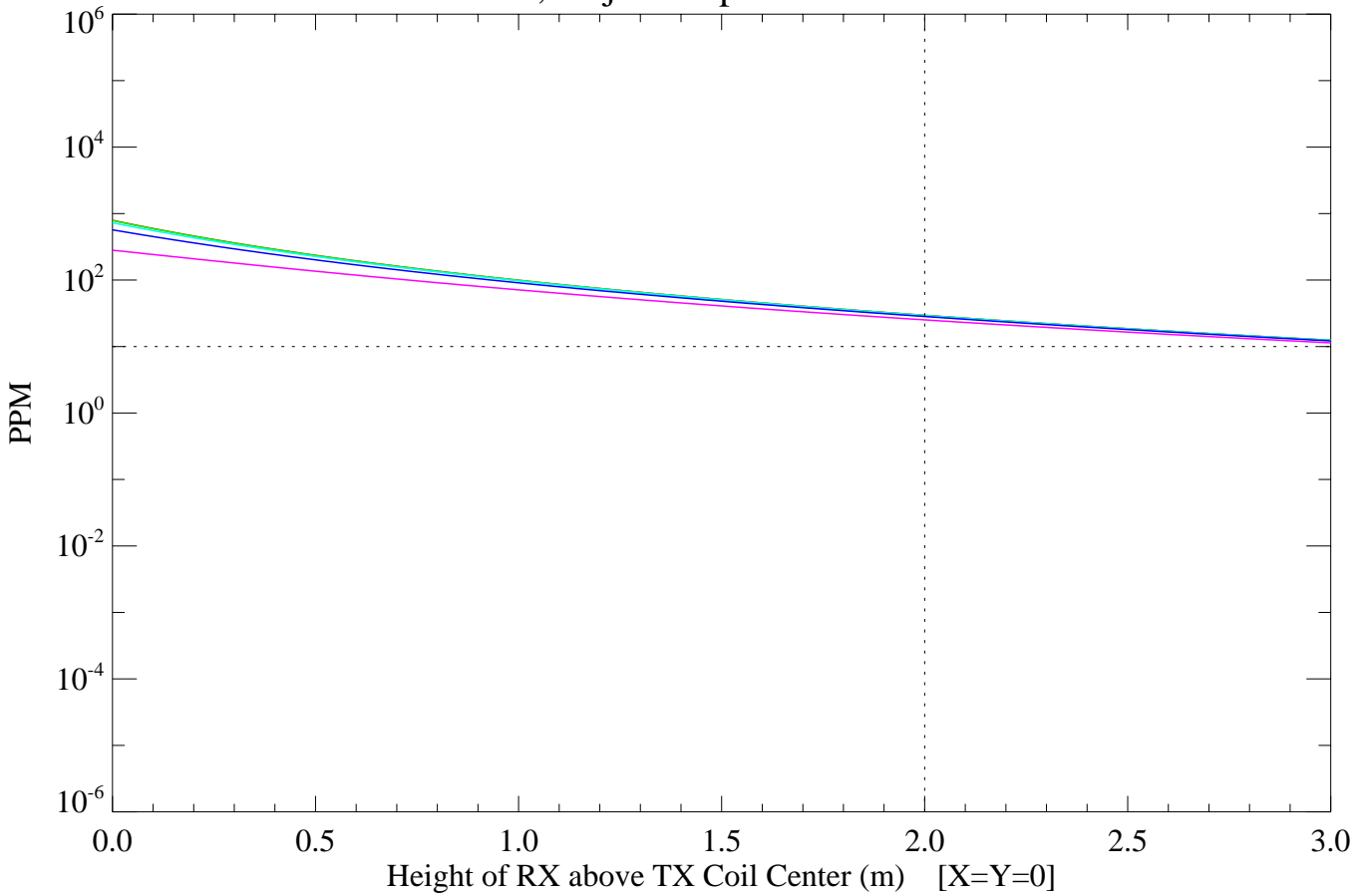
Appendix 2A

Results of calculating the signal strength in nano-volts and ppm for a 1 km square ground based transmitter and Case 1 / Case 2 circular receive coil(s)

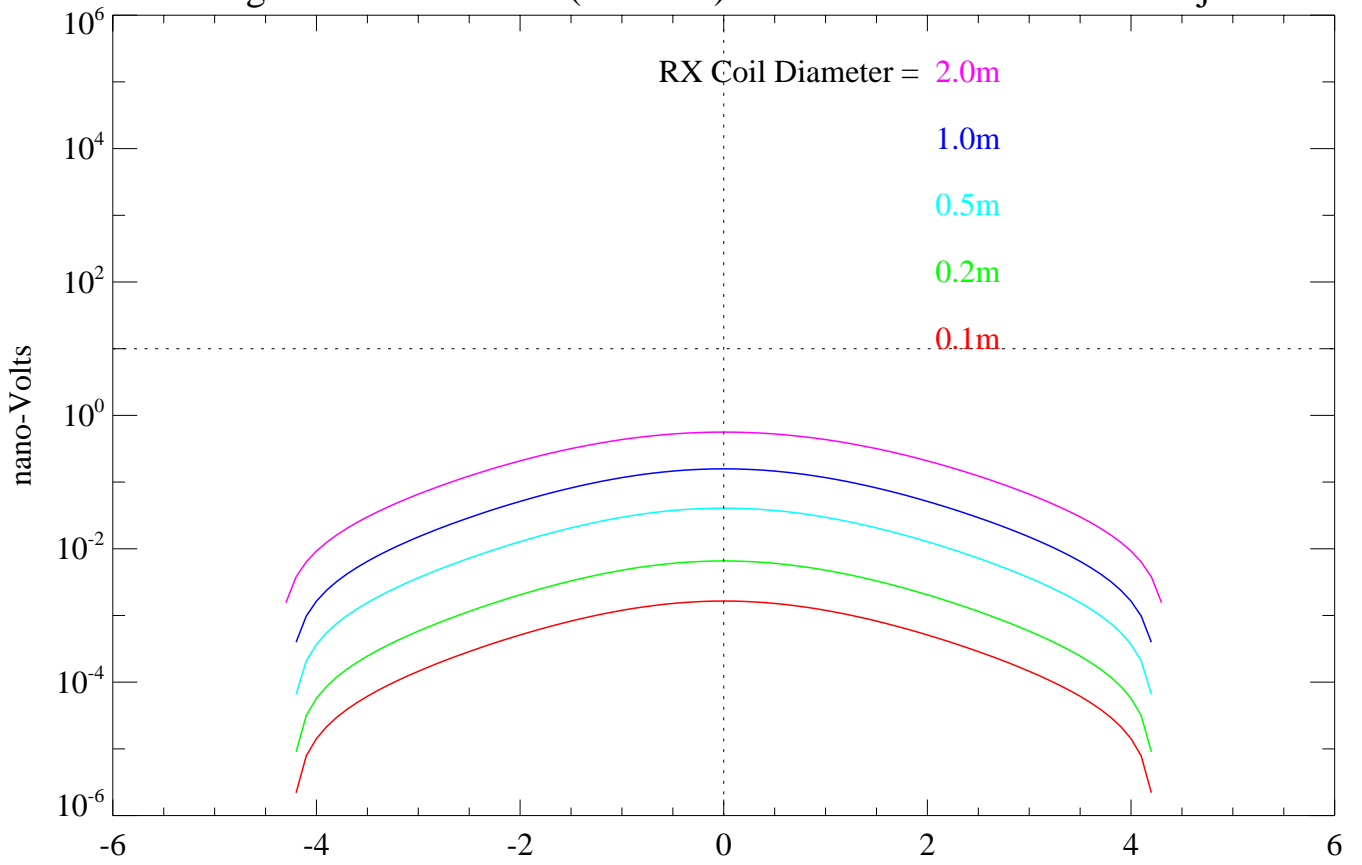
Large Ground TX Coil (CASE 1) - Signal Strength with Height



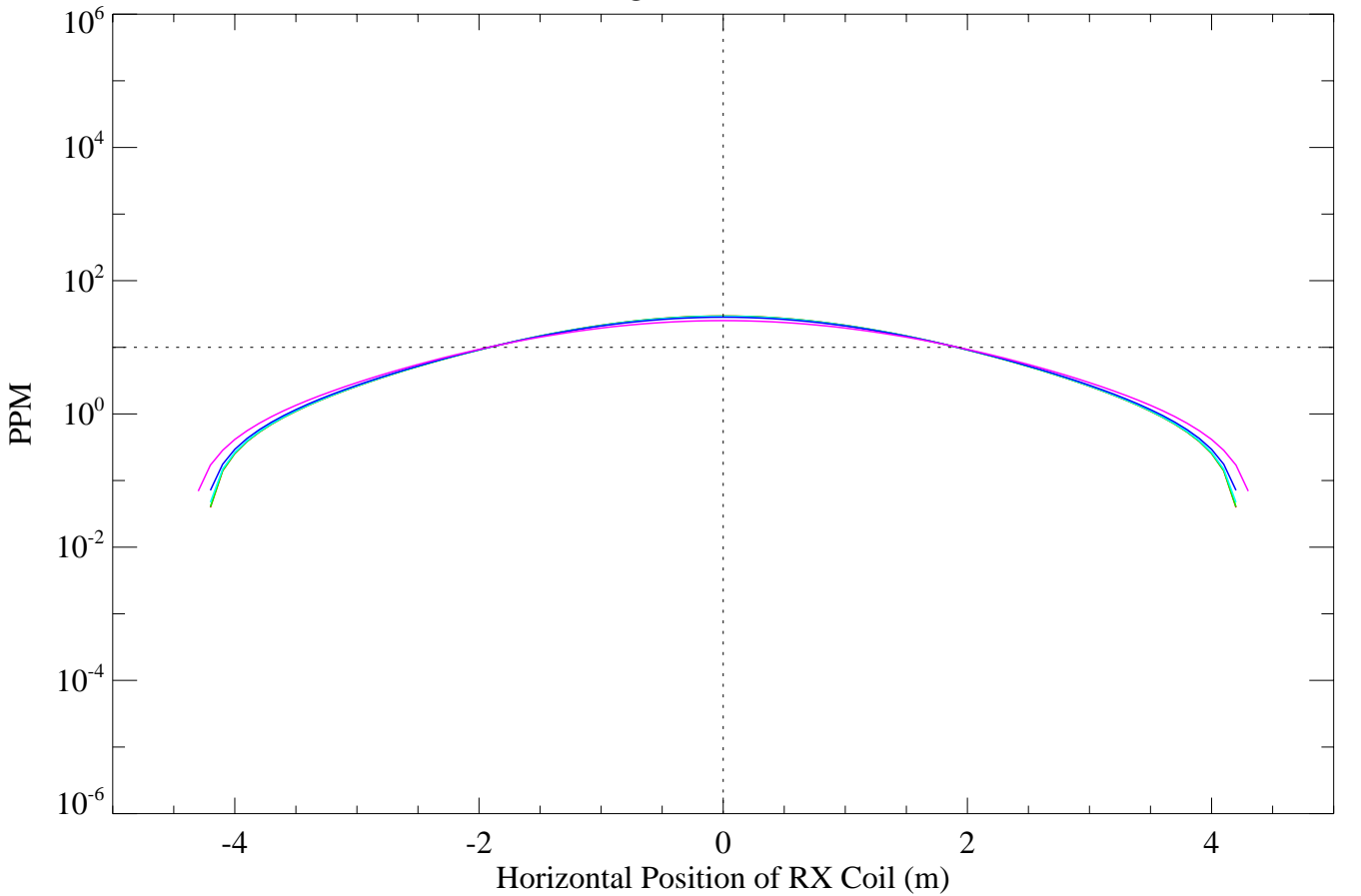
1km X 1km TX Coil, Object Depth=1.0m below TX Coil Center



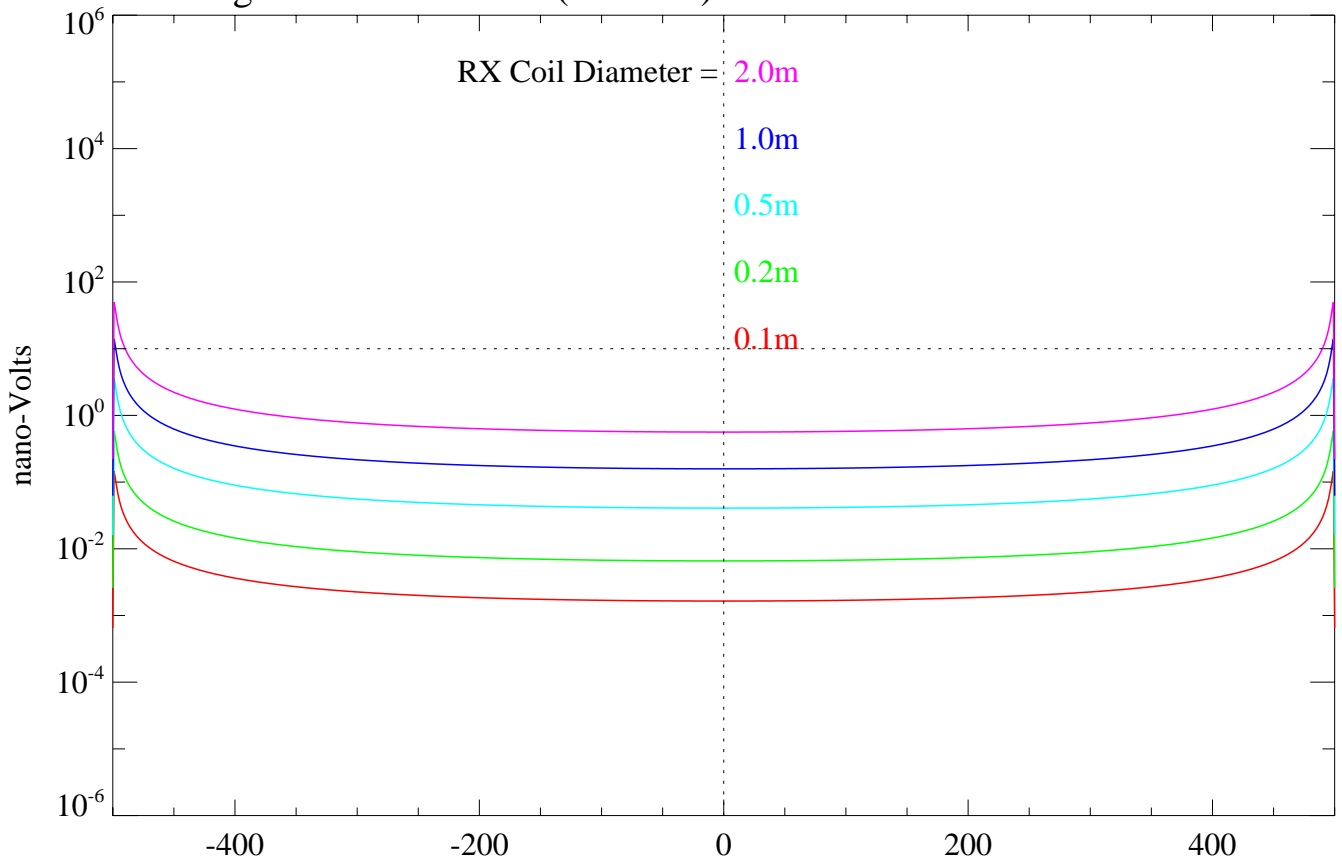
Large Ground TX Coil (CASE 1) - Horizontal Profile Over Object



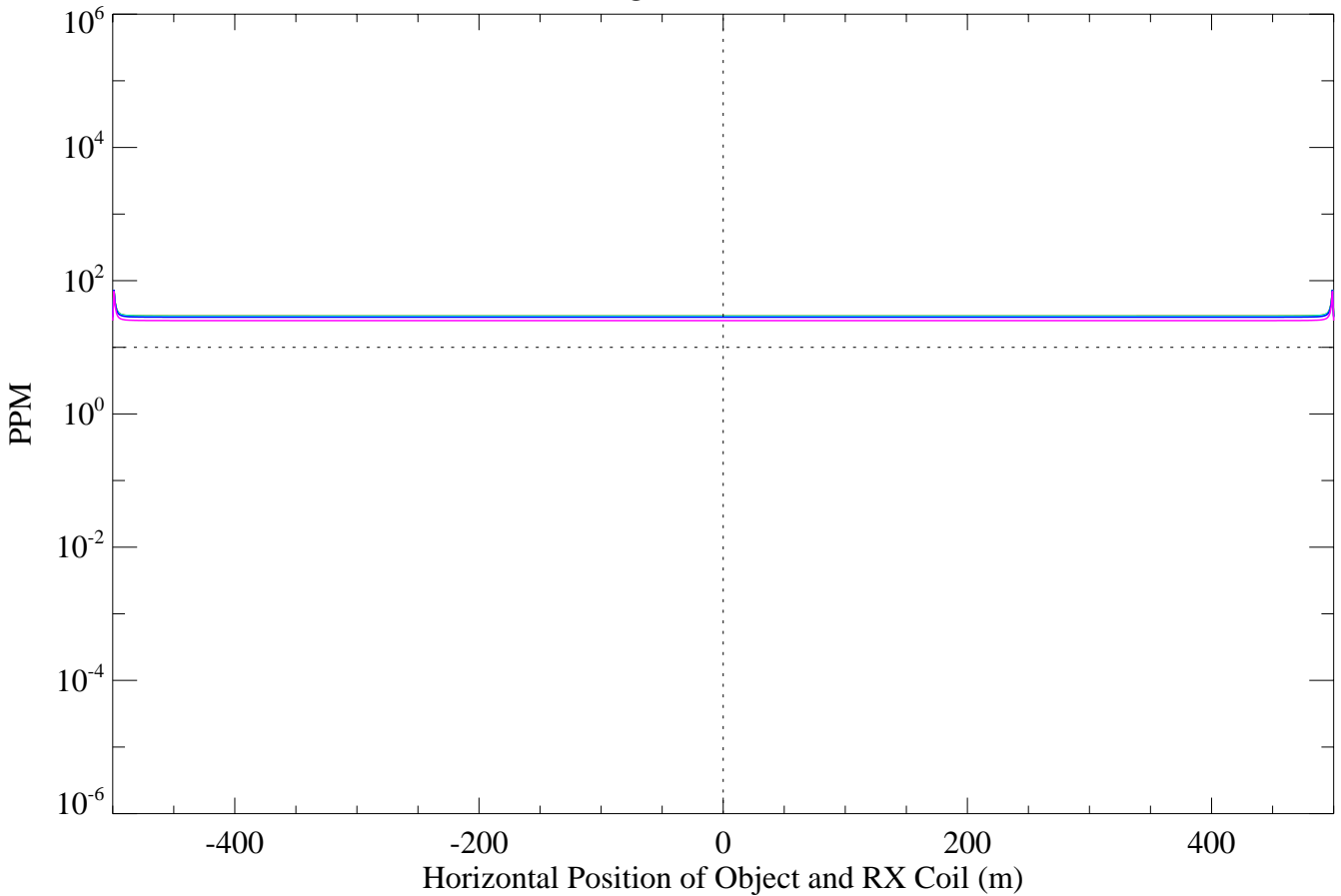
1km X 1km TX Coil, Object Depth=1.0m below TX Coil Center, RX Coil Height above Ground=2.0m



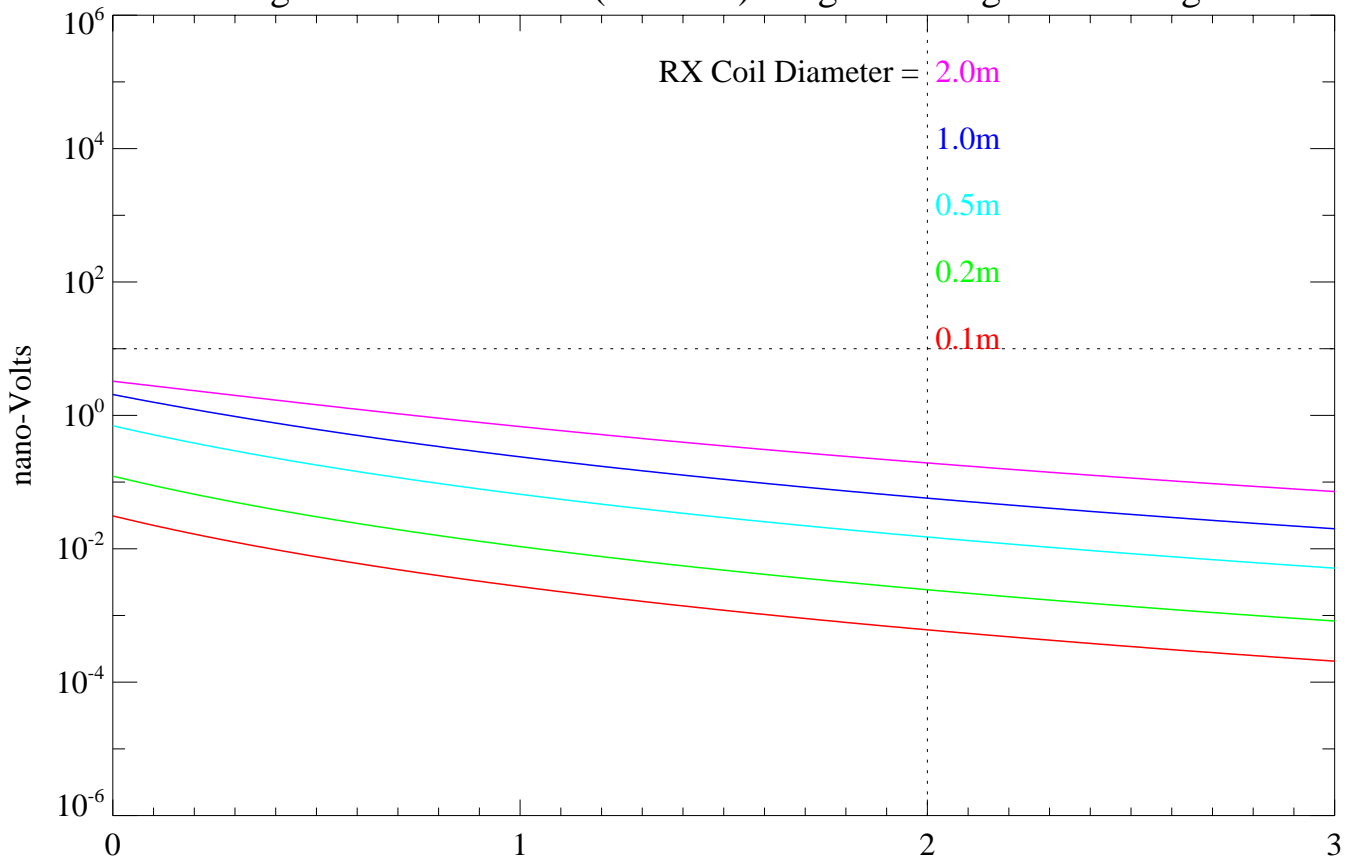
Large Ground TX Coil (CASE 1) - Horizontal Profile Over TX Coil



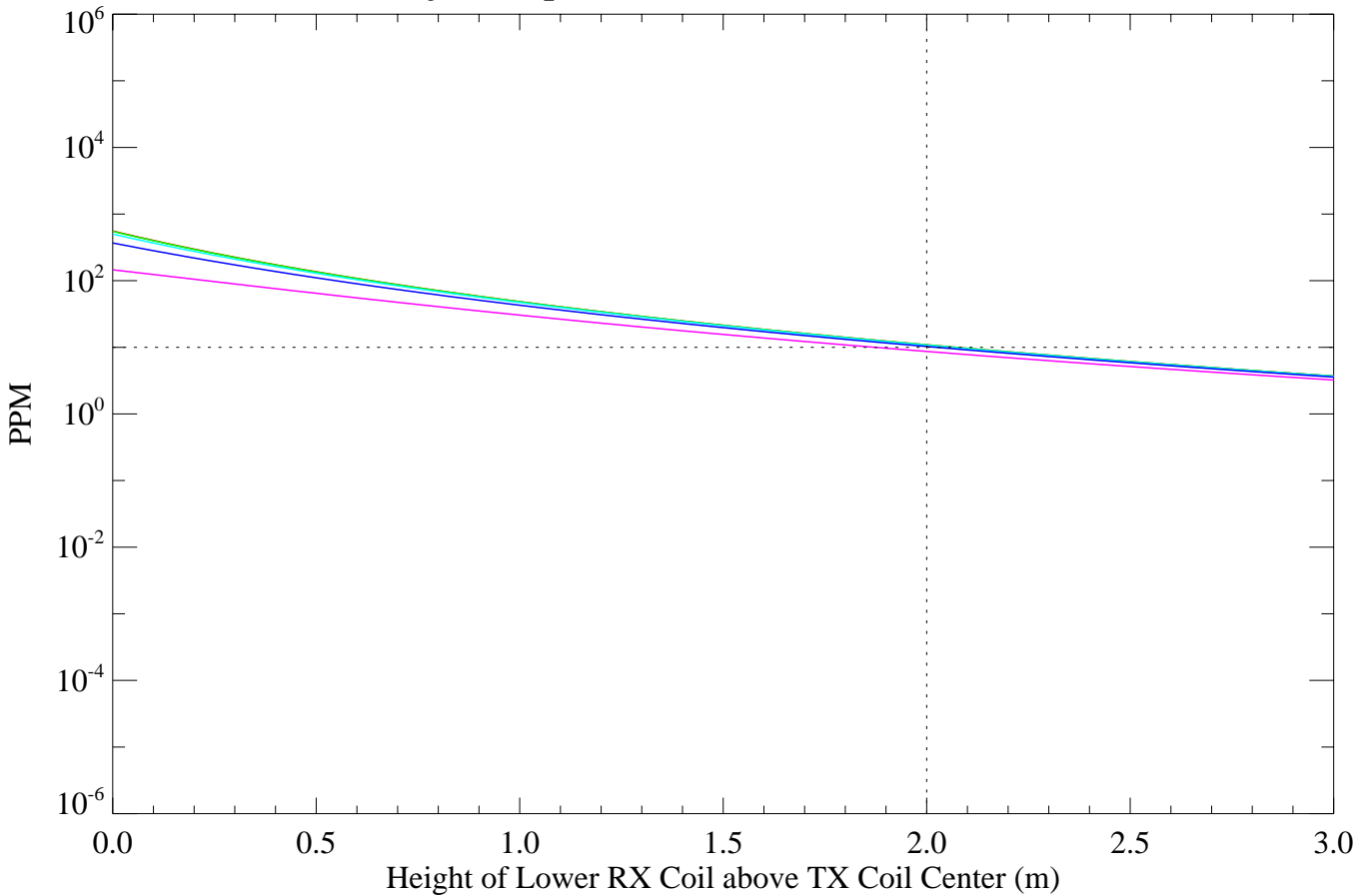
1km X 1km TX Coil, Object Depth=1.0m,
RX Coil Height above Ground=2.0m



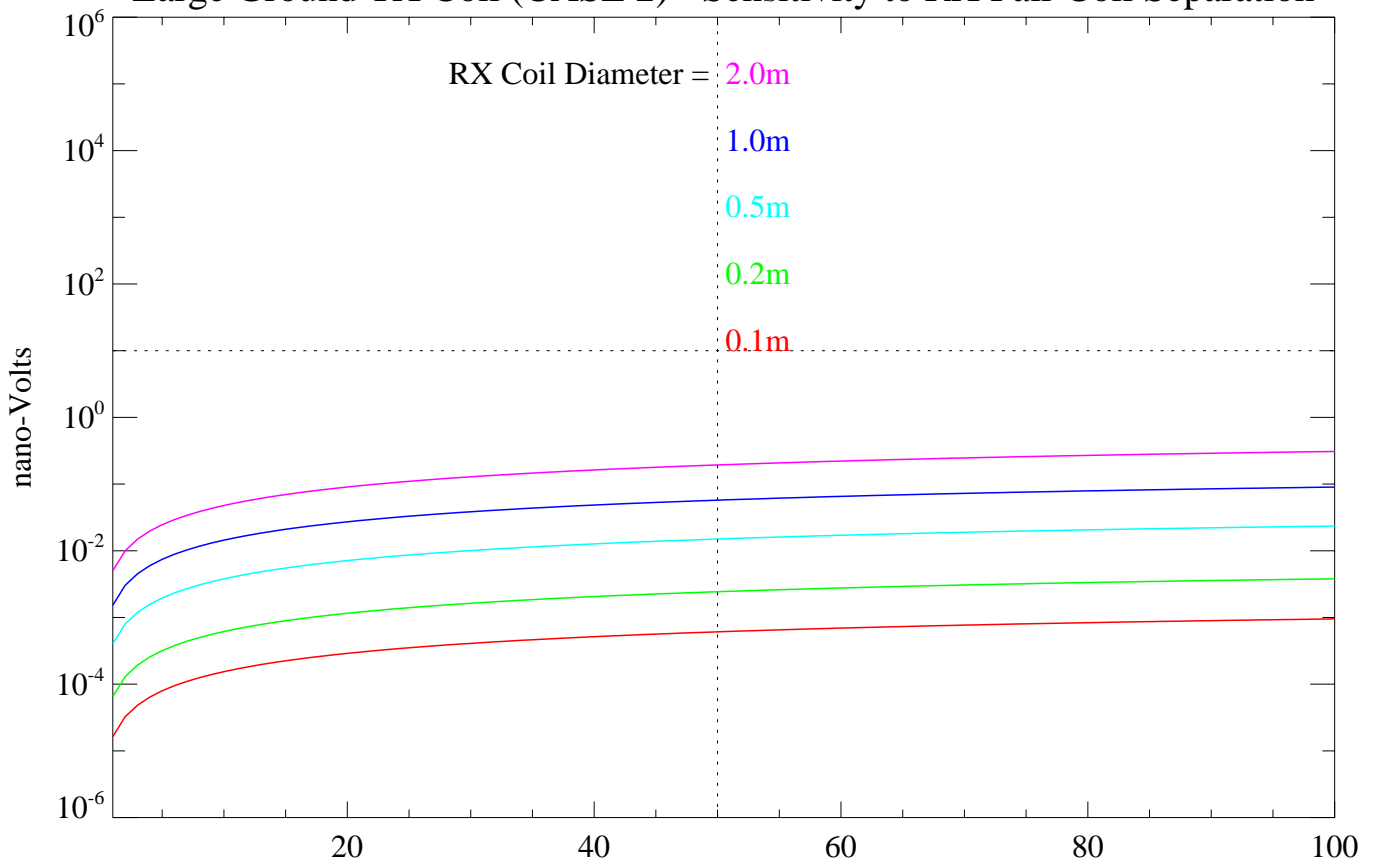
Large Ground TX Coil (CASE 2) - Signal Strength with Height



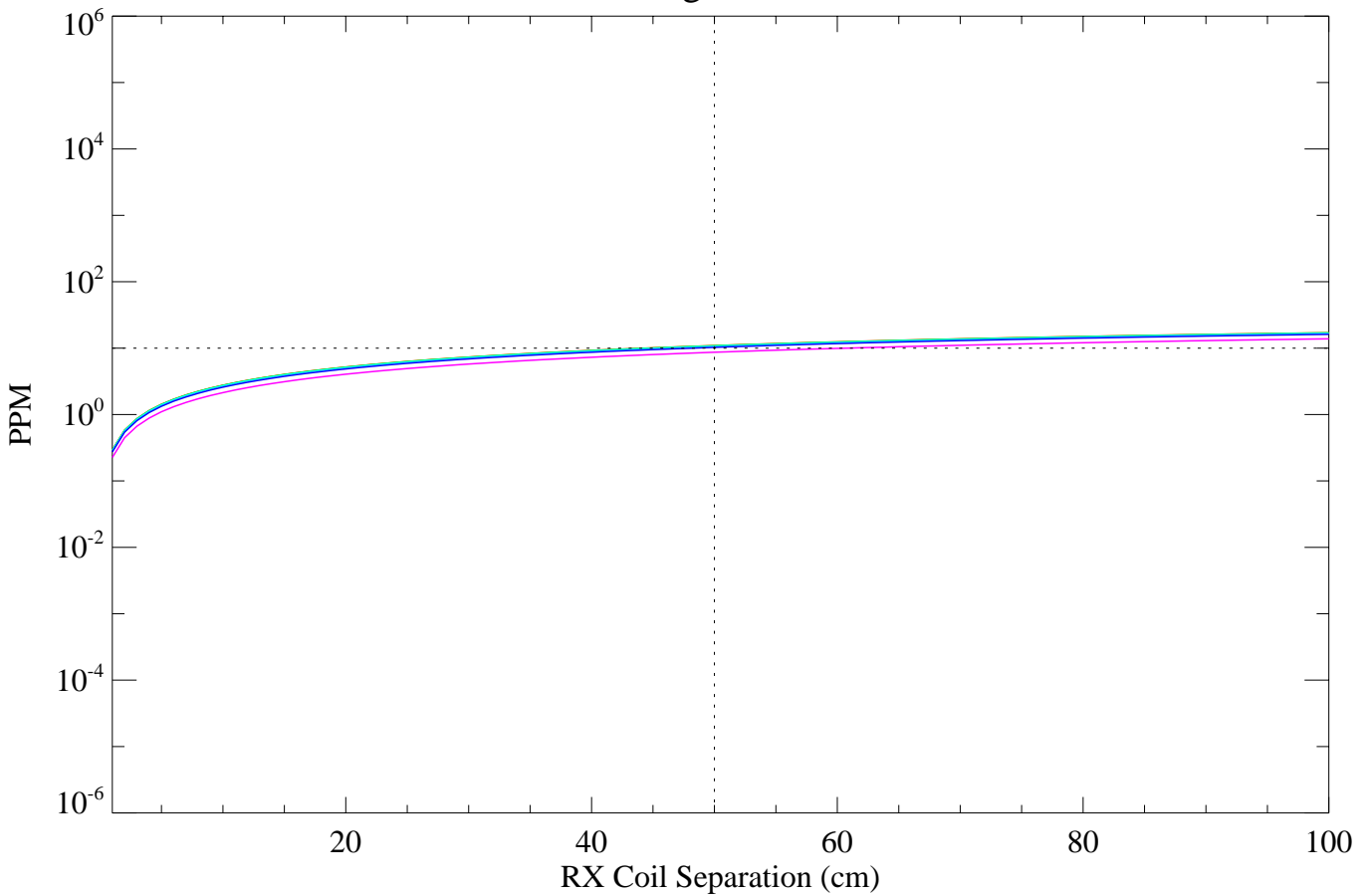
1km X 1km TX Coil, RX Coil Separation=0.5m, Object Depth=1.0m below TX Coil Center



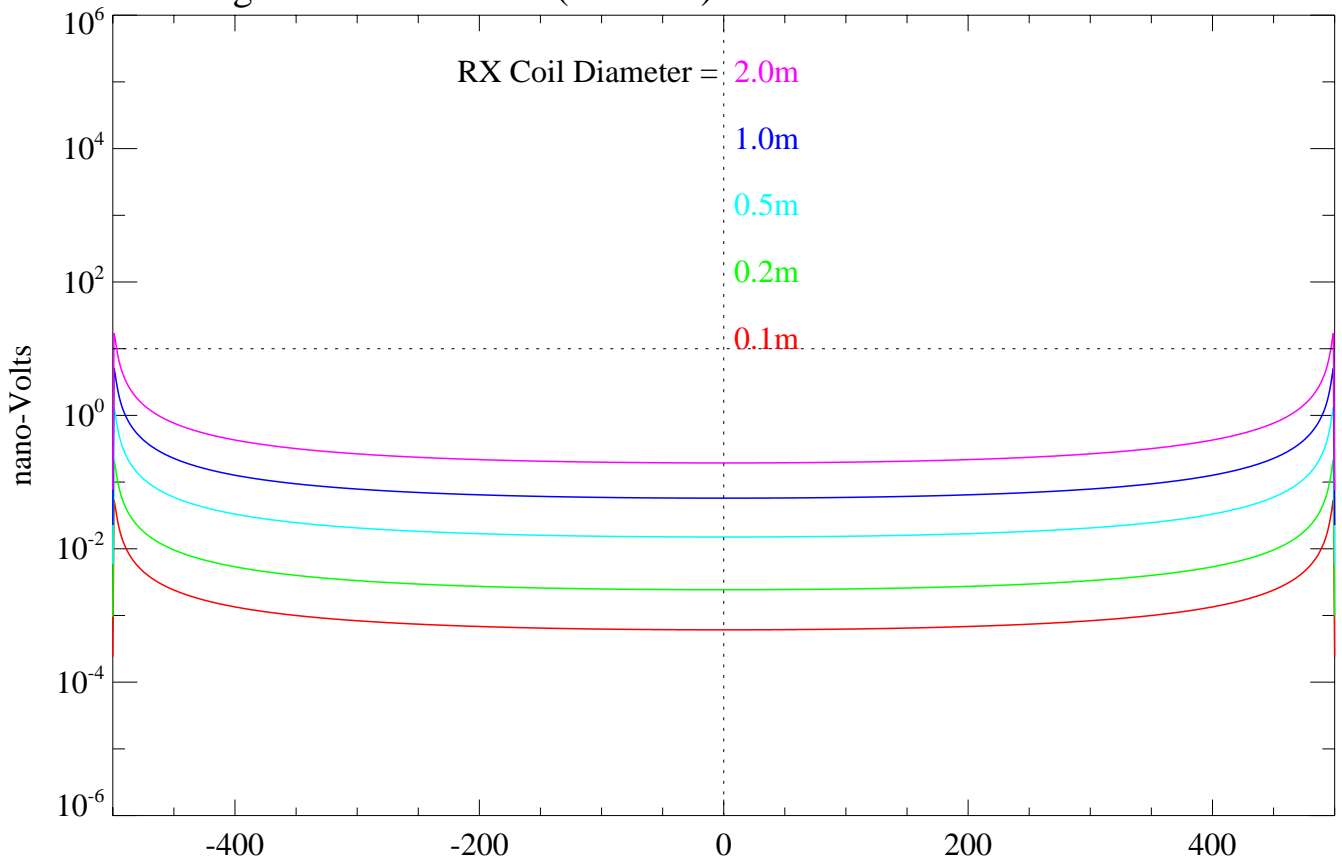
Large Ground TX Coil (CASE 2) - Sensitivity to RX Pair Coil Separation



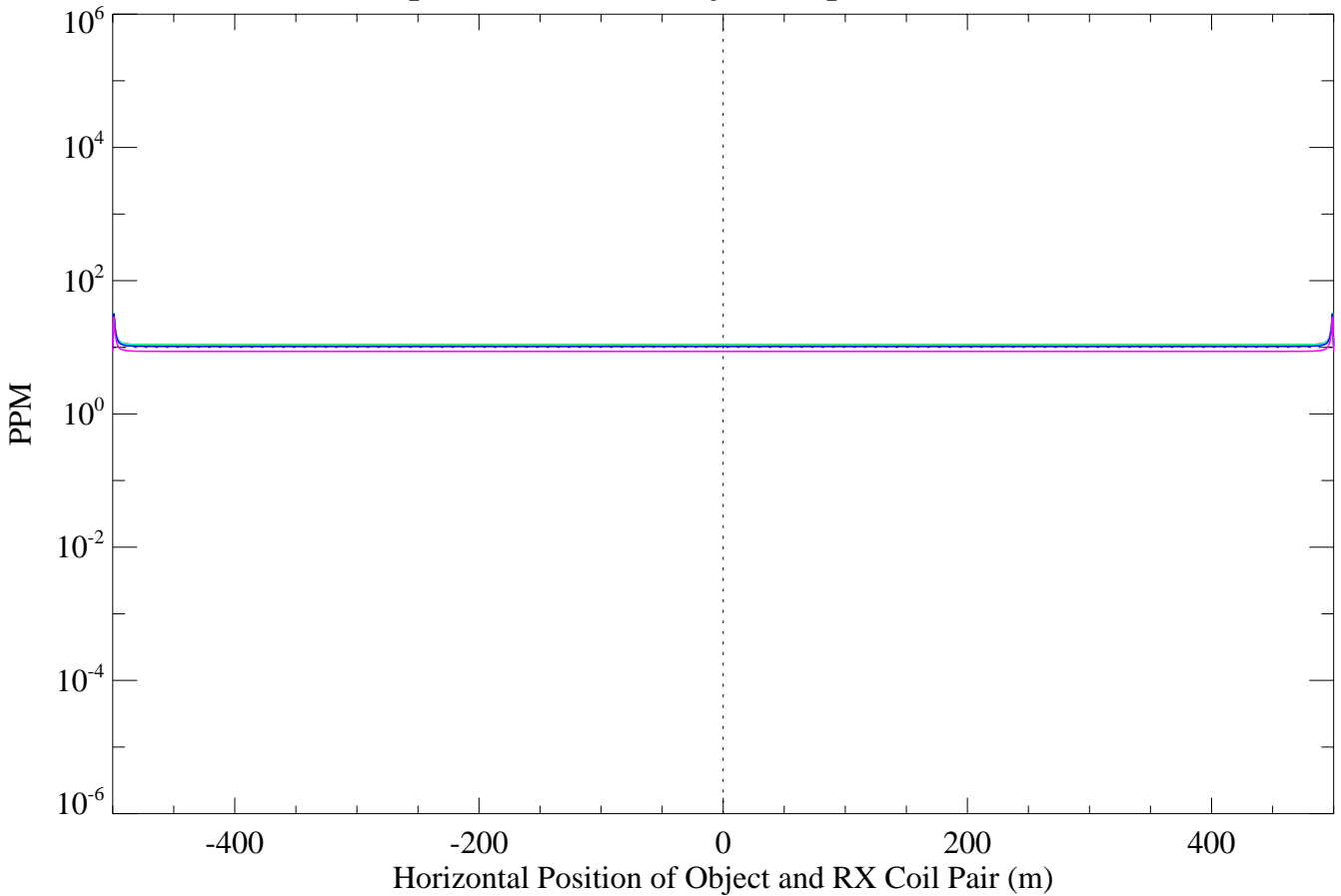
1km X 1km TX Coil, Object Depth=1.0m below TX Coil Center,
Lower RX Coil Height above Ground=2.0m



Large Ground TX Coil (CASE 2) - Horizontal Profile Over TX Coil



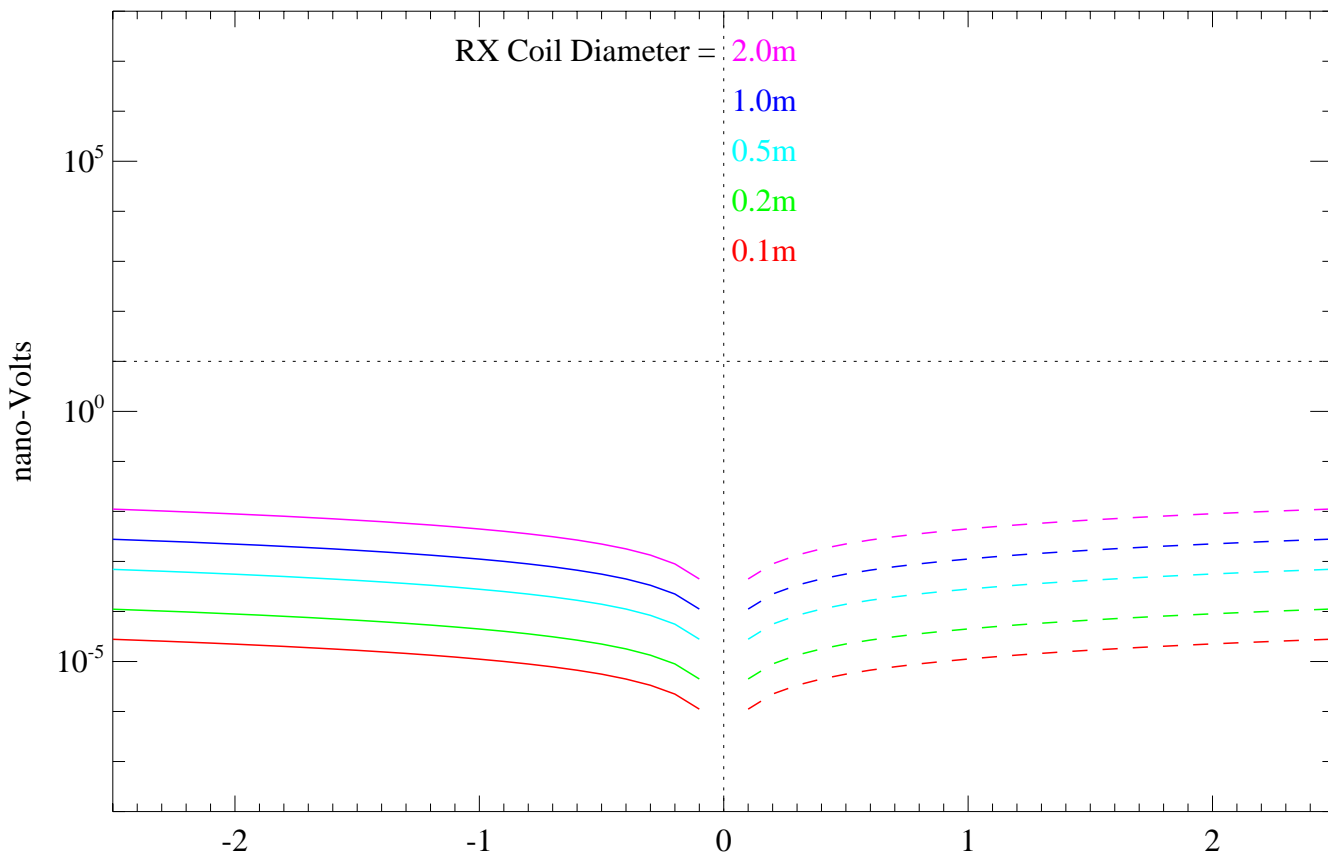
1km X 1km TX Coil, Lower RX Coil Height above Ground=2.0m, RX Coil Separation=0.5m, Object Depth=1.0m below Ground



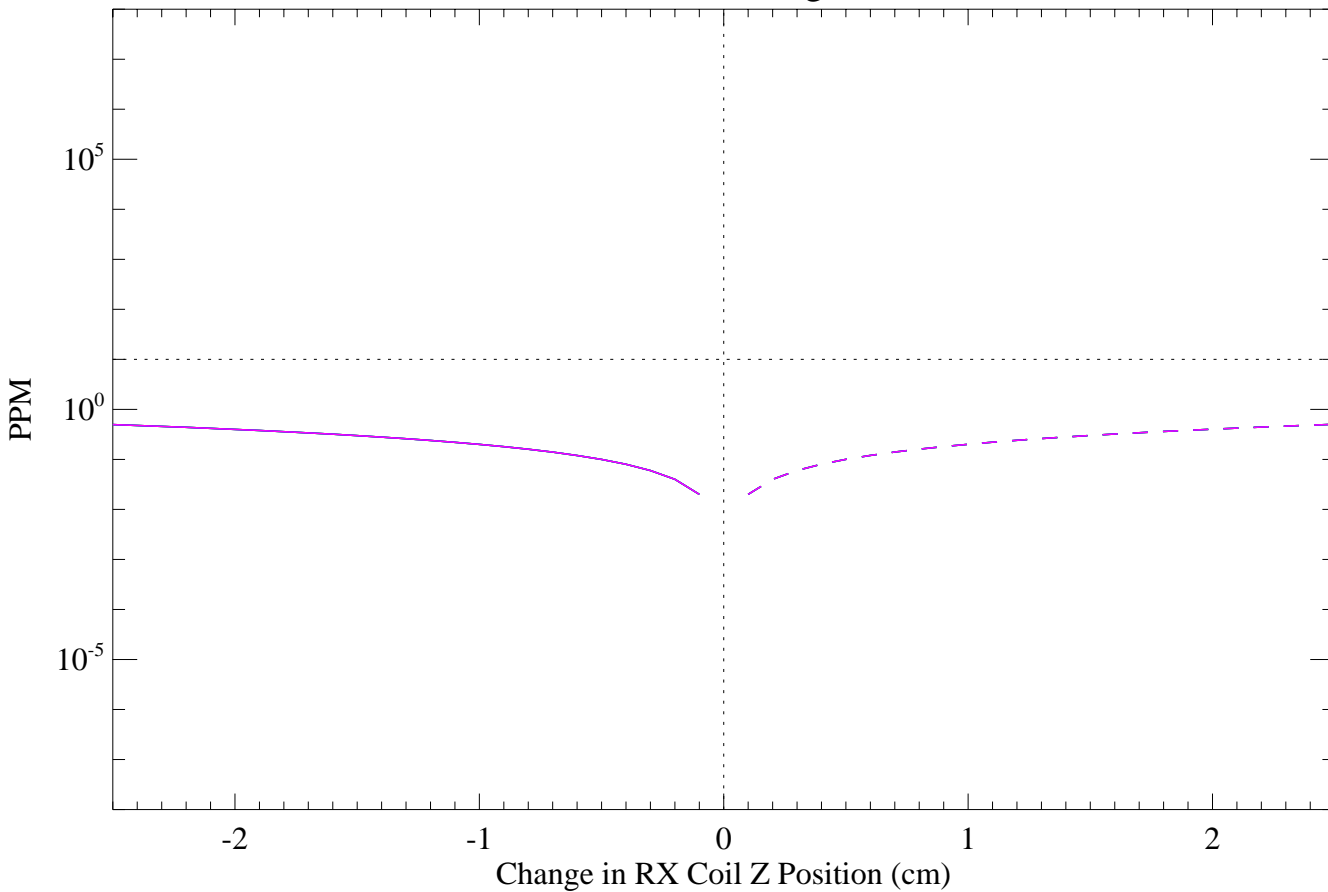
Appendix 2B

Plots of various perturbation levels for Case 1 and Case 2 receive coils and a 1 km square transmitter coil

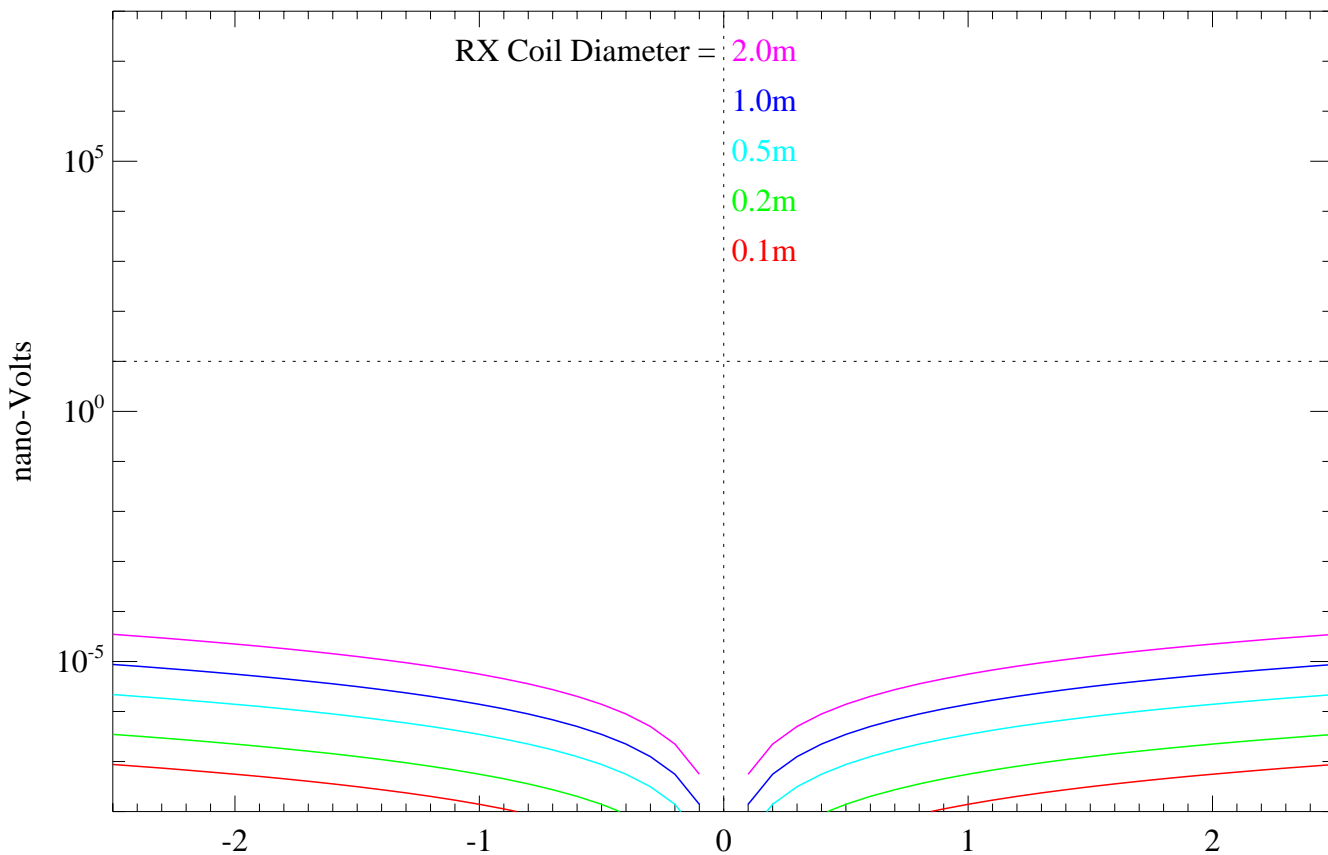
Large Ground TX Coil (CASE 1) - Change in Primary Field Coupling due to dZ Perturbations on RX Coil



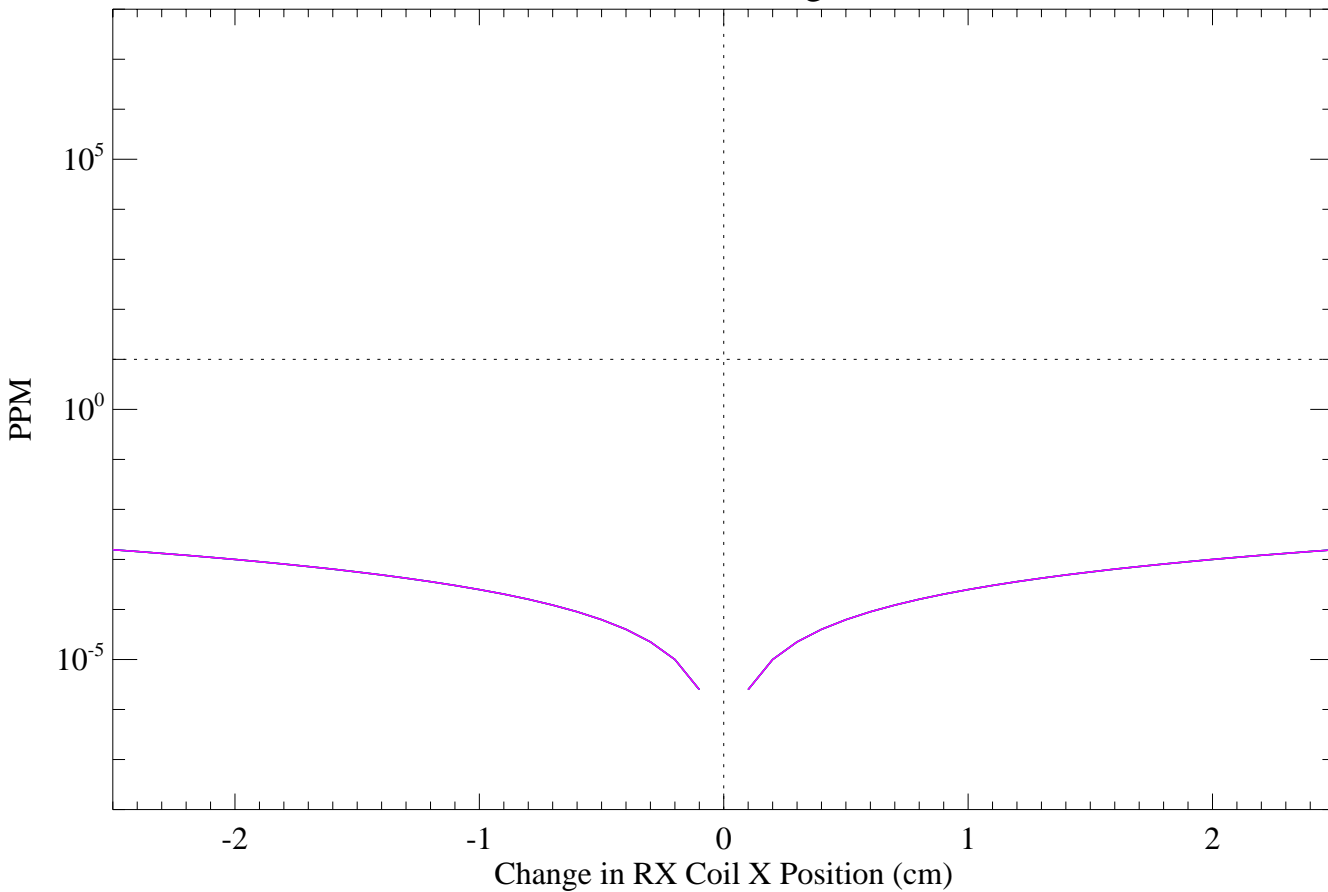
1km X 1km TX Coil, RX Coil Height above Ground=2.0m



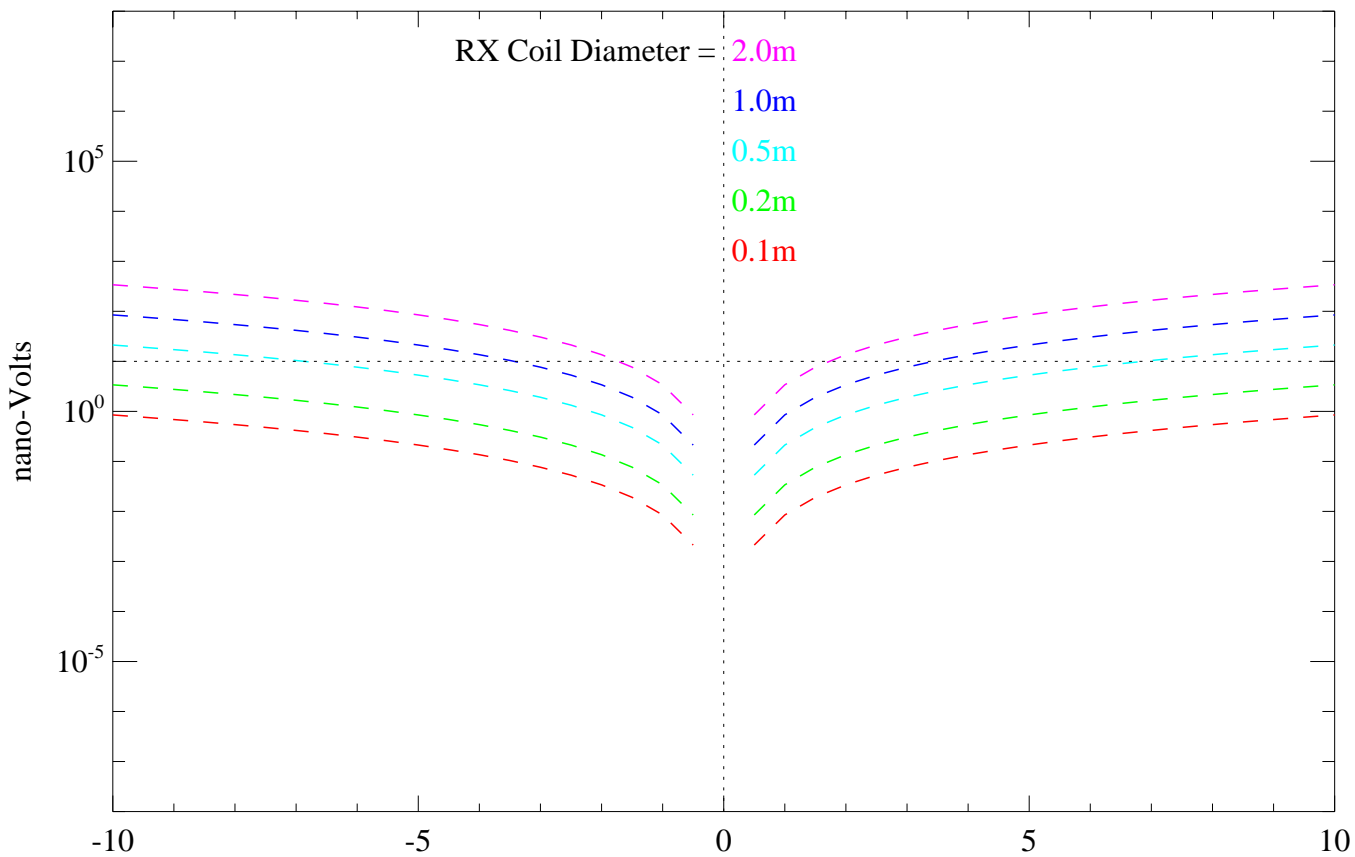
Large Ground TX Coil (CASE 1) - Change in Primary Field Coupling due to dX Perturbations on RX Coil



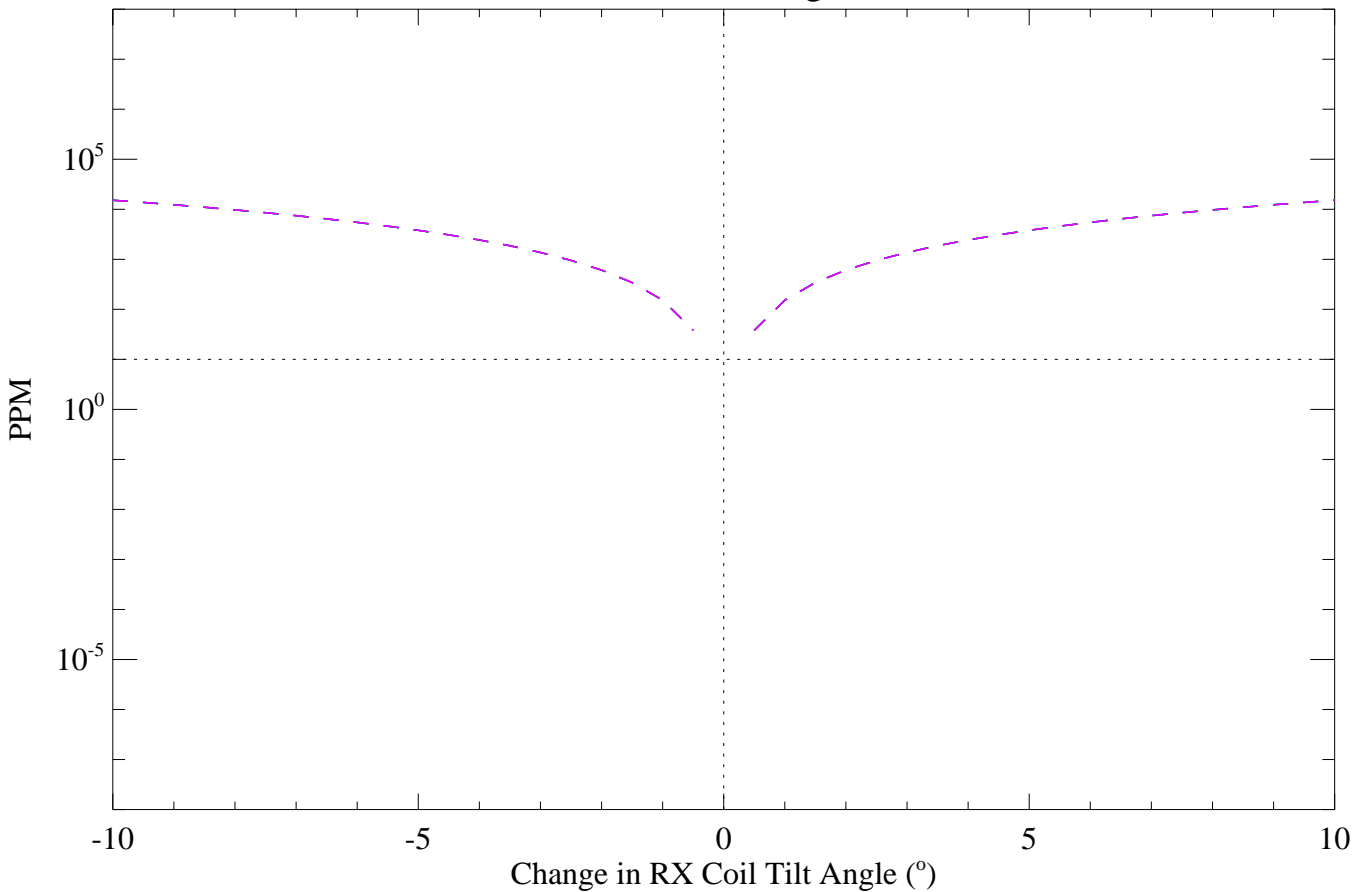
1km X 1km TX Coil, RX Coil Height above Ground=2.0m



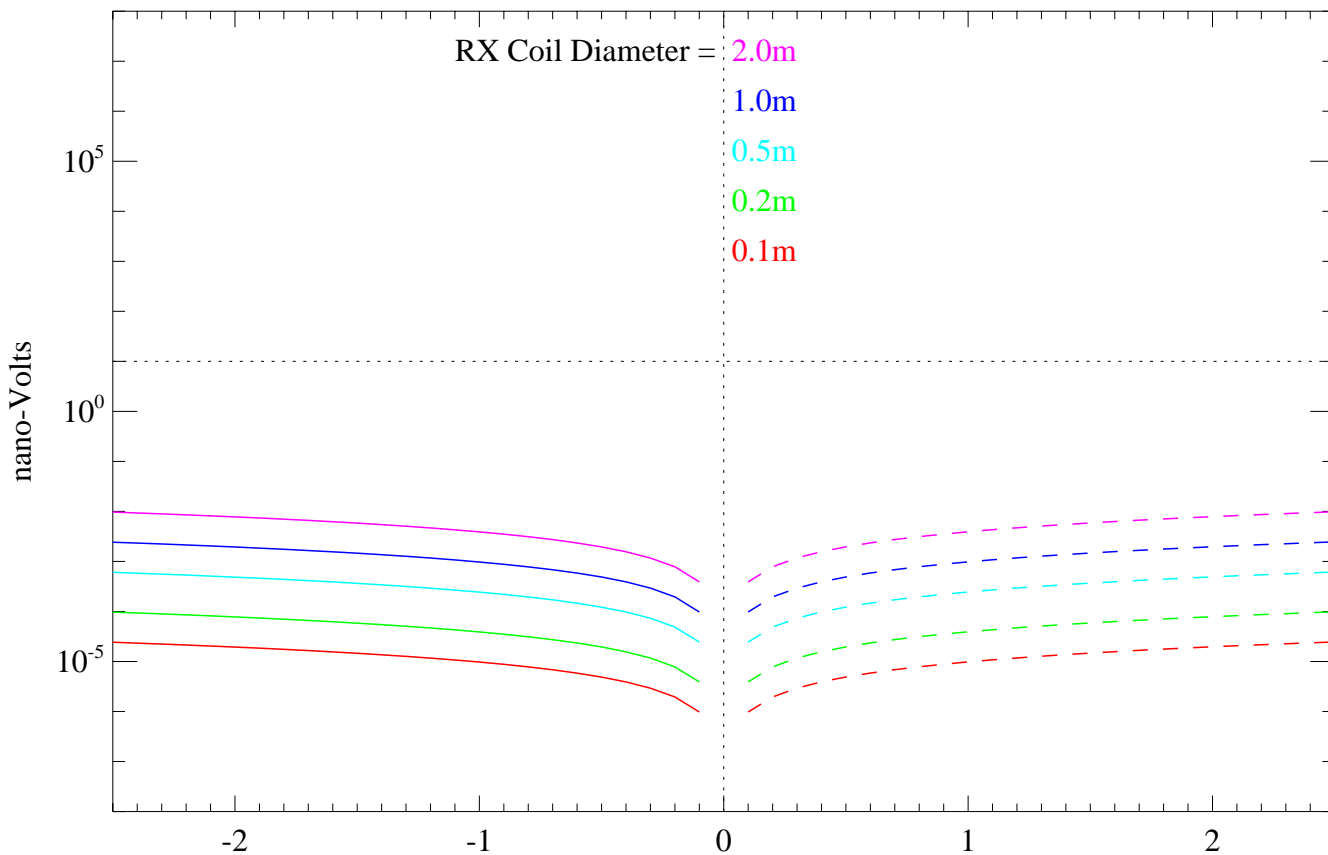
Large Ground TX Coil (CASE 1) - Change in Primary Field Coupling due to Pitch Perturbations on RX Coil



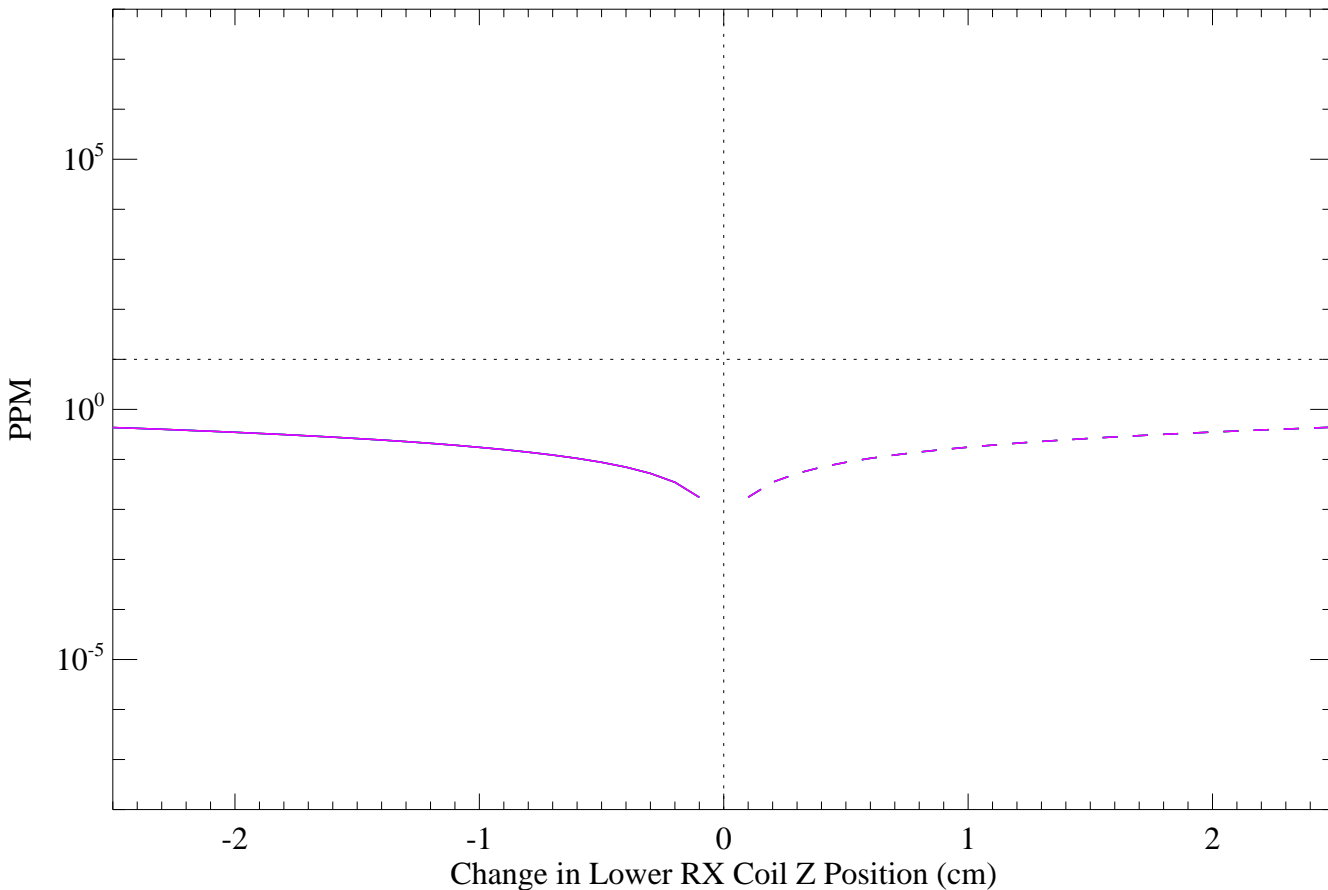
1km X 1km TX Coil, RX Coil Height above Ground=2.0m



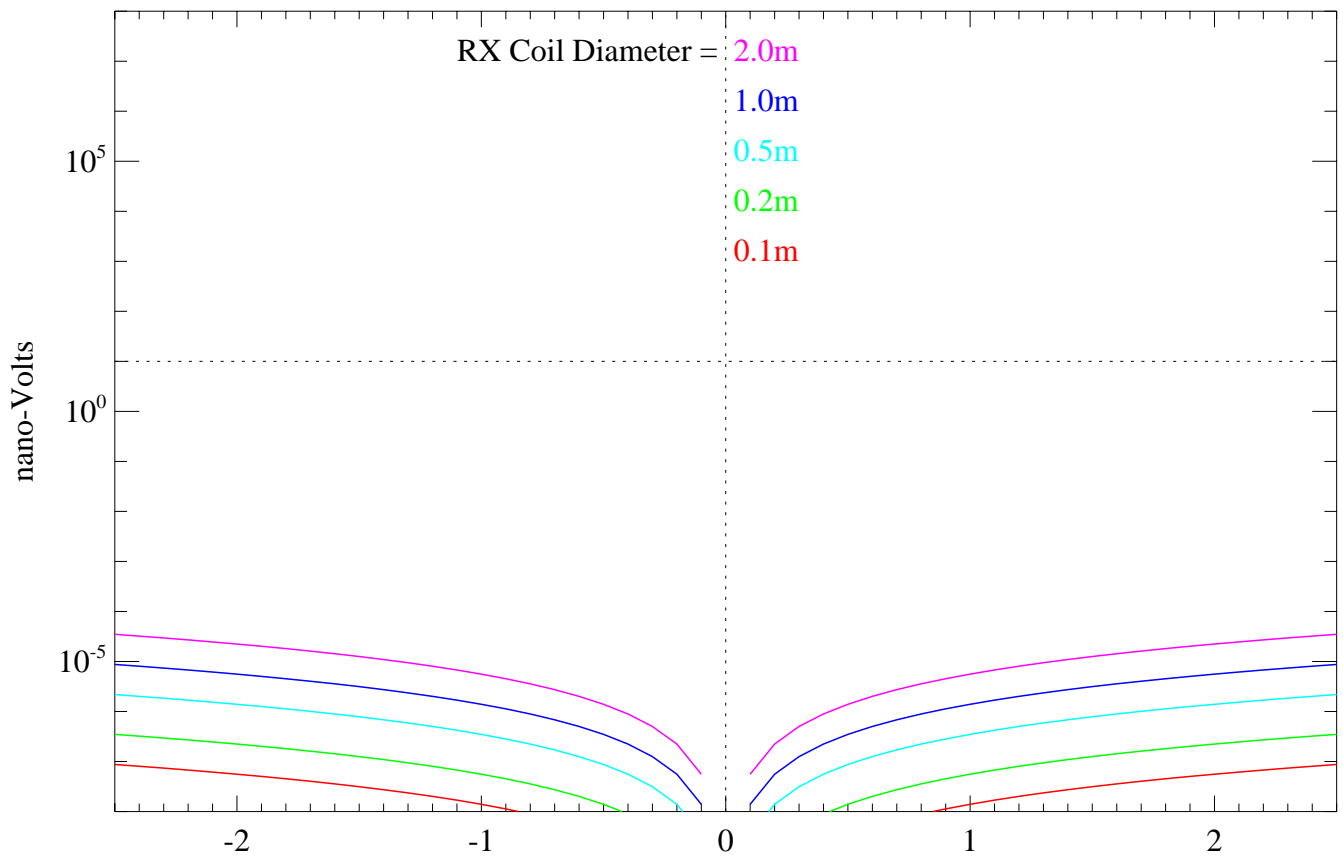
Large Ground TX Coil (CASE 2) - Change in Primary Field Coupling due to dZ Perturbations on a single RX Coil in a Gradient Pair



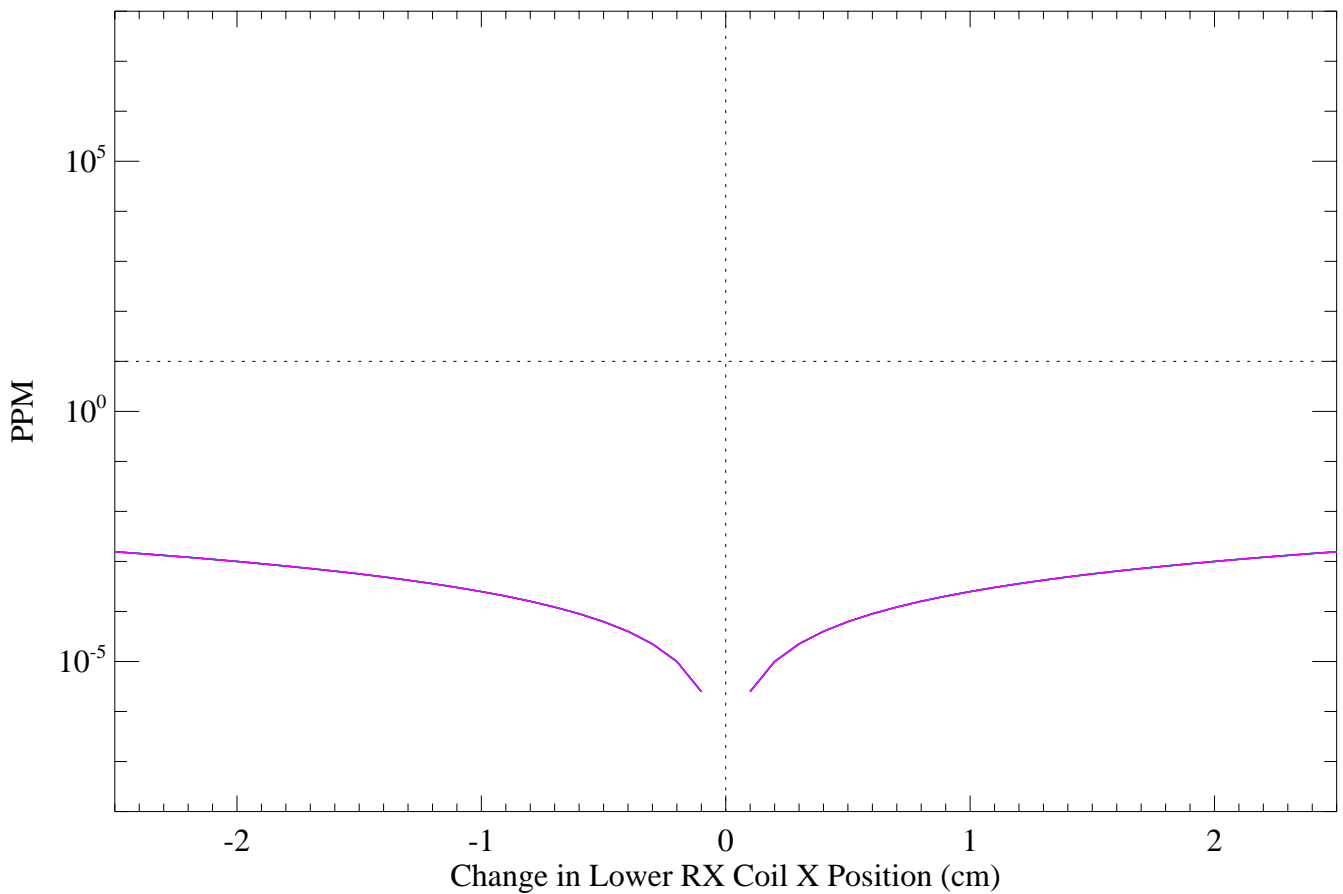
1km X 1km TX Coil, RX Coil Separation=0.5m,
Center of RX Coil Pair Height above Ground=2.0m



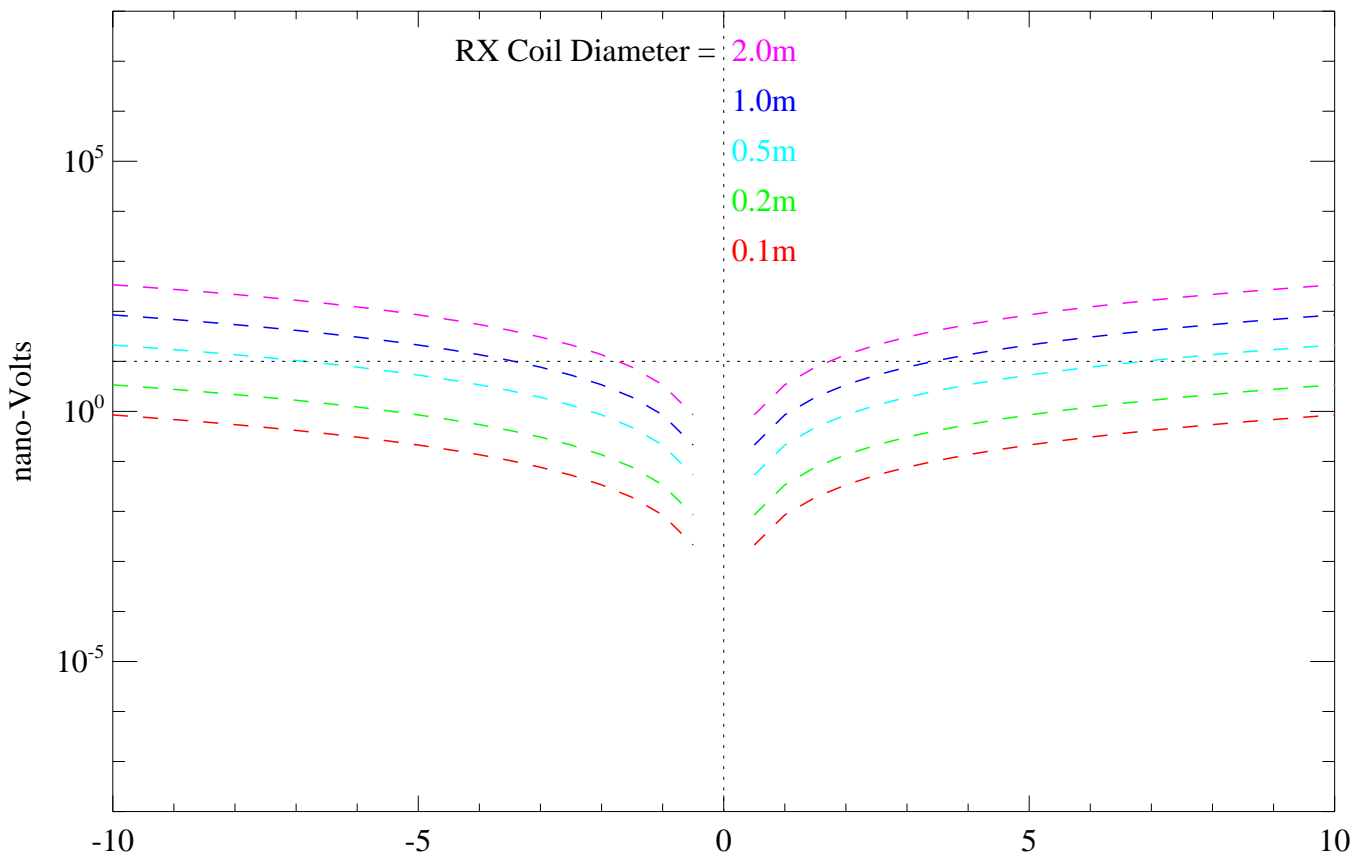
Large Ground TX Coil (CASE 2) - Change in Primary Field Coupling due to dX Perturbations on a single RX Coil in a Gradient Pair



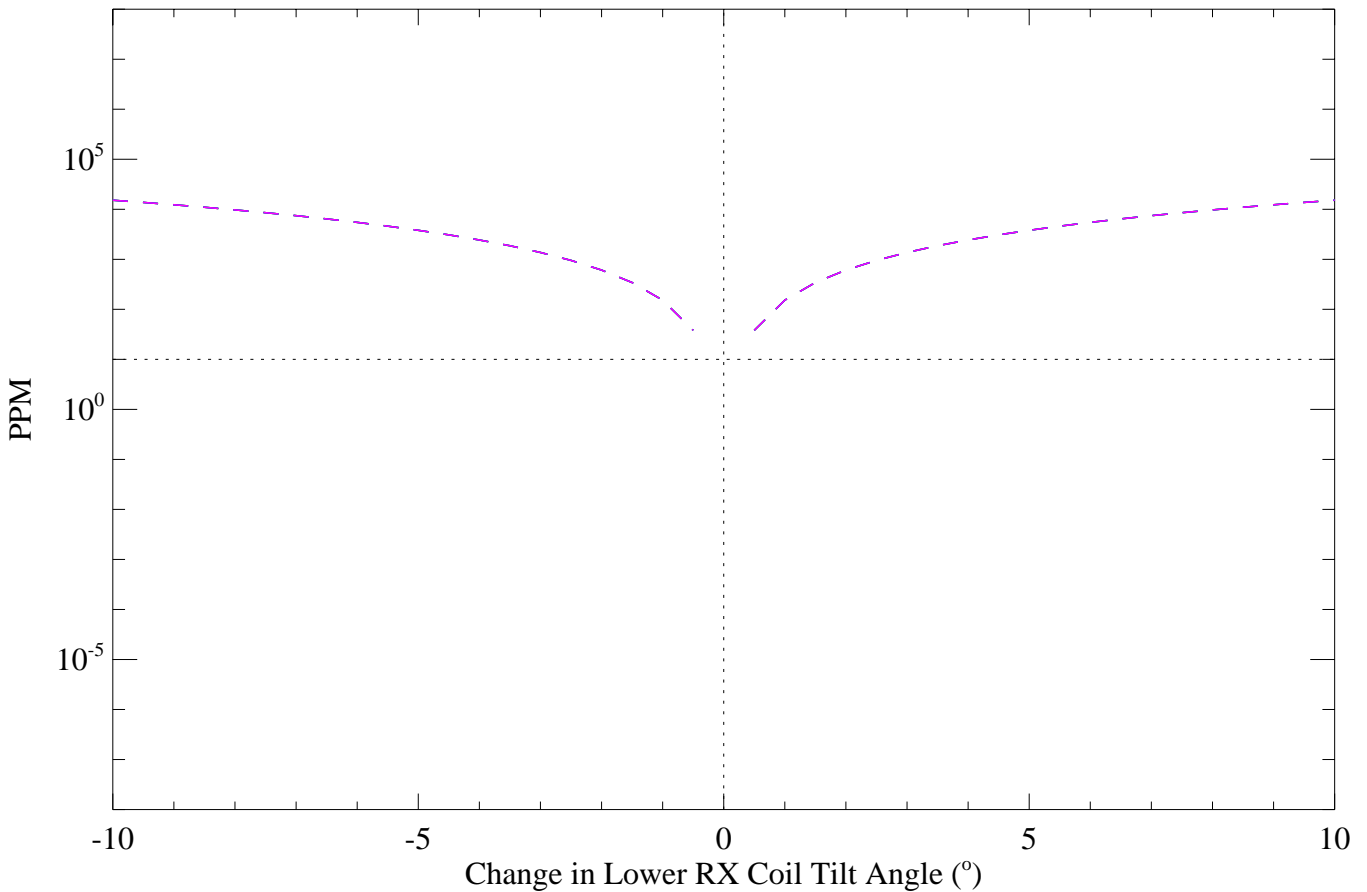
1km X 1km TX Coil, RX Coil Separation=0.5m,
Center of RX Coil Pair Height above Ground=2.0m



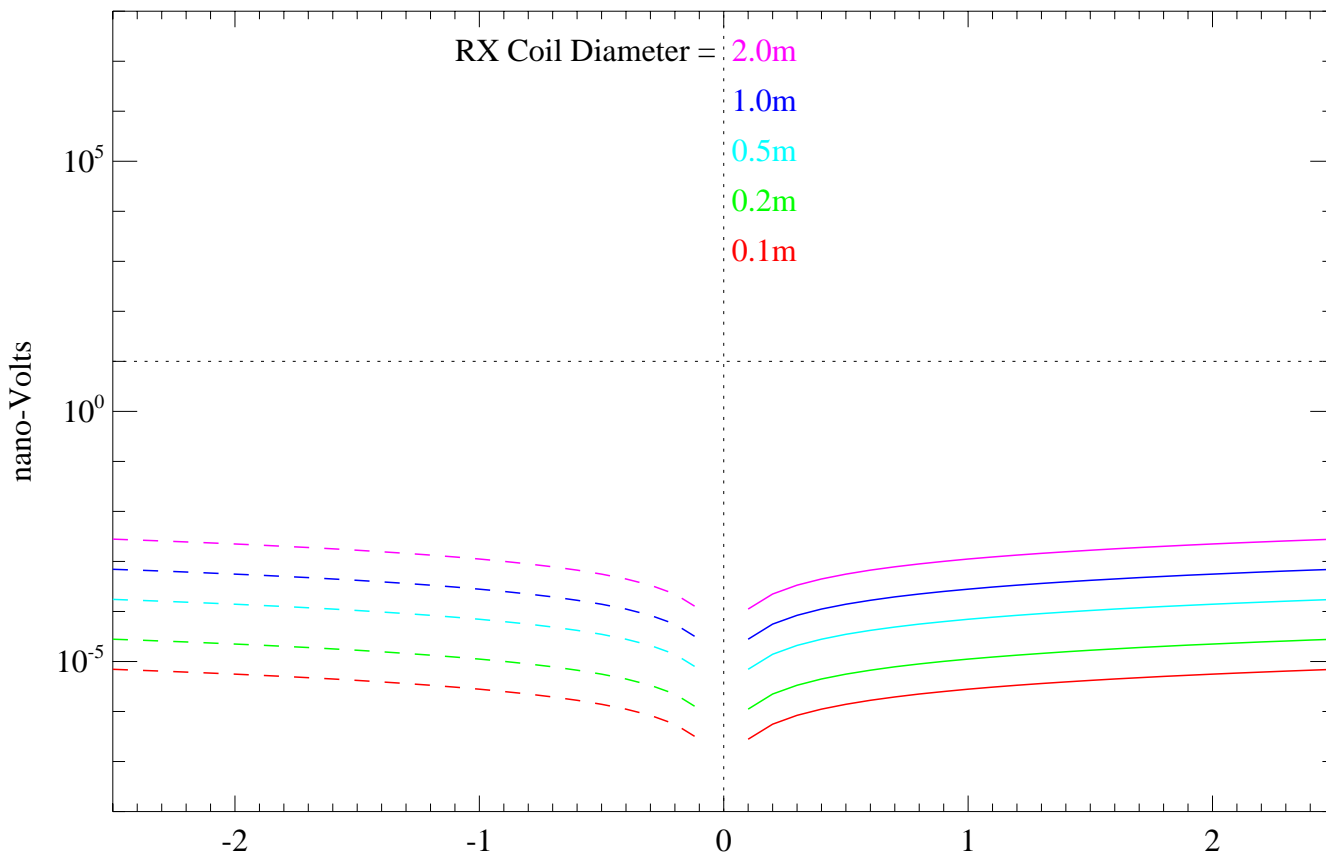
Large Ground TX Coil (CASE 2) - Change in Primary Field Coupling
due to Pitch Perturbations on a single RX Coil in a Gradient Pair



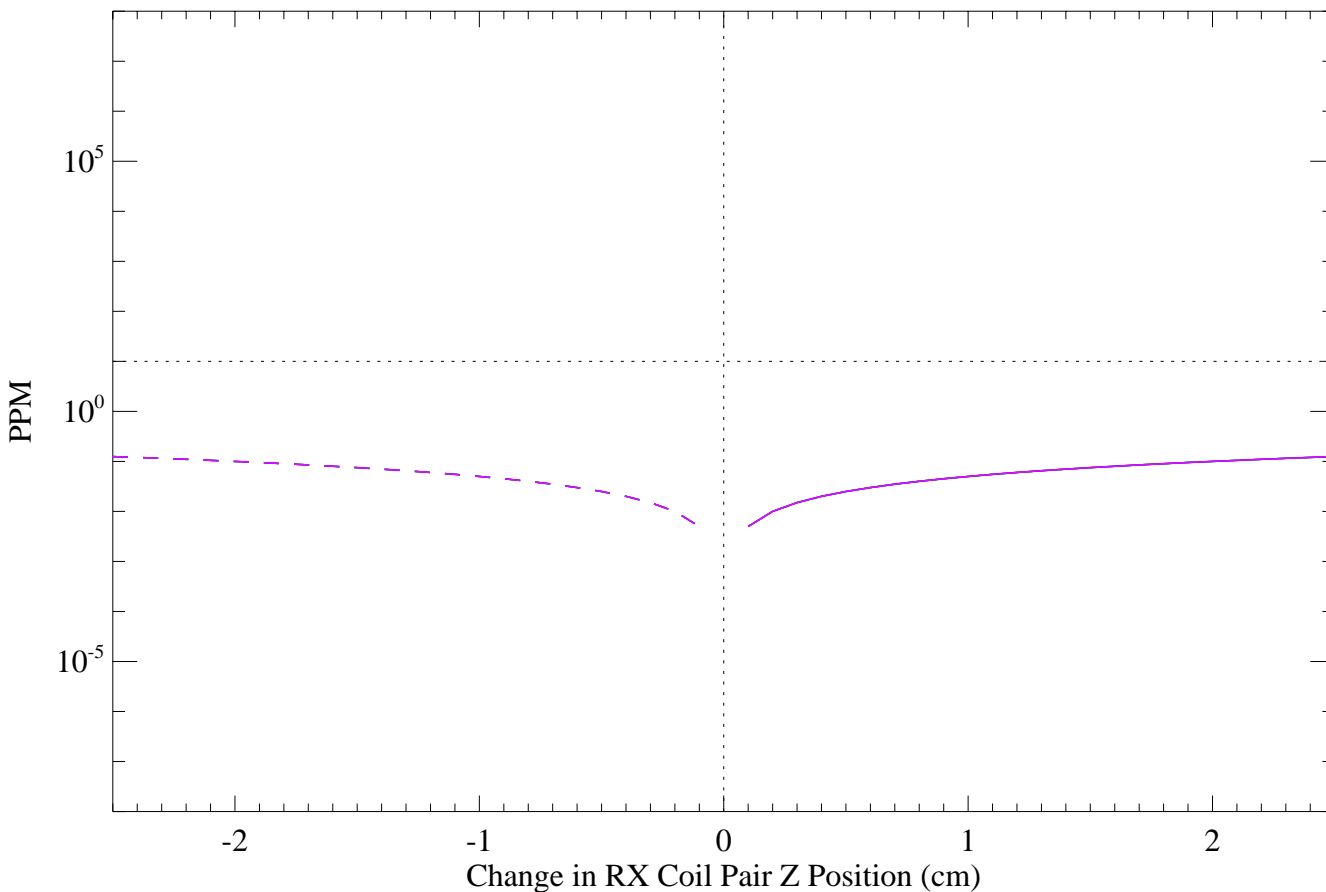
1km X 1km TX Coil, RX Coil Separation=0.5m,
Center of RX Coil Pair Height above Ground=2.0m



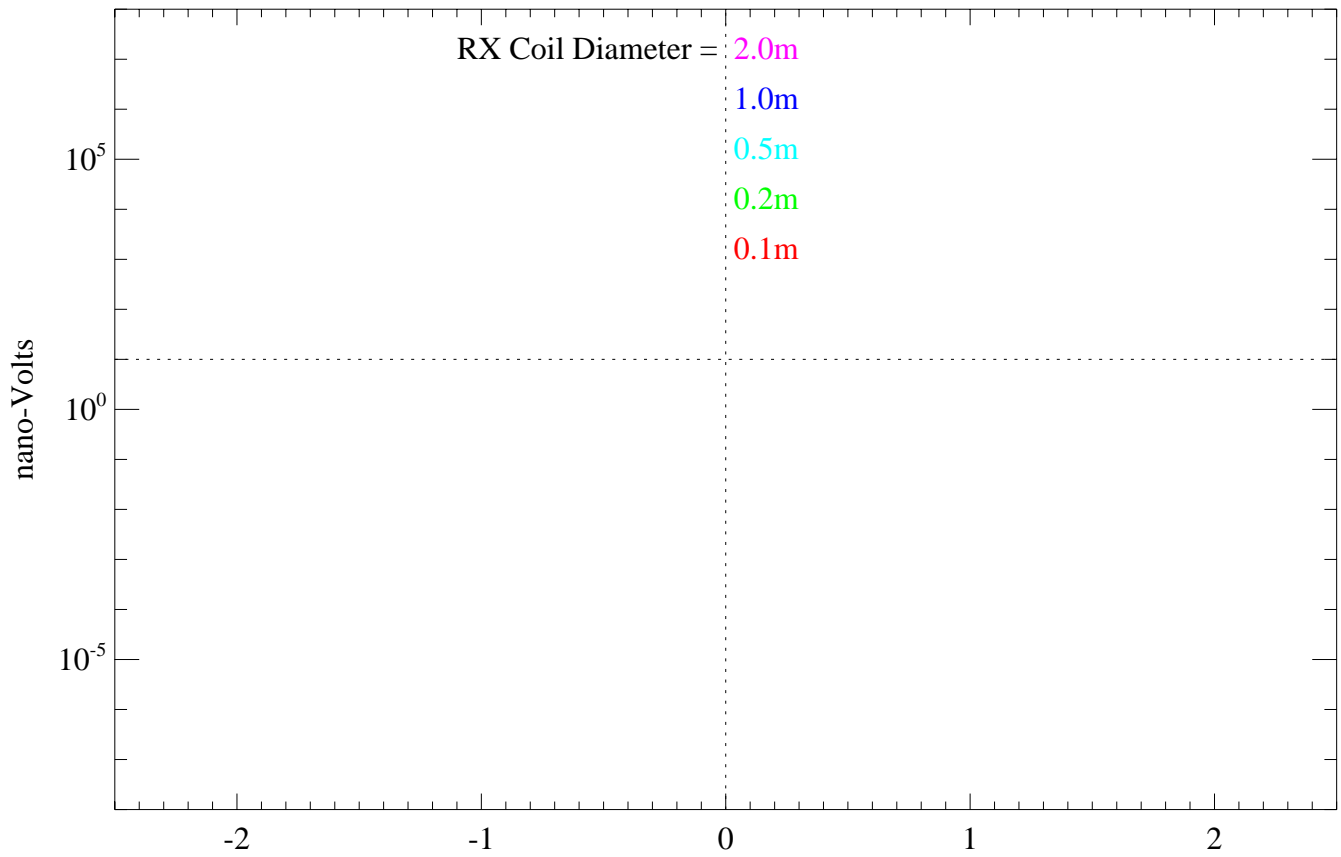
Large Ground TX Coil (CASE 2) - Change in Primary Field Coupling due to dZ Perturbations on a rigid Gradient RX Coil Pair



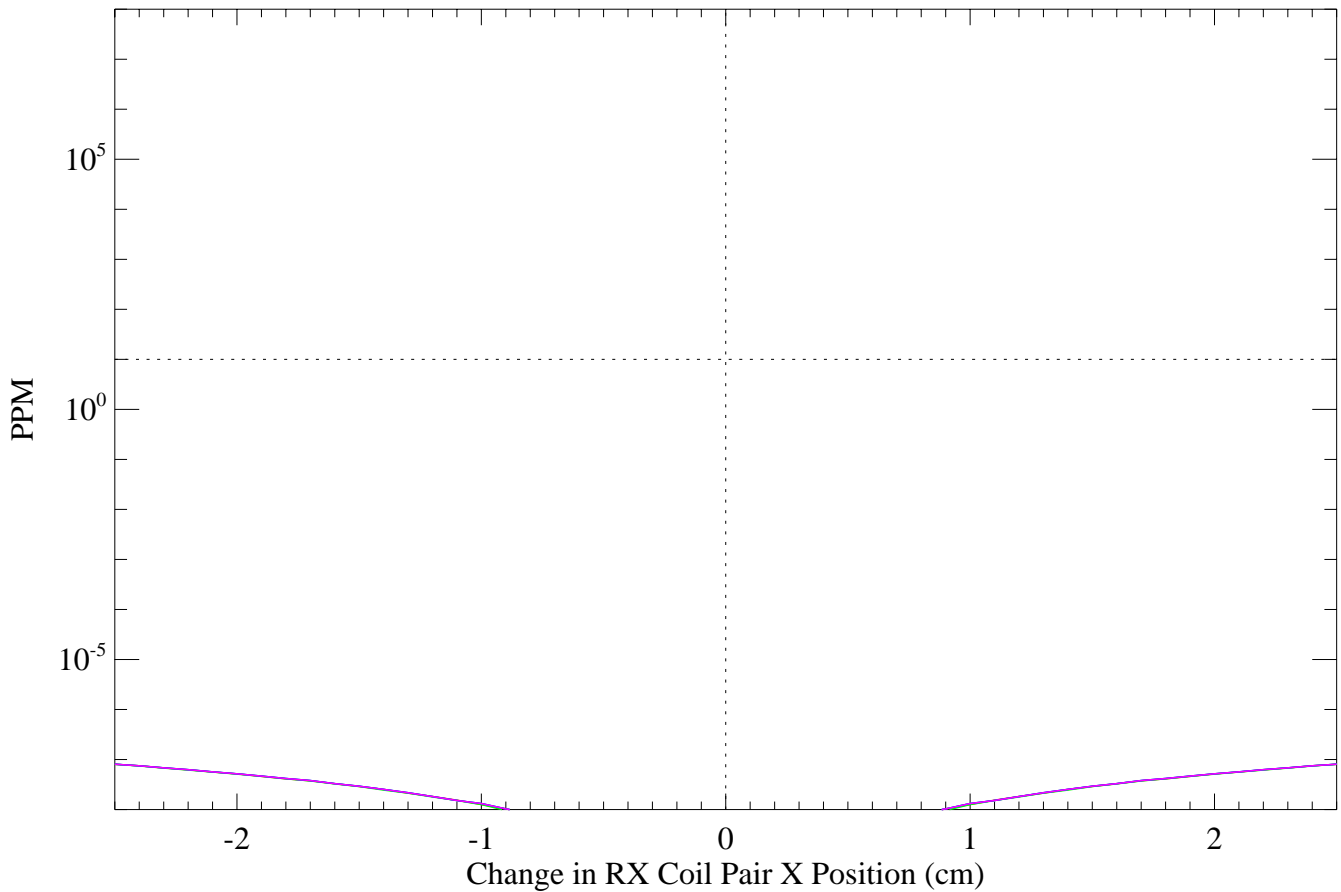
1km X 1km TX Coil, RX Coil Separation=0.5m,
Center of RX Coil Pair Height above Ground=2.0m



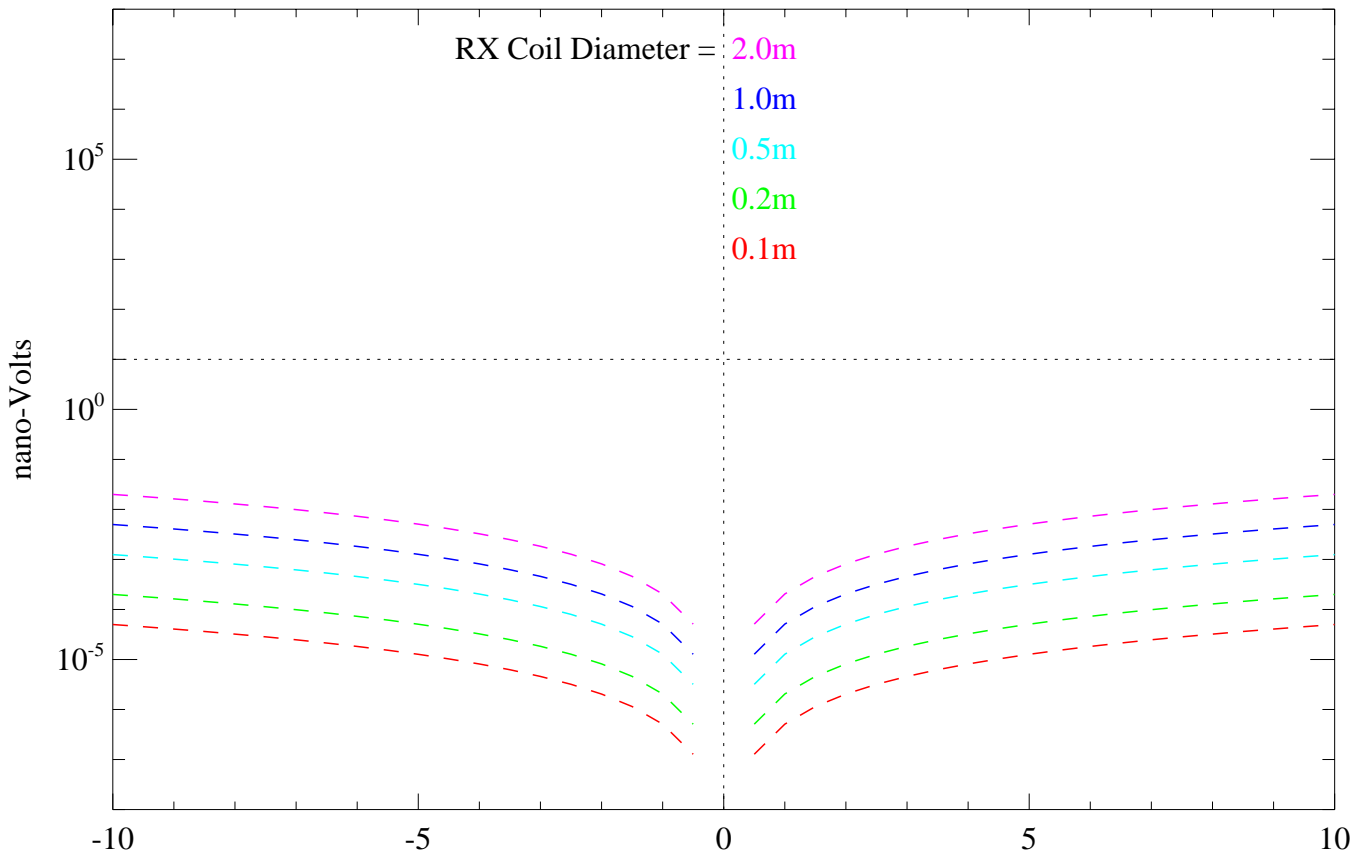
Large Ground TX Coil (CASE 2) - Change in Primary Field Coupling due to dX Perturbations on a rigid Gradient RX Coil Pair



1km X 1km TX Coil, RX Coil Separation=0.5m,
Center of RX Coil Pair Height above Ground=2.0m



Large Ground TX Coil (CASE 2) - Change in Primary Field Coupling due to Pitch Perturbations on a rigid Gradient RX Coil Pair



1km X 1km TX Coil, RX Coil Separation=0.5m,
Center of RX Coil Pair Height above Ground=2.0m

